



Politecnico di Torino

Master's Degree in Aerospace Engineering

MASTER THESIS

Thermal Analysis of 6U CubeSats

Candidate:

Gianluca Marraffa

Thesis supervisors:

Prof. Sabrina Corpino
Ing. Fabrizio Stesina

Company advisor:

Ing. Fabio Nichele

Contents

Abstract	10
Introduction	11
1 Thermal Problem	14
1.1 Design Phases	15
1.2 Spacecraft Thermal Environment	17
1.2.1 Ground Environment	17
1.2.2 Launch Thermal Environment	18
1.2.3 In-orbit Thermal Environment	19
1.3 Heat Transfer	22
1.3.1 Conduction	22
1.3.2 Radiation	25
2 Thermal Control System	29
2.1 Active Control	29
2.1.1 Heaters	29
2.1.2 Heat Pipes	30
2.1.3 Louvers	32
2.1.4 Pumped Fluid Loops	33
2.2 Passive Control	35
2.2.1 Radiators	35
2.2.2 Insulation Systems	36
2.2.3 Coatings and Surface Finishes	38
2.2.4 Phase Change Capacitors	40
3 Thermal Analysis	43
3.1 Fundamentals of Thermal Modeling	44
3.1.1 Network Solutions	44
3.1.2 Nodes	45
3.1.3 Conductors	48
3.1.4 TMM Computer Codes	54
3.1.5 Radiation Analysis Codes	66

3.2	Thermal Desktop	70
3.2.1	Optical and Thermophysical Properties	72
3.2.2	Thermal Models	76
3.2.3	External Heating Environments and Orbits	91
3.2.4	Case Set Manager	96
3.2.5	Post-Processing	102
4	Case Study	105
4.1	Mission 1	105
4.2	Mission 2	114
5	Results	126
5.1	Mission 1	126
5.1.1	Worst Hot Case	126
5.1.2	Worst Cold Case	134
5.1.3	Nominal Case	142
5.2	Mission 2	150
5.2.1	Alodine/Anodizing Valuation	150
5.2.2	Mission 2.a Worst Hot Case	154
5.2.3	Mission 2.a Worst Cold Case	161
5.2.4	Mission 2.b Worst Hot Case	168
5.2.5	Mission 2.b Worst Cold Case	175
5.2.6	Payload PCB Addition	181
6	Conclusions	184
	Acronyms	186
	Bibliography	188
	Acknowledgements	189

List of Figures

1	Different CubeSats configuration (Credits: NASA)	12
1.1	Environmental heat fluxes for a planet-orbiting spacecraft (Credits: J. Meseguer, I. Pérez-Grande, A. Sanz-Andrés, <i>Spacecraft Thermal Control</i>).	19
1.2	Solar and room temperature body spectral distribution (Credits:J. R. Wertz, <i>Space Mission Analysis and Design</i>).	20
1.3	One-dimensional heat conduction across a solid wall, whose surfaces are at different temperatures (Credits:J. Meseguer, I. Pérez-Grande, A. Sanz-Andrés, <i>Spacecraft Thermal Control</i>).	22
1.4	Differential element for energy equation in Cartesian coordinates (Credits:J. Meseguer, I. Pérez-Grande, A. Sanz-Andrés, <i>Spacecraft Thermal Control</i>).	24
1.5	Thermal radiation interactions on a surface (Credits:Kari Hyll, <i>Infrared Emittance</i>).	25
1.6	Spectral emissive power of a blackbody vs. wavelength (Credits:J. Meseguer, I. Pérez-Grande, A. Sanz-Andrés, <i>Spacecraft Thermal Control</i>).	27
2.1	Kapton film heater kit (Credits: Omega Engineering).	30
2.2	Heat-pipe schematic (Credits: D. G. Gilmore, <i>Spacecraft Thermal Control Handbook</i>).	31
2.3	Common louver design (Credits:J. Meseguer, I. Pérez-Grande, A. Sanz-Andrés, <i>Spacecraft Thermal Control</i>).	32
2.4	Schematic representation of a fluid loop showing the main components: 1 – heat exchanger; 2 – pump; 3 – heat source (Credits:J. Meseguer, I. Pérez-Grande, A. Sanz-Andrés, <i>Spacecraft Thermal Control</i>).	34
2.5	Schematic representation of a radiator ((Credits: D. G. Gilmore, <i>Spacecraft Thermal Control Handbook</i>).	36
2.6	Sketch of a typical multilayer insulation (Credits: J. Meseguer, I. Pérez-Grande, A. Sanz-Andrés, <i>Spacecraft Thermal Control</i>).	38
2.7	Solar absorptance vs. hemispherical total emissivity (Credits: J. Meseguer, I. Pérez-Grande, A. Sanz-Andrés, <i>Spacecraft Thermal Control</i>).	39
2.8	Phase change material radiator (Credits: D. G. Gilmore, <i>Spacecraft Thermal Control Handbook</i>).	41

3.1	Nodalization (Credits:TRW under NASA contract 9-10435, <i>Thermal Network Modeling Handbook</i>).	45
3.2	Temperature distribution (Credits:TRW under NASA contract 9-10435, <i>Thermal Network Modeling Handbook</i>).	45
3.3	Polygonal nodalization vs. rectangular nodalization (Credits:TRW under NASA contract 9-10435, <i>Thermal Network Modeling Handbook</i>).	47
3.4	Use of arithmetic nodes to model surfaces (Credits:TRW under NASA contract 9-10435, <i>Thermal Network Modeling Handbook</i>).	48
3.5	Thermal network Elements (Credits:TRW under NASA contract 9-10435, <i>Thermal Network Modeling Handbook</i>).	49
3.6	Conduction conductor (Credits:TRW under NASA contract 9-10435, <i>Thermal Network Modeling Handbook</i>).	49
3.7	Convection conductor (Credits:TRW under NASA contract 9-10435, <i>Thermal Network Modeling Handbook</i>).	49
3.8	Radiation conductor (Credits:TRW under NASA contract 9-10435, <i>Thermal Network Modeling Handbook</i>).	50
3.9	Simple conductor representing a heat-flow path through material (Credits:TRW under NASA contract 9-10435, <i>Thermal Network Modeling Handbook</i>).	51
3.10	Area and length equivalents for circular section nodes. (Credits:TRW under NASA contract 9-10435, <i>Thermal Network Modeling Handbook</i>).	51
3.11	Series conductor paths (Credits:TRW under NASA contract 9-10435, <i>Thermal Network Modeling Handbook</i>).	52
3.12	Configuration-factor algebra (Credits:TRW under NASA contract 9-10435, <i>Thermal Network Modeling Handbook</i>).	54
3.13	Finite-difference method (Credits:D. G. Gilmore, <i>Spacecraft Thermal Control Handbook</i>).	56
3.14	Finite-element method (Credits:D. G. Gilmore, <i>Spacecraft Thermal Control Handbook</i>).	63
3.15	Radiative interchange between two black differential area elements (Credits:D. G. Gilmore, <i>Spacecraft Thermal Control Handbook</i>).	67
3.16	Case Set Manager Dialog Box (Credits: <i>Thermal Desktop User's Manual</i> by C&R Technologies, Inc.).	70
3.17	Edit Optical Properties Dialog Box (Credits: <i>Thermal Desktop User's Manual</i> by C&R Technologies, Inc.).	72
3.18	Edit Optical Property Dialog Box to Define Optical Property Values (Credits: <i>Thermal Desktop User's Manual</i> by C&R Technologies, Inc.).	73
3.19	Edit Thermophysical Properties Dialog (Credits: <i>Thermal Desktop User's Manual</i> by C&R Technologies, Inc.).	75
3.20	Edit Thermophysical Property - Property Name Dialog (Credits: <i>Thermal Desktop User's Manual</i> by C&R Technologies, Inc.).	76
3.21	Radiation Analysis Group Manager Dialog Box (Credits: <i>Thermal Desktop User's Manual</i> by C&R Technologies, Inc.).	77

3.22	SINDA/FLUINT Submodel Manager Form Dialog Box (Credits: <i>Thermal Desktop User's Manual</i> by C&R Technologies, Inc.).	78
3.23	Thermal Desktop Thin Shell Edit Form and Subdivision Tab (Credits: <i>Thermal Desktop User's Manual</i> by C&R Technologies, Inc.).	79
3.24	Thin Shell Data Dialog Box Numbering Tab (Credits: <i>Thermal Desktop User's Manual</i> by C&R Technologies, Inc.).	80
3.25	Thin Shell Data Dialog Box Radiation Tab (Credits: <i>Thermal Desktop User's Manual</i> by C&R Technologies, Inc.).	81
3.26	Thin Shell Data Dialog Box Conductance-Capacitance Tab (Credits: <i>Thermal Desktop User's Manual</i> by C&R Technologies, Inc.).	82
3.27	Conductor Dialog Box (Credits: <i>Thermal Desktop User's Manual</i> by C&R Technologies, Inc.).	84
3.28	Contacto Dialog Box (Credits: <i>Thermal Desktop User's Manual</i> by C&R Technologies, Inc.).	86
3.29	Heat Load Edit Form Dialog Box (Credits: <i>Thermal Desktop User's Manual</i> by C&R Technologies, Inc.).	89
3.30	Heater Edit Form Dialog Box (Credits: <i>Thermal Desktop User's Manual</i> by C&R Technologies, Inc.).	90
3.31	Heating Rate Case Manager Dialog (Credits: <i>Thermal Desktop User's Manual</i> by C&R Technologies, Inc.).	91
3.32	Specifying the Orientation of the Spacecraft in Basic and Keplerian Orbits (Credits: <i>Thermal Desktop User's Manual</i> by C&R Technologies, Inc.). . .	92
3.33	Specification of Planetary Data For an Orbit (Credits: <i>Thermal Desktop User's Manual</i> by C&R Technologies, Inc.).	94
3.34	Keplerian Heating Rate Case Dialog Box (Credits: <i>Thermal Desktop User's Manual</i> by C&R Technologies, Inc.).	95
3.35	Case Set Manager Dialog Box (Credits: <i>Thermal Desktop User's Manual</i> by C&R Technologies, Inc.).	97
3.36	Case Set Dialog Box Calculations Tab (Credits: <i>Thermal Desktop User's Manual</i> by C&R Technologies, Inc.).	98
3.37	Case Set Dialog Box Radiation Task Tab (Credits: <i>Thermal Desktop User's Manual</i> by C&R Technologies, Inc.).	101
3.38	Case Set Dialog Box Output Tab (Credits: <i>Thermal Desktop User's Manual</i> by C&R Technologies, Inc.).	102
3.39	Post-processing with Four Color Bars for Node, Lump, Path and Tie Data (Credits: <i>Thermal Desktop User's Manual</i> by C&R Technologies, Inc.). . .	103
4.1	Mission 1 overview.	106
4.2	Mission 1 external surfaces mesh.	108
4.3	Mission 1 payload and bus component.	109
4.4	Mission 1 contactor.	110
4.5	Mission 1 heat loads.	111
4.6	Mission 1 orbit.	112

4.7	Mission 2.a overview.	114
4.8	Mission 2.b overview.	115
4.9	Mission 2.a external surfaces mesh.	117
4.10	Mission 2.b external surfaces mesh.	118
4.11	Mission 2.a payload and bus component.	120
4.12	Mission 2.b payload and bus component.	120
4.13	Mission 2 conductors.	122
4.14	Mission 2.a heat loads.	123
4.15	Mission 2.b heat loads.	123
4.16	Mission 2 orbit.	124
5.1	Mission 1 Worst Hot Case color post-processing.	126
5.2	Mission 1 6U/Y+ Worst Hot Case x-y plotting.	127
5.3	Mission 1 6U/Y- Worst Hot Case x-y plotting.	127
5.4	Mission 1 3U/X+ Worst Hot Case x-y plotting.	128
5.5	Mission 1 3U/X- Worst Hot Case x-y plotting.	128
5.6	Mission 1 2U/Z+ Worst Hot Case x-y plotting.	129
5.7	Mission 1 2U/Z- Worst Hot Case x-y plotting.	129
5.8	Mission 1 Camera 1 Worst Hot Case x-y plotting.	130
5.9	Mission 1 Camera 2 Worst Hot Case x-y plotting.	130
5.10	Mission 1 Camera 3 Worst Hot Case x-y plotting.	131
5.11	Mission 1 brackets Worst Hot Case x-y plotting.	131
5.12	Mission 1 Payload Component Worst Hot Case x-y plotting.	132
5.13	Mission 1 Bus Component Worst Hot Case x-y plotting.	132
5.14	Mission 1 battery 1 Worst Hot Case x-y plotting.	133
5.15	Mission 1 battery 2 Worst Hot Case x-y plotting.	133
5.16	Mission 1 Worst Cold Case color post-processing.	134
5.17	Mission 1 6U/Y+ Worst Cold Case x-y plotting.	135
5.18	Mission 1 6U/Y- Worst Cold Case x-y plotting.	135
5.19	Mission 1 3U/X+ Worst Cold Case x-y plotting.	136
5.20	Mission 1 3U/X- Worst Cold Case x-y plotting.	136
5.21	Mission 1 2U/Z+ Worst Cold Case x-y plotting.	137
5.22	Mission 1 2U/Z- Worst Cold Case x-y plotting.	137
5.23	Mission 1 Camera 1 Worst Cold Case x-y plotting.	138
5.24	Mission 1 Camera 2 Worst Cold Case x-y plotting.	138
5.25	Mission 1 Camera 3 Worst Cold Case x-y plotting.	139
5.26	Mission 1 brackets Worst Cold Case x-y plotting.	139
5.27	Mission 1 Payload Component Worst Cold Case x-y plotting.	140
5.28	Mission 1 Bus Component Worst Cold Case x-y plotting.	140
5.29	Mission 1 battery 1 Worst Cold Case x-y plotting.	141
5.30	Mission 1 battery 2 Worst Cold Case x-y plotting.	141
5.31	Mission 1 Nominal Case color post-processing.	142
5.32	Mission 1 6U/Y+ Nominal Case x-y plotting.	143

5.33	Mission 1 6U/Y- Nominal Case x-y plotting.	143
5.34	Mission 1 3U/X+ Nominal Case x-y plotting.	144
5.35	Mission 1 3U/X- Nominal Case x-y plotting.	144
5.36	Mission 1 2U/Z+ Nominal Case x-y plotting.	145
5.37	Mission 1 2U/Z- Nominal Case x-y plotting.	145
5.38	Mission 1 Camera 1 Nominal Case x-y plotting.	146
5.39	Mission 1 Camera 2 Nominal Case x-y plotting.	146
5.40	Mission 1 Camera 3 Nominal Case x-y plotting.	147
5.41	Mission 1 brackets Nominal Case x-y plotting.	147
5.42	Mission 1 Payload Component Nominal Case x-y plotting.	148
5.43	Mission 1 Bus Component Nominal Case x-y plotting.	148
5.44	Mission 1 battery 1 Nominal Case x-y plotting.	149
5.45	Mission 1 battery 2 Nominal Case x-y plotting.	149
5.46	Mission 2.a 3U/X+ alodine/anodizing x-y plotting.	151
5.47	Mission 2.b 6U/Y+ alodine/anodizing x-y plotting.	152
5.48	Mission 2.b Battery 1 alodine/anodizing x-y plotting.	153
5.49	Mission 2.a Worst Hot Case color post-processing.	154
5.50	Mission 2.a 6U/Y+ Worst Hot Case x-y plotting.	155
5.51	Mission 2.a 6U/Y- Worst Hot Case x-y plotting.	155
5.52	Mission 2.a 3U/X+ Worst Hot Case x-y plotting.	156
5.53	Mission 2.a 3U/X- Worst Hot Case x-y plotting.	156
5.54	Mission 2.a 2U/Z+ Worst Hot Case x-y plotting.	157
5.55	Mission 2.a 2U/Z- Worst Hot Case x-y plotting.	157
5.56	Mission 2.a Payload Component 1.a Worst Hot Case x-y plotting.	158
5.57	Mission 2.a Payload Component 2.a Worst Hot Case x-y plotting.	158
5.58	Mission 2.a Payload Component 2.a Antenna Worst Hot Case x-y plotting.	159
5.59	Mission 2.a Bus Component 1.a Worst Hot Case x-y plotting.	159
5.60	Mission 2.a Bus Component 2.a Worst Hot Case x-y plotting.	160
5.61	Mission 2.a Battery 1.a Worst Hot Case x-y plotting.	160
5.62	Mission 2.a Battery 2.a Worst Hot Case x-y plotting.	161
5.63	Mission 2.a Worst Cold Case color post-processing.	161
5.64	Mission 2.a 6U/Y+ Worst Cold Case x-y plotting.	162
5.65	Mission 2.a 6U/Y- Worst Cold Case x-y plotting.	162
5.66	Mission 2.a 3U/X+ Worst Cold Case x-y plotting.	163
5.67	Mission 2.a 3U/X- Worst Cold Case x-y plotting.	163
5.68	Mission 2.a 2U/Z+ Worst Cold Case x-y plotting.	164
5.69	Mission 2.a 2U/Z- Worst Cold Case x-y plotting.	164
5.70	Mission 2.a Payload Component 1.a Worst Cold Case x-y plotting.	165
5.71	Mission 2.a Payload Component 2.a Worst Cold Case x-y plotting.	165
5.72	Mission 2.a Payload Component 2.a Antenna Worst Cold Case x-y plotting.	166
5.73	Mission 2.a Bus Component 1.a Worst Cold Case x-y plotting.	166
5.74	Mission 2.a Bus Component 2.a Worst Cold Case x-y plotting.	167
5.75	Mission 2.a Battery 1.a Worst Cold Case x-y plotting.	167

5.76	Mission 2.a Battery 2.a Worst Cold Case x-y plotting.	168
5.77	Mission 2.b Worst Hot Case color post-processing.	168
5.78	Mission 2.b 6U/Y+ Worst Hot Case x-y plotting.	169
5.79	Mission 2.b 6U/Y- Worst Hot Case x-y plotting.	169
5.80	Mission 2.b 3U/X+ Worst Hot Case x-y plotting.	170
5.81	Mission 2.b 3U/X- Worst Hot Case x-y plotting.	170
5.82	Mission 2.b 2U/Z+ Worst Hot Case x-y plotting.	171
5.83	Mission 2.b 2U/Z- Worst Hot Case x-y plotting.	171
5.84	Mission 2.b Payload Component 1.b Worst Hot Case x-y plotting.	172
5.85	Mission 2.b Payload Component 2.b Worst Hot Case x-y plotting.	172
5.86	Mission 2.b Bus Component 1.b Worst Hot Case x-y plotting.	173
5.87	Mission 2.b Bus Component 2.b Worst Hot Case x-y plotting.	173
5.88	Mission 2.b Battery 1.b Worst Hot Case x-y plotting.	174
5.89	Mission 2.b Battery 2.b Worst Hot Case x-y plotting.	174
5.90	Mission 2.b Worst Cold Case color post-processing.	175
5.91	Mission 2.b 6U/Y+ Worst Cold Case x-y plotting.	175
5.92	Mission 2.b 6U/Y- Worst Cold Case x-y plotting.	176
5.93	Mission 2.b 3U/X+ Worst Hot Case x-y plotting.	176
5.94	Mission 2.b 3U/X- Worst Cold Case x-y plotting.	177
5.95	Mission 2.b 2U/Z+ Worst Cold Case x-y plotting.	177
5.96	Mission 2.b 2U/Z- Worst Cold Case x-y plotting.	178
5.97	Mission 2.b Payload Component 1.b Worst Cold Case x-y plotting.	178
5.98	Mission 2.b Payload Component 2.b Worst Cold Case x-y plotting.	179
5.99	Mission 2.b Bus Component 1.b Worst Cold Case x-y plotting.	179
5.100	Mission 2.b Bus Component 2.b Worst Cold Case x-y plotting.	180
5.101	Mission 2.b Battery 1.b Worst Cold Case x-y plotting.	180
5.102	Mission 2.b Battery 2.b Worst Cold Case x-y plotting.	181
5.103	Mission 2.b Payload Component 2.b PCB (a) and 3U face PCB (b).	181
5.104	Mission 2.b Payload Component 2.b PCB color post-processing (a) and x-y plotting (b-c).	182
5.105	Mission 2.b 3U Face PCB color post-processing (a) and x-y plotting (b-c).	183
5.106	Mission 2.b Payload Component 2.b PCB vs. 3U Face PCB x-y plotting.	183

List of Tables

1	Classification of small satellites.	11
1.1	Examples of Typical Thermal Requirements for Spacecraft Components (Credits: J. R. Wertz, <i>Space Mission Analysis and Design</i>)	14
1.2	Design phases (Credits:J. R. Wertz, <i>Space Mission Analysis and Design</i>).	16
1.3	Albedo values.(Credits:J. R.Wertz, <i>Space Mission Analysis and Design</i>).	21
3.1	Electrical-Thermal analogy (Credits:TRW under NASA contract 9-10435, <i>Thermal Network Modeling Handbook</i>).	44
3.2	Node type classification (Credits:TRW under NASA contract 9-10435, <i>Thermal Network Modeling Handbook</i>).	46
3.3	Contact from Edges/Faces (Credits: <i>Thermal Desktop User's Manual</i> by C & R Technologies, Inc.).	87
4.1	Mission 1 thermophysical properties.	106
4.2	Mission 1 optical properties.	107
4.3	Mission 1 external surfaces characteristics.	107
4.4	Mission 1 payload and bus components characteristics.	109
4.5	Mission 1 contactor parameters.	110
4.6	Mission 1 heat loads.	111
4.7	Mission 1 orbital data.	112
4.8	Mission 1 case scenarios.	113
4.9	Mission 2 thermophysical properties.	115
4.10	Mission 2 optical properties.	116
4.11	Mission 2.a external surfaces characteristics.	116
4.12	Mission 2.b external surfaces characteristics.	117
4.13	Mission 2.a payload and bus components characteristics.	119
4.14	Mission 2.b payload and bus components characteristics.	119
4.15	Mission 2.a conductors parameters.	121
4.16	Mission 2.b conductors parameters.	121
4.17	Mission 2 heat loads.	122
4.18	Mission 2 orbital data.	124
4.19	Mission 2 case scenarios.	125

Abstract

Recently, there has been an increase in emphasis on small satellites, however their small size results in small surface areas which often imply thermal and power constraints. For this reason, thermal analysis and design have become of crucial importance for every phases of a space mission project. In particular, since satellites limited power, the active thermal control systems are less employed, so it is important properly choose the passive systems and exploit them to the full.

The aim of this study is to present a quite complete description of a thermal analysis, starting from discussing the thermal problem in every aspect, to describing the mathematical methods, which are at basis of the analysis, and finally presenting the computer thermal model.

This thesis study has been conducted during a four months internship at *Tyvak International SRL*, a *Terran Orbital Corporation*, which provides Nanosatellite and CubeSat space vehicle products and services.

During the months of work at *Tyvak's* headquarters, the thermal models built have been adopted to carry out a first preliminary thermal analysis, useful for the design and testing phases, of 6U CubeSats developed by *Tyvak International SRL* for two different European space missions, concerning Earth observation and testing innovative equipment.

To solve the analysis, an highly specific software was adopted, *Thermal Desktop* by *Cullimore & Ring Technology*, which allows to implement Finite Difference or Finite Element solution to thermal model. A description of the model and how build it has been provided, in particular it has been focused on the Finite Difference Method which permits to achieve an accurate model, adopting the proper amount of nodes for the meshing, which is a compromise between accuracy and execution time.

Moreover, the choice concerning the electronic boards modeling was particularly interesting, since they have been modeled as black bodies inside the different components.

The results obtained during the internship job gave an experienced confirmation of the thermal model discussed. In fact, after being also validated by other partner companies, they supported the missions feasibility, since every components temperature analysed falls within the operative range, and the design, since thanks to the analyses realised it has been possible to improve the passive thermal control systems, discerning which different superficial treatments was the most effective for the mission.

Introduction

Interest in small satellites, mainly having a mass of 500 kg or less, has increased in the last decades exponentially.

Numerous commercial entities, government, and academic are attempting small satellite projects around the world. This raised interest is due to the concurrence of various reasons: the miniaturization of various enabling technologies, the changing economics of space, the need for rapid-response platforms for applications or the appeal of launching a personal satellite into orbit.

Since the size of a satellite corresponds directly to expenses associated with materials and parts, labour for development, and launch vehicle fuel, it is obvious to conclude that the major advantages of small satellites are lower cost and shorter development time. However, small satellites have technological and mission-related advantages in their own right. The shorter development cycle implies that newer payload and bus technologies can be inserted. In addition, compared to a solitary, large, conventional satellite, a network of several small satellites is potentially more flexible, as it can be reconfigured depending on mission needs. The inherent redundancy of a small-satellite network also implies lower susceptibility to single-point failure.

Despite these potential benefits of small satellites, the principal challenge is finding opportunities to launch them. The typical scenario is to wait for a piggy-back opportunity, i.e. to fly as an auxiliary payload on a rocket accommodating a larger satellite.

In Table 1 is reported the general classification of small satellites, where "wet mass" refers to the launched satellite with fuel.

Class	Wet Mass [kg]
Mini-satellite	100 - 500
Micro-satellite	10 - 100
Nano-satellite	1 - 10
Pico-satellite	0.1 - 1

Table 1: Classification of small satellites.

This thesis focuses specifically on the so-called CubeSats, which belong at nano-satellite class.

CubeSats Definition

CubeSats are miniature satellites that are commonly used in low Earth orbit for applications such as remote sensing or communications, even if now they are being used for interplanetary missions as well.

The term "CubeSat" refers to a cube-shaped satellite measuring $10\text{ cm} \times 10\text{ cm} \times 10\text{ cm}$ and having a mass no greater than 1 kg.

This standard size is called 1U, with U representing a "unit", but variations on the theme are possible. CubeSats are often configured in 2U, 3U, and 6U sizes as well, flanking respectively two, three or six single CubeSats 1U, for more complicated missions.

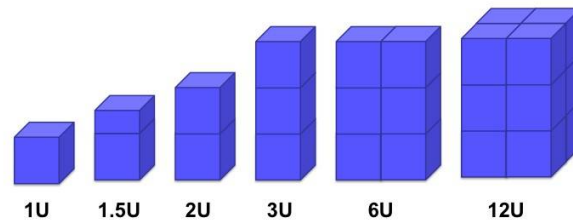


Figure 1: Different CubeSats configuration (Credits: NASA)

The CubeSat design was first proposed in the late 1990s by two professors: Jordi Puig-Suari of California Polytechnic State University and Bob Twiggs of Stanford University. They were trying to help students gain engineering experience in satellites.

CubeSats reduce launch costs in two fundamental ways. They don't weigh much, which means a rocket doesn't need a lot of fuel to transport them.

However, there are some design challenges with CubeSats:

- the electronics are smaller and are therefore more sensitive to radiation;
- because they are small, they cannot carry large payloads with them;
- their low cost also means they are generally designed to last only a few weeks, months or years before ceasing operations (and for those in low Earth orbit, falling back into the atmosphere).
- small size results in small surface areas which imply thermal and power constraints.

For these reasons, thermal analysis and design have become of crucial importance for every phases of this mission project. In particular, since CubeSats limited power, the active thermal control systems are less employed, so it is important properly choose the passive systems and exploit them to the full.

Hence, this thesis job focuses on the thermal design of CubeSats, on the design choices made during the mission development and on the result obtained from the analysis, which are relevant for many mission phases, as explained in the following.

Purposes Definition

The work object of this thesis is to perform a thermal analysis of different CubeSats, which operate in different conditions, in order to provide effective information during the design and the development phases of the space programme.

In particular the thermal analysis is especially required:

- to ensure the feasibility of the mission from the thermal point of view;
- to support the valuation during the design phase;
- to define the criteria and parameters for the environmental verifications.

The work has been split in several chapters.

Ch. 1: Thermal Problem. Herein it has been explained the thermal problem: the design phase, the thermal environment and a brief section about the heat transfer. Moreover it is explained how this factors influence the mission and therefore why the analysis is so important for the thermal control system on CubeSats.

Ch. 2: Thermal Control System. In this chapter is presented the state of the art for the principal strategies related to the thermal control system. Focusing in particular on the difference between the active and the passive systems.

Ch. 3: Thermal Analysis. This chapter shows what the thermal analysis consists in. In particular focusing on what are the instruments and the thermal math models useful for it. Later it has been described which software has been adopted for the analysis: *Thermal Desktop* by *Cullimore & Ring Technology* and some of its main features.

Ch. 4: Case Study. Here is presented the case study. In this chapter the two space mission developed by *Tyvak International SRL*, that have been the object of the internship work, have been defined and the thermal models obtained during the months of work at *Tyvak International* headquarters have been discussed.

Ch. 5: Results. In this chapter are summarised the results obtained during the previous analyses.

Ch. 6: Conclusions. Finally, in the conclusions are discussed the achieved results, with technical comments and observation that have emerged from them.

Chapter 1

Thermal Problem

The principal purpose of the thermal control is to maintain the temperature of the whole system and its subsystems within the required temperature limits during all mission phases. It is possible to specify two types of limits, the operational limits and the survival limits, the first type is about temperature ranges that the subsystem or component shall not exceed during the operations, while the second concerns the range in which the component must be kept even when it is not working, in order to ensure its survival [Wertz et al., 1991].

Components	Typical Temperature Ranges [°C]	
	Operational	Survival
Batteries	0 to 15	-10 to 25
Power Box Baseplates	-10 to 50	-20 to 60
Reaction Wheels	-10 to 40	-20 to 50
Gyros/IMUs	0 to 40	-10 to 50
Star Trackers	0 to 30	-10 to 40
C & DH Box Baseplates	-20 to 60	-40 to 75
Hydrazine Tanks and Lines	15 to 40	5 to 50
Antenna Gimbals	-40 to 80	-50 to 90
Antennas	-100 to 100	-120 to 120
Solar Panels	-150 to 110	-200 to 130

Table 1.1: Examples of Typical Thermal Requirements for Spacecraft Components (Credits: J. R. Wertz, *Space Mission Analysis and Design*)

The thermal control involves also the temperature gradients requirements to be satisfied. Moreover it is remarkable that a failure in the thermal control system may be catastrophic in terms of completing the mission.

In order to avoid these problems an efficient thermal design is needed, to protect the equipment from damaging hot or cold temperatures, either by proper insulation from external

heat sources or heat removal from internal ones.

To achieve these aims, the designer must select some preliminary thermal control configurations and then develop a model of the spacecraft and the environment to predict in the most accurate way the system thermal response.

The model shall then be validated to verify the results. By the way, the thermal control does not end with ground design and verification, but continues during the operational life of the spacecraft, monitoring data until the satellite's end-of-life [Wertz et al., 1991].

1.1 Design Phases

In Table 1.2 are summarized the different steps which are followed during the design process of the thermal control system.

At the beginning constraints and requirements are developed, focusing in particular on those events or equipments that may likely cause problems.

The second step is to define the thermal environment of the spacecraft, so it is important to characterize which are the heat inputs during all the entire mission life. The most important external heat source during the majority of mission time would be the Sun, supplying continuously about $1367 \left[\frac{W}{m^2} \right]$ at the mean distance of the Earth from the Sun.

This input decreases with distance from the Sun $\left(as \frac{1}{r^2} \right)$ and during eclipse period it becomes null.

Step three regards a review of the requirements and constraints. To compare them with the effective heat sources and equipment placement becomes necessary. In this way it is possible to identify and correct situations where the required limits for the equipments are overtaken by the maximum and minimum equilibrium temperatures.

In step four the configuration of the thermal control system is defined, in terms of what equipment is adopted and where components are placed.

Once a preliminary configuration has been carried out it is possible to move on the fifth phase: the determination of the heater and radiator requirements for the spacecraft and its components. In this step it is fundamental consider two worst case condition: the hottest case and the coolest case. The first one concerns a situation characterized by the maximum power dissipated by the system, but mostly by the Sun heat incident on the spacecraft surfaces. The second one instead is related to the eclipse situation combined with the minimum power dissipation.

Furthermore during this phase, it is important to take into account the possible degradation and extraordinary events, so an accurate analysis of thermal control performances shall be carried out.

In step six the information acquired from the previously analysis are used to approximate the mass and power budget of thermal control system.

In the last step all the results are gathered together. This process is iterated until it is obtained a thermal control system which meets all the requirements and constraints [Wertz et al., 1991].

Table 1.2: Design phases (Credits: J. R. Wertz, *Space Mission Analysis and Design*).

Step	Input	Output	Key Issues
1. Identify thermal requirements and constraints	Component thermal requirements	System level thermal requirements. Specialized requirements for specific equipment	Identify payload thermal requirements and major elements that may present thermal challenges.
2. Determine thermal environment	Orbit/attitude history. Spacecraft size and shape. Internal heat sources.	Total energy input to the spacecraft. Profile of energy input vs. Time.	Max and min distance from Sun, Earth and other central body. Chemical or nuclear internal heat sources.
3. Identify thermal challenges or problem areas	Thermal requirements. Heat sources. Equipment placement and attitude history.	List of specific thermal problem areas or problem times or event (hot, cold or stability)	Identify major elements that: <ul style="list-style-type: none"> • Generate large amount of heat. • Need cryo operating temperatures. • Have boiling or freezing problems. • Require a narrow temperature range.
4. Identify applicable thermal control techniques	Thermal requirements and energy profile from above. Additional constraints.	Preliminary list of thermal control mechanisms for mission duration and principal spacecraft components, areas or times.	Identify extraordinary thermal events or actions. Prefer passive over active means. Component placement often key. Pay particular attention to problem areas or severe thermal constraints. Watch for mission critical issues (freezing propellant or hinge, fluid boiling or potential explosions). Take into account: <ul style="list-style-type: none"> • Degradation of thermal surfaces over mission life. • Longest eclipse furthest from a warm central body. • Extraordinary thermal events or circumstances.
5. Determine radiator and heater requirements	List of thermal environments and events. Thermal control approach. Component temperature requirements.	Radiator sizes and temperatures to manage hot case with margin. Heater power for cold case thermal control.	
6. Estimate TCS mass and power	List of TCS methods and components	TCS mass and power	Typically 2% to 10% dry mass. May impact mass and power of other subsystems.
7. Document and iterate			Thermal robustness can be key to system design exibility and reducing operations costs.

1.2 Spacecraft Thermal Environment

Analysing the thermal control problem it is fundamental to consider the environment the spacecraft will encounter during operational life and also before and during the launch phase. It is understandable that ground operations, launch and orbit operation phases may present very different elements in terms of what environment surrounds the satellite. All these details must be taken into considerations during the design and development of the thermal control system, in order to guarantee the survival of the whole system.

Convection with ambient air and radiant heat exchange with surrounding objects are the main environmental influences during ground operations, while during launch phase, radiant heating from the inside surfaces of the booster fairing and free molecular heating due to the friction with the atmosphere after the fairing is jettisoned are the dominant drivers. Instead when the spacecraft reaches the orbit the main sources of environmental heat are direct sunlight, sunlight reflected off of Earth or other planets (albedo) and infrared energy emitted from a planet's atmosphere or surface [Wertz et al., 1991].

Commonly the thermal control system is designed to achieve temperature requirements in the environment encountered on-orbit, while compatibility with ground operations and launch ascent condition is assured by controlling the environment or limiting the spacecraft's exposure to it. The global thermal control of the spacecraft is purchased as a balance between the heat emitted by the system by radiation, the heat dissipated inside the system by its components and the heat absorbed from the surrounding environment. The heat exchanged by convection is absent in space so commonly it is not taken into consideration in this balance. Furthermore, since a generic thermal control system capable of achieving thermal requirements in all environmental conditions would be excessively expensive in terms of mass and costs, it is desirable to custom-tailor a thermal design for a specific spacecraft and its mission. This imply that the thermal analysis must consider the worst hot and worst cold cases combinations of heat developed by spacecraft components in every different operative modes and the changeable environmental heat loads on the spacecraft.

1.2.1 Ground Environment

On the ground, the spacecraft and all its components are exposed to a large assortment of potentially aggressive environments, the most problematic one is Earth's atmosphere. The terrestrial atmosphere has water and oxygen, therefore it is highly corrosive for many materials, including the light alloys used for structural purpose in spacecraft.

Another origin of problems associated with the terrestrial atmosphere is dust, which falls on the horizontal surfaces of the bodies. To avoid dust contamination, spacecraft and their different subsystems are assembled and integrated in so-called clean rooms. A clean room is an artificial place whose internal surfaces are made of materials which do not generate dust, moreover it is equipped with an air-conditioning system with appropriate dust filters. In some particular cases, when it is needed a specific clean environment, a smooth air flow is established through the clean area in order to further reduce the dust deposition, in fact even after filtration some particles of dust remain in the air [Pérez-Grande et al., 2012].

Moreover, spacecraft are subjected to particulate contamination. With particulate are meant those pieces of matter with micrometric sizes, which unavoidably deposit on the spacecraft surfaces during operations like manufacturing, integration, testing and launching. Particulate contamination becomes notably relevant with optical instruments, whose performances are related not only to the rate of transmission and reflectance, but also to the amount of scattering present in the optics.

The amount of particulates that deposit on a given surface is a function of the amount of particulate per unit volume existing in the surrounding air. So it is needed to define the air quality in terms of the maximum allowable number of particles per unit of volume of air (air class) [Pérez-Grande et al., 2012].

1.2.2 Launch Thermal Environment

The launch phase is critical because, over a brief period of time, the spacecraft is subject to extreme stresses due to launcher acceleration or atmosphere friction.

Furthermore the spacecraft has to withstand a considerable quantity of mechanical vibrations, as well as a large amount of acoustic energy, especially at the lift-off when the rocket noise is reflected on the ground, and of aerodynamic noise, due to the launcher passing through the aerodynamic transonic regime [Pérez-Grande et al., 2012].

In addition it shall be included also shock mechanical loads due to the processes of launcher stages separation and spacecraft separation.

Moreover, when the launcher varies its altitude, the atmospheric pressure decrease from the atmospheric pressure at the launch site to the outer space vacuum, which can lead to depressurization loads if there are not present any countermeasure to properly expel the air trapped in the spacecraft and in the fairing.

Another significant form of environmental heating is the molecular heating caused by molecular flow at the upper atmosphere, this effect can appear after fairing jettisoning (115 km of altitude) or at very low perigees at orbital velocities.

Aerodynamic heating also occurs when to modify the orbit of a spacecraft reaching a planet with an atmosphere it is adopted aerobreaking. This manoeuvre reduces the eccentricity of an elliptical orbit with less fuel consumption than directly using the rocket engine, but with an immediate impact on the thermal control subsystem [Pérez-Grande et al., 2012].

Free molecular heating is due to the bombardment of the spacecraft by individual molecules (free molecular flow). Therefore a residual atmosphere is needed for the manifestation of this effect. Commonly, this only appears at the end of the launching phase, after fairing jettisoning. Although fairing jettisoning would be desirable occurring as soon as possible after lift-off (in order to transport less mass), this requirement is in opposition to that of spacecraft heating. In fact free molecular flow is caused if fairing jettisoning takes place where the density of the atmosphere is still significant, so at low altitude.

In a first approximation, the free molecular heating rate can be estimated by the expression $Q_{fmh} = k_{fmh}\rho U^3/2$, where k_{fmh} is a factor between 0.6 and 0.8 (although in most cases the value $k_{fmh} = 1$ is considered for conservatism), ρ the air density, and U the magnitude of the velocity parallel to the heated surface. Although when the precedent expression is

applied, it must be taken into consideration that at particularly high altitudes the atmosphere density is very variable [Pérez-Grande et al., 2012].

However, it must be remarked that the launch phase is a small fraction of the whole operational life of the spacecraft, while there are satellites that orbit with very low perigee altitudes, so the satellite can experience free molecular heating. Generally, this effect has to be considered for perigee altitudes below 200 km approximately.

1.2.3 In-orbit Thermal Environment

Once the spacecraft reached the orbit, besides the thermal requirements of the different subsystems, the thermal control subsystem has to ensure the achievement of those requirements associated with the payloads. This point is crucial in case of scientific missions, where each device has its own operating range [Pérez-Grande et al., 2012].

The space environment depends on whether the particular mission is Earth-orbiting or deep space. For a spacecraft orbiting the Earth (or any other planet or moon), the main sources of environmental heating are solar radiation, both direct and reflected by the planet, and the infrared energy emitted by the planet itself (Figure 1.1).

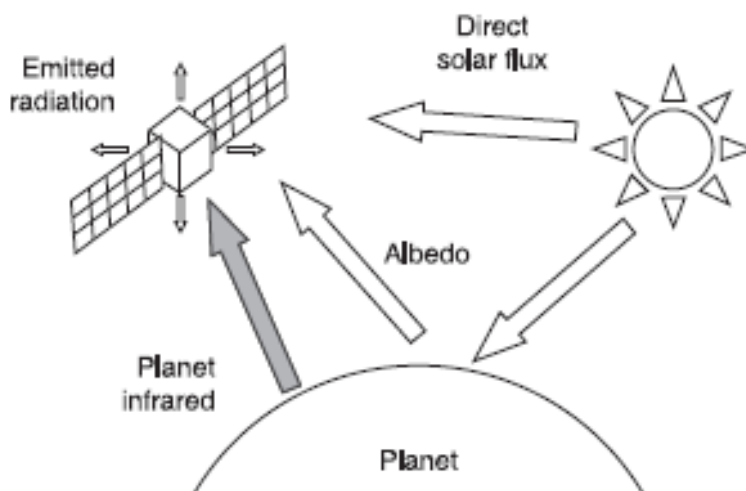


Figure 1.1: Environmental heat fluxes for a planet-orbiting spacecraft (Credits: J. Meseguer, I. Pérez-Grande, A. Sanz-Andrés, *Spacecraft Thermal Control*).

Solar Radiation The Sun is the main source of heating and power for a spacecraft close enough to the Sun (up to a distance of 2 AU, Astronomical Unit). The spectral distribution of solar irradiation is approximated by a blackbody at 5762 K; therefore its effects are primarily perceived as shortwave radiation. The energy emitted by the Sun is quite constant, even if, considering a satellite orbiting the Earth, it is necessary to take into consideration that the Earth's orbit is elliptical, so the intensity of the Sun radiation

reaching the planet changes along every orbit positions. This variation depends on the relative distance between Earth and Sun. When the Earth is in the farthest point from the Sun (situation occurring at summer solstice) the radiation intensity reaches its minimum value, while at winter solstice occurs its maximum value. At Earth's mean distance from Sun, the intensity of the solar radiation is equal to $1367 \left[\frac{W}{m^2} \right]$ and is known as the solar constant G_s . Moreover, the solar radiation intensity is not constant and it varies as a function of the wavelength, as shown in Figure 1.2 and this aspect is fundamental for selecting the spacecraft finishes.

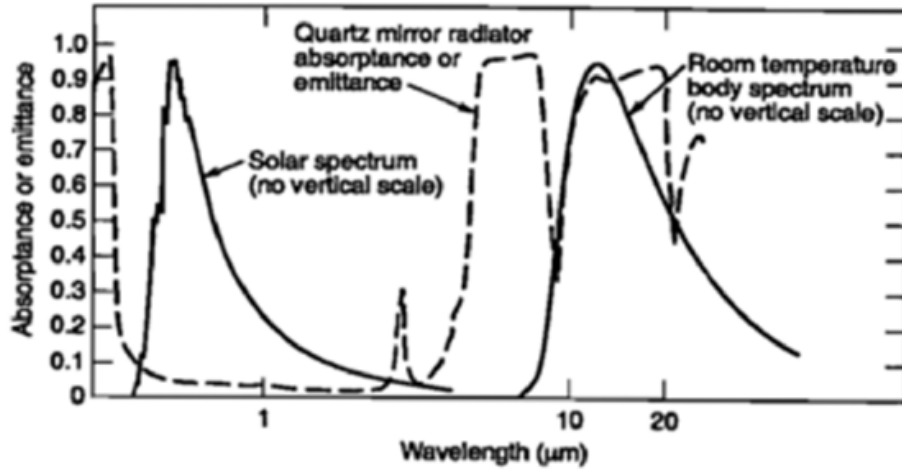


Figure 1.2: Solar and room temperature body spectral distribution (Credits:J. R. Wertz, *Space Mission Analysis and Design*).

The calculation, with a simple analytical expression, of the solar radiation absorbed by a flat surface of area A , whose normal vector forms an angle θ with the solar rays is

$$\dot{Q}_{Sun} = \alpha G_s A \cos \theta_s$$

where α is the solar absorptance of the surface [Pérez-Grande et al., 2012].

Albedo Albedo is the percentage of sunlight reflected by a planet and it is expressed as the fraction of incident solar radiation reflected back to space. It can be calculated for simplified analysis, assuming that the planet behaves as a reflecting sphere as follows:

$$\dot{Q}_{alb} = a G_s A F_{sc/p} \cos \phi$$

for $-\pi/2 < \phi < \pi/2$, where a is the planetary albedo coefficient, G_s the solar constant, ϕ the solar zenith angle and $F_{sc/p}$ the view factor between the surface and the planet. It is a very changeable parameter and this is due to the variability of the reflectivity on the whole Earth's surface. In particular, it is greater over land than over oceans and commonly

increases when solar elevation angles decreases or cloud coverage increases. Furthermore the reflectivity increases with latitude because of the greater presence of snow and ice, the decreasing of solar elevation angle and the grater cloud coverage. From these examination it is clear the strong interaction between the albedo values and the different mission analysed, in terms of orbit shape, height and inclination. Representative values for orbits of different inclinations are shown in the following Table 1.3 [Pérez-Grande et al., 2012].

Inclination [deg]	Angle of Sun out of orbit plane [deg]	Emitted radiation [W/m^2]		Albedo [%]	
		Min	Max	Min	Max
0-30	0	228	275	18	28
	90	228	275	45	55
30-60	0	218	257	23	30
	90	218	257	50	57
60-90	0	218	244	23	30
	90	218	244	50	57

Table 1.3: Albedo values.(Credits:J. R.Wertz, *Space Mission Analysis and Design*).

Earth IR Radiation The further radiation that reaches the Earth and is not reflected off is absorbed. The Earth behaves as any other object reached by radiation, so part of this radiation is reflected and part absorbed and then re-emitted as IR radiation or blackbody radiation. Globally this balance maintains fairly but it varies particularly when the analysis is limited to a small region of the Earth. The intensity of the radiation emitted is function of different parameters, such as the local surface’s temperature and the amount of cloud coverage. The highest values of Earth emitted IR are recorded in tropical and desert regions, while it decrease as the latitude increases. By the way, these variations are less important than the ones in albedo values. The IR energy emitted by the Earth is almost of the same wavelength as that emitted by a spacecraft and is of much longer wavelength than the energy emitted by the Sun. For this reason, Earth IR loads incident on a spacecraft cannot be reflected away from radiator surfaces with thermal control coatings, since the same coatings would prevent the radiation of waste heat away from the spacecraft. So this source of heat represents a problem for spacecraft radiators, especially in low altitude orbits. Eventually, it is important to consider that commonly the spacecraft is warmer than the effective Earth temperature, so the net heat flux is from the spacecraft to Earth and not the contrary. From the blackbody temperature of the planet, T_p , the planetary infrared thermal load on a spacecraft surface of area A can be calculated from:

$$\dot{Q}_{planet} = \varepsilon A F_{sc/p} \sigma T_p^4$$

where ε is the infrared emissivity of the surface, σ is the Stefan-Boltzmann constant and $F_{sc/p}$ is the view factor between the spacecraft surface and the planet [Pérez-Grande et al., 2012].

1.3 Heat Transfer

Commonly heat transfers from an object to another with three methods: conduction, convection and radiation.

In this section are presented conduction and radiation. Convection in space can be neglected since it is the heat transfer due to the bulk movement of molecules within fluids such as gases and liquids, which are absent in vacuum space.

1.3.1 Conduction

Heat conduction is the transfer of thermal energy due to a temperature gradient between regions of matter.

It is related to the transfer of free electrons from regions with higher energy to regions with lower energy and to grid vibration. So, heat conduction demands the presence of matter. The equation that governs heat conduction is Fourier's law. It allows the calculation of heat fluxes for a given temperature field. Temperatures are calculated from the principle of energy conservation [Pérez-Grande et al., 2012].

Fourier's law is an empirical law derived from experimental evidence and observation. Consider a wall of thickness Δx and area A , as shown in Figure 1.3. The temperature is considered uniform over the area A on both wall surfaces.

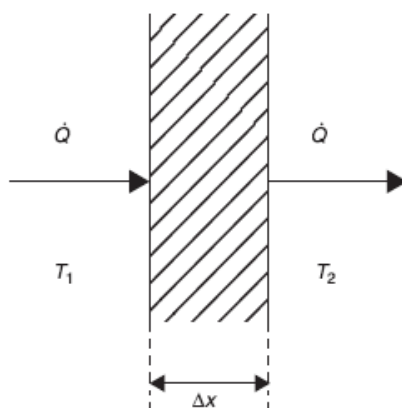


Figure 1.3: One-dimensional heat conduction across a solid wall, whose surfaces are at different temperatures (Credits:J. Meseguer, I. Pérez-Grande, A. Sanz-Andrés, *Spacecraft Thermal Control*).

It is assumed the temperature on the left face of the wall is higher than on the right face [Pérez-Grande et al., 2012].

Fourier's law affirms that the rate of heat flux, \dot{Q} , through a uniform material is directly proportional to the area of heat transfer and to the temperature difference, ΔT , in the

direction of heat flux, and is inversely proportional to the length of the path flow, Δx :

$$\dot{Q} \propto A \frac{\Delta T}{\Delta x} \quad (1.1)$$

The constant of proportionality is the so-called thermal conductivity. Thus,

$$\dot{Q} = kA \frac{\Delta T}{\Delta x} \quad (1.2)$$

Thermal conductivity, k , is a characteristic of the materials, which represents how fast heat flows in the materials. It is measured in $W/(m \cdot K)$ in SI units.

Evaluating equation (1.2)* in the limit $\Delta x \rightarrow 0$, the heat rate is given by

$$\dot{Q} = -kA \frac{dT}{dx} \quad (1.3)$$

The negative sign indicates that the transfer of heat occurs from higher to lower temperatures. Differentiating equation (1.3) with respect to the area gives the heat flux density or the heat flux per unit of time and area, q , whose SI units are W/m^2 :

$$q = -k \frac{dT}{dx} \quad (1.4)$$

Fourier's law has been introduced under simplified conditions (one-dimensional, steady-state conduction in a plane wall). Therefore, the temperature distribution can straightforwardly be deduced to be linear.

However, Fourier's law also applies to multidimensional and transient conduction in complex geometries. In these situations, the temperature field is not evident. So, a more general form of Fourier's law for a three-dimensional case can be written as:

$$q = -k \nabla T = q_x u_x + q_y u_y + q_z u_z = -k \left(\frac{\partial T}{\partial x} u_x + \frac{\partial T}{\partial y} u_y + \frac{\partial T}{\partial z} u_z \right) \quad (1.5)$$

where u_x, u_y, u_z are unit vectors of a Cartesian reference system.

Fourier's law analysed previously allows the heat fluxes for a given temperature field to be calculated.

By the way, one of the major purposes in a conduction analysis is to determine the temperature field in a domain, as a result of the boundaries conditions imposition. Heat fluxes would then be calculated from this temperature field.

To do this, the energy balance equation is applied to a differential element. In the following, this is done for the Cartesian coordinates system, but it could be eventually done also for the Cylindrical and Spherical system.

*The equations in this section are taken from the *Spacecraft Thermal Control* [4] by J. Meseguer, I. Pérez-Grande, A. Sanz-Andrés, 2012

The energy balance equation for an elemental volume, such as the one depicted in Figure 1.4 is

$$\frac{\partial}{\partial x} \left(k \frac{\partial T}{\partial x} \right) + \frac{\partial}{\partial y} \left(k \frac{\partial T}{\partial y} \right) + \frac{\partial}{\partial z} \left(k \frac{\partial T}{\partial z} \right) + \dot{q}_v = \rho c_p \frac{\partial T}{\partial t} \quad (1.6)$$

where \dot{q}_v is the rate at which energy is generated per unit volume of the medium and $\rho c_p \partial T / \partial t = \dot{E}_v$ is the time rate of change of the internal energy of the medium per unit volume, where ρ is the medium density and c_p the specific heat.

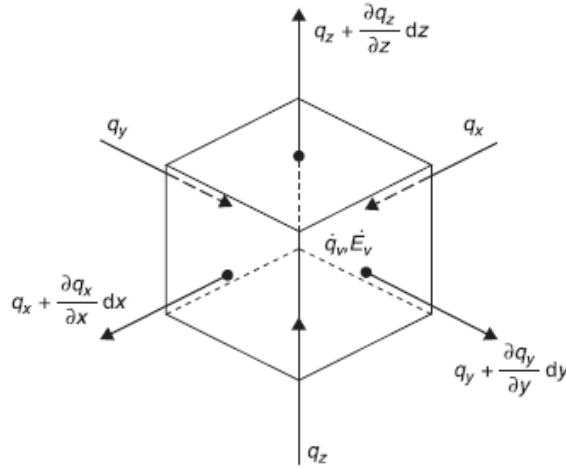


Figure 1.4: Differential element for energy equation in Cartesian coordinates (Credits: J. Meseguer, I. Pérez-Grande, A. Sanz-Andrés, *Spacecraft Thermal Control*).

If the thermal conductivity is constant, equation (1.6) can be simplified and written in the form

$$\frac{\partial^2 T}{\partial x^2} + \frac{\partial^2 T}{\partial y^2} + \frac{\partial^2 T}{\partial z^2} + \frac{\dot{q}}{k} = \frac{1}{\alpha} \frac{\partial T}{\partial t} \quad (1.7)$$

where $\alpha = k / (\rho c_p)$ is the thermal diffusivity [Pérez-Grande et al., 2012].

To determine the temperature field in a medium it is needed to solve the heat diffusion equation (equations (1.6)). To do this, knowing physical boundaries conditions is necessary. These can be given as temperatures, heat fluxes, or a combination of both. If the problem is time dependent, conditions existing in the medium at some initial time also have to be provided. Mathematically, the heat diffusion equation is a differential equation that needs integration constants in order to have a unique solution. These are provided by boundaries conditions in fact. The equations shown in the previous sections cannot be solved by analytical methods in every situations, but only in certain particular cases. These solutions are available in the literature for different geometries. When it is not possible to obtain an exact mathematical solution, the best alternative is often to use numerical techniques.

1.3.2 Radiation

Thermal radiation is electromagnetic radiation emitted from all a non-zero temperature matter in the wavelength range from $0.1\mu m$ to $100\mu m$. It is included part of the ultraviolet (UV) and all of the visible and infrared (IR).

It is called thermal radiation because it is caused by and affects the thermal state of matter. For its propagation is not required a material medium. The mechanism of radiation emission is associated to energy released as a result of oscillations or transitions of the electrons that constitute matter [Pérez-Grande et al., 2012].

Since thermal radiation is electromagnetic radiation, the properties of the propagation of electromagnetic waves can be applied.

The study of thermal radiation is quite complex for two of its features: one is its spectral nature, while the second one is related to its directionality.

A surface may have specific directions with preferential emission; so the distribution of the emitted radiation is directional. A surface is called termed diffuse when the radiative properties do not depend on the direction.

As previously said, all surfaces emit thermal radiation. This emission will strike other surfaces and will be partially reflected, partially absorbed, and partially transmitted. Figure 1.5 shows the different thermal radiation interactions on a body's surface.

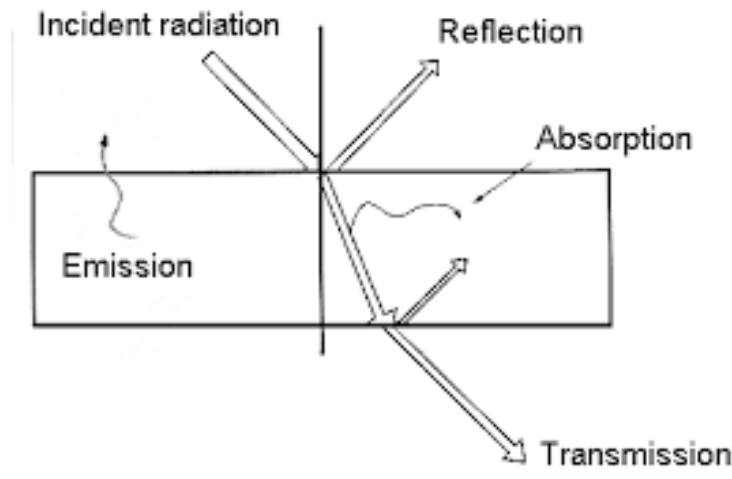


Figure 1.5: Thermal radiation interactions on a surface (Credits:Kari Hyll, *Infrared Emission*).

As can be noted, the surface emits Φ_e , receives the incident radiation Φ_i , out of which Φ_a is absorbed, Φ_r is reflected and Φ_t is transmitted [Pérez-Grande et al., 2012].

The intensity of emitted radiation, $I_{\lambda,e}$, is defined as the rate at which radiant energy, $\delta\dot{Q}$, is emitted at the wavelength λ in the (θ, ϕ) direction, per unit area of the emitting surface normal to this direction, per unit solid angle $d\omega$ about this direction and per unit

wavelength interval $d\lambda$ about λ . Thus, the spectral intensity is

$$I_{\lambda,e}(\lambda, \theta, \phi, T) = \frac{\delta\dot{Q}}{dA \cos\theta d\omega d\lambda} \quad (1.8)$$

To obtain the thermal interactions in all directions and wavelengths the intensity of radiation is successively integrated [Pérez-Grande et al., 2012].

Blackbody radiation A blackbody is an ideal surface that absorbs all incident radiation, at all wavelengths and all directions. So this makes of it the perfect absorber. As a consequence, the blackbody has three properties: (i) for a given wavelength and temperature it is the surface that emits the most, (ii) blackbody radiation is diffuse, it does not depend on the direction, and (iii) total blackbody radiation in a vacuum depends only on temperature [Pérez-Grande et al., 2012].

Since the blackbody is the perfect absorber and emitter, it will be used as a reference to compare the radiative properties of real surfaces.

The spectral emissive power of a blackbody at a temperature T was obtained by Planck as

$$E_{b,\lambda}(\lambda, T) = \frac{2\pi hc^2}{\lambda^5 \left(\exp\left(\frac{hc}{\lambda kT}\right) - 1 \right)} \quad (1.9)$$

where h is the Planck constant ($h = 6.6261 \cdot 10^{-34} J \cdot s$), $c = 2.9979 \cdot 10^8 m/s$ the speed of light in vacuum, λ the wavelength and in this case k is the Boltzmann constant ($k = 1.3807 \cdot 10^{-23} J/K$).

This expression is the Planck distribution, and the graphical representation of constant temperature lines, Figure 1.6, gives valuable information about its trend.

Equation (1.9) represents the spectral emissive power of a blackbody. It can be integrated to obtain the total emissive power of a blackbody, giving

$$E_b(T) = \int_0^\infty E_{b,\lambda}(\lambda, T) d\lambda = \sigma T^4 \quad (1.10)$$

where $\sigma = 5.67 \cdot 10^{-8} W/(m^2 \cdot K^4)$. This result, $E_b = \sigma T^4$, is known as the Stefan-Boltzmann law, and can be used to obtain the energy emitted by a blackbody in all directions and all wavelengths [Pérez-Grande et al., 2012].

Real surfaces The blackbody has been described as an ideal surface to be taken as a reference to define the behaviour of real surfaces.

Since the blackbody is the perfect emitter, any real surface emits less than the blackbody at the same temperature, same wavelength and same direction. For this reason, the spectral directional emissivity is characterized as the ratio between the real emission, $I_{\lambda,e}$, and the blackbody emission, $I_{b,\lambda}$, that is

$$\varepsilon(\lambda, \theta, \phi, T) = \frac{I_{\lambda,e}(\lambda, \theta, \phi, T)}{I_{b,\lambda}(\lambda, T)} \quad (1.11)$$

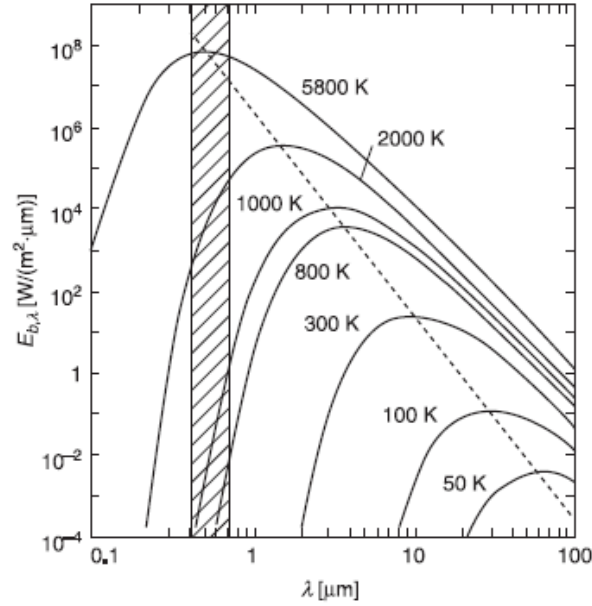


Figure 1.6: Spectral emissive power of a blackbody vs. wavelength (Credits: J. Meseguer, I. Pérez-Grande, A. Sanz-Andrés, *Spacecraft Thermal Control*).

The spectral hemispherical emissivity is defined as the ratio

$$\varepsilon(\lambda, T) = \frac{E_\lambda(\lambda, T)}{E_{b,\lambda}(\lambda, T)} \quad (1.12)$$

If the surface is diffuse, the spectral hemispherical emissivity is equal to the spectral directional emissivity. When the properties of the surface are function of the direction, the spectral hemispherical emissivity can be properly obtained integrating equation (1.11), according to equation (1.12). The second group of radiant properties is about irradiation. As already said, a surface will be irradiated by the radiation coming from other surfaces. This incident radiation will be partially reflected, partially absorbed and partially transmitted (as pictured in Figure 1.5).

For this reason, three radiative properties are presented [Pérez-Grande et al., 2012]. Firstly, the spectral directional absorptance is defined as the fraction of the incident radiation, $I_{\lambda,i}$, that is absorbed for a given direction and wavelength, $I_{\lambda,i,abs}$:

$$\alpha(\lambda, \theta, \phi, T) = \frac{I_{\lambda,i,abs}(\lambda, \theta, \phi, T)}{I_{\lambda,i}(\lambda, \theta, \phi)} \quad (1.13)$$

Secondly, it is described the spectral directional reflectance as the fraction of the incident radiation, $I_{\lambda,i}$, that is reflected for a given direction and wavelength, $I_{\lambda,i,reflec}$. For this case,

$$\rho(\lambda, \theta, \phi, T) = \frac{I_{\lambda,i,reflec}(\lambda, \theta, \phi, T)}{I_{\lambda,i}(\lambda, \theta, \phi)} \quad (1.14)$$

Lastly, the spectral directional transmittance is characterized as the fraction of the incident radiation, $I_{\lambda,i}$, that is transmitted for a given direction and wavelength, $I_{\lambda,i,trans}$:

$$\tau(\lambda, \theta, \phi, T) = \frac{I_{\lambda,i,trans}(\lambda, \theta, \phi, T)}{I_{\lambda,i}(\lambda, \theta, \phi)} \quad (1.15)$$

As for the emissivity, these coefficients will be integrated to get their values for all directions and all wavelengths. So, the spectral hemispherical absorptance is determined as

$$\alpha(\lambda, T) = \frac{\int_0^{2\pi} \int_0^{\pi/2} \alpha(\lambda, \theta, \phi, T) I_{\lambda,i}(\lambda, \theta, \phi) \cos \theta \sin \theta d\theta d\phi}{G_\lambda(\lambda)} \quad (1.16)$$

where

$$G_\lambda(\lambda) = \int_0^{2\pi} \int_0^{\pi/2} I_{\lambda,i}(\lambda, \theta, \phi) \cos \theta \sin \theta d\theta d\phi \quad (1.17)$$

is the spectral irradiance incident on the surface.

The spectral hemispherical reflectance is defined as

$$\rho(\lambda, T) = \frac{\int_0^{2\pi} \int_0^{\pi/2} \rho(\lambda, \theta, \phi, T) I_{\lambda,i}(\lambda, \theta, \phi) \cos \theta \sin \theta d\theta d\phi}{G_\lambda(\lambda)} \quad (1.18)$$

and the spectral hemispherical transmittance is designated as

$$\tau(\lambda, T) = \frac{\int_0^{2\pi} \int_0^{\pi/2} \tau(\lambda, \theta, \phi, T) I_{\lambda,i}(\lambda, \theta, \phi) \cos \theta \sin \theta d\theta d\phi}{G_\lambda(\lambda)} \quad (1.19)$$

For each of the levels of definition of these coefficients given previously (spectral directional and spectral hemispherical), the following relationship is verified

$$\alpha + \rho + \tau = 1 \quad (1.20)$$

For opaque surfaces transmittance is zero. So $\alpha + \rho = 1$.

Kirchhoff's law states that $\alpha(\lambda, \theta, \phi, T) = \varepsilon(\lambda, \theta, \phi, T)$; that is, for each direction and wavelength emissivity equals absorptance. When the surface is diffuse, from Kirchhoff's law it can be determined that $\alpha(\lambda, T) = \varepsilon(\lambda, T)$.

A surface is designated as grey when its properties are independent of the wavelength, in particular $\alpha(\lambda, T) = \alpha(T)$ and $\varepsilon(\lambda, T) = \varepsilon(T)$ [Pérez-Grande et al., 2012].

Chapter 2

Thermal Control System

It can be individuated two main categories regarding the thermal control strategies: the active control and the passive control system.

2.1 Active Control

In the active thermal control system are included all those control actions that ensure the temperatures within acceptable ranges through the use of some active means. This characteristic makes the active control usually more complex and expensive than the passive control. This strategy takes into consideration the use of heaters, thermo-electrical cooler, heat pipes, heat exchangers. Moreover modifying the spacecraft attitude may be useful to achieve the temperatures requirements.

2.1.1 Heaters

The fulfilment of some temperature range demands, in many cases, the generation of heat within the spacecraft. In these instances, heaters are commonly required to achieve specific requirements such as the protection of components from low temperatures, to provide accurate temperature control for specific devices or to warm up equipment to its operating temperature [Sanz-Andrés et al., 2012].

When a local uniform heat source or a heating area is required, electrical heaters can provide it properly due to their versatility, even if other types of heaters (such as chemical or nuclear) are also used in spacecraft. of course, using electrical heaters demands the availability of a power source.

Electrical heaters are substantially resistance elements, based on Ohm's and Joule's laws and they are part of a closed loop system made by a temperature sensing element and a temperature controller. They can be used in on-off control modes, ground controllable modes or in continuously-on modes.

Two types of heaters typically used on spacecraft are film heaters (or patch heaters) and cartridge heaters. By the way the most commonly used type is the film heater, because

of its flexibility it can be mounted on both flat and curved surfaces [Sanz-Andrés et al., 2012].

These heaters are made of electrical resistance filaments sandwiched between two layers of electrically insulating material, such as Kapton, attached to the leads. They come in different sizes to fit any applications or they can be custom-shaped too, to adapt them to very specific applications.

Commonly, the heating power density on the film heaters is limited to less than 0.8 W/cm^2 . The temperature control usually includes a relay which is actuated from the ground (the local control) to enable or disable the power supplied to the heater, a fuse to protect the spacecraft from a short circuit, and typically a thermostat or a solid-state controller to turn the heater on and off at fixed temperatures.

The most common type of control is a thermostatic control using a bimetallic mechanical thermostat which opens or closes the heater circuit at a predetermined temperature [Sanz-Andrés et al., 2012].

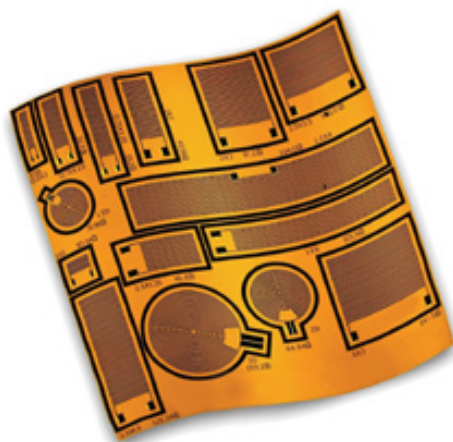


Figure 2.1: Kapton film heater kit (Credits: Omega Engineering).

2.1.2 Heat Pipes

The heat pipe is a device that allows an effective transport of thermal energy. It is made of a closed structure whose internal surface is lined with a thin layer of porous material, commonly called wick. The container may have a cylindrical shape, or any other shape that can be cleverly manufactured [Sanz-Andrés et al., 2012].

The pores of the wick are filled with a working liquid fitting to the application and the vapour of the liquid fills the remaining internal volume. Since the liquid and its vapour are in equilibrium, the pressure inside the container is equal to the vapour pressure corresponding to the saturation conditions.

This simple configuration permits a very efficient heat transfer from one end of the heat pipe to the other, following a quite simple heat transfer mechanism (Figure 2.2).

As heat is applied to one end (the evaporator), the working liquid evaporates from the wick, while the removal of heat from some other portion of the surface (the condenser) makes the vapour to condensate on the wick. The pressure gradient that results from the accumulation of vapour at one end of the heat pipe and its depletion at the other end makes the vapour to flow through the core region of the container. But, as the liquid evaporates, it retreats into the wick pores, then the meniscus there is depressed and the liquid pressure drops below the pressure of the adjacent vapour. At the other end condensation takes place, so that the working liquid fills in the wick, maintaining a flat surface without any depression of the pressure in the liquid [Sanz-Andrés et al., 2012].

Because of capillary forces, the final result is a pressure gradient in the liquid that makes the working liquid to flow through the wick towards the evaporator end, in the opposite direction to that of the flowing vapour in the core region, completing the flow circuit.

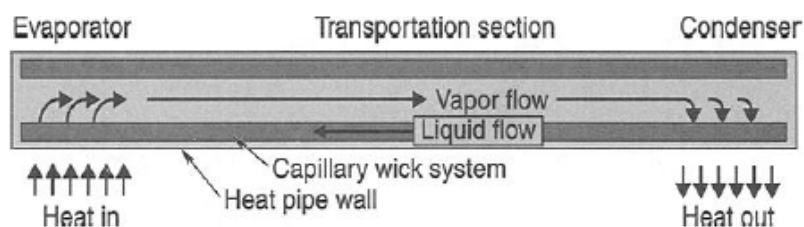


Figure 2.2: Heat-pipe schematic (Credits: D. G. Gilmore, *Spacecraft Thermal Control Handbook*).

There is a great number of heat pipes in terms of different geometry, function and methods used to transport the liquid from the condenser to the evaporator.

The previously described heat pipe, consisting of a working fluid, a wick structure and an envelope, is the most basic type and it is known as a constant conductance heat pipe.

There are other more complex heat pipe designs, namely: variable conductance heat pipes, thermal diodes, pulsating (oscillating) heat pipes, micro-heat pipes, rotating heat pipes, sorption heat pipes (SHPs), magnetic fluid heat pipes, loop heat pipes, and capillary pumped loops (LHPs and CPLs, respectively).

A large amount of fluids ranging from cryogenes to liquid metals have been used as heat pipe working fluids. The choice of a working fluid for a heat pipe application is due to several physical properties of the fluid, one of the most important is the temperatures of the desired operating range or the chemical compatibility of the fluid with the container and the wick [Sanz-Andrés et al., 2012].

The physical properties to be taken into consideration selecting a heat pipe working fluid are: the vapour pressure, latent heat of vaporization and surface tension; moreover the density, dynamic viscosity and thermal conductivity of both the liquid and vapour phases. Furthermore there are requirements which should be considered in the selection of a heat pipe working fluid: a large latent heat of vaporization, high thermal conductivity, low viscosity, high surface tension, high wetting ability, and a boiling point suited to the

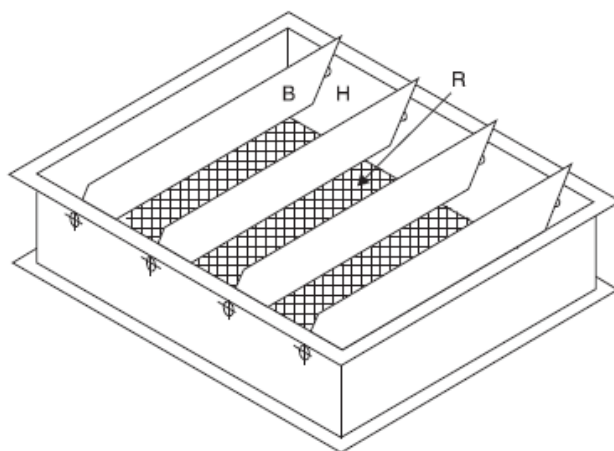
required operating temperature.

Typically one of the most used working fluid in space application is ammonia.

Heat pipes are often classified according to the type of wick structure used. In situations in which a porous wick structure is adopted, the wick may be formed from a variety of small elements, including screens, particles, and fibres. The wick structure may also involve grooves cut into the heat pipe wall. Moreover the condensed liquid can also be transported to the evaporator through one or more arteries, which are placed within the pipe where vapour returns to the condenser [Sanz-Andrés et al., 2012].

2.1.3 Louvers

Louvers are mechanical equipment that consist of a frame which includes an array of highly reflective blades, commonly identical, which can pivot about their longitudinal axis thanks to some actuators, similarly to a Venetian blind, as shown in Figure 2.3. The ends of the shafts are joined to the frame by bearings. This assembly is situated over the spacecraft radiator [Sanz-Andrés et al., 2012].



Key: R, radiator; H, housing; B, blades.

Figure 2.3: Common louver design (Credits: J. Meseguer, I. Pérez-Grande, A. Sanz-Andrés, *Spacecraft Thermal Control*).

When the temperature of the radiator grows the actuators rotate the blades towards their open position, normally perpendicularly to the radiator surface, in this way the radiator has the maximum view of outer space.

When the temperature of the radiator diminishes, the actuators move the blades towards the closed position, completely blocking the radiator's view of outer space. The highly reflective and so low-emissive, finish of the blades cuts off the energy radiated to space.

The two most relevant louver system components are the blades and actuators [Sanz-

Andrés et al., 2012].

Even if for each application louver blades have different sizes and thickness, the principles of design are common to most commercial louvers. Louver blades are typically thin, rectangular, aluminium pieces made from one or two individual sheets. If two are adopted, they are bonded along their longitudinal edges and to a hollow central aluminium shaft. The thickness of the blades is in the order of 0.3 to 0.5 mm, its system has to withstand high vibration loads, a reason which constrains the design.

Louver actuators are the devices that orient the blades, allowing or impeding the view between the radiator and the outer space. They modify the angle of their blades depending on the temperature of the radiator, according to previously calibrated values. The actuators can act passively or actively, but in the latter case electrical power is needed.

Although, most of the louvers flown are actuated by means of bimetallic helicoidal springs formed by two bonded strips of materials with different coefficients of thermal expansion. These bimetallic actuators are located within a housing that provides thermal insulation from the environment, and good thermal coupling with the radiator surface, so that they can react to changes of temperature of the radiator without any power consumption [Sanz-Andrés et al., 2012].

2.1.4 Pumped Fluid Loops

For relatively small heat loads ($< 10kW$) and small transport distances, heat pipes have demonstrated effective options for simple, reliable, and quiet thermal energy transport and temperature control. The main limitation for these devices is the capillary pressure limit, which continues to be extended through the development of higher performance wick materials and geometries. Obviously, the capillary driving force is the advantage of the traditional heat pipe because no pump power and no moving parts are needed for the operation [Sanz-Andrés et al., 2012].

For high heat loads mechanically pumped loops are arguably unchallenged. Despite a pump power penalty and the presence of moving parts, mechanically pumped loops have proven their value in many spacecraft thermal control systems. In both cases heat transfer is fulfilled through the motion of a working fluid, by using capillary forces for a heat pipe or by using a pumping device, centrifugal or positive displacement pump, commonly driven by an electric motor, for a pumped fluid loop.

The action of heat transfer involves the absorption of heat at a relatively steady rate from the component whose temperature has to be controlled and to transfer it to a heat sink which can be placed distant from the source.

Focusing on pumped fluid loops, they can be classified as single-phase heat transfer loops (liquid or gaseous), or two-phase fluid loops. A simplified pumped fluid loop is shown in Figure 2.4. The cooling is accomplished by the use of a coolant as the thermal energy transport agent. The coolant absorbs the dissipated thermal energy from a component and transfers it to a heat sink [Sanz-Andrés et al., 2012].

The final heat rejection process depends on whether the coolant is expendable or non-expendable. With the expendable one, the working fluid is rejected from the space vehicle

once it has ended its mission. In the case of non-expendable, the working fluid is recirculated within the system once its thermal energy has been emitted to space via a radiator.

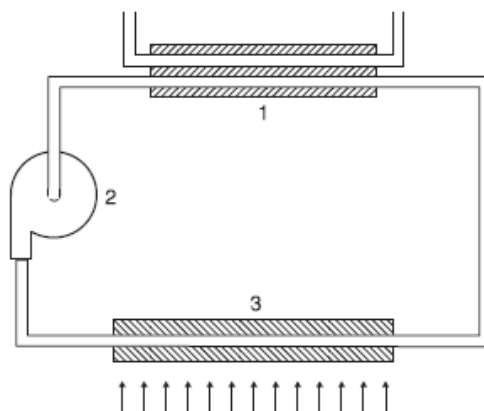


Figure 2.4: Schematic representation of a fluid loop showing the main components: 1 – heat exchanger; 2 – pump; 3 – heat source (Credits:J. Meseguer, I. Pérez-Grande, A. Sanz-Andrés, *Spacecraft Thermal Control*).

As showed in Figure 2.4 , the different components within a pumped fluid system (pump, heat exchanger, radiator, etc.) are linked mainly by conduits. As previously said, the simplest model of a pumped fluid loop consists of a circuit formed by fluid-carrying tubes which connect a heat sink to a heat source. A circulation pump moves the fluid through the loop to transport the heat from source to sink by forced convection.

Coolant fluids can be gaseous or liquid (molten metals can be used at higher temperatures). The selection of the coolant is due to thermal and power requirements for fulfilling a given cooling duty.

In the case of non-expendable coolants, the basic parameters are: density, specific heat, thermal conductivity and viscosity, as well as temperature limits, that should be compatible with the desired application.

This properties, however, do not give the complete picture of the problem. In fact several fluids fitting the appropriate thermal and frictional requirements can be aggressive to metallic or elastomeric materials. Many coolants are toxic and their use has to be ruled out when manned operations are expected [Sanz-Andrés et al., 2012].

2.2 Passive Control

The passive control is that group of thermal control methods ensuring the components to maintain their temperature in the desired range by control of conductive and radiative heat paths through the selection of the geometrical configuration of surfaces and optical properties of materials.

For this type of control it can be used materials and devices like sun shields, insulation blankets, phase change materials, thermal coatings and certain surface finishes to ensure the achievement of the temperature requirements for the whole spacecraft life cycle.

Now it will be introduced some of the most common means of a passive thermal control.

2.2.1 Radiators

To reject waste heat to space are largely used radiators, which are devices that take the waste thermal energy from a heat source and reject it by infrared radiation (IR) to the external space, through radiating surfaces.

Even if spacecraft radiators may have different forms (from simple flat plate radiators mounted on the side of the spacecraft, to radiating panels deployed after the spacecraft reaches the orbit), whatever the configuration is, all radiators reject heat by infrared radiation from their surfaces. So the radiating power depends on the emissivity and temperature of the radiating surfaces [Sanz-Andrés et al., 2012].

Of course, the radiator rejects the spacecraft waste heat, but also any radiant heat loads from the environment or from other spacecraft surfaces that are absorbed by the radiator. For this reason radiators are given surface finishes with high infrared emissivity ($\varepsilon > 0.8$) to maximize heat rejection and low solar absorptance ($\alpha < 0.2$) to limit heat loads from the surroundings.

The net heat leaving a radiator surface per unit time (assuming a view factor of 100% to space) is given by the simple expression

$$\dot{Q}_{rad} = A\varepsilon\sigma(T^4 - T_0^4) \cong A\varepsilon\sigma T^4 \quad (2.1)$$

where A is radiator surface area, ε the infrared emissivity, σ the Stefan-Boltzmann constant ($\sigma = 5.67 \cdot 10^{-8} W/(m^2 K^4)$), T the absolute radiator temperature, and T_0 the deep space temperature ($T_0 \lll T$).

Depending on how the heat is moved from the source to the radiating surfaces, radiators can be categorized as passive radiators and active radiators. The main advantage of passive radiators is their simplicity.

Passive cryogenic radiators can have one stage or more than one stage (multi-stage). The efficiency of these coolers is function of the thermal decoupling from the spacecraft temperature and the degree of insulation from external radiant fluxes. Moreover in case of multi-stage coolers, the efficiency is based on the thermal insulation between the successive stages by means of multilayer insulations and low-conductance supports, that respectively reduce the heat exchange by radiation and by conduction.

Furthermore, low-conductance supports can also provide high mechanical coupling which

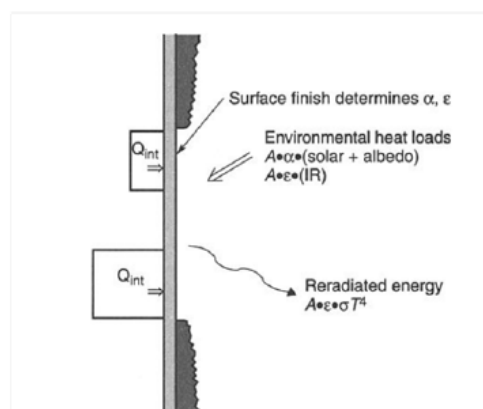


Figure 2.5: Schematic representation of a radiator ((Credits: D. G. Gilmore, *Spacecraft Thermal Control Handbook*).

are fundamental during the launch/ascent phase.

In multi-stage radiant coolers each stage arrests the heat leakage from the insulation below and radiates it to space, permitting the successive stages to reach colder temperatures. The lowest temperature stage is defined as the radiator cold stage and it dissipates the waste thermal energy. Typically, the radiator stages are shielded from environmental heat sources, such as solar radiation, terrestrial infrared and albedo radiation with devices such as Sun shield [Sanz-Andrés et al., 2012].

Many parameters shall be taken into account for the design of passive cryogenic radiators. Starting from those relative to the type of orbit, the orbit altitude, the spacecraft orientation relative to the Earth and Sun and the location of the radiator and ending to other parameters such as the thermo-optical properties of the radiator stages and of the multilayer insulations, the thermal properties of the insulating materials, the heat load applied to the radiator cold plate, and the geometry.

Passive radiator coolers also have potential problems about the contamination of cold surfaces by outgassing from either the spacecraft or the radiator itself.

2.2.2 Insulation Systems

A typical design strategy for the thermal control subsystem of many spacecraft is based on the insulation of the spacecraft from the environment. To reject to space the heat from dissipating devices, radiators are appropriately sized and mounted on the outer surface of the spacecraft. On the other hand, compensation heaters are sized for the worst cold case scenarios to avoid malfunctioning of the equipment.

This insulation design strategy reduces the impact of the highly variable environmental conditions and of the cold external radiative sink on the spacecraft components. In this way the power requested for the compensating heaters is minimized.

Insulation systems are requested too when different temperature levels must be reached

within the spacecraft at the same time. For example, in case of cryogenic devices, that operate at extremely low temperatures, whereas their corresponding proximity electronics run at room temperature [Sanz-Andrés et al., 2012].

In the following it is described one of the main insulation systems, multilayer insulations. A multilayer insulation (MLI), or thermal blanket, is composed of several layers of closely spaced, highly reflecting shields, that are located perpendicular to the heat flow direction. Each internal layer is a very thin layer (from $7\mu m$) of material, usually Kapton or Mylar, coated with vapour deposited aluminium (VDA) on each sides. This mirror-like aluminium finish makes the sheets highly reflective and of low emissivity, which takes to a high resistance to radiative heat transfer between layers.

The outer cover instead is commonly thicker (from $125\mu m$) than the internal ones to intensify its mechanical strength. The external layer is typically covered in aluminium only on its internal side, that because aluminium degrades when it is exposed to ultraviolet radiation. The external layer can be made just in bare Kapton or can be painted with a black carbon paint, in this way it is possible to avoid undesired reflections.

When better mechanical properties are requested, for instance to protect it from micrometeoroids, more resistant materials, such as beta-cloth, can be adopted for this outer layer. By the way, since the outer cover can be hit by solar radiation, its behaviour when exposed to UV radiation has to be carefully checked.

In order to avoid direct contact between shields, and so heat conduction between sheets, low-conductivity, non-metallic spacers are used. To minimize the contact they are typically in the form of a mesh. Common materials for this netting spacer are Dacron and Nomex. The pile of layers is stacked together by stitches sewn with special non-metallic thread that has to be free of volatile components. Small Kapton pieces can be used to prevent the blanket from tearing due to thread tension. To close the lateral gaps and avoid the degradation of the internal layers, the outer cover is folded back on the internal layer. This continuity between the external and the internal layers reduces the performance of the blanket in a small area close to the edges and seams. The blankets are mounted to the structure with hook-and-pile (Velcro) fasteners and pins [Sanz-Andrés et al., 2012].

Figure 2.6 shows a common cross-section of a multilayer insulation.

Moreover it should be provided a proper venting of the multilayer insulation in order to avoid undue pressure loads on the shields during the ascent flight. Otherwise, the blanket would billow out like a balloon and the dynamic pressure could detach it from the spacecraft. So, to permit the proper venting of the blanket, the sheets are perforated.

The size and separation of the perforations depend on the type of mission. Typical values can be $0.8mm$ holes every $6mm$.

An other aspect to prevent is electrostatic charge and the consequent discharges, so all the layers of the blanket have to be grounded to the spacecraft structure. This can be achieved with a bolt connected to the spacecraft structure and that passes through the blanket with washers touching each layers or using a metallic strip, folded in such a way that it touches all the layers of the blanket [Sanz-Andrés et al., 2012].

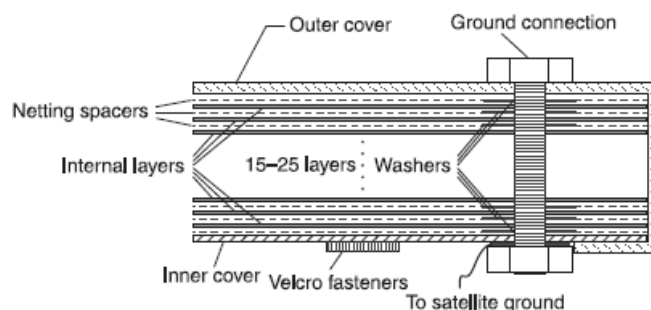


Figure 2.6: Sketch of a typical multilayer insulation (Credits: J. Meseguer, I. Pérez-Grande, A. Sanz-Andrés, *Spacecraft Thermal Control*).

2.2.3 Coatings and Surface Finishes

A coating consists of one layer, or more, of any material upon a substrate. Optical coatings have been adopted to control the temperature of spacecraft since the first successful orbital flight. Since then, coating substances have been developed to the point where reasonably stable coatings are available, which give any desired value of ε or α [Sanz-Andrés et al., 2012].

However, when optical properties are considered, thermal control surfaces are categorized into four basic types:

- solar reflector;
- solar absorber;
- total or flat reflector;
- total or flat absorber.

A plot of solar absorptance, α , versus hemispherical total emissivity, ε , is represented in Figure 2.7.

Solar absorbers absorb solar energy while emitting only a limited percentage of infrared energy. So, this class of thermal coatings is identified by the highest values of the α/ε ratio. Such materials are not very common, but high values of α/ε can be reached using certain polished metal surfaces, like polished beryllium, metal films, or thin films of metal oxides. Flat absorbers absorb completely the spectral range and have relatively high solar absorptances and high emissivities. Paints that are flat absorbers can be made from black pigments such as the oxides or mixed oxides (e.g. Cr_3O_4 , $Fe_2O_3 \cdot NiO$, Fe_3O_4 , or $Mn_2O_3 \cdot NiO$). The pigments are ground and dispersed in silicone elastomers or alkaline metal silicate vehicles and applied to the base structure. These kind of paints are the so-called black paints because their behaviour is very similar to the blackbody. Typical black paints' α values are in the order of 0.95, while typical ε values are about 0.88.

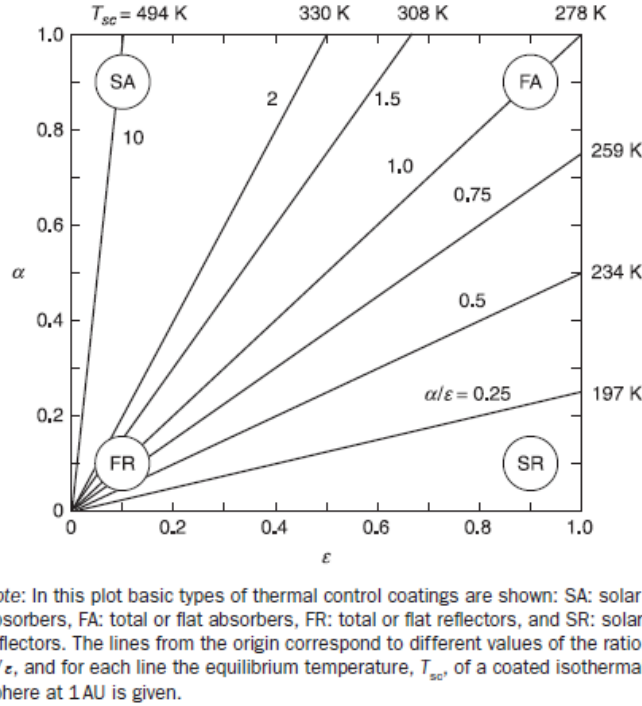


Figure 2.7: Solar absorptance vs. hemispherical total emissivity (Credits: J. Meseguer, I. Pérez-Grande, A. Sanz-Andrés, *Spacecraft Thermal Control*).

An alternate approach is to cover the substrate material with metals, such as copper or nickel and then oxidizing the coating. Because the base materials are often alloys of aluminium or magnesium, experimental work is also being carried out with anodizing. Through anodizing it can be obtained protection from corrosion as well as a coating with the desired optical properties. Moreover the interior of many spacecraft is painted black because it helps to distribute heat and provides uniform temperatures [Sanz-Andrés et al., 2012].

The third class is flat reflectors, which differ from flat absorbers because they reflect energy in the entire spectral range (in both the solar and infrared spectral range). Materials which have these optical properties are not typical so flat reflectors are usually obtained with highly polished metals or with paints pigmented with metal flakes. These surface treatments are adopted to thermally decouple a part of the spacecraft.

Solar reflectors are identified by limited values of the ratio α/ϵ , they reflect most incident solar energy while absorbing and emitting infrared energy. Usually materials that belong to this kind of coatings are white paints, with α values in the order of 0.20 and ϵ values in the order of 0.90, and optical solar reflectors (OSR) or second surface mirrors (SSM), like fused silica mirrors or silvered Teflon tapes, adopted where lower α values are needed (≈ 0.10) while ϵ values are in the order of 0.90. These surfaces are indicated for coatings where low temperatures are requested and are typically used for radiator surfaces that can be exposed to the Sun.

The basic requirement for a spacecraft coating is its long-term space stability for mid-long periods, months or years. Even if, in many instances this object has not yet been achieved. In fact, in space thermal control finishes experiences different very destructive effects, such as thermal loads, mechanical loads (vibration, acceleration, shock), general spacecraft contamination (contaminant films that deposit on most spacecraft surfaces), radiation, atomic oxygen (only in low Earth orbits) and micrometeorites and space debris. Furthermore, the loads due to ground operations at atmospheric conditions (assembly operations, testing, integration, transport and storage) shall be considered for the design of thermal coatings. For these reasons, coating materials can degrade irreversibly their physical characteristics of design (optical, thermal, electrical and mechanical). The general result of these effects is an increase in solar absorptance with little or no effect on infrared emissivity. This higher solar absorptance becomes relevant in the thermal control design of a spacecraft because spacecraft radiators have to be sized considering the substantial increase in absorbed solar energy that occurs due to degradation during the whole mission phases [Sanz-Andrés et al., 2012].

2.2.4 Phase Change Capacitors

An effective method of storing thermal energy is using a latent heat storage system through the use of a phase change material (PCM), that is identified by a high-energy storage density and an isothermal process too. Adopting a phase change material is an option to be taken into account when the thermal loads, such as the incident orbital heat fluxes, or the internal equipment heat dissipation, variate widely.

The process at the base of energy storage is the heat absorption or release that occurs when a given storage material changes phase. The phase transition can be solid to liquid, liquid to gas, or vice versa and also a solid–solid phase change. These phenomena absorb or release heat at a nearly constant temperature. In space applications, solid–liquid transitions have been most widely used because of the smaller volume variation than liquid–gas or solid–gas phase changes [Sanz-Andrés et al., 2012].

The phase change material as a thermal control system consists of a container filled with a substance capable of undergoing a phase change. When the temperature of the spacecraft surface raises, either due to external radiation or to inner heat dissipation, the phase change material will absorb the excess heat through phase change and will re-establish it through the inverse transition when the temperature decreases again.

Because of the electrical analogy, this thermal control system is also defined phase change capacitor.

Phase change capacitor systems can be adopted to control the temperature of equipment in several ways. In case of equipment that operates cyclically, the object is to avoid temperature extremes of short duration.

The phase change material cell is usually sandwiched between the equipment and the heat sink. When the equipment is active and so generating heat, the energy is stored in the phase change capacitor through a phase change. During the off part of the cycle, the heat of fusion energy is removed through the heat sink.

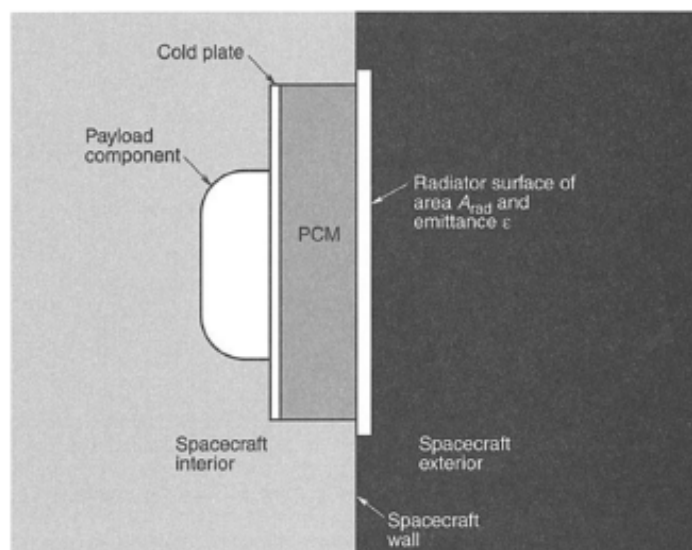


Figure 2.8: Phase change material radiator (Credits: D. G. Gilmore, *Spacecraft Thermal Control Handbook*).

If the purpose of the thermal control system is to protect a component from excessive heat dissipation, as is the case of equipment that transfers its dissipated heat to a sink, the phase change material is connected to the equipment but without interfering with the normal heat path [Sanz-Andrés et al., 2012].

When it is considered an insulated equipment instead, the phase change capacitor can be used as the sole heat sink, ensured that the heat transferred does not exceed that required to completely melt the material.

The characteristics that a phase change material should have are:

- Appropriate phase-transition temperature. The melting point (in a solid–liquid system) should be within the permitted temperature range of the component being thermally controlled, commonly between $260K$ and $320K$.
- High latent heat of fusion, or enthalpy of fusion. It is important to reduce the mass and/or volume of the system.
- Good thermal conductivity. This characteristic helps to minimize thermal gradients and facilitates the charging and discharging of energy storage. Since most phase change materials have low thermal conductivity, fillers have to be considered to increase the conductivity of the system.
- High density. This takes to a storage container of smaller dimensions.
- Small volume change on phase transformation and low vapour pressure, which reduce container design complexity.

- Reversible phase-to-phase transition. The chemical compositions of both phases should be equal.
- Long-term reliability and chemical stability during repeated cycles.
- Non-toxic, non-corrosive, compatible with container materials, not a fire hazard.
- No propensity to supercool. This is a problematic aspect of a phase change material, especially for salt hydrates. If it is more than a few degrees, it will interfere with the proper functioning of the system.
- Available and cost effective.

Two devices based on paraffin waxes, dodecane (melting point 10.5°C) and hexadecane (melting point 18.5°C), have been adopted in thermal storage capsules to control the battery temperatures in the NASA Mars rovers (ref. *Swanson and Birur*, 2003).

The main elements of a phase change capacitor are: phase change material, container and fillers or thermal conductivity enhancers. Containers vary for their outer shape (circular or rectangular) and for the flexible element that is adopted to compensate the volume variation of the material during the phase transition. Between flexible elements of the container, the most diffused are metallic bellows, metallic membrane and rubber diaphragm.

Instead if a rigid container is adopted, it is mandatory to provide a void or gas volume to allow the melting expansion of the phase change material [Sanz-Andrés et al., 2012].

Focusing on the thermal conductivity enhancers, they are of two types: fillers and fins.

Fillers are used to raise the thermal conductivity of non-metallic phase change materials which have low conductivities. The fillers that are most widely adopted are: aluminium (as powder, foam, wool, or honeycomb), copper (as foam), alumina (Al_2O_3 , as powder or foam), graphite (as foam or fibre).

Regarding fins, aluminium fins are used instead of honeycomb because of the problems related to the contact conductance between the honeycomb and the cold plate. Aluminium can be welded to the cold plate whereas honeycomb is normally attached to it with epoxy, that can result in an undesirably high contact resistance. However, the compatibility of phase change capacitors with materials adopted as fillers is limited by the corrosion induced by the phase change material itself or by impurities in it. This negative aspect can be reduced by appropriate inhibitors such as oxide films and additives.

Chapter 3

Thermal Analysis

Thermal analysis subsists in a sequence of design selection and supporting analysis. The system requirements associated to reduce weight, cost and test complexity are commonly achieved by keeping the thermal design as simple as possible and by avoiding the use of active components. A passive control will be lighter, less expensive to build, more reliable and easier to test than a systems that relies on an active one.

To prepare for the design phase, it is indispensable to collect a large amount of data and information about the system. This data typically consists of drawing and sketches of the hardware, a geometry model, predicted heat dissipation and components weight, determination of orbit and attitude, information about thermal environments from pre-launch phase to on orbit phase, spacecraft's operating modes, thermal and optical property data for materials. These information are crucial to define a preliminary thermal design approach and to build the thermal model.

Lastly before to begin the thermal analysis is important to identify the thermal design approach. Using the data gathered as stated previously, the analyst can start to construct the thermal models: a geometric model for the calculation of radiation view factors and a thermal model for predicting temperatures.

The first model is a mathematical representation of the physical surfaces of the satellite or component and is used to compute the radiation couplings between all surfaces in the model, as well as heating rates to each surface from external flux sources such as solar, Earth IR and albedo radiation.

The thermal model instead, is usually a lumped parameter model of the thermal capacitance of each node and thermal conduction terms between nodes. This kind of model is directly analogous to an electrical resistance-capacitance network. These models are obtained using a mix of computer aided design (CAD) technologies and calculations.

Once the model is completed and debugged it is run to predict hardware temperatures under worst hot and worst cold condition cases. It could be necessary to perform also a certain number of parametric runs to close in on optimum sizing of radiators, heaters and so on. The analysis must also be rerun to reflect changes in design or updates to new analysis inputs. The final step of the analysis is the documentation, that have to include the complete description of the geometry, the thermal model and the tests.

3.1 Fundamentals of Thermal Modeling

To comprise the fundamentals of thermal math modeling, a brief introduction to the basic techniques of thermal modeling is introduced in this chapter*. Usually, the questions to face during the development of a proper thermal math model are related to the necessity to achieve the greatest accuracy with the lowest cost. Cost factors are categorized into two classes: (i) the cost of developing the model and (ii) the cost of using the model.

In addition, the issue of achieving accuracy is related to costs constraints and differs widely from one thermal math model to another.

3.1.1 Network Solutions

Two systems are defined analogous when they are described by similar equations and boundary conditions, therefore the equations representing the behaviour of one system can be changed into the equations for the other by simply modifying symbols of the variables. Thermal and electrical systems are two such analogous systems, as illustrated in Table 3.1.

Quantity	Thermal System	Electrical System
Potential	T	E
Flow	\dot{Q}	I
Resistance	R	R
Conductance	G	$1/R$
Capacitance	C	C
Ohm's Law	$\dot{Q} = GT$	$I = E/R$

Table 3.1: Electrical-Thermal analogy (Credits:TRW under NASA contract 9-10435, *Thermal Network Modeling Handbook*).

The analogy between thermal and electrical systems let the thermal engineer to make widely use of known basic electrical laws such as Ohm's Law and Kirchhoff's Laws, that are utilized for balancing networks. Numerical techniques employed to solve the partial differential equations describing such electrical systems have been opportunely adapted to computer solutions of thermal networks, enabling in this way the thermal engineer to easily compute temperature distributions and gradients of difficult physical thermal networks. Thermal-analysis computer programs have been developed requiring to the user to define a system thermal network analogous to an electrical circuit. When data representing the network components are input, preprogrammed routines calculate the transient or steady-state solutions [McMurchy et al., 1972].

In the following sections are described the development of a thermal network and the numerical techniques for solving it.

*The notions in this chapter are taken from the *Thermal Network Modeling Handbook* [7] prepared by TRW under NASA contract 9-10435.

3.1.2 Nodes

To develop a thermal network and apply numerical techniques to the relative solution, it is important to subdivide the thermal system into finite subvolumes defined nodes. The thermal characteristic of each node are thought to be concentrated at the central nodal point of each subvolume. Each node describes two thermal-network elements, a temperature (potential) and a capacitance (thermal mass), as shown in Figure 3.1.

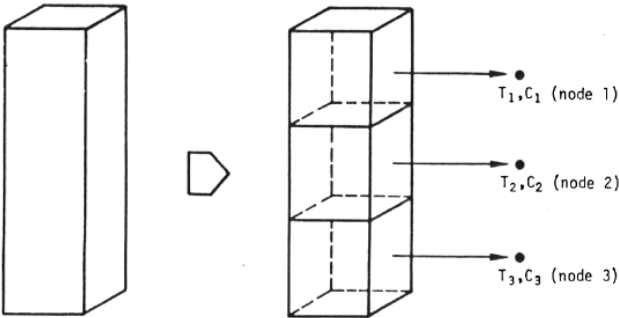


Figure 3.1: Nodalization (Credits:TRW under NASA contract 9-10435, *Thermal Network Modeling Handbook*).

The temperature, T , designated to a node defines the average mass temperature of the subvolume. The capacitance, C , designated to a node is calculated from the thermophysical properties of the subvolume material at the temperature of the node, and it is thought to be concentrated at the nodal center of the subvolume [McMurchy et al., 1972]. Because a node represents a concentration of parameters at a single point in space, the temperature distribution through the subvolume implicated by the nodal temperature is linear, as represented in Figure 3.2c and not a step function as shown in Figure 3.2b.

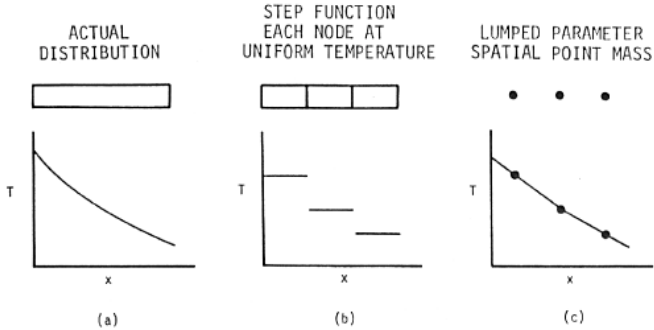


Figure 3.2: Temperature distribution (Credits:TRW under NASA contract 9-10435, *Thermal Network Modeling Handbook*).

In a homogeneous material, the temperature at a point different than the nodal point can be approximated by interpolation between adjacent nodal points where the temperatures are well known. The error considered by dividing a system into finite-sized nodes, rather than volume dx^3 , where dx goes to zero, is dependent on numerous aspects: material thermal properties, boundary conditions, node size, node-center placement and time increment of transient calculations [McMurchy et al., 1972].

However to this moment, it has been considered only nodes representing subvolumes with a finite thermal mass (capacitance), but in many cases, two other kind of nodes are needed to describe a thermal network. Thermal analyzers such as the program SINDA (Systems Improved Numerical Differencing Analyzer) commonly call and define the three types of nodes as resumed in Table 3.2:

Node Name	Node Type
diffusion	finite thermal mass
arithmetic	zero thermal mass
boundary	infinite thermal mass

Table 3.2: Node type classification (Credits:TRW under NASA contract 9-10435, *Thermal Network Modeling Handbook*).

The diffusion node (finite capacitance) is adopted to describe normal material, the temperature of which can change as a result of heat flow into or out of the nodes. It is defined by a gain or loss of potential energy, which depends on the capacitance value, the net heat flow entering the node and the time during which the heat is flowing. Mathematically, a diffusion node is described by the expression:

$$\Sigma \dot{Q} - \frac{C \Delta T}{t} = 0 \quad (3.1)$$

The arithmetic node (zero capacitance) is a physically unreal element, but using it in numerical solutions can be helpful to interpret results in applications such as surface temperatures, bondline temperatures and node-coupling temperatures. It also can be used to represent thermal-system elements that have small capacitance values respect to the most of the other nodes in the system, resulting in computer run-time reduction with less changes in overall accuracy. These elements could be small components like bolts, films or fillets; gaseous contents of small ducts or tubes; and low-mass insulations [McMurchy et al., 1972].

By the way the number of arithmetic nodes should be a very limited part of the total number of nodes in the network. Mathematically, an arithmetic node is described by the expression:

$$\Sigma \dot{Q} = 0 \quad (3.2)$$

The boundary node (infinite capacitance) is adopted to describe a boundary or sink whose temperature is set and will not vary independently how much heat flows into or out of

it. Typical uses are representation of deep-space sink temperature, recovery temperature and planet-surface temperature. Moreover, boundary nodes may represent thermal-system components that have a particular large capacitance compared to the other nodes, like the bulk propellant in a large tank. Mathematically, a boundary node is described as:

$$T = \text{constant} \quad (3.3)$$

The disposition of the diffusion-node centers and the choice of node shapes refer on many factors: (i) the points where temperatures are desired, (ii) the expected temperature distribution, (iii) physical reasonableness and (iv) the ease of computation.

For the size of the node shall be also taken into account: (i) the accuracy desired, (ii) the structural design, (iii) the computer storage capabilities and (iv) computer time required. In general, the shape of a diffusion node is thought to be a simple geometric figure having areas and volumes that can be simply calculated. In some instances, nodal divisions are decided first, with the node-center locations obtained as a consequence. In these cases, nodal edges will commonly be placed along structural edges, while structural members will be separated in a symmetric and equal fashion [McMurchy et al., 1972].

This suggests that rectangularly shaped nodes are usually desirable, that is true simply because with this kind of nodes, the areas and volumes needed for the input calculations are easy to compute. Using such simple nodal shapes is in keeping with current engineering practice. On the contrary, it has been suggested that nodalization should be performed in a manner that the paths of heat flow assumed a triangular pattern, as illustrated in Figure 3.3a. The only disadvantage to this approach is that the engineer must calculate the volumes of the consequent irregular polygonal nodes, as represented in Figure 3.3b. It is notable how much easier the rectangular nodalization approach is, as shown in Figure 3.3c.

In the same way, to simplify the calculations for circular structures, they are nodalized in pie-wedge shapes, annular shapes, or a combination of the two.

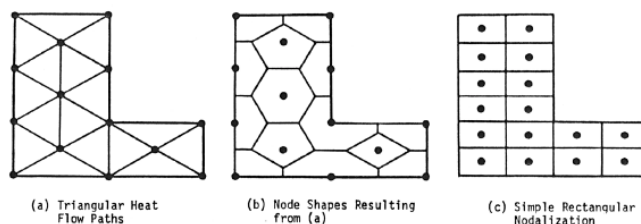


Figure 3.3: Polygonal nodalization vs. rectangular nodalization (Credits:TRW under NASA contract 9-10435, *Thermal Network Modeling Handbook*).

Boundary nodes are adopted to define points, lines or surfaces of constant temperature in, respectively, one-, two-, or three-dimensional models. The physical placement of a boundary node is caused exclusively by the conduction paths connected to it. A single

boundary node can be used to model all boundaries at the same temperature.

Instead arithmetic nodes have an amount of uses that are consequences of the fact that these nodes serve as an engineering model of the proverbial "wafer of thickness dx , where dx approaches zero". A typical application is the modeling of exterior surfaces of re-entry vehicles, that experience severe, fastly changing boundary conditions [McMurphy et al., 1972]. In the physical system, the surface temperature stays very close to radiation equilibrium with the surface heating rate, this indicates that the system can be properly simulated by the employ of a surface arithmetic node, as shown in Figure 3.4.

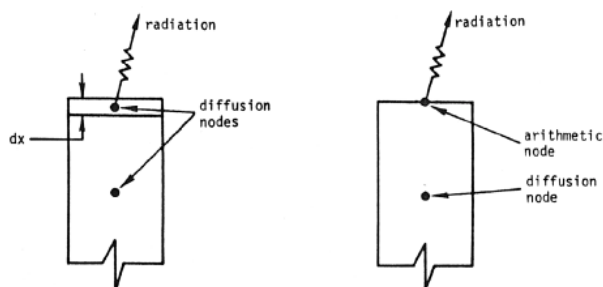


Figure 3.4: Use of arithmetic nodes to model surfaces (Credits:TRW under NASA contract 9-10435, *Thermal Network Modeling Handbook*).

In the making of a thermal network, calculations with respect to nodes are generally limited to computing the capacitance of diffusion nodes. The following formula is implemented:

$$C = \rho \cdot V \cdot C_p \quad (3.4)$$

where C is thermal capacitance [$J/^\circ C$], ρ is density [kg/m^3], V is volume [m^3], and C_p is specific heat [$J/kg^\circ C$].

The specific heat and the density of materials may vary with temperature. The necessity to use temperature dependent properties for analysis refers to the degree to which the properties modify and the temperature range over which the capacitance of the material will be calculated. Most thermal analysis computer codes can accommodate temperature-varying thermal properties [McMurphy et al., 1972].

3.1.3 Conductors

Conductors are the thermal math modeling network elements that perform the heat-flow paths through which energy is moved from one node to another. Figure 3.5 shows the element node temperatures (T), capacitances (C) and conductors (G) that comprehend a thermal network.

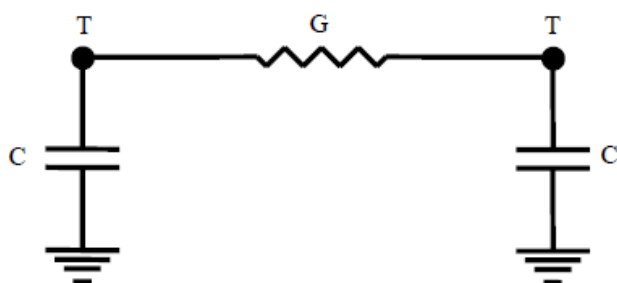


Figure 3.5: Thermal network Elements (Credits:TRW under NASA contract 9-10435, *Thermal Network Modeling Handbook*).

The three processes by which heat transfers from a hotter region to a colder region are conduction, convection, and radiation. Conduction is the process by which heat flows within a medium or between different mediums in direct physical contact. The energy is transmitted by molecular communication. Figure 3.6 shows the conduction conductor.

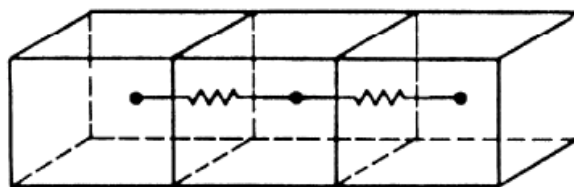


Figure 3.6: Conduction conductor (Credits:TRW under NASA contract 9-10435, *Thermal Network Modeling Handbook*).

On the other hand, convection is the process of energy transport by combined action of heat conduction, energy storage and mixing motion. Heat will transfer by conduction from a surface to next particles of fluid; then the fluid particles will move to a colder region, where they will mingle with, and give a part of their energy to, other fluid particles. The energy is actually stored in the fluid particles and is transferred as a result of their mass motion. Figure 3.7 shows the convection conductor.



Figure 3.7: Convection conductor (Credits:TRW under NASA contract 9-10435, *Thermal Network Modeling Handbook*).

Conduction or convection conductors are defined linear conductors, because for those paths, the heat-flow rate is a function of the temperature difference between nodal temperatures to the first power.

$$\dot{Q} = G_{ij}(T_i - T_j) \quad (3.5)$$

Instead, radiation is the process by which heat flows between two bodies separated in space. Energy is transferred through electromagnetic wave phenomena. Radiation conductors (shown in Figure 3.8) are said non-linear, because the heat flowing between two surfaces by radiation is a function of the difference of the fourth powers of the surface temperatures:

$$\dot{Q} = G_{ij}(T_i^4 - T_j^4) \quad (3.6)$$

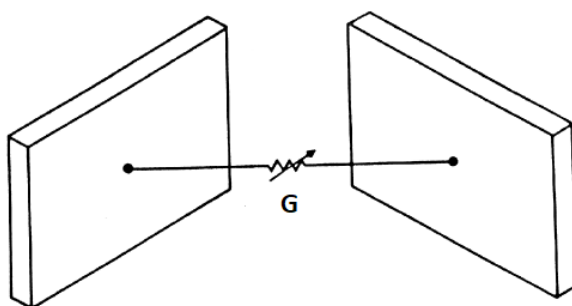


Figure 3.8: Radiation conductor (Credits:TRW under NASA contract 9-10435, *Thermal Network Modeling Handbook*).

Conduction

Conduction conductors for rectangular nodes are computed from this equation:

$$G = \frac{k \cdot A}{L} \quad (3.7)$$

where G is thermal conductance [$W/^\circ C$], k is thermal conductivity [$W/m^\circ C$], A is cross-sectional area through which heat flows [m^2], and L is the distance between adjoining nodes [m]. The thermal conductivity of materials may differ with temperature or other influencing parameters within the system; the cross-sectional area through which the heat flows and distance between node centers are defined by the size and shape of the adjacent nodes [McMurchy et al., 1972]. As with the capacitance calculations, necessity to use temperature dependent properties refers on the degree to which the conductivity changes over the temperature range expected during the analysis.

Rectangular Nodes The length, L , of the heat-flow path, utilized for conduction-conductance computations for rectangular nodes, is the distance between node centers

and the area, A , to be adopted is the area of a node cross-section perpendicular to the line connecting the node centers. The convention is shown in Figure 3.9.

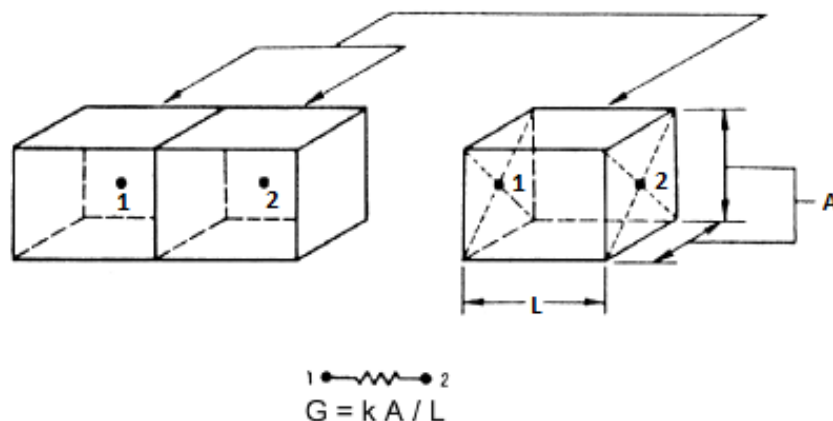


Figure 3.9: Simple conductor representing a heat-flow path through material (Credits:TRW under NASA contract 9-10435, *Thermal Network Modeling Handbook*).

Circular Section For conductors between nodes that are circular sections, the conventions illustrated in Figure 3.10 should be adopted.

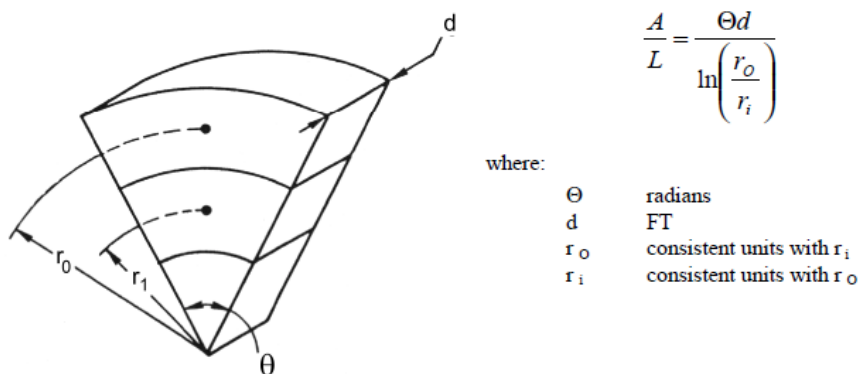


Figure 3.10: Area and length equivalents for circular section nodes. (Credits:TRW under NASA contract 9-10435, *Thermal Network Modeling Handbook*).

Parallel and Series Conductors Two or more parallel conduction paths between nodes can be summed to make one conductor value by the following equation:

$$G_T = G_1 + G_2 + \dots + G_n. \quad (3.8)$$

Two or more series conduction paths between nodes can be combined to make one conductor value by the following equations:

$$\frac{1}{G_T} = \frac{1}{G_1} + \frac{1}{G_2} + \dots + \frac{1}{G_n} \quad G_T = \frac{1}{\frac{1}{G_1} + \frac{1}{G_2} + \dots + \frac{1}{G_n}} \quad (3.9)$$

To model the conductors between two differently shaped nodes or two nodes of different materials, as depicted in Figure 3.11, the equation (3.9) may be useful.

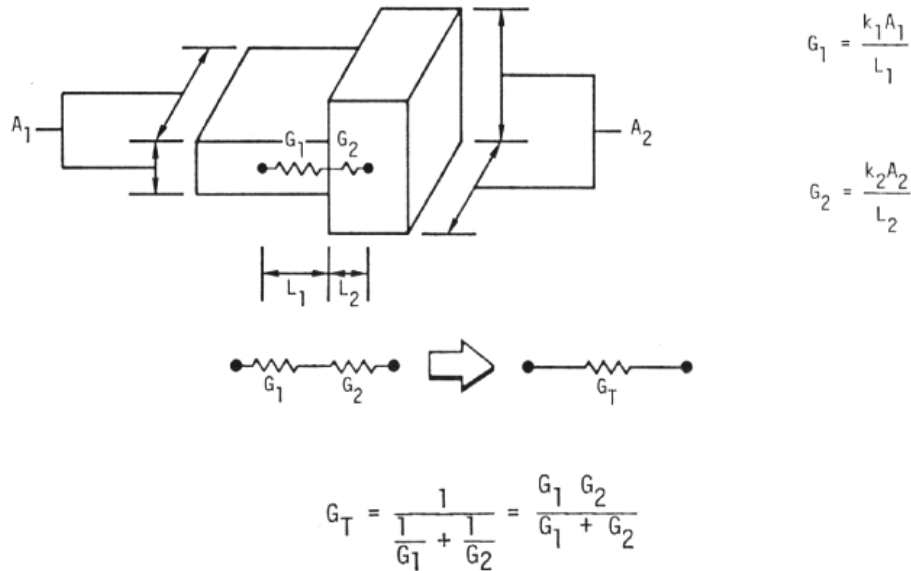


Figure 3.11: Series conductor paths (Credits:TRW under NASA contract 9-10435, *Thermal Network Modeling Handbook*).

Convection

Convection conductor calculations are not analysed in this section because they will not be used in the case study thermal analysis presented in the following chapter. However, if the reader would study deeper the matter a complete description is presented in the referenced text *Thermal Network Modeling Handbook* [7] by TRW under NASA contract 9-10435.

Radiation

The great majority of thermal-analysis computer programs linearise the radiation term prior to executing the heat balance at each time-step. This operation simply corresponds to factoring $(T_i^4 - T_j^4)$ into $(T_i^3 + T_i T_j^2 + T_i^2 T_j + T_j^3)$ and $(T_i - T_j)$. Then the term $(T_i^3 + T_i T_j^2 + T_i^2 T_j + T_j^3)$ is estimated by the computer each time-step for the current values of T_i and T_j [McMurphy et al., 1972].

The quantity got by this operation is then multiplied by the input value of the radiation conductor, reducing the radiation equation to a linear form. The thermal engineer have

only to be interested in the input value of the radiation conductor, which takes the following form:

$$G_{ij} = \sigma \varepsilon_i F_{i-j} A_i \quad \text{for radiation to a blackbody, and}$$

$$G_{ij} = \sigma \zeta_{i-j} A_i \quad \text{for radiation between gray surfaces,}$$

where G_{ij} is the input value for radiation conductors [W/K^4]; σ is the Stefan-Boltzmann constant, $5.669 \cdot 10^{-8}$ [$W/m^2 K^4$]; ε_i is the emittance of surface i (dimensionless); F_{i-j} is the geometric (configuration) factor from surface i to surface j (dimensionless); A_i is the area of surface i [m^2] and ζ_{i-j} is the gray-body radiation factor (dimensionless).

The emittance, ε , is the ratio of the total emissive power of a real surface at temperature T to the total emissive power of a black surface at the same temperature. The emittance of a surface is a function of the material, the surface condition and the temperature of the body. This can be modified by polishing, roughing, painting, etc. The values of ε for many common materials and surface conditions have been measured at various temperatures and are available in literature, in many reference engineering manuals.

The engineer have to understand the value of emittance to be utilized and whether the variation of ε with temperature is significant over the temperature range expected for the surface [McMurchy et al., 1972].

The geometric (configuration) factor from surface i to surface j , F_{i-j} , is the fraction of total radiated energy from surface i that is directly incident on surface j , assuming surface i is emitting energy diffusely. F_{j-i} would be the fraction of total radiant energy from surface j that is intercepted by surface i . The configuration factors for finite regions of diffuse areas are related by the equation

$$A_i F_{i-j} = A_j F_{j-i} \quad (3.10)$$

So the configuration factor is only function of the geometry of the system. Many computer software have been programmed to compute the shape factors between surfaces with complex geometries and they will be presented later.

The gray-body shape factor ζ_{i-j} is the product of the geometric shape factor F_{i-j} and a factor that permits the departure of the surface from blackbody conditions. For radiation enclosures, the ζ_{i-j} factors are generally estimated with a computer program. The inputs for the program are the $A_i F_{i-j}$ values from every surface of the enclosure to every other surface, the emittance and area for each surface.

Simplified equations for ζ_{i-j} can be written for two-component gray enclosures.

Infinite parallel flat plates: $F_{1-2} = F_{2-1} = 1$.

$$\zeta_{1-2} = \frac{1}{\left(\frac{1}{\varepsilon_1} + \frac{1}{\varepsilon_2} - 1\right)} \quad (3.11)$$

Concentric cylinders of infinite height or concentric spheres: $F_{1-2} = 1$, $F_{2-1} \neq 0$

$$\zeta_{1-2} = \frac{1}{\frac{1}{\varepsilon_1} + \frac{A_1}{A_2} \left(\frac{1}{\varepsilon_2} - 1\right)} \quad (3.12)$$

For nonenclosed surfaces, an effective emittance, ε_{eff} , between the surfaces can be adopted to compute the gray-body form factor with the following equation:

$$\zeta_{i-j} = \varepsilon_{eff_i} F_{i-j} \quad (3.13)$$

The effective emittance is a function of the emittances of the two surfaces and the configuration factors between them. The error introduced with using the ε_{eff} is the result of neglecting secondary reflections from surfaces other than the two for which the effective emittance was determined [McMurphy et al., 1972]. ε_{eff} can be determined with the following equation:

$$\varepsilon_{eff} = \frac{\varepsilon_1 \varepsilon_2}{1 - F_{1-2} F_{2-1} (1 - \varepsilon_1)(1 - \varepsilon_2)} \quad (3.14)$$

The examples of configuration-factor algebra in Figure 3.12 may be useful to fully understand the precedent discussion.

$$\begin{aligned} A_1 F_{1-3} &= A_3 F_{3-1} \\ A_1 F_{1-34} &= A_1 F_{1-3} + A_1 F_{1-4} \\ A_{12} F_{12-34} &= A_1 F_{1-34} + A_2 F_{2-34} \\ A_{12} F_{12-34} &= A_1 F_{1-3} + A_1 F_{1-4} + A_2 F_{2-3} + A_2 F_{2-4} \\ A_1 F_{1-4} &= A_3 F_{3-2} \text{ (symmetrically positioned)} \end{aligned}$$

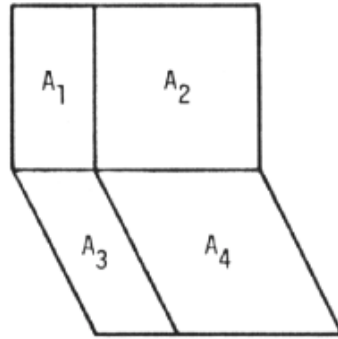


Figure 3.12: Configuration-factor algebra (Credits:TRW under NASA contract 9-10435, *Thermal Network Modeling Handbook*).

3.1.4 TMM Computer Codes

Solving the general heat-transfer equation is the purpose of all thermal-analysis codes in the spacecraft industry. The general partial differential equation of heat conduction with source term for a stationary heterogeneous, anisotropic solid is

$$\rho C_p \frac{\partial T}{\partial t} = \nabla \cdot (K \cdot \nabla T) + Q(T, t) \text{ (Energy rate per unit volume)} \quad (3.15)$$

where ρ is density [kg/m^3], C_p is specific heat [$J/kg \text{ } ^\circ C$], ∇ is gradient operator [$1/m$], K is conductivity tensor [$W/m \text{ } ^\circ C$], T is temperature [$^\circ C$], t is time [sec] and Q is the source term [W/m^3].

Equation (3.15)[†] is a parabolic differential equation in which the Fourier conduction law

[†]The equations in this section are taken from the *Spacecraft Thermal Control Handbook* [3] prepared by David G. Gilmore.

($q = -K \cdot \Delta T$) is implemented. Even if temperature (T) is a scalar that can differ with position, the heat flow is function of the temperature gradient in a particular direction and so is a vector quantity.

Several methods may be used to solve the equations describing the thermal problem.

Most aerospace companies in the spacecraft industry implement finite-difference numerical techniques to solve Eq.(3.15) for many heat-transfer problems with proper boundary conditions. For this reason, these companies usually have either SINDA/1987, written by J. Gaski, or SINDA85/FLUINT, developed by Martin Marietta for NASA Johnson Space Center (JSC).

SINDA consists of a preprocessor and an execution library. The preprocessor reads a SINDA input file and, following certain rules, constructs a FORTRAN executable. The analyst chooses subroutines from the SINDA library to get temperatures. SINDA permits the user to include the necessary FORTRAN logic to solve a specific heat-transfer problem. FORTRAN code can be added into any of the SINDA operation blocks. The Gaski SINDA has a one-dimensional incompressible-fluid thermal-analysis capability for evaluating pumped-fluid heat-transfer networks.

SINDA85 is a relevant evolution from the previous SINDA-type codes. It has fluid-network analysis capability for evaluating various types of thermal networks, including incompressible, compressible, two-phase flow, and others, moreover it also allows the analyst to build a thermal model from separate submodels [Gilmore et al., 2002]. However, both features are very powerful.

Now some of the most implemented methods for thermal analysis are discussed.

Finite-Difference Method (FDM)

These codes define the solution to a finite-difference model that approximates the physical object. The nodes or subvolumes are assumed to be isothermal and physical properties are assumed to be constant within a node. Several heat-transfer books define finite-difference-node meshes as lumped-parameter representations. The nodes are linked by conduction and/or radiation. The governing partial differential equation is converted into a system of finite-difference equations by constructing an FDM mesh [Gilmore et al., 2002]. The basis for this step is the Taylor series approximation. A three-dimensional Cartesian coordinate system is assumed for this discussion. From Figure 3.13, which illustrates typical one- and two dimensional FDM meshes, the Taylor series about x_0 for $T(x)$ is written for the one-dimensional mesh:

$$T(x_0 + \Delta x) = T(x_0) + \left. \frac{\partial T}{\partial x} \right|_{(x=x_0)} \cdot \delta x + \left. \frac{\partial^2 T}{\partial x^2} \right|_{(x=x_0)} \cdot \Delta x^2 / 2! + \left. \frac{\partial^3 T}{\partial x^3} \right|_{(x=x_0)} \cdot \Delta x^3 / 3! + \dots \quad (3.16)$$

From this approximation, the first and second derivatives can be derived:

$$\begin{aligned} \left. \frac{\partial T}{\partial x} \right|_{(x=x_0)} &= \frac{T(x_0 + \Delta x) - T(x_0)}{\Delta x} + 0(\Delta x) \\ \left. \frac{\partial^2 T}{\partial x^2} \right|_{(x=x_0)} &= \frac{\frac{T(x_0 + \Delta x) - T(x_0)}{\Delta x} - \frac{T(x_0) - T(x_0 - \Delta x)}{\Delta x}}{\Delta x} + 0(\Delta x^2) \end{aligned} \quad (3.17)$$

where $0(\Delta x)$ and $0(\Delta x^2)$ are a means of expressing the order of the truncation error associated with the approximation.

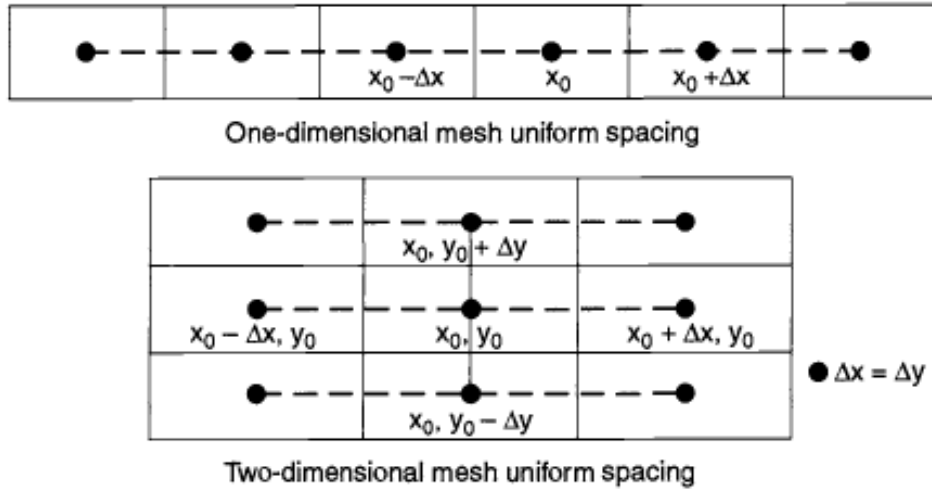


Figure 3.13: Finite-difference method (Credits:D. G. Gilmore, *Spacecraft Thermal Control Handbook*).

Equation (3.15) can be written for a heterogeneous, anisotropic solid, the conductivity of which in each of the three principal directions is a function of temperature:

$$\rho C_p \frac{\partial T}{\partial t} = \frac{\partial}{\partial x} \left[k_x(T) \frac{\partial T}{\partial x} \right] + \frac{\partial}{\partial y} \left[k_y(T) \frac{\partial T}{\partial y} \right] + \frac{\partial}{\partial z} \left[k_z(T) \frac{\partial T}{\partial z} \right] + Q(T, t) \quad (3.18)$$

The x-partial derivative, $\frac{\partial}{\partial x} \left[k_x(T) \frac{\partial T}{\partial x} \right]$ can be written as

$$\begin{aligned} & \left[k_x(\delta^+) \cdot \left(\frac{T_{n+1}(x + \Delta x, y, z, t) - T_n(x, y, z, t)}{\Delta x} \right) \right. \\ & \left. - k_x(\delta^-) \cdot \left(\frac{T_n(x, y, z, t) - T_{n-1}(x - \Delta x, y, z, t)}{\Delta x} \right) \right] / \Delta x \end{aligned} \quad (3.19)$$

where n is the node number about which the Taylor series is applied, and

$$\delta^\pm = \frac{T_n(x, y, z, t) + T_j(x \pm \Delta x, y, z, t)}{2}, \quad j = n + 1 \text{ or } n - 1 \quad (3.20)$$

$$\text{or} \quad \delta = T_n(x, y, z, t)$$

where j is the adjacent node, x , y and z are the spatial coordinates of n and t is time. Multiplying Eq.(3.19) by the volume $\Delta x \cdot A$, where $A = \Delta y \cdot \Delta z$, it can be got

$$A \cdot k_x(\delta^+) \cdot \frac{(T_{n+1} - T_n)}{\Delta x} - A \cdot k_x(\delta^-) \cdot \frac{(T_n - T_{n-1})}{\Delta x} \quad (3.21)$$

where T is reductive for $T_i(x, y, z, t)$ and $i = n$.

The coefficient $A \cdot k_x(\delta^\pm)/\Delta x$ is resumed by the parameter G , the conductance. In this way, Eq.(3.21) becomes

$$G_{n+1} \cdot (T_{n+1} - T_n) - G_{n,n-1} \cdot (T_n - T_{n-1}) \quad (3.22)$$

where $G_{n+1,n} = \frac{k(\delta^+) \cdot A}{\Delta x}$ and $G_{n,n-1} = \frac{k(\delta^-) \cdot A}{\Delta x}$ [Gilmore et al., 2002]. Similar expressions can be written for the other terms in y and in z , in Eq.(3.18).

The conductance, G , is placed in the conduction block of SINDA. So, using the Taylor series approximation, a partial differential equation has been converted into a set of finite-difference equations that can now be solved numerically. The source term in Eq.(15.18), $Q(t)$, is the means by which external and internal radiation, convection, and heat sources are considered into the difference equation. The radiation term is commonly written as

$$\sigma A \zeta_{n,n+1} (T_n^4 - T_{n+1}^4) \quad (3.23)$$

where σ is the Stefan-Boltzmann constant, A is the surface area of the radiating surface, and $\zeta_{n,n+l}$ represents the net radiation exchanged between two real surfaces, including all possible reflection paths. From the SINDA perspective $A \zeta_{n,n+l}$ is just another conductance, except it is a radiation coefficient. In SINDA, radiation conductances are differentiated from convection and conduction coefficients by a minus sign; for example, $-G$ indicates a radiation conductor and G denotes a normal (conduction or convection) conductor.

In constructing a thermal model the analyst chooses how many nodes to utilize, how to distribute them and how to link them by radiation, conduction or convection. The resulting model network provides a system of finite-difference equations with either constant or variable coefficients. The number of equations to be solved is function of the number of nodes decided by the user in the thermal model minus any boundary nodes, which have a defined temperature history.

To convert the finite-difference equations to a set of algebraic equations that are then solved within SINDA, the time derivative has to be approximated, just as the spatial derivatives. The $\frac{\partial T}{\partial t}$ in Eq.(3.18) can be approximated in the following way:

$$T(t^* + \Delta t) = T(t^*) + \theta \cdot \left. \frac{\partial T}{\partial t} \right|_{t^* + \Delta t} \cdot \Delta t + (1 - \theta) \cdot \left. \frac{\partial T}{\partial t} \right|_{t^*} \cdot \Delta t \quad (3.24)$$

where θ is a variable-weighted implicit factor. Multiplying Eq.(3.18) by the volume ($\Delta x \cdot A$), it can be observed that the coefficient for $\frac{\partial T}{\partial t}$ becomes

$$C_n = \rho \cdot C_p \cdot \Delta x \cdot A \quad (3.25)$$

where C_n denotes the capacitance of node n and A is the cross-sectional area $\Delta y \cdot \Delta z$. Mixing Eqs.(3.22), (3.23) and (3.24), it is found that Eq.(3.19) becomes

$$\begin{aligned} & C_n \frac{T_n(t + \Delta t) - T_n(t)}{\Delta t} \\ &= \theta \cdot \left[\sum_{j=1}^N G_{jn}(T_j - T_n) + \sigma \cdot \sum_{j=1}^N \zeta_{jn} A_n (T_j^4 - T_n^4) + Q_n(T_n, t) \right]_{t^* + \Delta t} \\ &+ (1 - \theta) \cdot \left[\sum_{j=1}^N G_{jn}(T_j - T_n) + \sigma \cdot \sum_{j=1}^N \zeta_{jn} A_n (T_j^4 - T_n^4) + Q_n(T_n, t) \right]_{t^*} \end{aligned} \quad (3.26)$$

This equation contains the parameter θ , which can be modified along with the FDM mesh size and time step to yield various finite-difference approximations with different local truncation errors. The values $\theta = 0, 1/2$ and 1 yield the forward-explicit, Crank-Nicolson, and backward-implicit approximations [Gilmore et al., 2002].

Selecting a particular FDM mesh scheme and evaluating the coefficients in Eq.(3.26) yields a system of n algebraic equations where n is the number of finite-difference nodes. To note that n does not include boundary nodes. If $\theta = 0$, each equation is explicit and has only one unknown temperature, T_n . If $\theta > 0$, a system of algebraic equations exists and must be solved by either iterative techniques, matrix-inversion schemes or decomposition procedures. Usually the system of equations is written as

$$T_{new} = [A] \cdot T_{old} \quad (3.27)$$

where $[A]$ is an $n \times n$ matrix and T is an $n \times 1$ or column matrix. For thermal models of ten or more finite-difference nodes, $[A]$ is typically a sparse matrix because each node is normally connected to a small subset of the total number of nodes in the model. For most heat-transfer problems, $[A]$ is not banded because of radiation interchange between the nodes. Consequently the efficient solvers for tridiagonal matrices are not generally useful.

FDM Errors Three types of errors can happen with the application of the FDM to heat-transfer problems. The first is the truncation error, which is the difference between the differential equation and the approximating difference equations. This type of error can be shown for the one-dimensional heat-transfer equation with constant conductivity. Let

$$F_{pde}(T) = \left(\frac{\partial T}{\partial t} - k \cdot \frac{\partial^2 T}{\partial x^2} \right) \quad (\text{partial differential equation}) \quad (3.28)$$

and

$$\begin{aligned} F_{fd}(T_i) &= \left(\frac{T_{t^* + \Delta t, x^*} - T_{t^*, x^*}}{\Delta t} \right) \\ &- k \left(\frac{T_{x^* + \Delta x, t^*} - 2T_{x^*, t^*} + T_{x^* - \Delta x, t^*}}{\Delta x^2} \right) \quad (\text{finite - difference equation}) \end{aligned} \quad (3.29)$$

then $[F_{fd}(T_i) - F_{pde}(T)]$ represents the truncation error at each node. T_i indicates the temperature at three successive nodes, $x^* + \Delta x, x^*$, and $x^* - \Delta x$, and t defines a discrete time. The temperature T in the analytical solution is a continuous function. The truncation error is determined from the finite-difference node spacing (mesh size) and the size of the time step. As the number of finite-difference nodes is increased and the time step decreased, the error associated with the Taylor series approximation (truncation) decreases and approaches zero in the limit. In this case the truncation errors go to zero and the difference equation is said to be consistent with the partial differential equation. However, as the number of nodes in the network expands, the corresponding number of difference equations to be solved increases. This, in turn, increases execution time [Gilmore et al., 2002].

From the viewpoint of algebraic simplicity, an analyst prefers the coarsest network possible. The best thermal model is a compromise between node size and computational cost. No specific rules are available for deciding the optimal network size. One way to judge the truncation errors introduced by too coarse a network is to estimate the truncation error as the calculation proceeds.

The second type of error refers to the stability of the numerical solution. If the effect of errors tends to diminish as the numerical solution progresses, then the solution is stable and converges. However, if the errors tend to grow with time, then the solution becomes unstable and diverges.

The third type of error is the computer rounding error made during numerical calculations. This is the difference between the exact numerical answer and the actual numerical answer (i.e., the truncated numerical answer generated by the computer). Rounding error is a relevant problem with 16-bit computers, somewhat of a problem with 32-bit machines and typically not a problem with 64-bit computers. The numerical temperature, T_{num} , is defined as

$$T_{num} = T_{ex} + (T_{num} - T_{exn}) + (T_{exn} - T_{ex}) \quad (3.30)$$

where T_{ex} is the analytical solution and T_{exn} is the exact numerical solution. The discrete error is the combination of the truncation and stability errors. As already discussed, these errors are directly coupled to the mesh size and time step assumed by the analyst. The truncation error for a uniform mesh is typically $0(\Delta x^2)$ (second-order). However, for a non-uniform mesh, the truncation error becomes $0(\Delta x)$ (first-order). So, a non-uniform FDM mesh reduces the order of the truncation error and decreases the accuracy of the approximation. The majority of spacecraft thermal models are not uniform; however, if sufficient thermal nodes are used, the numerical answers will be reasonably accurate [Gilmore et al., 2002].

Forward-Differencing Approach to Heat-Transfer Equations

The forward-differencing expression is got from Eq.(3.24) by setting $\theta = 0$; so,

$$T(t^* + \Delta t) = T(t^*) + \left. \frac{\partial T}{\partial t} \right|_{t^*} \cdot \Delta t \quad (3.31)$$

This method needs that the calculation of T_i at $t_* + \Delta t$ are based on values of T_i that are known at t^* , the previous time. This is shown by setting $\theta = 0$ in Eq.(3.26). The forward-differencing assumption is explicit and the solution can be unstable if the time step, Δt , is too large [Gilmore et al., 2002]. The criteria for stability are defined by calculating the minimum value

$$\tau_n = \frac{C_n}{\sum_j G_{nj}} \quad (3.32)$$

for each finite-difference node, where τ is the stability factor and j is the sum of all conductors connecting other nodes to n by conduction or radiation. The thermal capacitance of the node is C_n , and the values of G_{nj} are the conductance values between successive nodes. If radiation occurs between two nodes, the value is linearised to get

$$G_{nj} = \sigma \zeta_{nj} A_j (T_n^2 - T_j^2) (T_n + T_j) \quad (3.33)$$

In SINDA, τ is called CSGMIN. CSGMIN is the smallest time constant in the thermal network at each time step. It can vary from time step to time step. CSGMIN includes the effect of boundary conditions if the node that has the smallest τ is connected to any boundary nodes. The solution process will remain stable if the time step, Δt , is always minor than CSGMIN. In SINDA $\Delta t = 0.95 \cdot CSGMIN / CSGFAC$ is always adopted, with CSGFAC defaulted to 1.0.

The forward-differencing equation has one unknown node temperature at $t^* + \Delta t$, with all the other temperatures known at t^* . Any radiation terms are approximated by Eq.(3.33). Even if this explicit equation is simple to solve, the time step, Δt , is limited by the stability criteria for the node with the smallest time constant. In this way, using this technique the analyst is trading simplicity for potentially many small time steps, a situation that can cause excessive execution time and fully consume the CPU on a local workstation. In applying the forward-differencing equations, the analyst does not have to specify the convergence criteria and a time step, since these can be opportunely calculated from the specified thermal data [Gilmore et al., 2002].

Backward-Differencing Approach to Heat-Transfer Equations

Another technique used to solve heat-transfer equations is backward differencing. In this case the heat balance is written in terms of the unknown temperatures at $t^* + \Delta t$,

$$T(t^* + \Delta t) = T(t^*) + \left. \frac{\partial T}{\partial t} \right|_{t^* + \Delta t} \cdot \Delta t \quad (3.34)$$

This equation is obtained by setting $\theta = 1$ in Eq.(3.24). This approach yields a system of n equations, where n is the total number of finite-difference nodes whose temperatures are computed at each time step. Boundary nodes are excluded. This formulation is called implicit. The minimum time constant CSGMIN is still calculated in SINDA for implicit methods. Since implicit methods are unconditionally stable, the time step Δt can exceed CSGMIN. However, if the time step decided is too large, although stable, the truncation

error can become significant. When using an implicit method, the analyst must specify the time step. The user should always compare the specific time step to *CSGMIN*. If the decided time step is five to ten times *CSGMIN*, it is probably too large. Of course, this judgement depends on the problem being solved [Gilmore et al., 2002].

Iterative schemes are usually used to solve systems of equations. Such techniques need a convergence criterion. For transient problems, the SINDA constants *DRLXCA* and *ARLXCA* must be specified to use the implicit schemes. Two constants are required because SINDA uses both diffusion and arithmetic nodes. *DRLXCA* is the convergence criterion for diffusion nodes, and *ARLXCA* is the convergence criterion for arithmetic nodes.

The advantage of backward differencing consists in the ability to vary the time step. During periods of rapidly varying boundary conditions, the time step can be decreased. In the same way, during periods of slowly changing boundary conditions, the time step can be increased. Commonly, implicit numerical schemes are faster than the explicit-forward method because of the large time steps permitted. By the way, the larger is the time step, more iterations are needed to get a solution. Each iteration is essentially equivalent to a time step. So, the actual implicit time step is approximately the specified Δt divided by the number of iterations required to obtain a solution. The user needs to confront this modified time step to *CSGMIN* to verify that the specified time step is providing the increased computational speed expected over the explicit method. For some problems the implicit scheme may not be any faster than the explicit method.

The following stability criteria are associated with Eq.(3.26):

- $\theta = 0$, $\Delta t < CSGMIN$;
- $\theta < 1/2$, conditionally stable, i.e., $CSGMIN < \Delta t < CSGMIN(1 + \Delta)$ where $\Delta \rightarrow \infty$ as $\theta \rightarrow 1/2$;
- $1/2 < \theta < 1$, unconditionally stable for any Δt ;

All the SINDA codes use three types of nodes: diffusion (with mass), arithmetic (no mass) and boundary (specified temperature). These definitions are particularly useful when solving equations whose time constants vary by many orders of magnitude or higher values. If arithmetic nodes were not allowed, the algebraic system of equations would be very stiff. This class of problem (stiff equations) can only be solved with implicit techniques. When *CSGMIN* is very small for some diffusion nodes, they can be converted to arithmetic nodes. This makes the equations less stiff and improves the computational efficiency without sacrificing accuracy. The temperature of an arithmetic node is achieved by noting that the total heat flow into the node is zero [Gilmore et al., 2002].

Finite-Element Method (FEM)

The FEM is a second approach to the numerical solution of heat-transfer problems. The FEM-mesh schemes are the real strength of this technique. Each finite-element model

usually has hundreds of elements. Two approaches are used to develop a solution with the FEM: the methods of weighted residuals (MWR) and the Ritz variational method. The most largely used finite-element approach is the Galerkin method, which is one of four MWRs. The FEM seeks an explicit expression for the temperatures, \tilde{T} , in terms of known functions that, on average, satisfy the governing differential equations and the boundary conditions exactly on an element. The \tilde{T} is the finite-element approximation to the actual temperature, T . The form used for \tilde{T} is

$$\tilde{T}(t, a_i) = \sum_{i=0}^N a_i \Phi_i(t) \quad (3.35)$$

where the a_i refers to as degrees of freedom (DOF), N is the total number of DOF and the $\Phi_i(t)$ are said, in several books ([3], [5], [7]), trial, basis, shape, interpolation or coordinate functions. Commonly the Φ_i are thought to be powers of x on the element. This approach parallels the analytical technique of finding a function or set of functions that solves the differential equation and also satisfies the prescribed boundary conditions. An example of a basis function is

$$\begin{aligned} \Phi_i &= 0, & t &= a \\ \Phi_i &= \frac{a-t}{a-b}, & a < t < b \\ \Phi_i &= 1, & t &= b \end{aligned} \quad (3.36)$$

So Φ_i is a linear function whose value varies from 0 to 1. A bar element has an element node at each end and a triangle element has a node at each corner (Figure 3.14). The a_i are specified at each element node. For a thermal problem, a_i equals T_i , where the T_i are the element-node temperatures. The essence of the method is to get a set of algebraic equations for the element-node temperatures T_i that form a column vector called \tilde{T} . The temperatures between element nodes are found by applying the basis function between those nodes. For example Eq.(3.36) for Φ_i would be utilized to find the temperature between element nodes a and b . For a reasonable FEM mesh, \tilde{T} should approach T , the exact temperature solution [Gilmore et al., 2002].

Basis functions used in Eq.(3.35) can be linear [Eq.(3.36)], quadratic, cubic, or quartic. Examples of element shapes are:

- bar (one-dimensional);
- triangular, rectangular, quadrilateral (two-dimensional);
- hexahedral, pentahedral, tetrahedral (three-dimensional).

To improve the accuracy of the finite-element method, either a smaller mesh (more elements) is adopted or higher-order basis functions (increased DOF) on the elements are required. This FEM-mesh technique does not provide the analyst with an error estimate like finite-difference, which is based on Taylor series expansions. So, the analyst either

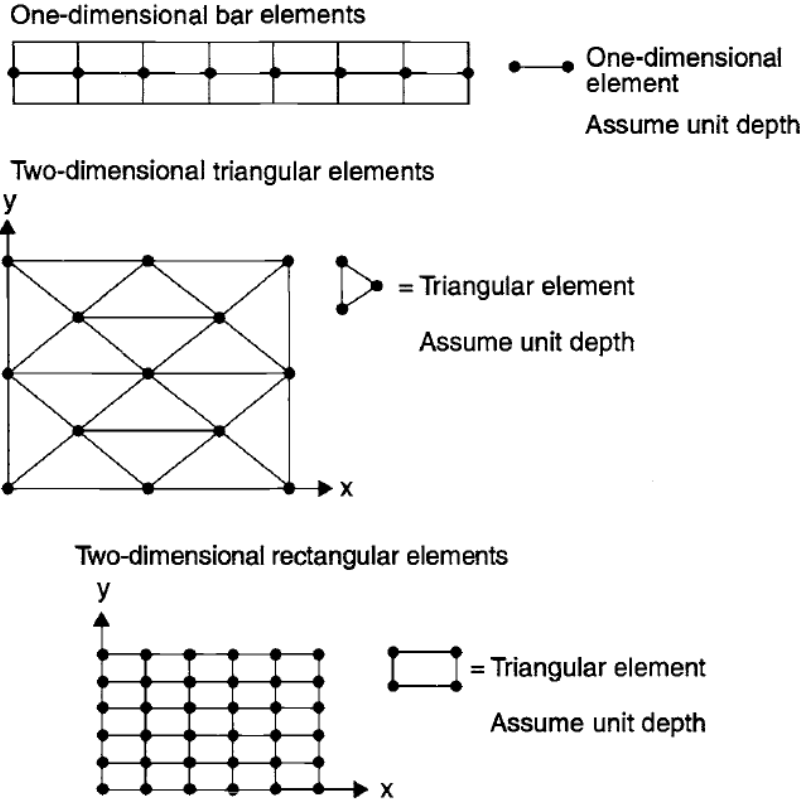


Figure 3.14: Finite-element method (Credits:D. G. Gilmore, *Spacecraft Thermal Control Handbook*).

repeats the problem with a more dense mesh or, according to the experience, develops an FEM mesh that seems to provide an acceptable solution. This process leads to detailed-mesh structures, since the associated errors are not easily calculated and the analyst does not want to solve the same problem twice for two different mesh sizes to establish a convergence criterion [Gilmore et al., 2002].

Many finite-element codes that can be utilized for thermal analysis are available in the aerospace industry. These include NASTRAN, ADINAT, ABAQUS, ANSYS, COSMOS, and TOPAZ. All were developed to perform structural analysis.

Finite-Difference vs. Finite-Element

In conclusion, both method, finite-difference or finite-element, can be adopted to solve heat-transfer problems. The FDM is based on Taylor series approximations to develop the algebraic equations that are solved numerically to find a set of temperatures. Each finite-difference node is located at the center of mass and is assumed isothermal throughout the volume occupied. The error associated with the calculation can be estimated.

The FEM is based on using elements that are one-, two-, or three-dimensional, depending

on the problem being solved. Each element has element nodes at its corners. Parameter values, for example temperatures, are usually specified or calculated at element nodes. Modification within the element are calculated by using interpolation (basis) functions within the element. So the properties and temperature can differ across the element. The Galerkin MWR is commonly utilized to develop the algebraic equations that define the element-node temperatures [Gilmore et al., 2002].

The FDM is very effective for building spacecraft-system models. It is compatible with the basic surface primitives (e.g., cones, cylinders, spheres) utilized to determine spacecraft surfaces in the radiation codes. Heat-transfer problems that are in first instance driven by radiation can be simply solved with this method. The FDM mesh does not need to be uniform, the truncation error decreases from $O(\Delta x^2)$ to $O(\Delta x)$. The accuracy of the method is defined by the truncation error from the Taylor series expansions. This assumes that the analyst is using an inherently stable integration scheme and that rounding error is small, which may not always be the case. The truncation error can be reduced with a more dense FDM mesh and lower time steps.

Confronting the accuracy of FDM and FEM is very difficult unless an exact solution is available. This never occurs for non-linear problems, which is usual for radiation-dominated thermal analyses. Thermal models developed with this method can have three types of isothermal nodes: diffusion, arithmetic and boundary. The arithmetic node, can be used to avoid stiff equations that always have a large spread in the time constants. In several spacecraft models one thermal node represents an electronics box. This is easily accommodated by finite-difference schemes, but not by finite-element schemes. To overcome the mesh-generation problem for finite-difference techniques, many aerospace companies have used FEM-mesh generators like PATRAN to build a mesh and then convert it to finite-difference for the finite-difference analysis codes like SINDA. The resulting temperatures are then returned to the finite-element mesh-generation code for display. Without a finite-difference pre- and post-processor, FDM has a serious disadvantage in building thermal models and displaying the results [Gilmore et al., 2002].

The FEM is widely used in structural analysis. The method is very effective for solving thermal/stress problems. Commonly the structural model needs conspicuously more detail than the equivalent thermal model. So the structural characteristics will normally drive the size of the thermal analysis for a combined thermal- stress analysis. The real strengths of finite-element techniques are the mesh-generation schemes. These techniques can easily manage irregular surface shapes and the interface between two different mesh schemes.

FEM-mesh-generating schemes are still utilized in most thermal software packages to develop and post-process finite-difference temperature results. The finite-element codes have the equivalent to diffusion (nodes with mass) and boundary nodes. They do not use arithmetic (zero-mass) nodes. Because of this the resulting algebraic equations can be very stiff and lead to excessive computational costs. Moreover, the finite-element codes cannot use just one node for an electronics box simulation, as finite-difference codes can. For normal thermal analysis, finite element models will always be larger than necessary. This condition is driven by the requirement that each element face must share a complete interface with another element, and it is also driven by the lack of information about the error associated

with the calculations. So, the analyst tends to construct smaller meshes than may be necessary. Commonly, curved surfaces like cones and cylinders need far more finite-element surfaces to define the shape than are required for finite-difference codes. One node of 360° may be all the analyst really needs. A representation like that is not allowed with finite-element codes. The Monte Carlo radiation codes recognize and adopt the actual surface description for a cone and cylinder. This provides radiation-interchange factors that are correct. Approximation of these surfaces by flat surfaces or polynomial fits can influence the accuracy of the interchange factors and inconveniently increase the cost and complexity of achieving them.

The great part of finite-difference codes, such as SINDA, allow the analyst to include extensive user logic (e.g., FORTRAN subroutines) in the thermal model. Finite-element codes, like NASTRAN, are far more restrictive in this aspect.

Implicit-solution schemes best fit for transient finite-element analysis. This is mainly due to the fact that the algebraic equations being solved can be very stiff. Many finite-element solution schemes are most effective with banded matrices; although, with radiation the matrices are not properly banded. The only way to check the accuracy of the finite-element codes is to run the problem again with a more dense mesh size or high-order elements. This is of course not an inexpensive procedure for determining the error. Commonly, error calculations are not made within the finite-element codes [Gilmore et al., 2002].

In the 1990s many integrated thermal-analysis programs were developed that allow the analyst to generate complete TMMs and GMMs, execute them, and display the results in a user-friendly, menu-driven environment on a workstation or PC. These newer systems typically have a model builder, an orbital display capability, a radiation analyser, a thermal analyser, and post-processing software to display temperature distributions and temperature heat-flux plots. Most have a limited capability to read in models built in other CAD systems. The thermal analysers are mostly finite-difference (e.g., SINDA). The radiation codes are based either on the Monte Carlo technique or the gray-diffuse assumption (these are presented in the next section).

The commercially available thermal-analysis software packages are the following:

- **Thermal Synthesizer System (TSS)** by *SPACEDESIGN* under license to *NASA/JSC*;
- **Thermal Desktop (TD)** by *Cullimore and Ring Technologies*, TD uses AUTOCAD and it is the software that will be adopted for the case study analysis in the next chapter;
- **THERMICA** by *Network Analysis Inc.* under license to *ASTRIUM*;
- **FEMAP/SINDAG Modeling System** by *Network Analysis Inc.*;
- **IDEAS TMG Thermal Modeling System** by *MAYA*; FEMAP can also be used instead of IDEAS;
- **ITAS** by *Analytix Corporation*;

- **Thermal Analysis System** by *Harvard Thermal*;

The model builders for these systems refer on either surface primitives (shapes) or elements, e.g., patches. The commercially available shape-based systems are TSS, THERMICA, and ITAS. TD can be shape or element based. The others are element-based systems. The object of these systems is to facilitate the analyst's ability to build thermal models in a fast, efficient way. The aim is to let the computer perform as many of the calculations as possible, so that the analyst can think more about the physics of the problem.

In addition to these commercially available thermal-analysis systems, many helpful commercial codes can assist an analyst in either building a thermal model or analysing results:

- **SINAPS** by *Cullimore and Ring Technologies, Inc.*
- **Pre-SINDA** by *VERIDIAN*.
- **SSPTA** by *Swales and Associates, Inc.*

3.1.5 Radiation Analysis Codes

Radiation interchange factors between surfaces and energy absorbed on surfaces of spacecraft are determined by radiation codes. The book *Thermal Radiation Heat Transfer* [6] by Siegel and Howell provides a complete summary of assumptions made by these radiation codes and the techniques that they use. The codes adopt either the gray-diffuse assumption or the Monte Carlo approach.

The Gray-Diffuse Assumption

Many codes, as industry standard for several years, assume a gray-diffuse surface to determine the emission and absorption of radiation on a surface. This assumption implies:

- i. The temperature is uniform over that surface.
- ii. The emittance, absorbance, and transmittance of a surface are independent of wavelength and direction.
- iii. All energy from a surface is emitted and reflected diffusely.
- iv. The incident and reflected energy flux is uniform over each surface.

With these assumptions a set of blackbody geometric configuration factors or view factors are determined. A blackbody is a surface that completely absorbs all incident radiation of all wavelengths and from all directions. The view factor, F_{ij} , is simply the fraction of energy leaving black surface i that arrives at black surface j . The view factor can be calculated from a double integral sum, the unit-sphere method, or the contour integration method [Gilmore et al., 2002].

The energy per unit time transferred from black element dA_1 to dA_2 over the distance S is given as:

$$dQ_{dA_1 \rightarrow dA_2} = F_{12} \sigma T_1^4 dA_1 \quad (3.37)$$

where

$$F_{12} = \frac{\cos G_1 \cos G_2}{\pi S^2} dA_2 \quad (3.38)$$

is the configuration or view factor (Figure 3.15). This assumes the blackbody total intensity, i_b , refers to the blackbody total hemispherical emissive power, e_b , by the equation

$$i_{b1} = \frac{e_{b1}}{\pi} = \frac{\sigma T_1^4}{\pi} \quad (3.39)$$

where σ is the Stefan-Boltzmann constant, π is 3.14159265, and T is the temperature of the surface.

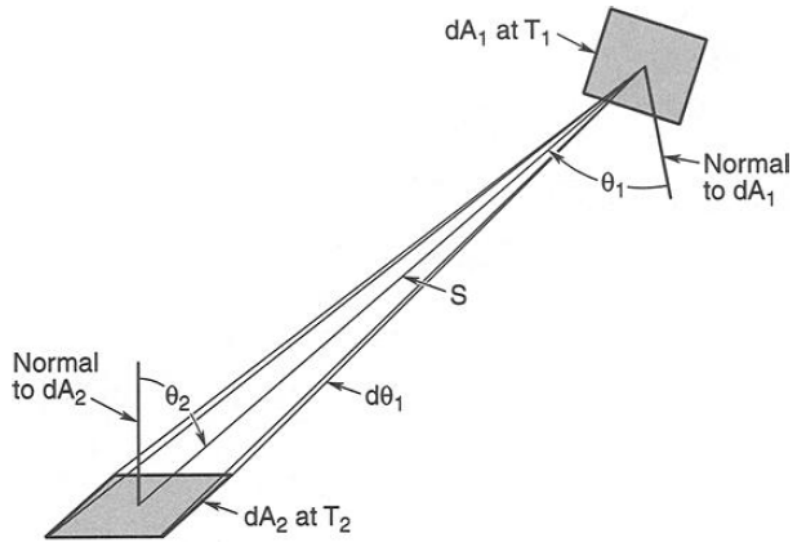


Figure 3.15: Radiative interchange between two black differential area elements (Credits:D. G. Gilmore, *Spacecraft Thermal Control Handbook*).

Once the values of F_{ij} are calculated, the values of B_{ij} can be determined. B_{ij} is the fraction of energy emitted by black surface i that is absorbed by real surface j , including all intervening reflections from other real surfaces, including i . The real surface is assumed to be gray, a diffuse emitter and a diffuse reflector. A gray surface has radiative properties that do not depend by wavelength. A gray surface emits and absorbs a fraction of what a black surface does. For these assumptions, the Gebhart Method [6] can be used to calculate the B_{ij} values from the F_{ij} values and the specified surface emittances.

It can be also determined the energy absorbed by a surface. To do this calculation it has

to be determined the shadow factors, i.e., how one surface shadows another. This information is of course dependent on the direction of the incident solar energy. The accuracy of the shadow factor depends on how a surface is subdivided into a mesh. The shadow factor needs each small mesh element to be either illuminated or shadowed.

To determine absorbed energy on a surface, whether shadowed or not, the code has to be able to specify the orientation of a surface in an orbit with respect to the Sun and Earth (these are the external-environment sources of heat for a spacecraft surface). After specified the orbit, the code defines a set of reference axes, e.g., solar-inertial, planet-centered, etc. The coordinate system for each surface is then defined in relation to the spacecraft reference axes. This reference axis is then oriented with respect to the orbital reference axes. In this way, the orientation of any surface with respect to the Sun or Earth can be defined and its illumination determined [Gilmore et al., 2002].

The Monte Carlo Approach

The Monte Carlo method was first used in the aerospace industry in the 1970s. The majority of the commercially available thermal-analysis systems include a Monte Carlo radiation code (i.e. TSS, TD, THERMICA, IDEAS, and ITAS).

Most of the Monte Carlo codes utilize surface primitives, i.e., they are shape based. Those thermal-analysis systems that utilize finite-element mesh-generating schemes cannot construct surface primitives with one element. For instance, many elements are required to create a cylinder or cone. This requirement can add unnecessary surfaces to a geometric model. As discussed previously, those extra surfaces can influence the execution time of a Monte Carlo code if several curved surfaces have to be built from smaller elements [Gilmore et al., 2002].

With the tendency to construct large detailed thermal models of subsystems and spacecraft, the geometric models can become very big. This can particularly increase the execution time of the Monte Carlo software.

The quantity of time spent in finding a ray/surface interaction can be excessive in Monte Carlo codes. Methods for speeding up the ray tracing within the code by reducing the number of time-consuming ray/surface intersection calculations have been developed. One of these, the OCTREE method, subdivides a three-dimensional surface geometric model into cells or compartments. Typically only a small number of surfaces are in each cell. Some surfaces may be divided between cells. When a ray is emitted from a surface in one cell, the code tries to determine if any surface in that cell is hit. If not, the code checks the next or adjacent cell in the direction the ray is moving. The technique significantly reduces the search time to find the surface the emitted ray intersects or hits. The key to this method is breaking the surface geometric model into a reasonable number of three-dimensional cells. If too many cells are used, then the Monte Carlo calculation time can become excessive [Gilmore et al., 2002].

The Monte Carlo codes, can determinate the energy absorbed on a surface. The shadowing of a surface by another surface automatically falls out from the ray/intersection calcula-

tions, i.e., a ray either hits the targeted surface or the shadowing surface. To determine energy absorbed on a surface whether shadowed or not, the code has to be able to define the orientation of a surface in an orbit with respect to the Sun or Earth. After a set of reference axes is defined in the orbit, the coordinate system for each surface is then defined in relationship to the spacecraft's reference axes. These reference axes are then oriented along the orbital reference axes. So, the orientation of any surface with respect to the Sun or Earth can be defined and its illumination can be determined.

All the radiation codes adopt the semi-gray approximation, a solution method that assumes that radiant interchange can be treated in two independent spectral regions, one solar and the other IR.

As previously stated, all surfaces are assumed gray diffuse, but the Monte Carlo codes are not limited by this assumption. The surfaces can be gray diffuse, specular or some combination of the two reflectances. Moreover, transmittance can be allowed. Direction-dependent surface properties can also be utilized, although they could influence Monte Carlo code execution time. The conservation of energy yields, for incident energy on a surface,

$$\alpha \text{ or } (\varepsilon) + \rho + \tau = 1 \quad (3.40)$$

where α is the absorptance of the surface at solar wavelengths, ε is the fraction of energy emitted or absorbed by a surface in the IR wavelengths, ρ is the fraction of energy reflected by a surface at solar or IR wavelengths (the reflectance could be diffuse, specular or directional), and τ is the fraction of incident energy transmitted through a surface.

As already noted, the OCTREE method is helpful for speeding up the determination of a ray/surface intersection in a single processor. Another powerful method is to develop a distributed-processing system for a Monte Carlo code. In this case tens of processors can be used. Such a system can greatly decrease execution times for problems with hundreds of surfaces. The efficiency of any of the commercially available Monte Carlo codes on a single processor is important. However, running a Monte Carlo code on multiple processors and on numerous computers has a significantly greater influence on reducing execution times for a given problem [Gilmore et al., 2002].

3.2 Thermal Desktop

C&R Thermal Desktop is a program that allows the user to easily construct, analyse and post-process complex thermal models. Thermal Desktop uses abstract network, finite difference and finite element modelling methods. RadCAD, a subset of Thermal Desktop, is a module to determine radiation exchange factors and orbital heating rates. FloCAD, another module of Thermal Desktop, develops flow networks and determines convective heat transfer factors. The title “Thermal Desktop” is normally adopted to refer to Thermal Desktop and its integrated modules, however, RadCAD and FloCAD may be licensed separately to allow the user to tailor the system to properly meet analysis needs [Cullimore et al., 2017].

The output of Thermal Desktop, RadCAD and FloCAD is automatically combined in order to create inputs for SINDA/FLUINT, CRTech’s industry standard thermal/fluid analyser. Thermal Desktop’s *Case Set Manager* feature (Figure 3.16) organizes conduction generation, radiation analysis, fluid flow network generation, SINDA execution and post-processing under a single one-click operation. Multiple cases may be specified and executed sequentially, automating and simplifying large analysis jobs.

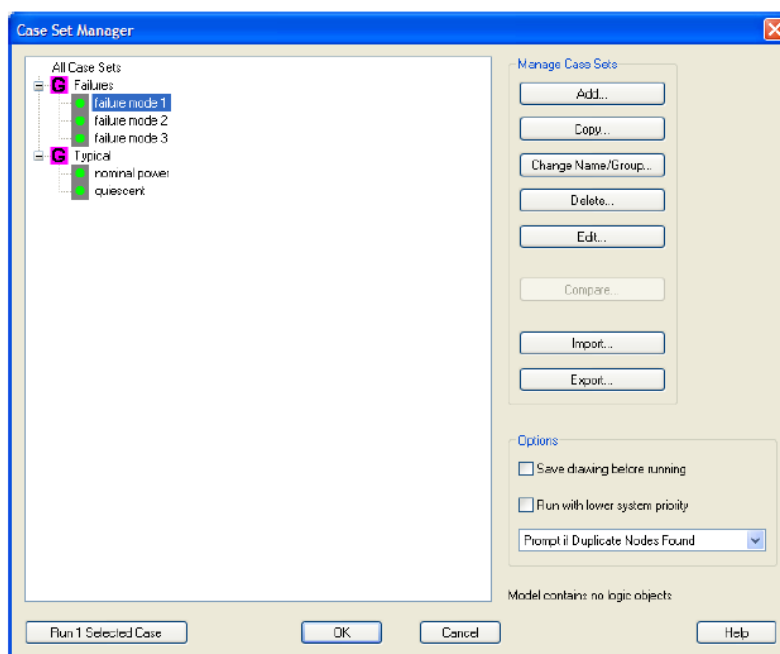


Figure 3.16: Case Set Manager Dialog Box (Credits: *Thermal Desktop User’s Manual* by C&R Technologies, Inc.).

Thermal Desktop is also parametric. Input fields for surface parameters, assembly positioning, optical and material properties, network elements and orbital data will accept either numerical values or expressions using arbitrary user-defined variables. Parametric trade studies and optimizations are simply executed, especially when managed

using *Case Sets*. A dynamic link between SINDA/FLUINT and Thermal Desktop allows SINDA/FLUINT to command Thermal Desktop to recalculate radks, heating rates, conduction and capacitance data on the fly from within a SINDA/FLUINT execution: SINDA/FLUINT can be utilized as a scripting language for controlling Thermal Desktop execution and any recomputations of radiation, contact, convection, etc. needed of Thermal Desktop by SINDA/FLUINT can be done to support the execution of parametric runs [Cullimore et al., 2017].

Using the SINDA/FLUINT Solver, optimizations may now be performed that include optical properties and geometric sizing as design variables. Thermal models may be automatically related to test data, modifying all aspects of the model including capacitance, conduction and radiation values.

Thermal Desktop runs as an AutoCAD application, completely integrated within an AutoCAD drawing session. Powerful CAD techniques for generating geometry can be utilized for generating thermal models. Custom menus, toolbars and dialog boxes allow the construction and analysis of thermal models directly within the AutoCAD environment. Thermal Desktop can analyse thermal models consisting of AutoCAD 3D faces, regular MxN meshes and arbitrary polyface meshes. These surfaces may be modelled directly or by using various AutoCAD mesh generation commands such as surfaces of revolution, ruled surfaces and edge defined patches. Thermal Desktop is not limited to just conic surfaces. Thermal Desktop can also import, display, and analyse existing TRASYS, TSS, NEVADA, I-deas/FEA, FEMAP, ANSYS, and NASTRAN models.

RadCAD is the radiation analyser module for Thermal Desktop. A very fast, oct-tree accelerated, Monte-Carlo ray-tracing algorithm is utilized by RadCAD to calculate radiation exchange factors and view factors. Innovations by CRTech to the ray-tracing process have resulted in an extremely efficient radiation analyser. A unique progressive radiosity algorithm has also been incorporated to calculate radiation exchange factors from view factor data. RadCAD has also incorporated the progressive radiosity algorithm into heating rate computations, resulting in faster performance. Automatic compression and decompression of internal database files reduces disk usage. Powerful thermal analysis can now be performed using modest desktop computers.

FloCAD is a Thermal Desktop module that permits a user to develop and integrate both fluid and thermal systems within a CAD based environment. FloCAD adds the capability of modelling flow circuits, including fans and convective heat transfer, connected directly to the surfaces and solids representing PCB boards, chips, heat fins, etc. It has singular tools for fastly modelling sophisticated heat pipes. FloCAD was originally thought for electronic packaging design tasks, but since it provides full access to the powerful and general-purpose SINDA/FLUINT thermo-hydraulic analyser, it can be adopted in many other applications as well [Cullimore et al., 2017].

The following sections present a complete description of the main Thermal Desktop / RadCAD / FloCAD commands.[‡]

[‡]The description of the following command in this chapter are taken from the *Thermal Desktop User's Manual* [8] prepared by C&R Technologies, Inc.

3.2.1 Optical and Thermophysical Properties

Optical Properties

The choices under the cascading *Thermal* → *Optical Properties* menu permit optical property database files to be created, edited and assigned to the current drawing. The optical property database file contains physical property values (emissivity, specularity, etc.) catalogued under a user defined name.

Thermal Desktop surfaces are assigned optical properties by defining a name for each side using an *Edit* dialog box. When computations are executed, the property names associated with the surfaces are translated into physical values using the currently specified database file. Assigning optical properties to surfaces indirectly by name, rather than with values, makes it easier to perform parametric analyses.

Property definitions (a name and values for emissivity, transmissivity, etc.) can be added to, deleted from, or modified in the current property database using the *Thermal* → *Optical Properties* → *Edit Property Data* menu choice. The current optical property database is displayed at the top of the *Edit Optical Properties* dialog box (Figure 3.17) and is taken from the current AutoCAD drawing, or the most recent *Open/Create Property DB* command. Property definitions that currently exist in the database are displayed in the table along with a resume of the solar absorptivity, IR emissivity and their ratio.

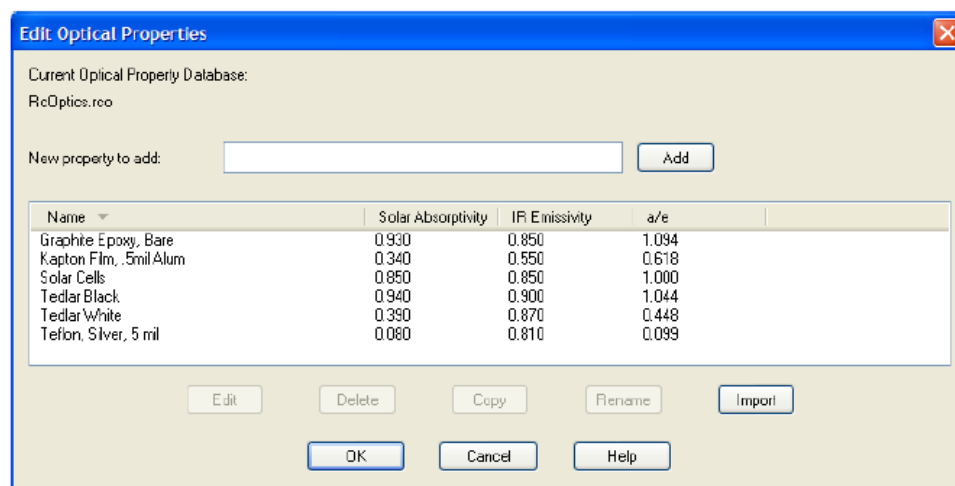


Figure 3.17: Edit Optical Properties Dialog Box (Credits: *Thermal Desktop User's Manual* by C&R Technologies, Inc.).

An existing property definition may be modified, copied, renamed or deleted from the database file by selecting the property in the list field and then selecting the *Edit*, *Copy*, *Rename* or *Delete* button, respectively. Alternatively, the user may right-click on the property name to access a context menu. If *Edit* is selected (or the property definition in the list field is double clicked), the *Edit Optical Property* dialog box for the chosen property will appear allowing property values to be changed (Figure 3.18). The *Copy* function copies

all values of the selected property and requires a new name. The *Rename* function will cycle through the model and will rename all references to the property. The *Delete* function may be performed on a single item or multiple properties. The program controls if a property is referenced and will not delete a property that is utilized by the current model. The *Import* button permits the user to import a property, or several properties, from another optical property database. New property definitions may be created by entering a name in the new property field and then selecting the *Add* button. An *Edit Optical Property* dialog box for the new property definition will be displayed with default optical property values. If the name entered already exists, the dialog box will show the previously defined values (same as *Edit*). The *Edit Optical Property* dialog box is illustrated in Figure 3.18.

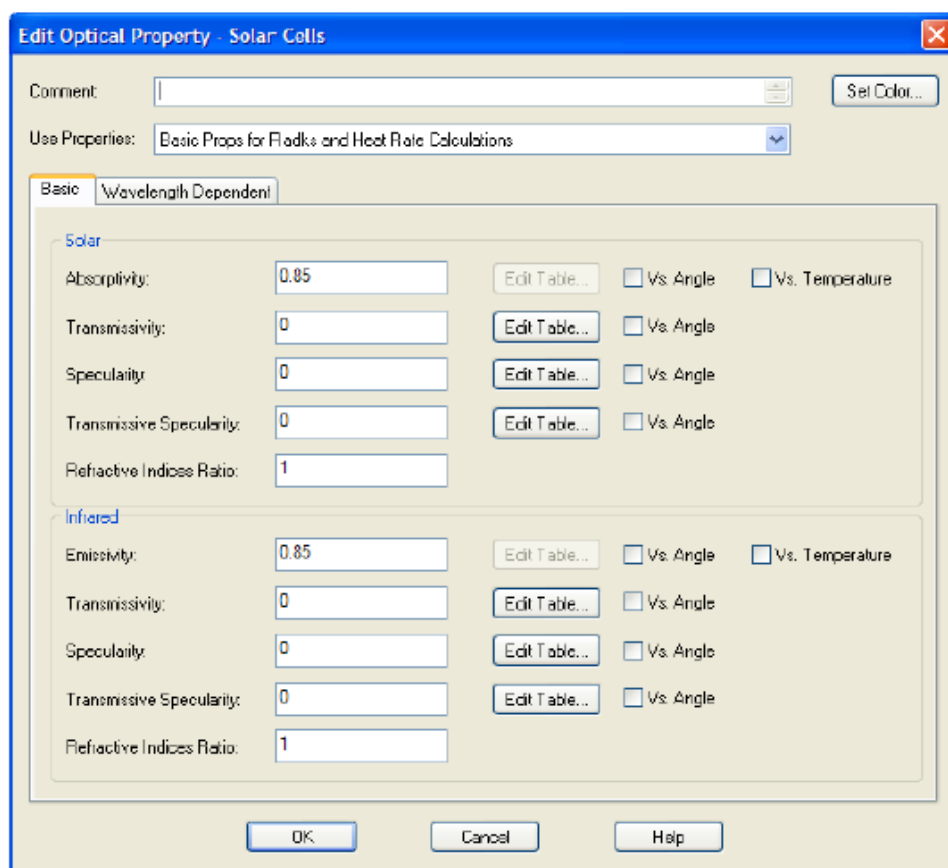


Figure 3.18: Edit Optical Property Dialog Box to Define Optical Property Values (Credits: *Thermal Desktop User's Manual* by C&R Technologies, Inc.).

The second field on the *Edit Optical Property* dialog box is the *Use Properties* field. The drop-down menu provides two options: *Basic Props for Radks and Heat Rate Calculations*, and *Wavelength Dependent for Radks, Basic for Heat Rate Calculations*.

For radk calculations, the choice of *Use Properties* field specifies whether the radks are based on the infrared properties on the *Basic* tab or the wavelength-dependent properties

on the *Wavelength-Dependent* tab. On either tab, the properties that can be defined are:

- **Emissivity/Absorptivity** Both values represent the fraction of incident radiation that is absorbed by the surface. Emissivity is also the fraction of energy emitted by the surface compared to a black-body at the same temperature. The values may be 0 to 1, inclusive. The sum of Emissivity (or Absorptivity) and Transmissivity at a given wavelength may not be greater than 1.
- **Transmissivity** The fraction of incident radiation that is transmitted through the surface. The values must be 0 to 1, inclusive, with 0 being a non-transmissive surface. The sum of Emissivity (or Absorptivity) and Transmissivity at a given wavelength may not be greater than 1. Non-zero transmissivity is only utilized for ray-tracing methods.
- **Reflectivity** The fraction of incident energy reflected away from the surface. The reflectivity of a surface is calculated by the program to be:

$$reflectivity = 1 - emissivity - transmissivity$$

- **Specularity** The fraction of reflected energy ($1 - emissivity - transmissivity$) that is reflected in a non-diffuse way. The values may be 0 to 1, inclusive, with 0 being diffuse (scattered) reflections, 1 being specular reflections and values in between being a combination of diffuse and specular. Non-zero specularity is only used for ray-tracing methods.
- **Transmissive Specularity** The fraction of transmitted energy that is transmitted in a non-diffuse way. The values may be 0 to 1, inclusive, with 0 being diffuse (scattered) transmission, 1 being specular transmission (optically clear) and values in between being a combination of diffuse and specular.
- **Refractive Indices Ratio** Specular transmissive rays may also model refraction. Refraction may be modelled by inserting a value for the *Refractive Index Ratio*. The ray is refracted through the surface according to Snell's Law

Thermophysical Properties

Thermophysical properties are physical properties of materials utilized for heat transfer and thermoelectric computations. Basic material properties are thermal conductivity, specific heat and density. Additional properties can be added to calculate phase change material loss (recession) due to added heat and Peltier effect devices. Thermophysical properties are saved in an external database and are referenced by name.

A thermophysical property database can be edited by adding new properties, editing existing properties, deleting properties, copying properties in the same database, importing properties from another database or renaming properties (*Thermal* → *Thermophysical*)

Properties → *Edit Property Data*, the *Edit Thermophysical Properties* dialog opens, as shown in Figure 3.19).

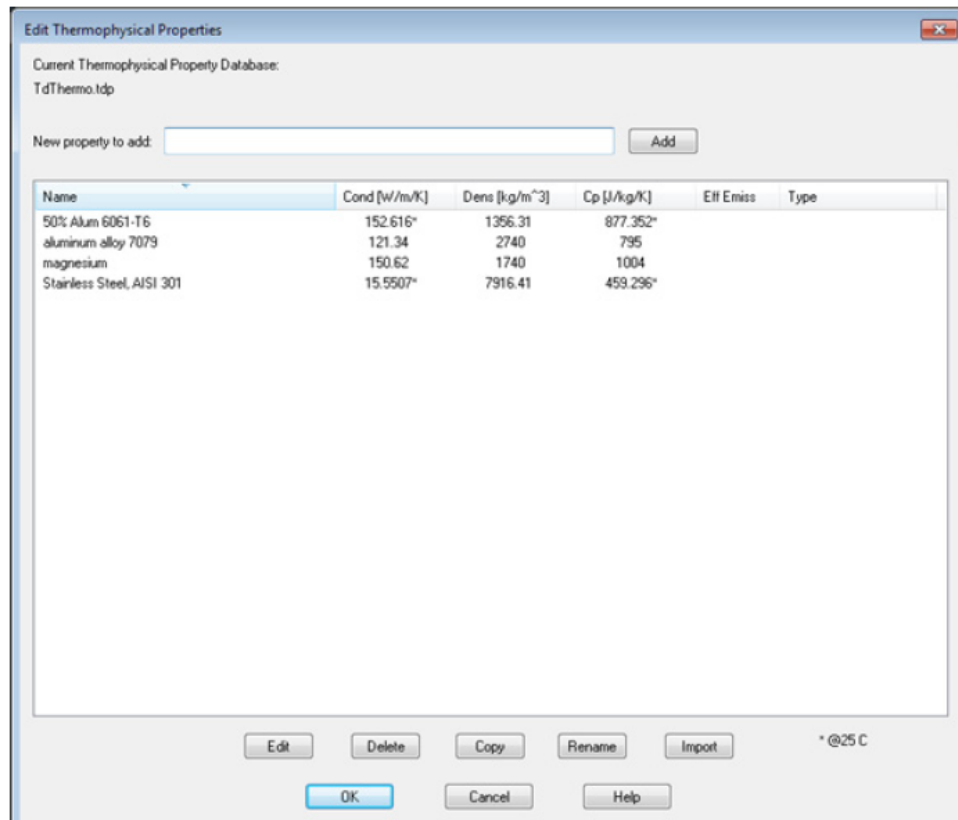


Figure 3.19: Edit Thermophysical Properties Dialog (Credits: *Thermal Desktop User's Manual* by C&R Technologies, Inc.).

To add a thermophysical properties, it has to be typed the name of the *New Property to Add* and selected *Add*, while to edit one it has to be selected the property to edit and then select *Edit* and make desired changes to the *Edit Thermophysical Property-Property Name* dialog, that opens in both cases and it is illustrated in Figure 3.20.

Basic Properties for Material is selected to specify primary material properties. The material may be a pure substance or a compound material with pre-calculated property values.

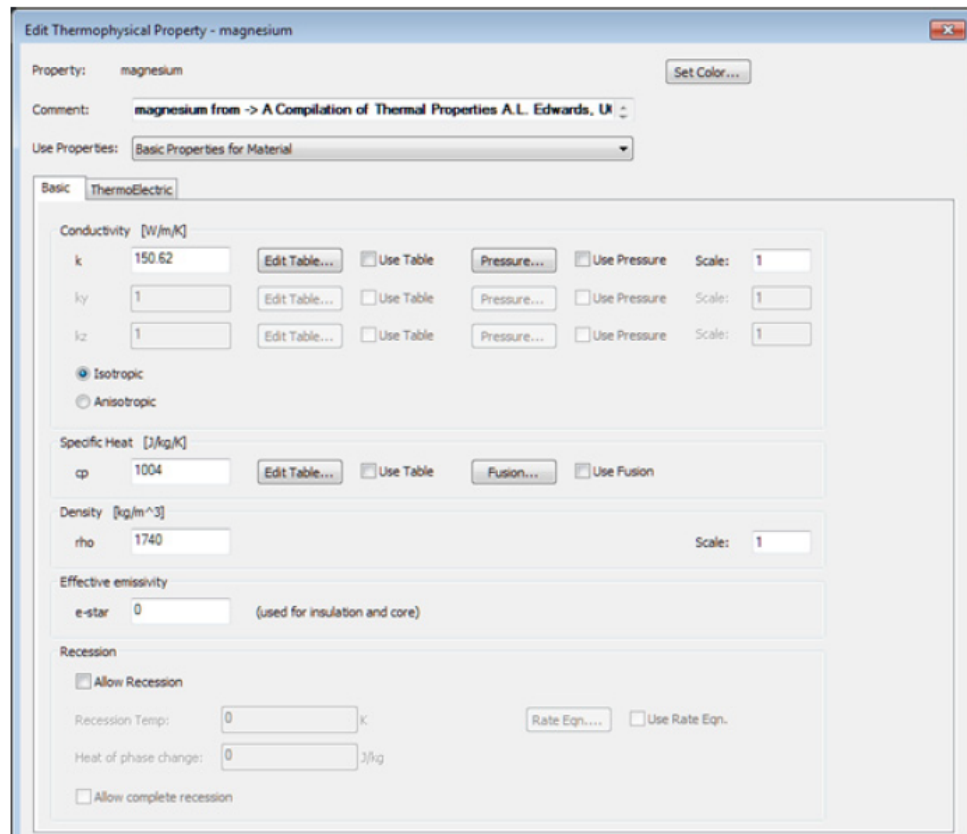


Figure 3.20: Edit Thermophysical Property - Property Name Dialog (Credits: *Thermal Desktop User's Manual* by C&R Technologies, Inc.).

3.2.2 Thermal Models

Radiation Analysis Groups

A common thermal model often consists of regions that are radiatively separate from one another. Less computer disk memory and CPU time will be utilized by dividing the problem into multiple radiation models, or analysis groups, rather than one unnecessarily large model. Furthermore, it may be useful to perform different types of radiation analysis for each part of the model. For example, energy absorbed from external heating sources may be calculated for the exterior surfaces of the model, while radiation exchange factors may be calculated for the interior and exterior surfaces of the model. Results for each of the radiation analysis groups (heating rates and/or radiation exchange factors) are put together when temperatures are computed with SINDA/FLUINT. Utilizing radiation analysis group also prevents the duplication of surfaces in separate models.

A radiation analysis group is thought as a set of surfaces, with the active side defined for each surface in the set. The active side is the side or sides of the surface that will take part in a radiation exchange calculation. An analysis group has a user-defined name and

this name is utilized when performing radiation calculations. A surface can belong to one or more analysis groups and can have the same or different active side specifications in each group. Names of analysis groups must be specified ahead of time before they may be utilized.

Selecting *Thermal* → *Radiation Analysis Groups* opens a dialog box to specify the names of RadCAD analysis groups. The *Thermal* → *Edit* dialog box is then utilized to assign surfaces to analysis groups. The *Radiation Analysis Group Manager* dialog box is illustrated in Figure 3.21. This dialog box permits new analysis group names to be added to the drawing database. Names have to be specified here before they can be utilized with the *Edit* dialog box.

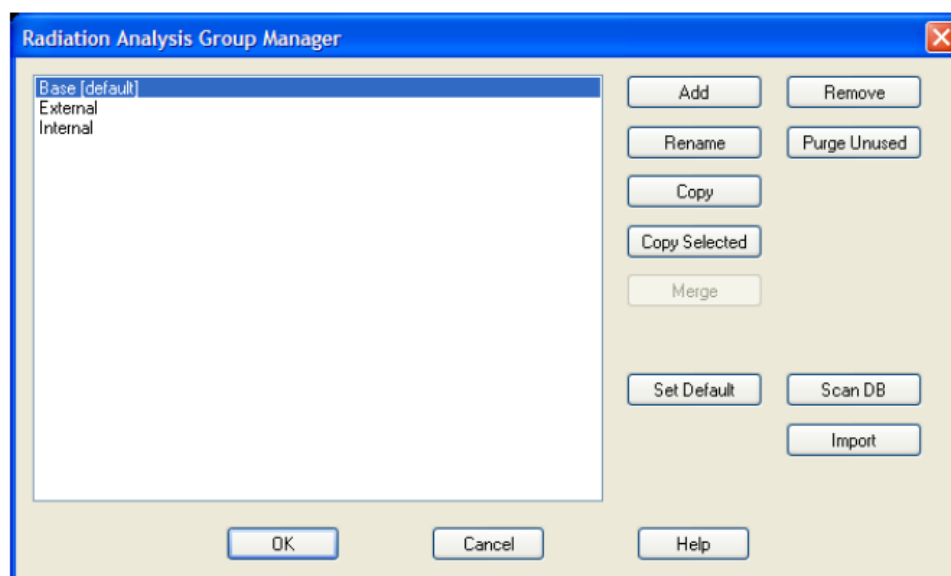


Figure 3.21: Radiation Analysis Group Manager Dialog Box (Credits: *Thermal Desktop User's Manual* by C&R Technologies, Inc.).

Thermal Submodels

Thermal submodels are arbitrary, user-defined subdivisions of the thermal model. At the least, submodels provide organization to the model. On a higher level, submodels permit to combine models without taking into account node or conductor ID conflicts. Moreover, submodels can be utilized for configuration changes and monitoring the behaviour of the solution. All thermal entities (nodes, conductors, heat loads, user logic) are put in a thermal submodel. If a submodel is cut out from the solution, the nodes, conductors, user logic and anything else included in that submodel are unavailable for that solution.

Selecting the *Thermal* > *SINDA Submodels* command opens the *SINDA/FLUINT Submodel Manager Form* dialog box that permits submodel names to be specified (as shown in Figure 3.22). These names will then be available on a pull-down lists when assigning node IDs to surfaces using the *Edit* dialog box. Submodel names should be specified here

before they are utilized to name thermal nodes, but, if a submodel name is manually typed into a field while editing a Thermal Desktop object, a dialog box will open asking for confirmation to add the submodel to the *Submodel Manager*, if it does not already exist. Submodel names may be added at any time during the creation of a model.

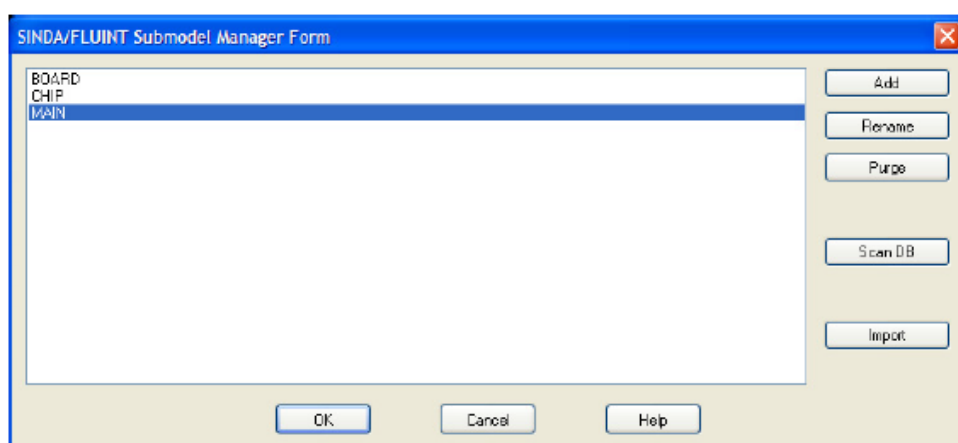


Figure 3.22: SINDA/FLUENT Submodel Manager Form Dialog Box (Credits: *Thermal Desktop User's Manual* by C&R Technologies, Inc.).

Thin Shell

Thin shells are geometrical thermal objects that are displayed without a displayed thickness. Each thin shell can have a thickness specified that is utilized for conductance and capacitance calculations, even if the thickness is not visible.

In Thermal Desktop, thin shells can be finite difference primitive shapes, finite difference arbitrary shapes or finite elements. The finite difference primitives are specific geometric shapes that have internal conductances calculated using finite difference conduction methods. The finite difference arbitrary shapes are usually assumed to be a single node without internal conduction. The finite element thin shells have internal conductances calculated using finite element methods.

The finite difference shells are created using the *Thermal* → *Surfaces/Solids* submenu and selecting the desired shape. Finite elements can be created manually, but they are more commonly created using *TD Mesher*, or created by *TD Direct* or a third-party tool and then imported.

When a thin shell is created or edited, the *Thin Shell Data* dialog is displayed. This is subdivided into tabs, which availability depends on the selected thin shell. The finite difference primitive shapes can provide computational efficiency unavailable to finite elements, because they maintain a mathematically correct shape regardless of nodal resolution, hence the surface area and radiation reflections will be accurate whether the number of nodes defining the shape is. The primitives can also be determined parametrically. Each thin shell has its own method of creation and its own set of parameters.

The finite difference primitive shapes are: *Box*, *Cone*, *Cylinder*, *Disk*, *Ellipse*, *Ellipsoid*, *Elliptic Cone*, *Elliptic Cylinder*, *Offset Paraboloid*, *Ogive*, *Parabolic Trough*, *Paraboloid*, *Rectangle*, *Scarfed Cone*, *Scarfed Cylinder*, *Sphere* and *Torus*. While, the finite difference arbitrary shapes instead are *From AutoCAD Surface* and *Polygon*.

When a thin shell is created, graphical nodes will also be drawn. These nodes are attached to the surface and will be updated if the surface is moved or resized, in the case of the finite difference shells. Finite elements are attached to nodes and the node must be moved to move the element or change its shape.

When a new Thermal Desktop surface is created or the *Edit* command is selected, a *Thin Shell Data* dialog box is opened (as shown in Figure 3.23).

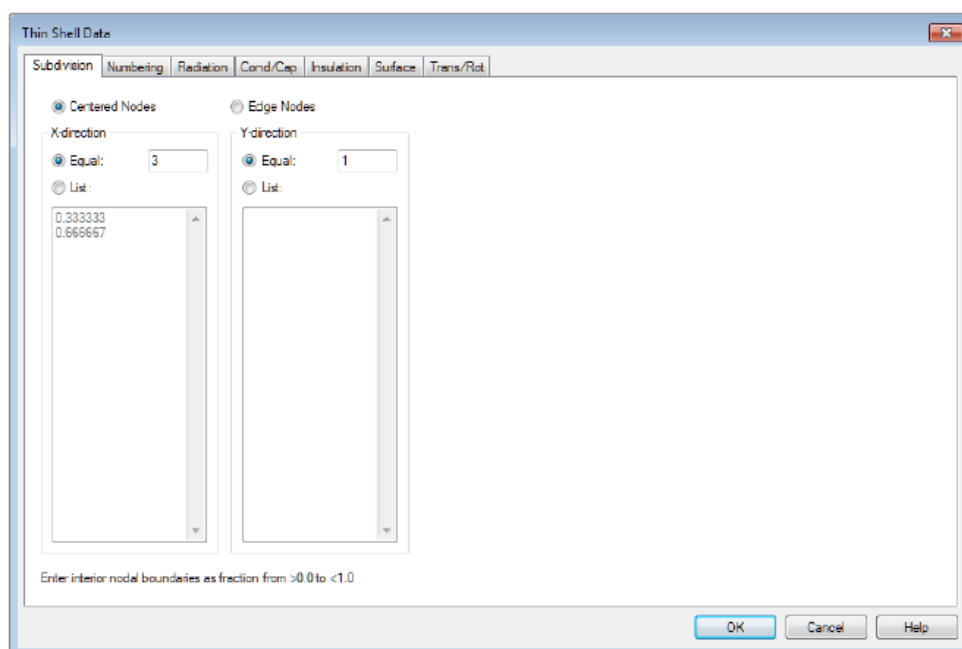


Figure 3.23: Thermal Desktop Thin Shell Edit Form and Subdivision Tab (Credits: *Thermal Desktop User's Manual* by C&R Technologies, Inc.).

Subdivision Tab If a custom conic surface is being edited, the *Subdivision* tab (illustrated in Figure 3.23) will be available in the *Thin Shell Data* dialog box, while it will not be present if more than one surface or a converted mesh surface is being edited.

First of all, the user has to decide the placement of the nodes on the surface. The *Centered Nodes* option locates the nodes at the node center. The *Edge Nodes* option also locates the nodes at the center of the nodal area, but will make the nodes span the entire surface by adding "half" nodes on the edges and "quarter" nodes at the corners. Users should adopt the *Edge Nodes* option when connections between custom conic surfaces is desired. When two surfaces that have edge nodes share a common edge and have the same nodal breakdown, the nodes that they share may be merged into a common set of nodes. The "half" nodes now become "whole" nodes again and the connection is equivalent to folding

a regular centered node surface along a nodal centerline. Edge nodes are usually preferred for edge contact calculations as well, since conductors will be computed all the way to the edge of the surface.

The *Subdivision* tab has two identical sections for defining the nodal breakdown in each of the two principle directions of the surface. The labels indicate the nodal breakdown directions according to the type of surface being edited. A uniform spacing of nodal boundaries can be obtained by selecting the *Equal* radio button and typing the number of nodes desired in the particular direction into the corresponding input field. Nodal boundaries can be located at arbitrary positions by selecting the *List* radio button, activating the *List* input field and typing nodal boundary values.

Numbering Tab The *Numbering* tab of the *Thin Shell Data* dialog box, illustrated in Figure 3.24, defines the submodels and node IDs for the *Top/Out* and the *Bottom/In* sides of a surface. The "top" side of a flat surface is in the +Z direction of the local coordinate system, determined by traversing the vertices in a counter-clockwise direction according to the right-hand rule. The "out" side refers to the exterior side of curved Thermal Desktop custom surfaces. The "bottom" or "in" side is the opposing side.

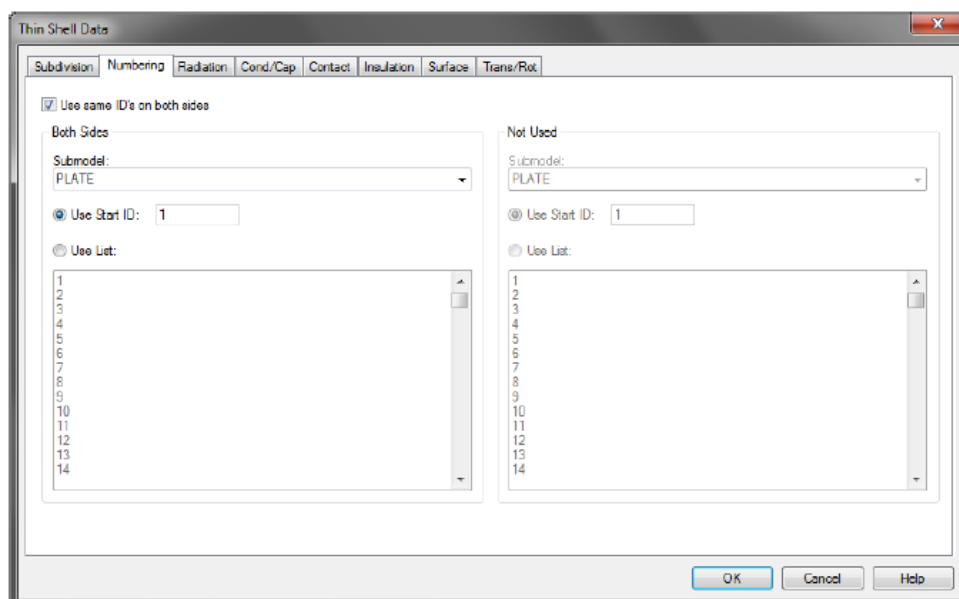


Figure 3.24: Thin Shell Data Dialog Box Numbering Tab (Credits: *Thermal Desktop User's Manual* by C&R Technologies, Inc.).

The *Use same IDs on both sides* check box permits to choose between a true 2D thermal network for the surface (checked) or a 3D thermal network which includes two nodes through the thickness of the surface (unchecked). This second method is utilized for simplified modeling of a sandwich or honeycomb panel. The materials and material thicknesses are defined on the *Cond/Cap* tab. This option is only available for finite difference surfaces.

Radiation Tab The *Radiation* tab of the *Thin Shell Data* dialog box, illustrated in Figure 3.25, permits the selected surface(s) to be assigned to one or more analysis groups and also permits the optical properties of the surface to be specified. Surfaces may be placed in any number of RadCAD analysis groups, with different active sides. Analysis group names have to be specified ahead of time with the *Radiation Analysis Groups* menu choice before they can be utilized in the *Thin Shell Data* dialog box.

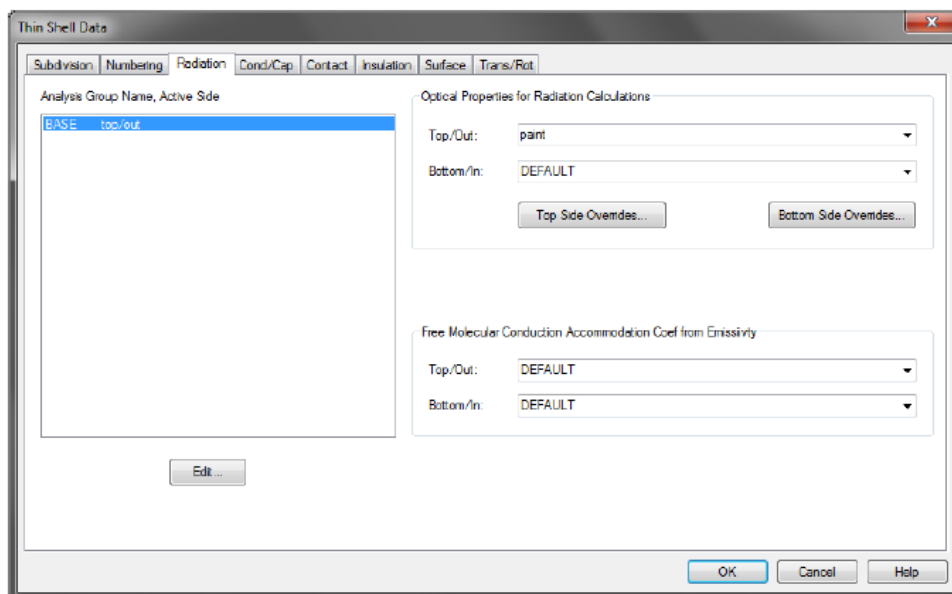


Figure 3.25: Thin Shell Data Dialog Box Radiation Tab (Credits: *Thermal Desktop User's Manual* by C&R Technologies, Inc.).

The user may modify the active side of an analysis group by either double clicking on the name in the list or by selecting one or more names in the list and then selecting *Edit*. Upon editing, an *Edit Active Side* dialog box will be displayed and user can select the active side for the edited set.

As said, this tab also assigns optical property references to each side of the surface. Names can be inserted directly into the fields or they can be set from the pull-down list of properties. The pull-down list contains the list of currently defined property aliases, followed by the list of properties defined in the actual property database file.

Cond/Cap Tab Output of capacitance and conductance data to SINDA/FLUINT may be defined by the *Thin Shell Data* dialog box *Cond/Cap* tab as illustrated in Figure 3.26.

The drop-down field permits to select a material from the thermophysical properties database or from alias names created in the current DWG file. When *Use same IDs on both sides* check box is unchecked on the *Numbering* tab, the material has to be defined for both sides (*Top/Out* and *Bottom/In*) and the user must also define the material and distance between the nodes (*Separation*). The material utilized for the *Separation* can have

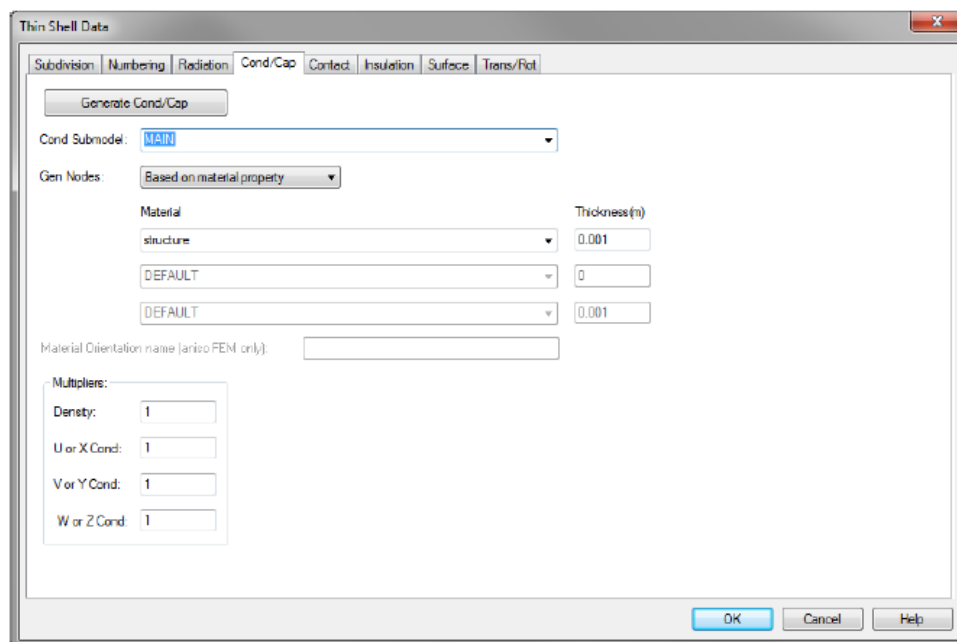


Figure 3.26: Thin Shell Data Dialog Box Conductance-Capacitance Tab (Credits: *Thermal Desktop User's Manual* by C&R Technologies, Inc.).

an effective emissivity specified.

For the other *Tabs* and *Surfaces* not described in this section a complete discussion is provided by *Thermal Desktop User's Manual* [8] by C&R Technologies, Inc.

Finite Difference (FD) Solids

Thermal Desktop supports three kinds of finite difference solids. They are bricks, cylinders and spheres. Arbitrary shaped solids may be built and analysed in Thermal Desktop using finite elements. Editing of *FD Solids* is very similar to editing surfaces. The *FD Solid Edit* dialog box utilizes a similar "tabbed" format.

Subdivision Tab The *FD Solid Edit* dialog box *Subdivision* tab permits the user to set the subdivision for the three primary directions of the solid.

Numbering Tab The *FD Solid Edit* dialog box *Numbering* tab permits the user to set the submodel name and node IDs for the nodes that are attached to the solids.

Cond/Cap Tab The *FD Solid Edit* dialog box *Cond/Cap* tab permits the users to select to *Generate Cond/Cap* as well as set the *Material* for the solid and the submodel that the conductors will be located in. The user may also select to generate the nodes based on the material property or as arithmetic.

Radiation Tab The *FD Solid Edit* dialog box *Radiation* tab permits the user to set the optical properties of each face as well as which faces will be active in each analysis group. The user is not only able to set the analysis groups and optical properties for the outside faces of the solid, but also the inside faces. This is useful in modelling of transparent solids and internal reflecting faces.

Conductors

A conductor, or set of conductors, can be created by utilizing one of the three menu choices under the *Thermal* → *FD/FEM Network* menu: *Node-to-Node Conductor*, *Node-to-Nodes Conductor* and *Node-to-Surface Conductor*.

When the *Node-to-Node Conductor* command or *Node-to-Nodes Conductor* command is selected, the user is prompted to specify a single node (the primary node) followed by either another single node or a group of nodes (the target node or nodes), respectively. Once the conductor is created the number of nodes is not limited, however, only nodes can be the target of the conductor.

When the *Node-to-Surface Conductor* command is selected, the user is prompted to select a single node (the primary node) and any number of thin shells (finite difference or finite element surfaces), finite difference solids or pipes (the conductor targets). Domain tag sets can also be adopted for the conductor target. Finite element solids cannot be chosen directly, but had to be surface coated with planar elements for the connection.

After completing the command, conductor lines will be displayed from the primary node to each of the target nodes. For *Node-to-Surface conductors*, the target nodes are the nodes associated with the target objects and arrows will specify the side or sides of an object to which the conductor is linked. The conductor definition may be modified by selecting any one of the conductor lines followed by the *Thermal* → *Edit* command. The *Conductor* dialog box is illustrated in Figure 3.27.

The conductor *Type* can be one of three general options: *Generic*, *Natural Convection* or *Function of Temperature Difference*. The *Natural Convection* options are not permitted for *Node-to-Node(s) conductors* unless the target nodes present in the *To* list of the *Conductor* form are associated with a geometric object.

Generic conductors may be specified to be bi-directional or one way. Bi-directional heat flow permits heat to flow in either direction depending on the temperatures of the two bodies. One-way conductors are typically adopted for abstract model duplication or simple (no pressure drop) flow calculations. *Generic* conductors can be time dependent (*Vs. Time* checkbox) or a function of the temperature difference between the two nodes of each generated conductor (*Vs. Temp Diff* checkbox). If either of these two options is checked, the user must input an array to determine the dependence by clicking the *Array...* button. For *Generic* conductor types, the conductor parameter is typed into the field just below the *Type* drop-down list. The name, use and units of the value are taken from the *Use material*, *Radiation conductor* and *Per Area* checkboxes.

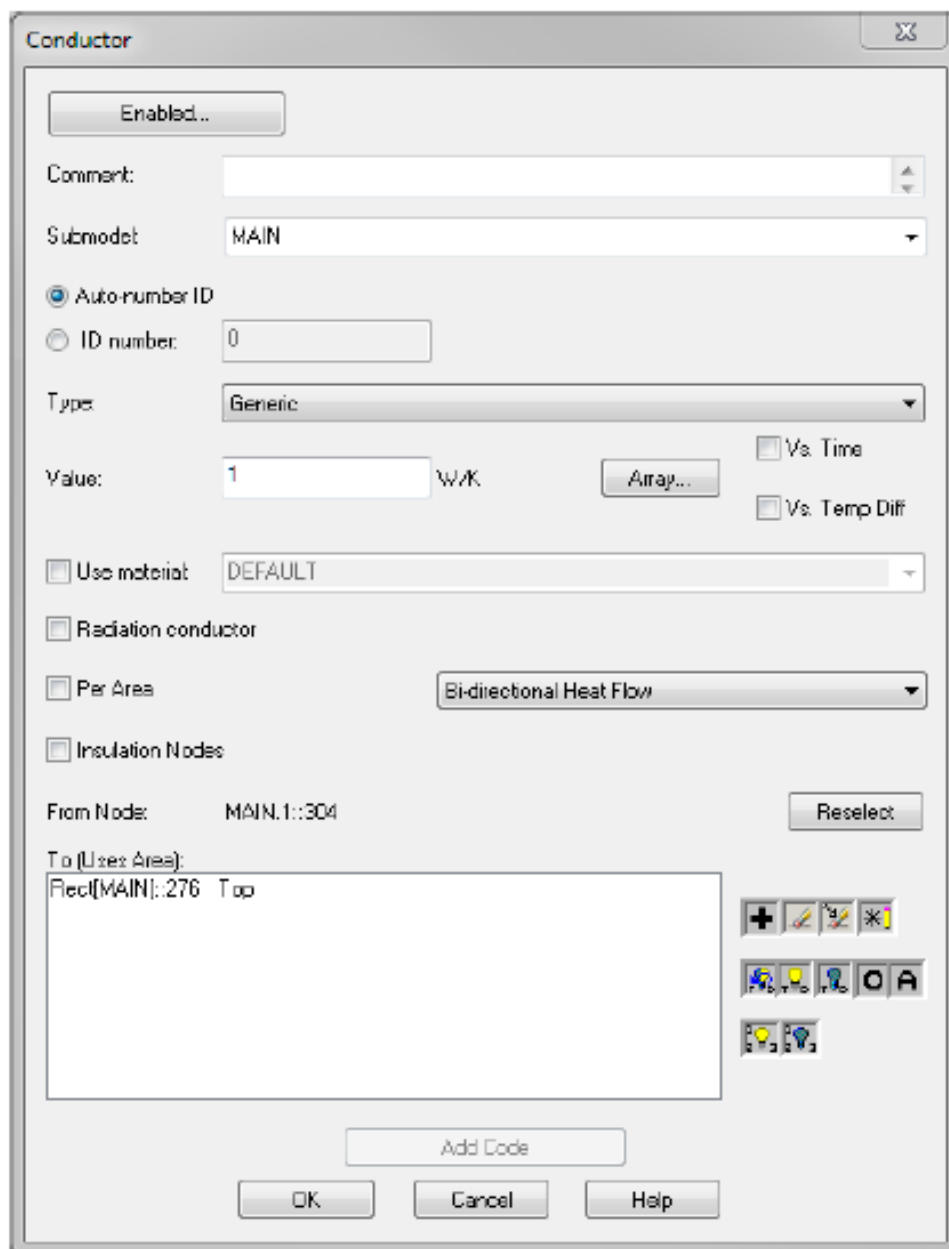


Figure 3.27: Conductor Dialog Box (Credits: *Thermal Desktop User's Manual* by C&R Technologies, Inc.).

With *Use material*, *Radiation conductor* and *Per Area* all unchecked, the *Value* field contains a conductance. This value is divided amongst the individual conductors weighted relative to the area of the *To nodes* (target nodes). For node-to-node(s) conductors, the value is evenly divided among the target nodes if any of the target nodes are free nodes (nodes not associated with geometric objects). The sum of all conductor conductances created by this conductor form will sum to the *Value* independent of the size of the sur-

faces. If the *Per Area* checkbox is checked and *Use material* and *Radiation* conductor are unchecked, then the *Value* is multiplied by the area of each node associated with objects in the *To* list. Therefore a change in the size of the *To* objects would result in a change in the total conductance. The *Per Area* option cannot be utilized with free nodes (nodes not associated with geometric objects) as the target nodes. If *Use material* is checked and *Per Area* is unchecked (*Radiation* conductor and *Use Material* are mutually exclusive), the input value is *Area/length*, where area is the cross-sectional area of the heat transfer path and length is the distance along the heat transfer path.

The conductance is computed internally by multiplying the conductivity of the defined material by the value in the *Area/length* field. The resulting total conductance is divided amongst the individual conductors weighted relative to the area of the *To* nodes. For node-to-node(s) conductors, the value is evenly divided among the target nodes if any of the target nodes are free nodes (nodes not associated with geometric objects). If *Use material* and *Per Area* are both checked, the input field is *Length*. The conductance is computed internally by dividing the specified material's conductivity by the *Length* value and then multiplying that value by the area of each node for each individual conductor.

Contactors

Contactors are a user-defined thermal conductance between two or more high-level objects, such as 2D surfaces, 3D solids (FE solids must first be surface coated) and FloCAD pipes. Contactors are defined as "from" one or more objects "to" one or more objects. The designation of "from" and "to" has a significant effect on how the connection is calculated.

The *FD/FEM Network* \rightarrow *Contactor* command will prompt the user to specify objects between which contact conductors are to be created. The user first selects a group of objects from which contactors are to be generated, then have to be selected the objects to which the contact might be made. Obviously an object cannot have a contactor to itself. When selection is complete, the *Contactor* dialog box opens as illustrated in Figure 3.28. The *Contactor* dialog box permits the user to:

- define the thermal submodel to contain the generated conductors;
- define whether the edges or the faces of the object are utilized to find connections;
- specify the conduction coefficient;
- select the number of integration intervals;
- set the tolerance (or allowable gap) for connections;
- select the connection testing algorithm;
- specify scaling factors;
- select the specific edges or faces of objects between which connections will be made;

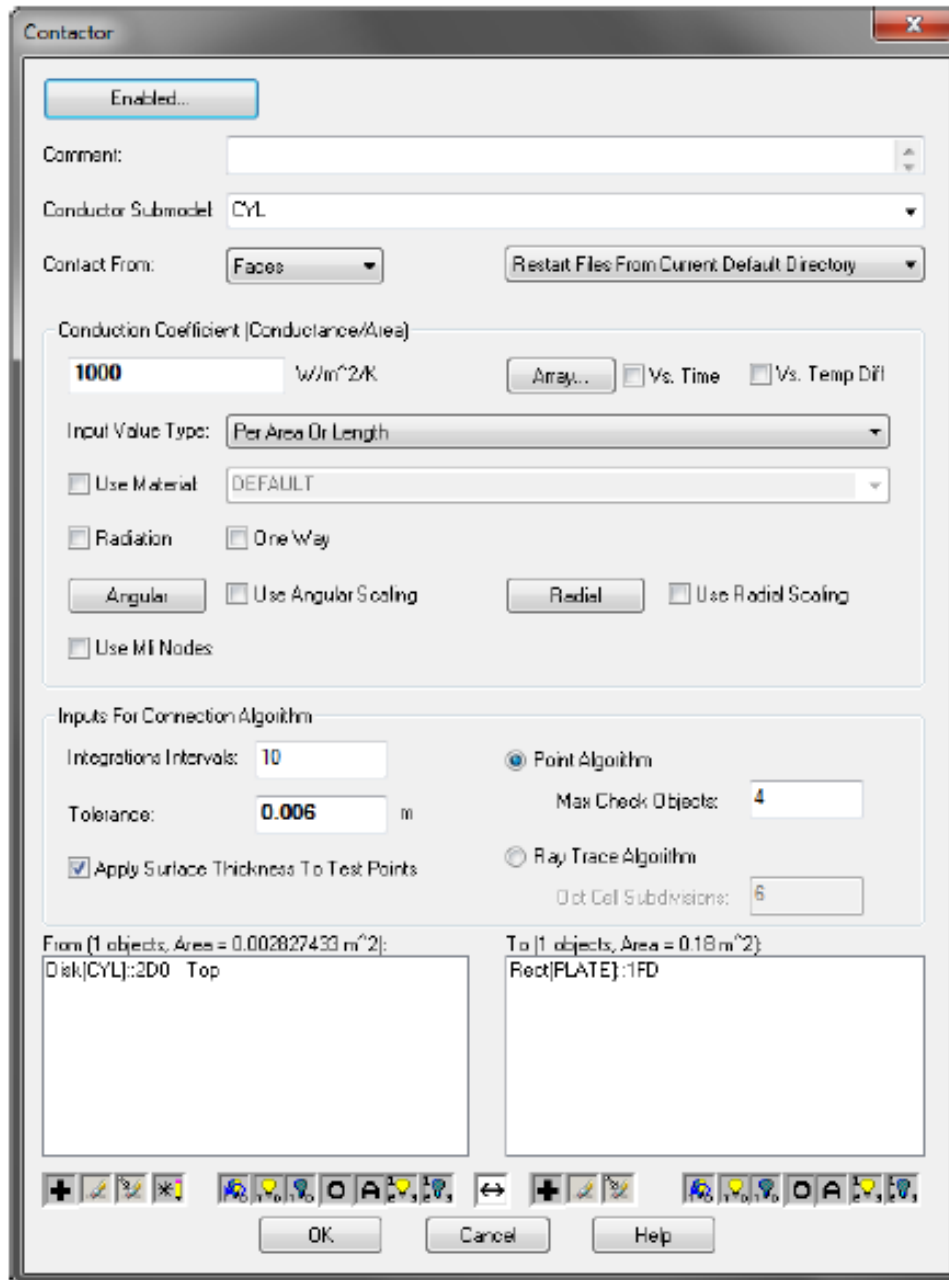


Figure 3.28: Contactor Dialog Box (Credits: *Thermal Desktop User's Manual* by C&R Technologies, Inc.).

The *Conduction Coefficient* section of the *Contactor* dialog box, along with the geometry of the *From* objects and the integrated contact area, form the basis for the conductors to be created for SINDA/FLUINT. In this section, the user can determine a fixed conduction coefficient or specify the value as a function of time or temperature. The user can also make selections to specify the contactor to be based on a conductive material, material

independent or even based on radiation. The *Input Value Type* defines how the *Conduction Coefficient* is distributed on the contacting areas.

- *Per Area Or Length* multiplies the *Conduction Coefficient* by the contacted area of each node on the *From* surfaces. The total value of conductors will be (*Conduction Coefficient*) · (total contacted area of *From* surfaces).
- *Absolute - (If not 100% connected, total cond output is less than input value)* determine the total conductance of all *From* surfaces. If the *From* surfaces are not completely in contact with *To* surfaces, then the total value of conductors will be minor than the given *Conduction Coefficient*. The total value of conductors is distributed among the nodes of the *From* surfaces proportional to their contacted areas. The total value of conductors will be (*Conduction Coefficient*) · (total contacted area of *From* surfaces) / (total area of *From* surfaces).
- *Absolute - (Total conductance output equals input value)* determines the total conductance of the contactor. The conductance coefficient is distributed among the nodes of the *From* surfaces proportional to their contacted areas.

Selecting *Use Material* will permit the user to select a material in the material properties database with the drop-down list; the conductivity of the material, even temperature- or pressure-dependent, is utilized in the calculation of the resulting conductances. Some common uses for contactors and suggested settings are provided in Table 3.3.

Type of Contact	Conduction Coefficient	Input Value Type	Use Material	Radiation
Conductance	conductance	Absolute	not checked	not checked
Conductance coefficient	conductance per edge length	Per area or length	not checked	not checked
Interface material	interface width/interface thickness	Per area or length	checked with desired material selected	not checked
Bolted interface	bolt conductance per number of bolts	Absolute	not checked	not checked
Interface pad or gasket with known resistance	1/resistance	Absolute	not checked	not checked
Radiation (F_{ij})	Interface width · ε_{eff} · F_{ij}	Per area or length	not checked	checked

Table 3.3: Contact from Edges/Faces (Credits: *Thermal Desktop User's Manual* by C & R Technologies, Inc.).

The *Integration Intervals* option defines the number of test points on nodes within the *From* surfaces for determining the interface area or length of the contactor. The *Tolerance* value specifies the distance a *To* object may be from a test point to allow a connection. If the *From* surface or edge is larger than the *To* surfaces, then a reasonable tolerance had to be set. Furthermore, adiabatic sections of the *From* surface can be specified by using small tolerances. When connecting from small objects to large objects and no adiabatic sections exist, then the tolerance may remain at a very large value.

Heat Loads

The *FD/FEM Network → Heat Load On Surfaces/Nodes/Solids* commands allows the user to apply a constant or time varying heat load to specific entities. After selecting the entities to receive the heat load, the *Heat Load Edit Form* dialog box, pictured in Figure 3.29, will open.

When adopting *Heat Load on Nodes*, only nodes can be used. If the node is associated with a surface or solid, the heat load can be specified as an absolute load or a flux. For a flux on a heat load on nodes, the surface area of the node is utilized based on the selection of top, bottom or both. When adopting *Heat Load on Surfaces*, surfaces or solids may be used. If a solid is chosen, the heat load will be applied to the selected faces of the solid. Finite element solids must be surface coated to be selected. Again, the heat load can be defined as absolute or a flux. When adopting *Heat Load on Solids*, only solids or solid elements may be used. The heat load may be defined as absolute or volumetric. When volumetric or flux heat loads are adopted, the value provided for the heat load is multiplied by the volume or area, respectively, of each node. When an absolute heat load is adopted, the value provided is the total for all objects and the heat load applied to each node is evenly divided among the nodes if the heat load was applied to nodes, proportional to the surface area of each node if the heat load was applied to surfaces, and proportional to the volume of each node if the heat load was applied to solids.

If the heat load is time dependent, the user must input an array of time dependency with an optional multiplier of the array data values. A time varying heat load is thought to be periodic. If a periodic heat load is not desired, the user should insert values that represent the entire time of a transient run. Also, if a time varying heat load is input and a steady state solution is being solved, then the time average heat load will be utilized for the steady state calculations.

If the heat load is temperature dependent, the user must input an array of temperature dependency utilizing the *Array* button or may define an existing SINDA array. For both options, an optional multiplier of the array data values can be defined.

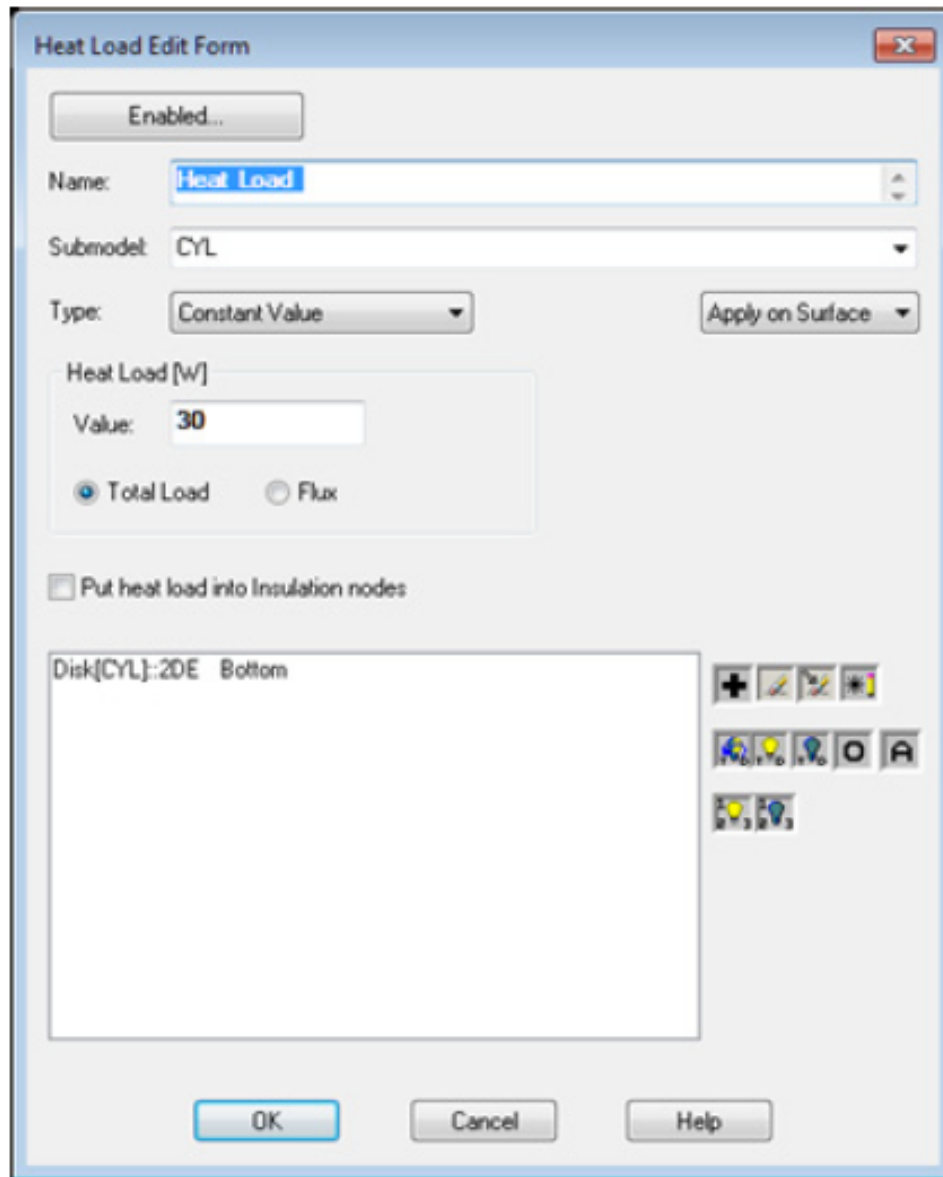


Figure 3.29: Heat Load Edit Form Dialog Box (Credits: *Thermal Desktop User's Manual* by C&R Technologies, Inc.).

Heaters

The *Thermal* → *FD/FEM Network* → *Heater* command permits the user to apply a temperature dependent heater to nodes or surfaces. A heater is a thermostatically controlled heat load. The temperature utilized for the control ("sensed" as with a thermocouple) can be a different placement than where the heat load is applied. The user is first prompted to choose the objects receiving heat, then the sensor objects. If no sensor objects are selected, the heated objects will be adopted as the sensing objects. Objects that may be utilized

for heaters or sensors are nodes, finite difference surfaces and solids, planar elements, and FloCAD pipes. Once the objects are chosen, the Heater Edit Form dialog box will be displayed, as illustrated in Figure 3.30.

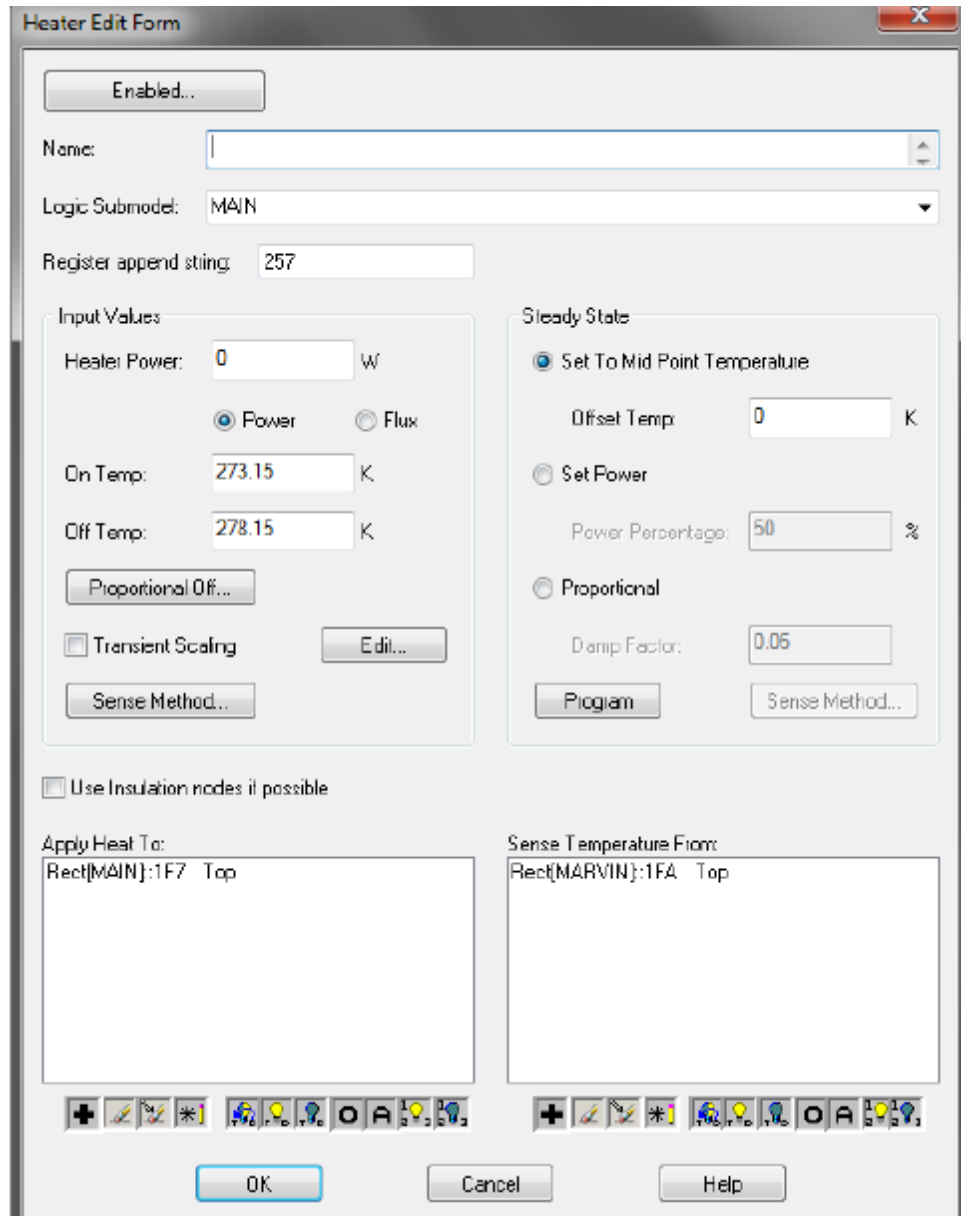


Figure 3.30: Heater Edit Form Dialog Box (Credits: *Thermal Desktop User's Manual* by C&R Technologies, Inc.).

On the left side of the dialog box the user types the available *Heater Power* and the set-point temperatures (*On Temp* and *Off Temp*) to cycle the heater on and off. The heater power may be input as a flux or power and may be negative as well. This permits the heater to perform as a cooler with thermostat.

For heaters and coolers, the *On Temp* must always be lower than the *Off Temp*; Thermal Desktop will write the proper logic for heaters or coolers.

3.2.3 External Heating Environments and Orbits

Thermal Desktop provides a complete external heating environment definition and viewing facility.

New heating rate cases are created by selecting *Thermal* → *Orbit* → *Manage Orbits*, which then opens the *Heating Rate Case Manager* dialog box, pictured in Figure 3.31. Multiple orbit definitions can be created and saved under user specified names pushing the *Add* button.

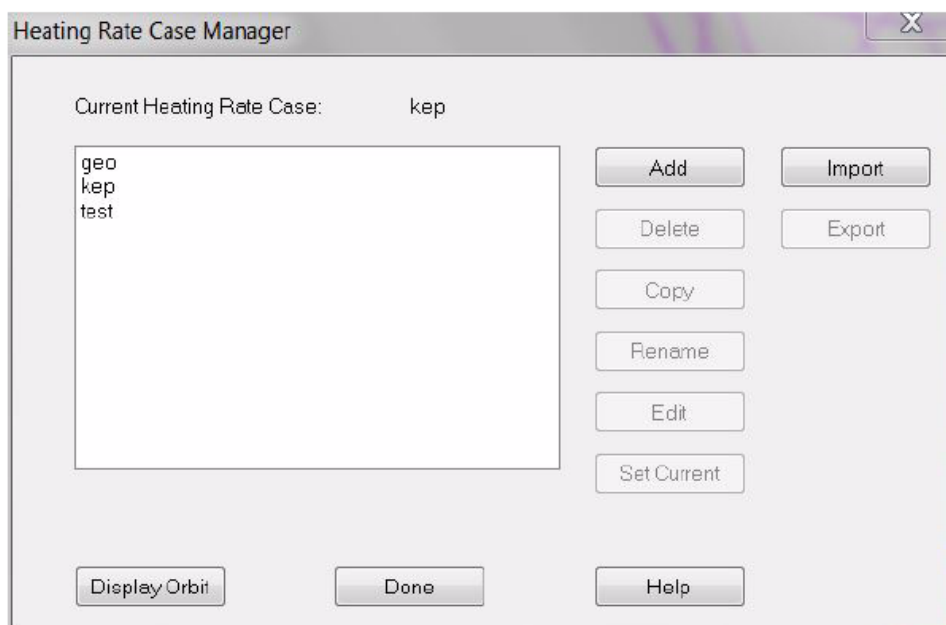


Figure 3.31: Heating Rate Case Manager Dialog (Credits: *Thermal Desktop User's Manual* by C&R Technologies, Inc.).

All menu operations using orbits are performed on the actual orbit. The user can choose an orbit from the list in the *Heat Rate Case Manager* dialog, then select the *Set Current* button to set the current orbit. The orbit will be edited when *Orbit* > *Edit Current Orbit* is selected. The current orbit will be used when heating rate calculations are performed utilizing commands from the menu, and for *Model Checks* > *View Model from Sun/Planet*. After orbits are specified and a heating rate environment case computed, heating rate data may be output for utilizing by a thermal analyser.

The type of external heating that can be created in the *Heating Rate Case Manager* dialog box are:

- *Basic Orbit*

- *Keplerian Orbit*
- *Planetary Latitude, Longitude, Altitude List*
- *Vector List*
- *Free Molecular Heating using a Vector List*
- *Free Molecular Heating with Reference Orbit*

The *Heating Rate Case* dialog box for the orbit is organized with tabs which provide the tools for defining the shape of the orbit, planet related data, the orientation of the vehicle, the number of orbit positions for heating rate calculations and optional spin.

Orientation Tab

The orientation of the spacecraft is defined using the *Orientation* tab, illustrated in Figure 3.32. This tab is available for *Basic*, *Keplerian*, or *Planetary* environments.

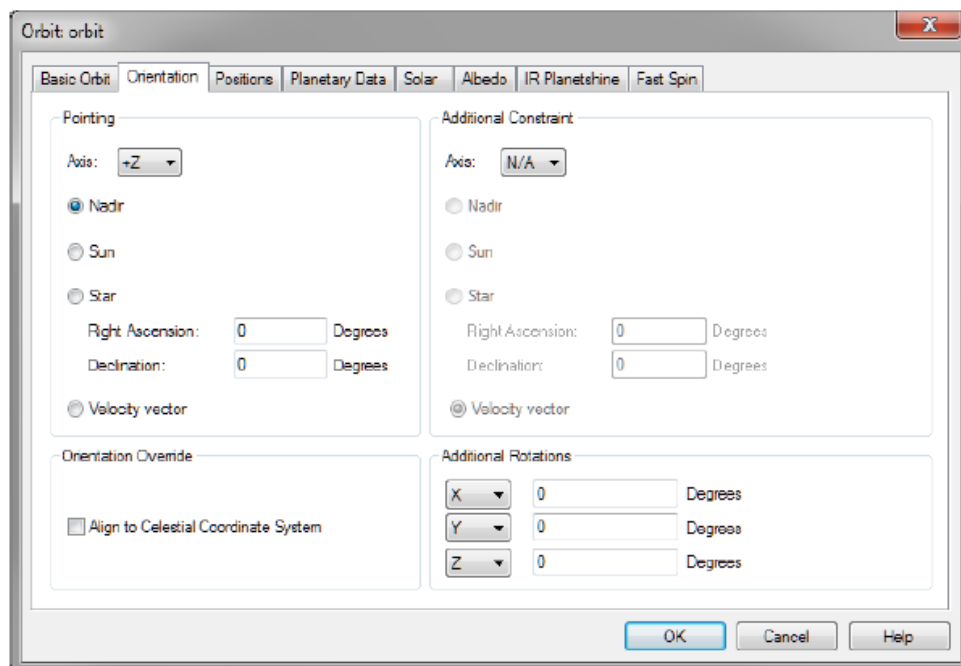


Figure 3.32: Specifying the Orientation of the Spacecraft in Basic and Keplerian Orbits (Credits: *Thermal Desktop User's Manual* by C&R Technologies, Inc.).

The regions *Pointing* and *Additional Constraint* permits aligning the entire system adopting the World Coordinate System. The + or - Z axis can be defined to point directly at a target. Optionally, another constraint can be applied by orienting a second axis. The selected constraint axis (+X, -X, +Y or -Y) will be rotated about the pointing axis to align

as close as possible to the additional constraint target.

The target that can be selected are:

- *Nadir/Zenith*. The Nadir is center of the orbital central body and will be an option in the *Basic* and *Keplerian* orbits. Zenith is normal to the planetary surface and will be an option for the *Planetary* environment.
- *Sun*. The center of the Sun.
- *Star*. A point in the celestial sphere defined by the *Right Ascension*, measured from the *Vernal Equinox* and the *Declination*.
- *Velocity vector*. The tangent to the orbit path or East for *Planetary* environment

When *Align to Celestial Coordinate System* is checked, the system will be aligned to the Celestial coordinate system. Any pointing and constraint options are ignored. This option is helpful when orbital manoeuvres are complex or if the spacecraft orientation is specified by data calculated in an external program.

The *Additional Rotations* can be utilized to perform the manoeuvres from a fixed coordinate system. After the vehicle coordinate system is aligned adopting one of the pointing operations, additional rotations may be applied by utilizing the input fields in *Additional Rotations* region, through the drop-down lists specifying the axis of rotation. The rotations are applied in order from top to bottom. Expressions may also be utilized to modify the spacecraft orientation during the orbit.

Planetary Data

The planet, moon or star about which the satellite orbits is defined by the data input on the *Planetary Data* tab on the *Orbit* dialog box illustrated in Figure 3.33. Parameters may be typed directly or set from default values utilizing the *Reset to* drop-down list.

- *Radius of Planet*. The mean radius of the planet.
- *Gravitational Mass (GM)*. The product of the gravitational constant (G) and the planet mass (M). This may also be referred to as the standard gravitational parameter in some references. The *Gravitational Mass* is always input in km^3/sec^2 .
- *Inclination of Equator*. It is the angle between the planet's equatorial plane and its ecliptic plane.
- *Sidereal Period*. It is the time for the planet to complete one revolution when viewed from a fixed inertial position.
- *Mean Solar Day*. It is the time for the planet to complete one revolution with respect to the Sun.

- *Color*. This button permits the user to choose the color of the sphere used to represent the planet in orbit view.
- *Reset to*. The user may modify the planet or reset the values to default values by choosing a new planet in the *Reset to* field drop-down list. Choosing the Sun in the *Reset to* field makes the orbit heliocentric.

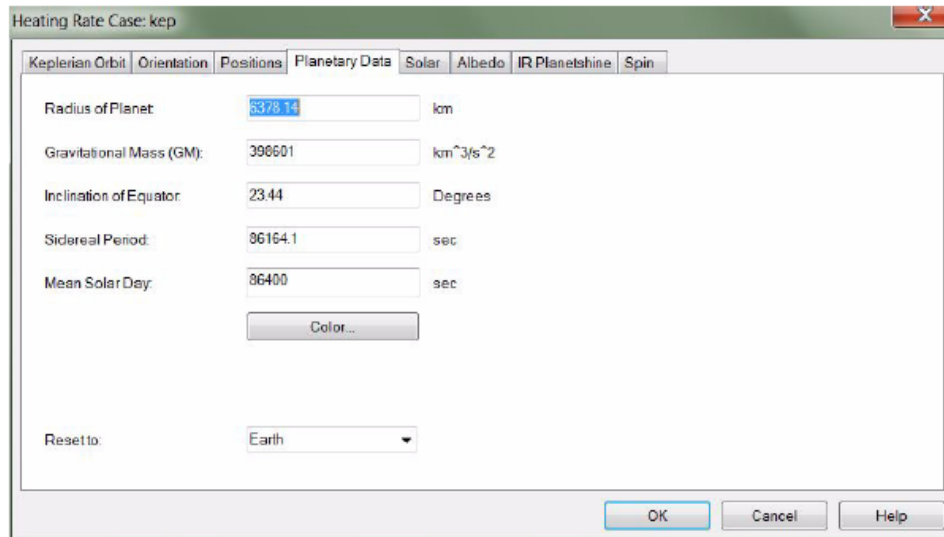


Figure 3.33: Specification of Planetary Data For an Orbit (Credits: *Thermal Desktop User's Manual* by C&R Technologies, Inc.).

Keplerian Orbit

The dialog box for specifying a *Keplerian* orbit is pictured in Figure 3.34. This tab contains input fields to specify the shape of the orbit and its orientation relative to the planet and Sun. Any two of the four parameters on the right side of the dialog box may be utilized to define the shape of the orbit. The remaining two parameters may be computed by selecting the *Update* button.

The following inputs and definitions are adopted to define the orbit:

- *Orbit Inclination* - The angle between the orbit plane and the equatorial plane. The angle is formed between the north pole of the planet and the orbit normal vector. Inclinations less than 90° will have the satellite travelling west-to-east at the ascending node. Inclinations greater than 90° , or retrograde orbits, will have the satellite travelling east-to-west at the ascending node. Input is in degrees between 0 and 180.
- *Ascending Node* - The point at which the orbit crosses the equatorial plane, travelling south to north. The line between the ascending node, center of the planet and the descending node is called the line of nodes.

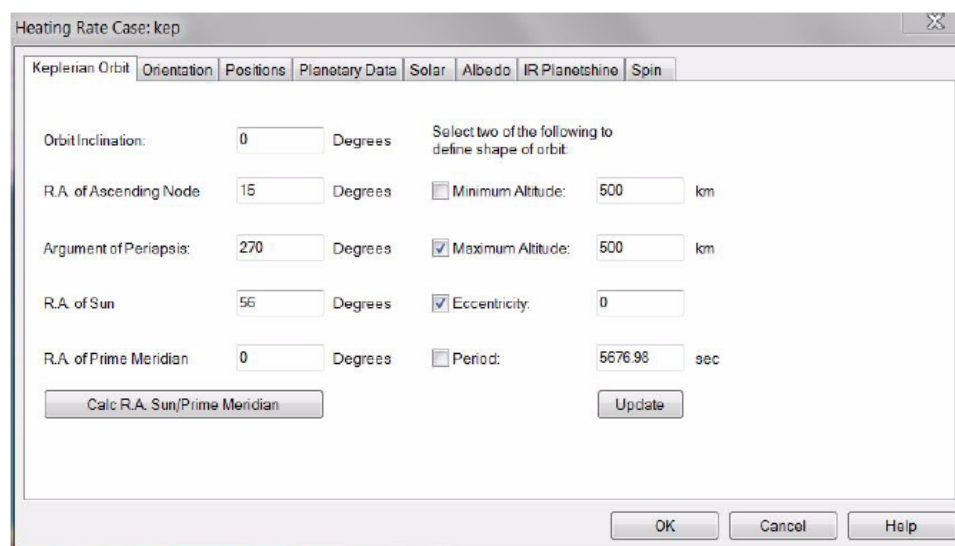


Figure 3.34: Keplerian Heating Rate Case Dialog Box (Credits: *Thermal Desktop User's Manual* by C&R Technologies, Inc.).

- *Right Ascension (R.A.)* - The right ascension is the angle measured in the equatorial plane from the Vernal Equinox. The angle is measured counter-clockwise using the right-hand rule about the north pole of the planet. The input is in degrees.
- *R.A. of Ascending Node* - The right ascension of the ascending node.
- *Argument of Periapsis* - The angle formed between the line connecting the center of the planet to the ascending node and the line connecting the center of the planet to point in the orbit closest to the planet (the periapsis). The angle is measured positive in the direction of motion of the satellite. The orbit begins at the periapsis point: this is Time = 0.
- *R.A. of Sun* - The right ascension of the Sun. The declination (angle from the equatorial plane, positive towards the north pole) of the Sun is automatically computed using information entered on the *Planetary Data* tab. A R.A. of Sun equal to 0° represents the vernal equinox. A value of 90° places the Sun at the max declination and represents the summer solstice for the northern hemisphere. A value of 180° represents the autumnal equinox, while a value of 270° represents winter in the northern hemisphere and the Sun is located at the minimum declination (the negative value of the Inclination of the Equator).
- *R.A. of Prime Meridian* - The right ascension of the prime meridian of the planet. In *GeoLatLong* heating environments, the Prime Meridian defines the subsolar longitude. The difference between the R.A. of Prime Meridian and R.A. of Sun defines the subsolar longitude at time zero. If the R.A. of Prime Meridian and R.A. of the Sun are equal, the zero Longitude will be at solar noon (subsolar) at time equal to 0.

- *Minimum Altitude* - The distance between the planet surface and the satellite at the periapsis point.
- *Maximum Altitude* - The distance between the planet surface and the satellite at the apoapsis (farthest away) point.
- *Eccentricity* - The ratio between half the distance between foci and the semi-major axis of the orbit ellipse.
- *Period* - The time to complete one revolution of the orbit.

If the Earth is being orbited, the right ascension of the Sun and the prime meridian may be calculated by selecting the *Calc RA Sun/Prime Meridian* button. The user may enter the desired date and time, and select the *Calculate* button to compute the right ascensions, then select the *Update* button to transfer the values to the *Keplerian Orbit* input form. The date and time used for this calculation would most likely be the mid-point of the solution since the *RA Sun* and *RA Prime Meridian* do not progress during the solution.

3.2.4 Case Set Manager

The primary purpose of the *Case Set Manager* is to permit the user to set up different thermal analysis cases and to make computations from radiation calculations to creating and running the SINDA/FLUINT model to post-processing temperatures with the click of a single button.

By default, when the *Run Selected Case* button is clicked, Thermal Desktop will first perform the radiation and heating rate tasks for the current case set, compute and output the nodes and conductors, build and run a SINDA/FLUINT model and finally, display the temperature results mapped into the thermal model in color.

The user may set up multiple case sets and each can be a different analysis for the actual model. Each case set may have different start and stop times for transient runs, different SINDA logic, different property databases or aliases, or even different symbol values, which might modify the geometry. Case sets can be organized into groups for organization and simplified selection for editing or running multiple cases.

The *Case Set Manager* dialog box, pictured in Figure 3.35, is opened by choosing *Thermal* → *Case Set Manager* or its corresponding tool-bar icon. The case sets are listed in a tree format and can be rearranged by dragging and dropping. When *Run Selected Case(s)* button is clicked, the case sets selected in the case set tree or all case sets in the selected case set groups will be executed. Multiple case sets will be run in the order they appear in the tree.

When editing a case set, the *Editing Case Set* dialog is utilized. The dialog is divided into nine tabs:

- *Case Set - Calculations* Tab

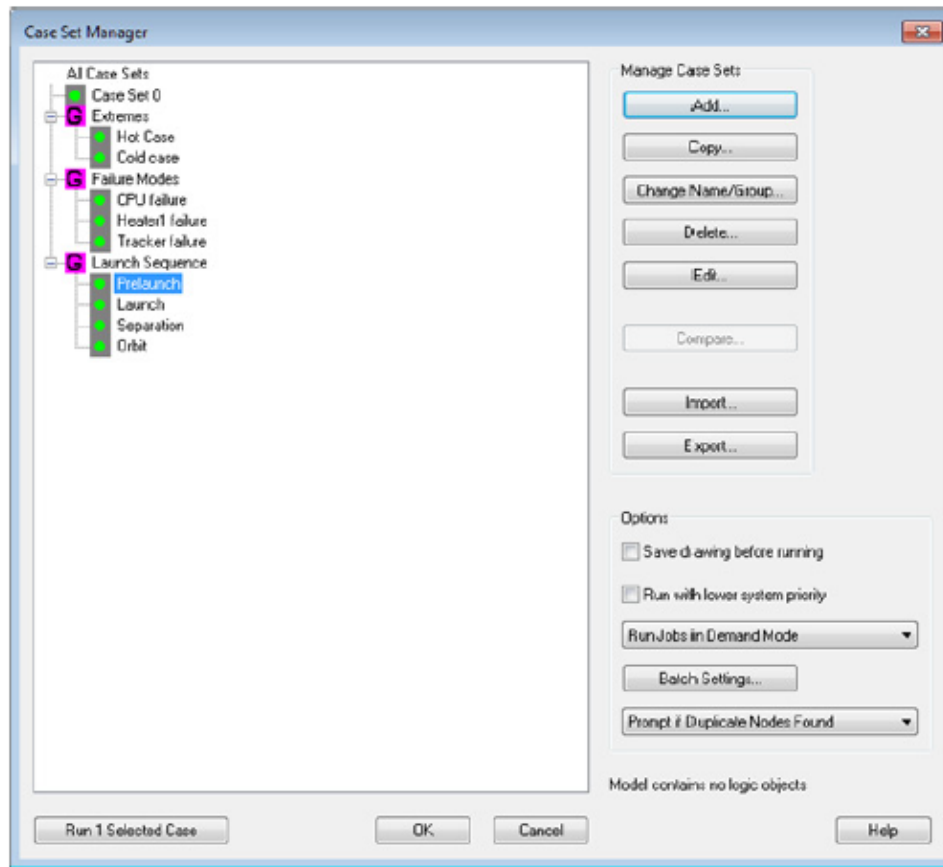


Figure 3.35: Case Set Manager Dialog Box (Credits: *Thermal Desktop User's Manual* by C&R Technologies, Inc.).

- *Case Set - Radiation* Tab
- *Case Set - Output* Tab
- *Case Set - SINDA* Tab
- *Case Set - Dynamic* Tab
- *Case Set - Advanced* Tab
- *Case Set - Property Database (Props)* Tab
- *Case Set - Symbols* Tab
- *Case Set - Comments* Tab

Case Set - Calculations Tab

The *Calculations* tab (shown in Figure 3.36) permits the user to set up a SINDA/FLUINT model and have it launched through the *Case Set Manager*. The user can select any, all

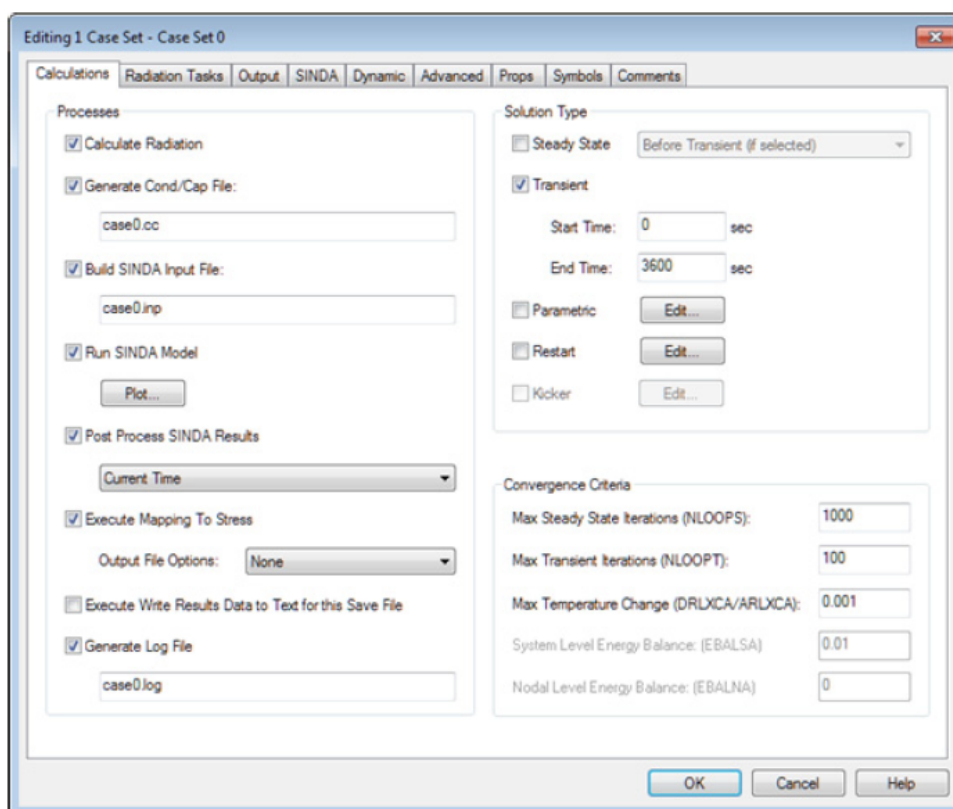


Figure 3.36: Case Set Dialog Box Calculations Tab (Credits: *Thermal Desktop User's Manual* by C&R Technologies, Inc.).

or none of the options listed in the *SINDA Model Options* field. If none of the options are chosen then the case will only perform any radiation tasks listed on the *Radiation Tasks* tab. The options are:

- *Calculate Radiation*. When checked, all radiation tasks on the *Radiation* tab are updated per the options on the tab. When unchecked, any existing radiation data will be loaded for the solution.
- *Generate Cond./Cap File*. Calculates and outputs the NODE DATA, CONDUCTOR DATA, REGISTER DATA and logic for heaters, heat loads, logic objects and data logger comparisons for the model. The SINDA/FLUINT input file will reference the file named in the field. If the option is unchecked, the conductance and capacitance information will not be updated to match changes in the Thermal Desktop model.

- *Build SINDA Input File.* Generates the primary input file for SINDA/FLUINT. This file commonly includes the OPTIONS, CONTROL, OPERATIONS, and OUTPUT CALLS blocks. If unchecked and *Run SINDA Model* is checked, SINDA will use the filename listed in this field.
- *Run SINDA Model.* Run the SINDA/FLUINT model listed under Build SINDA Input File.
- *Post Process SINDA Results.* Post-processes the SINDA/FLUINT results at the defined time. Results can be in either the SAVE file format or the Compressed Solution Results (CSR) directory format.
- *Execute Mapping to Stress.* Maps data to existing Data Mappers. This option is only available when post-processing is selected. The *Output File Options* determines if the mapping output goes directly to the Mapper's output file (None), if the Mapper output file is appended with the case set name or SINDA file name, or if the Mapper output file is written to the Run directory chosen on the *Advanced tab*.
- *Execute Write Results Data to Text for this Save File.* When checked, the data defined in the *Save to Text Manager* is written to the appropriate files using the results of the current solution.
- *Generate Log File.* Generates a log file that contains all of the information written to the AutoCAD status window.

The user may direct the type of solution SINDA/FLUINT utilizes to calculate the steady state or transient response. The options in the *Solution type* region defines the SINDA/FLUINT OPERATIONS logic for basic solution combinations. Any combination of solution types can be chosen, however, if steady state or transient are not selected a solution will not be solved. For steady state solutions, the SINDA/FLUINT routine STEADY is adopted. The options for a steady state solution are:

- *Before Transient (if selected):* When adopted with heating environments, this option will utilize the orbital average heating. Other time-varying conditions, such as boundary node temperatures will use the *Initial Value*. If a transient solution has been chosen, it will be executed after the steady state solution.
- *At Each Orbit Time Position:* When adopted with a heating environment, a steady state solution will be executed at each orbit positions. This is useful for low capacitance models.
- *After Transient:* This option is the same as the first option, but the steady state solution will be executed after the transient solution.
- *Before & After Transient:* This option is the same as the first option, but a steady state solution will be executed before and after the transient solution.

For transient solutions, the SINDA/FLUINT solution routine TRANSIENT is adopted. The user may override these defaults by specifying a custom *Operations* block. If both *Steady State* and *Transient* are selected, then the user should choose when the *Steady State* should run: before the transient, after the transient, or before and after the transient. The user must type the *Start Time* and *End Time* if a transient run is selected.

For more information on the various solution types available, it could be reviewed the *SINDA/FLUINT User's Manual* [9]. On the referenced manual it can be found also the convergence criteria used for the solution, that in the following are presented:

- *Max Steady State Iterations (NLOOPS)*: Maximum number of iterations for steady state solution.
- *Max Transient Iterations (NLOOPT)*: Maximum number of iterations for a transient time step.
- *Max Temperature Change (DRLXCA/ARLXCA)*: Maximum allowable temperature change per iteration. DRLXCA is applied to diffusion nodes and ARLXCA is applied to arithmetic nodes. The value is adopted for both diffusion and arithmetic nodes in both transient and steady state solutions.
- *System Level Energy Balance (EBALSA)*: Represents an acceptable relative energy balance of the system. This convergence criterion is adopted for steady state solutions.
- *Nodal Level Energy Balance (EBALNA)*: Represents an acceptable absolute energy balance of all nodes in each submodel. This criterion is adopted for steady state solutions. The default value of zero means that the nodal energy balance is skipped.

Case Set - Radiation Tab

The case set radiation tasks (*Radiation* tab) are illustrated in Figure 3.37. The information grouped on this tab is utilized to specify which analysis groups and which orbits are to be adopted to calculate radiation conductors and heating rates. The *Add* function has intelligent defaults so that the output name and output submodel for that case will not only be valid names, but will also be unique. The radiation options on the right side of the *Radiation* tab permits the user to inform the program what to do in case a database for that job is found. A database is defined by the *Radiation Analysis Group* name, the *Orbit* name (if required) and the *Optical Properties* database name.

When the *Add* button is clicked, or an existing radiation task and the *Edit* button are selected, then the *Radiation Analysis Data* dialog box is opened. On the first tab, the *Job* tab, the user specify the *Calculation Type*, the *Analysis Group* and the *Orbit* (if necessary for the *Calculation Type*), the *Calculation Method* and the text to *Add to Database Name*. The *Calculation Type* that can be chosen are:

- *Radks* - surface-to-surface radiation exchange.

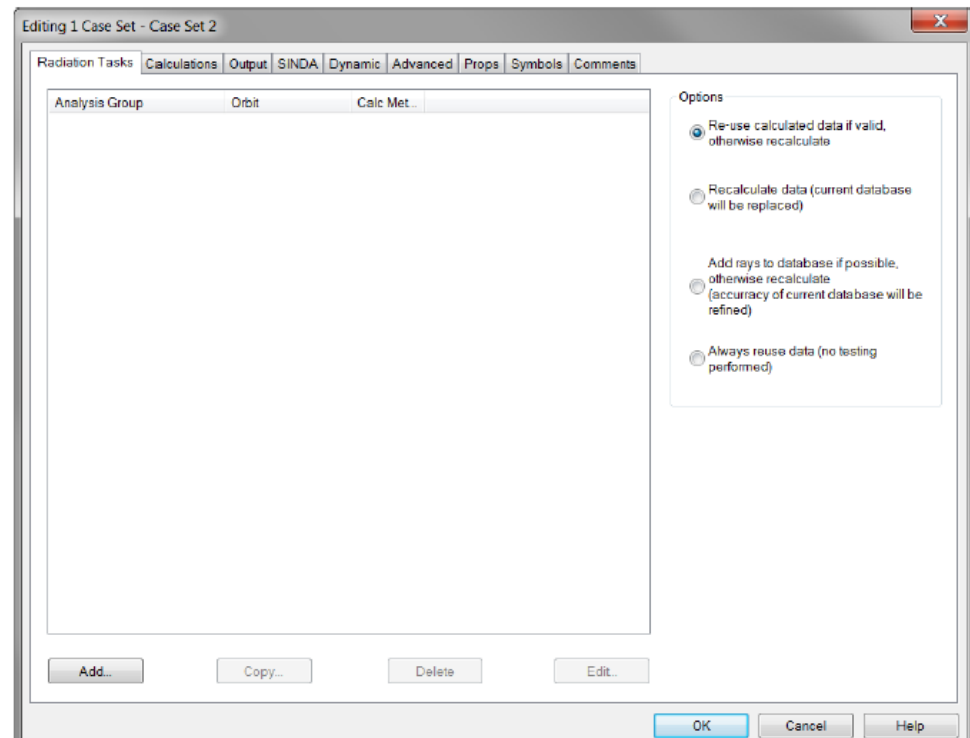


Figure 3.37: Case Set Dialog Box Radiation Task Tab (Credits: *Thermal Desktop User's Manual* by C&R Technologies, Inc.).

- *Heating Rates* - heating rates due to heating environments (requires *Orbit*).
- *Articulating Radks* - surface-to-surface radiation exchange for articulating geometries (requires *Orbit*).
- *Free Molecular Conduction* - free molecular conduction calculation between fixed surfaces.
- *Articulating Free Molecular Conduction* - free molecular conduction between articulating surfaces (requires *Orbit*).
- *View Factors* - black-body view factors for use prior to calculations using radiosity method. Utilizing this option for heating rates permits defining a maximum number of rays for the view factor calculation while having a different number of rays for the heating sources.
- *Articulating View Factors* - black-body view factors for articulating geometry (requires *Orbit*) for use prior to calculation using radiosity method.

Once the calculation type is specified the user chooses the desired *Radiation Analysis Group* from the drop-down list and desired heating environment for the radiation task.

Case Set - Output Tab

The *Output* tab permits the user to monitor the types of output that are written during the SINDA/FLUINT run. This tab is pictured in Figure 3.38. For transient runs, the user may specify the *Output Increment* at the top left of the dialog box. If *Output Increment* is set to "0", then the current output increment becomes $TIMEND \cdot 0.01$, where $TIMEND$ is the solution end time. The user can also monitor the submodel name utilized for the output in the drop-down list located at the top right corner. If the pull-down says (AUTO), then the GLOBAL submodel will be utilized for the output calls. The GLOBAL and GLOBAL_FLUID submodels are included in all solutions regardless of built submodels.

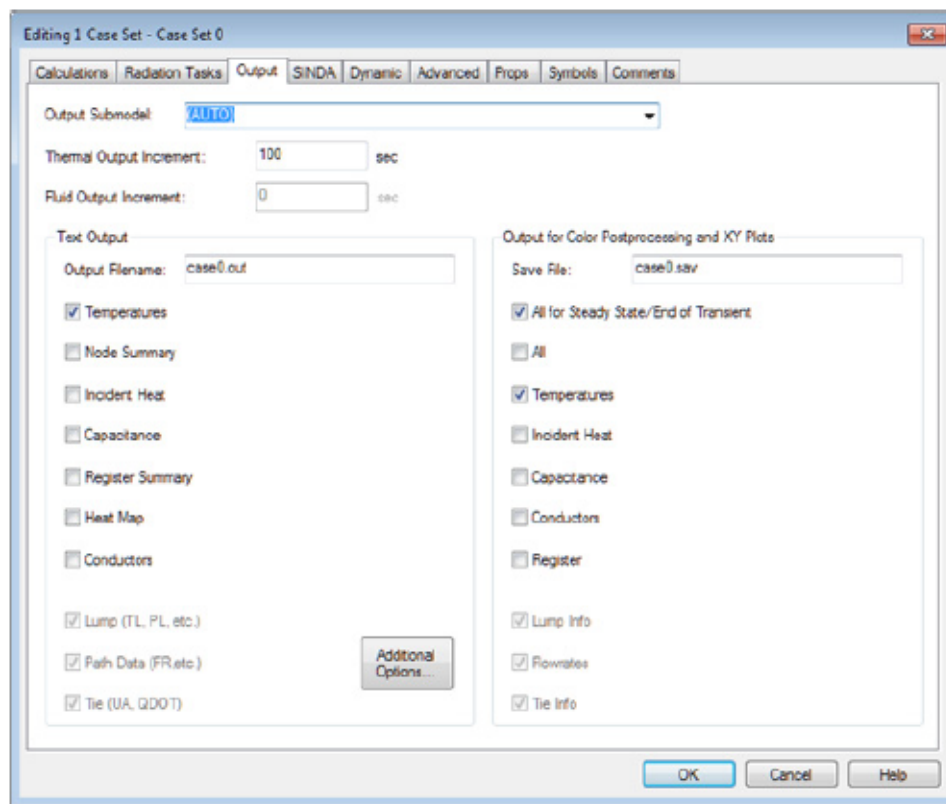


Figure 3.38: Case Set Dialog Box Output Tab (Credits: *Thermal Desktop User's Manual* by C&R Technologies, Inc.).

3.2.5 Post-Processing

Post-processing, examining calculation results, in Thermal Desktop can be performed through:

- *Color Post-processing* - displaying calculation values on graphical objects as colors or shades;

- *X-Y Plotting* - displaying calculation values on an X-Y plot, typically as a function of time;
- *Query Node* - obtaining calculation values by selecting graphical objects;
- *Results Queries* - generating summary files based on one or more results files.

Color Post-processing

After calculations are performed, the results may be viewed utilizing Thermal Desktop's post-processing facility. View factors, radks, heating rates, SINDA/FLUINT results and generic text files can all be post-processed directly on the graphical entities. Multiple color bars may be pictured so that data from various objects may be examined at the same time, or objects in different viewports can have different scales.

For example, temperatures may be pictured for thermal nodes simultaneously pressures are pictured for fluid lumps. Figure 3.39 illustrates a combined fluid/thermal model with results displayed adopting all four available color bars.

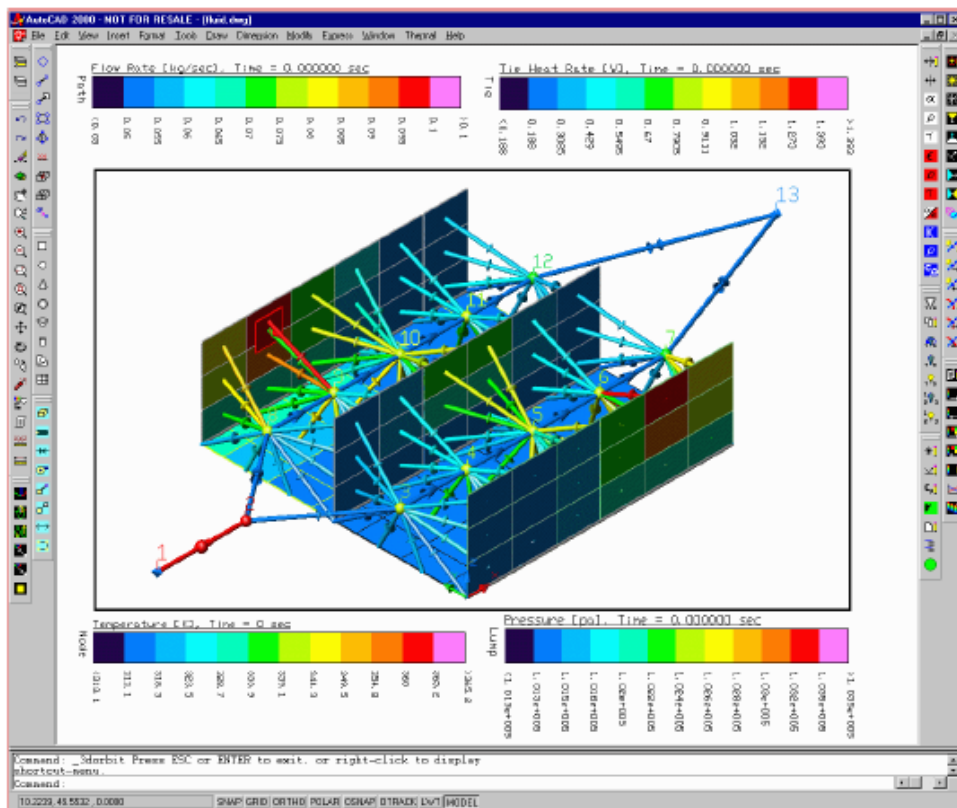


Figure 3.39: Post-processing with Four Color Bars for Node, Lump, Path and Tie Data (Credits: *Thermal Desktop User's Manual* by C&R Technologies, Inc.).

Node values are displayed as contours, by default, with colors interpolated between node

locations on a continuous surface or solid. For finite difference objects, the contouring can be turned off such that the entire nodal area or volume displays the node value.

Thermal Desktop saves information about data to be post-processed in a post-processing dataset. The dataset stores the file name containing the data, the type of data to be plotted, the current time value if appropriate and a comment to describe the data.

X-Y Plotting

The *Thermal → Post Processing → X-Y Plot Data vs. Time* command plots transient, or parametric, results in the *EZXY Plotter*. Performing X-Y plot commands will display *EZXY Plotter* and prompt for objects to be plotted, unless items were preselected. The plots have several options and export features that can be explored using the on-line help provided on the *EZXY Plotter* forms.

EZXY Plotter will plot whatever the currently selected dataset for post-processing contains. Temperatures, heating rates or even radiation conductors vs. time for articulating geometry may be plotted. The *X-Y Plotter* also accepts a generic ASCII format for making plots of data calculated by user written programs or SINDA/FLUINT logic.

Parametric steady-state results will be plotted as a function of record number since the time value will always be zero. The X axis values can be changed to any value stored in the results through the *EZXY Plotter* interface.

Chapter 4

Case Study

The case study of this thesis are two 6U CubeSats developed for two different space missions by *Tyvak International*.

Tyvak International, a *Terran Orbital Corporation*, is a start-up which provides Nanosatellite and CubeSat space vehicle products and services that target advanced state-of-the-art capabilities for government and commercial customers to support operational and scientifically relevant missions.

During the months of work at *Tyvak's* headquarters, the aim of this thesis has been to carry out a first preliminary thermal analysis, useful for the design and testing phases, of the two space mission described in the following.

However, to not disclose sensitive information, the name of the missions and of their main equipments will be concealed. They will be referred to, in the following sections, as "*Mission 1*" and "*Mission 2*".

4.1 Mission 1

Mission 1 is a project, in partnership with other Italian companies and co-funded by the European Union, which address the sector of spacecraft attitude determination from star measurements, in particular providing an innovative multi-camera system for spacecraft autonomous attitude determination by means of star observation.

The purpose of the thermal analysis was to provide an effective representation of the thermal environment in order to support the feasibility of the project and give an input for the payload testing phase.

Using *Thermal Desktop* and the features described in the previous chapter the model pictured in Figure 4.1 has been built.

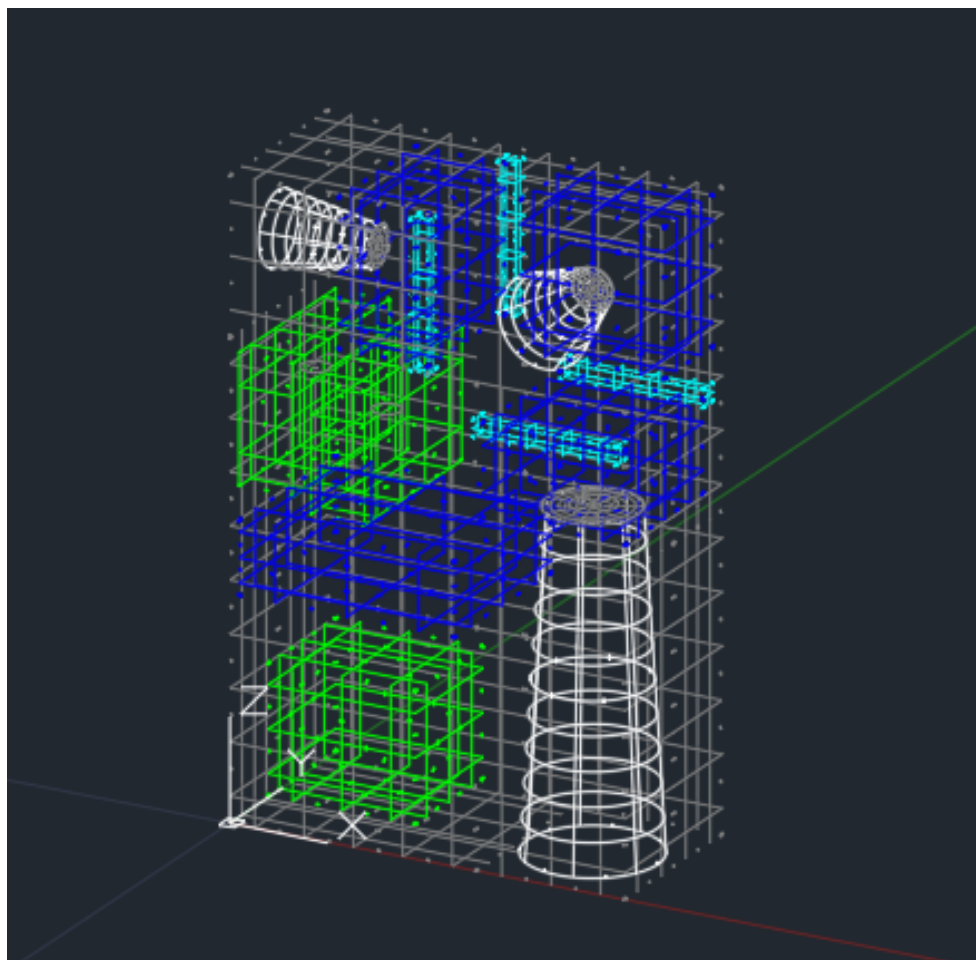


Figure 4.1: Mission 1 overview.

Optical and Thermophysical Properties

The material's optical and thermophysical properties implemented in the model are summarized in Table 4.1 and Table 4.2*.

Name	Conductivity $\left[\frac{W}{m \cdot K}\right]$	Density $\left[\frac{kg}{m^3}\right]$	Specific Heat $\left[\frac{J}{kg \cdot K}\right]$
Al7075	173	2810	960
FR4	0.23	1900	1200
Lithium Ion Cell	0.5	2140	870
Solar Cell	64	5323	322
Titanium	2.2	4500	540

Table 4.1: Mission 1 thermophysical properties.

*Values from *NASA Reference Publication 1121, April 1984* and *NASA/TM—2014–218195*.

Name	Solar Absorptivity	IR Emissivity
Al7075 Alodine	0.3	0.1
Al7075 Anodized	0.65	0.88
FR4	0.40	0.90
Black Painting	1	1
Solar Cell	0.90	0.80

Table 4.2: Mission 1 optical properties.

External Surfaces

The spacecraft's external surfaces are modelled with Finite Difference elements. The edge nodes are distributed on the surfaces and their number for the mesh has been chosen as a compromise between the analysis accuracy and execution time. A representation of the mesh is illustrated in Figure 4.2, while in Table 4.3 are resumed the main characteristics of each surfaces.

It is important to note that to distinguish the external face from the internal one there are two nodes in the same location but with different properties, while the coincident nodes belonging to two different surfaces have been merged to avoid errors during the analysis.

Face	Side	Material	Optical	Thickness [mm]	Mesh
3U/X+	Top/Out	Solar Cell	Solar Cell	0.3	5x13
	Bottom/In	FR4	FR4	1	
3U/X-	Top/Out	Al7075	Anodized	1.5	5x10
	Bottom/In	FR4	FR4	1	
6U/Y+	Top/Out	Solar Cell	Solar Cell	0.3	9x13
	Separation	FR4	n.a.	1	
6U/Y-	Bottom/In	Al7075	Alodine	2.3	9x13
	Top/Out	Al7075	Anodized	1.5	
2U/Z+	Bottom/In	Al7075	Alodine	1	9x5
	Top/Out	Al7075	Anodized	0.8	
2U/Z-	Bottom/In	Al7075	Alodine	0.8	6x5
	Top/Out	Al7075	Anodized	0.8	

Table 4.3: Mission 1 external surfaces characteristics.

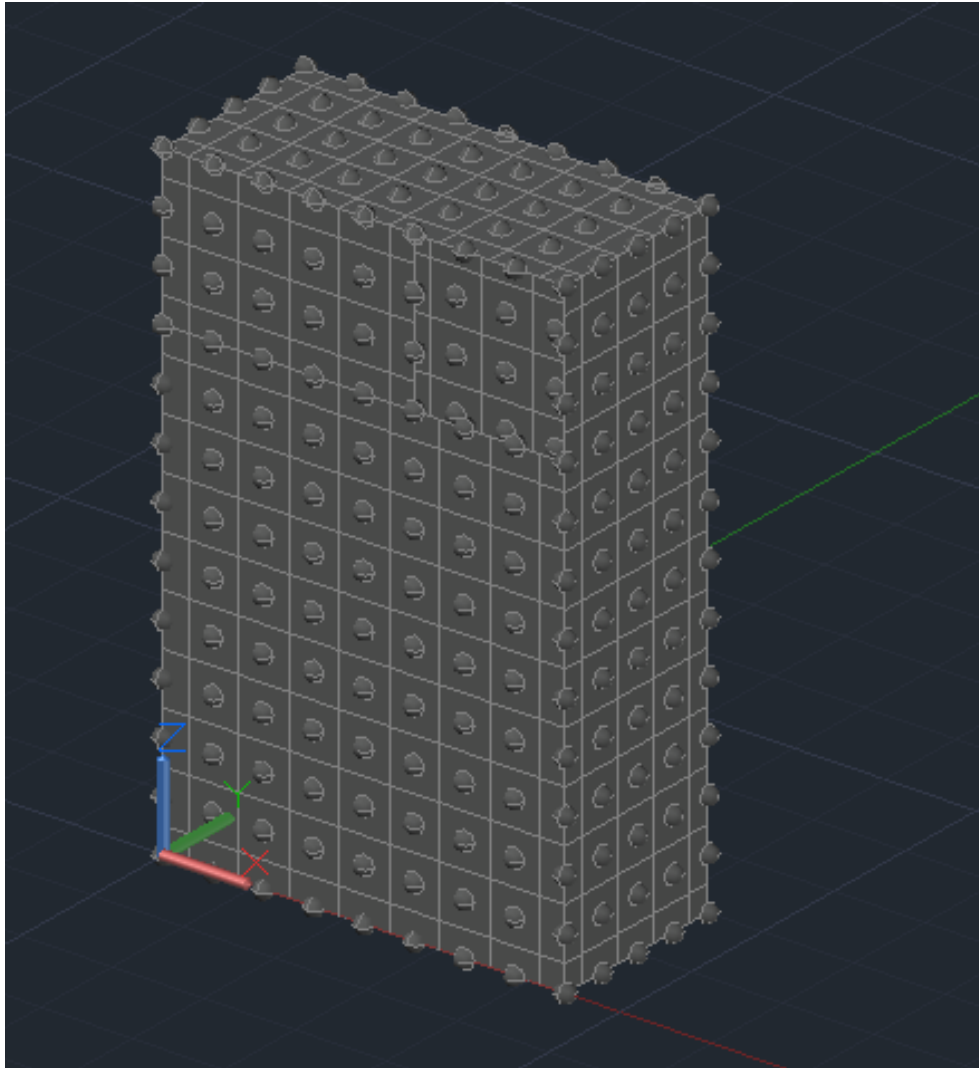


Figure 4.2: Mission 1 external surfaces mesh.

Payload and Bus Components

The components modelled inside the spacecraft, shown in Figure 4.3, are the following:

- Three payload cameras;
- One payload component;
- Four brackets connecting the cams to the structure;
- Two batteries;
- One bus component.

These components have been modelled as aluminium boxes with a black body inside (the red boxes pictured in Figure 4.3), where the heat loads are applied on. However the batteries and the brackets represents an exception, since they have been modelled as FD solids.

In Table 4.4 are reported some of the main characteristics of the different components.

Component	Mesh	Material	Optical
Camera 1	3x4x4	Al7075	Alodine
Baffle Cam1	8x5	Al7075	Black Painting
Camera 2	4x3x4	Al7075	Alodine
Baffle Cam2	8x4	Al7075	Black Painting
Camera 3	4x4x3	Al7075	Alodine
Baffle Cam3	8x6	Al7075	Black Painting
Payload Component	4x4x4	Al7075	Alodine
Brackets	2x2x5	Al7075	Alodine
Battery 1 and 2	1x5x3	Lithium Ion Cell	Alodine
Bus Component	4x4x4	Al7075	Alodine
Black Body	1x1x1	FR4	Black Painting

Table 4.4: Mission 1 payload and bus components characteristics.

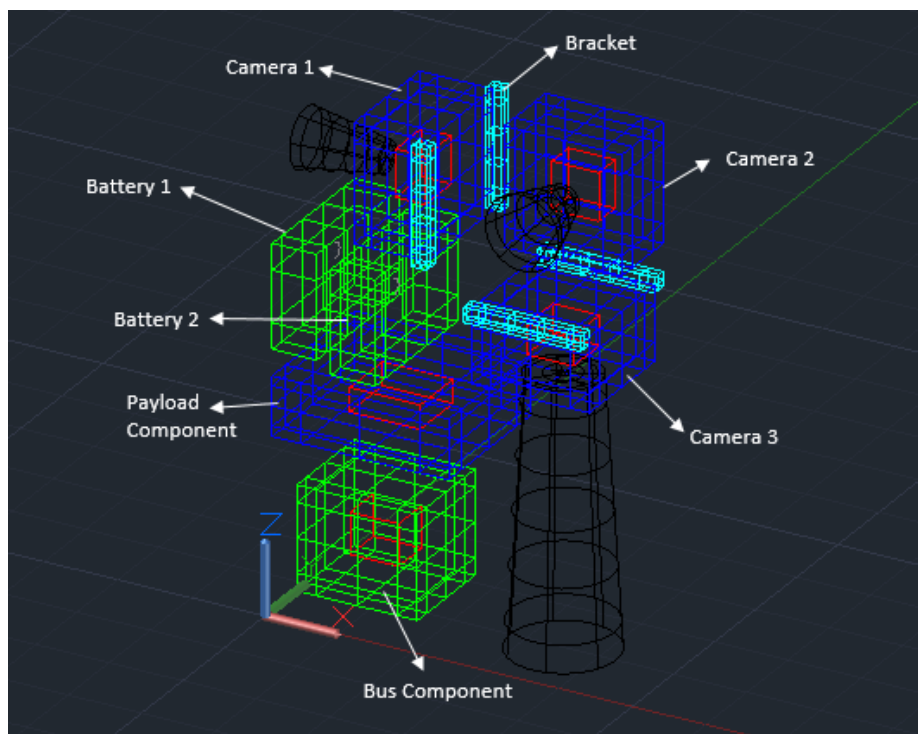


Figure 4.3: Mission 1 payload and bus component.

Contactors

To connect the internal components to the external surfaces and to model the conductive paths at the interfaces it has been used the *Contactor* function.

In Figure 4.4 is shown a contactor representation, while in Table 4.5 the input parameters used for the conductance calculation at the interfaces have been reported. These parameters have been calculated according the instruction in Table 3.3 for bolted interfaces and in literature for bolt thermal conductance [3].

Instead contactors between baffle and body of each cameras have been modelled with a titanium disk, thickness 5 mm, hence the conductance coefficient have been calculated using the material and geometrical properties of the disk.

Interface	Conductance [W/K]
Camera 1 - Brackets	12
Camera 2 - Structure	8
Camera 3 - Brackets	12
Brackets - Structure	12
Payload Component - Structure	8
Battery 1 and 2 - Structure	4
Bus Component - Structure	8

Table 4.5: Mission 1 contactor parameters.

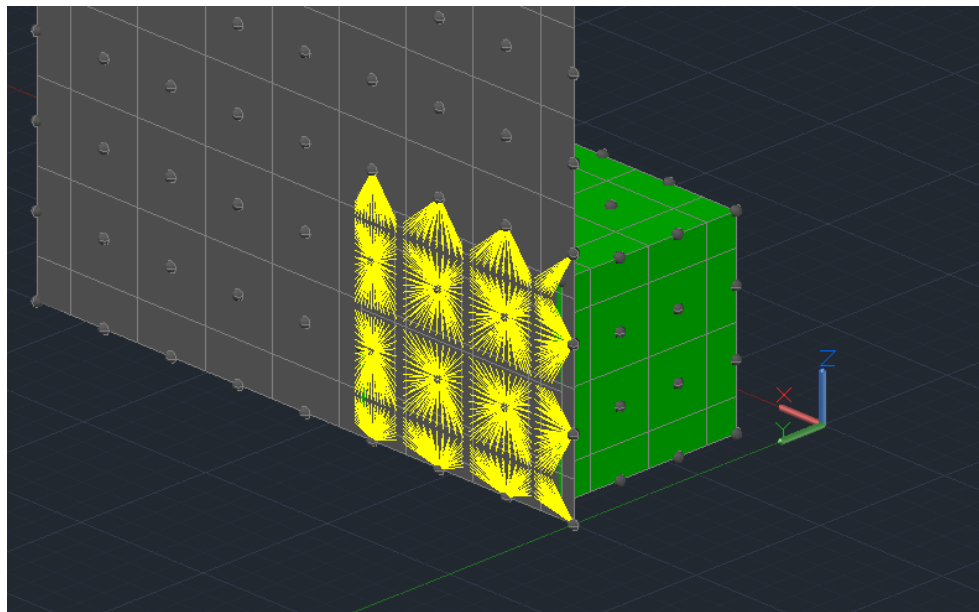


Figure 4.4: Mission 1 contactor.

Heat Loads

The heat loads, as previously stated, have been applied on the black body inside every component. These are solid heat loads, since they are applied to FD solids. Moreover, there are also surface heat load applied to the baffles and heaters to the batteries, which are temperature dependent so they switch on only if $T < 5^\circ\text{C}$. The heat loads included into the model are illustrated in Figure 4.5, while Table 4.6 shows their power.

Heat Load	Power [W]
Camera Body	1.5
Camera Baffle	0.5
Payload Component	1.5
Battery 1 and 2	0.5
Bus Component	5.5

Table 4.6: Mission 1 heat loads.

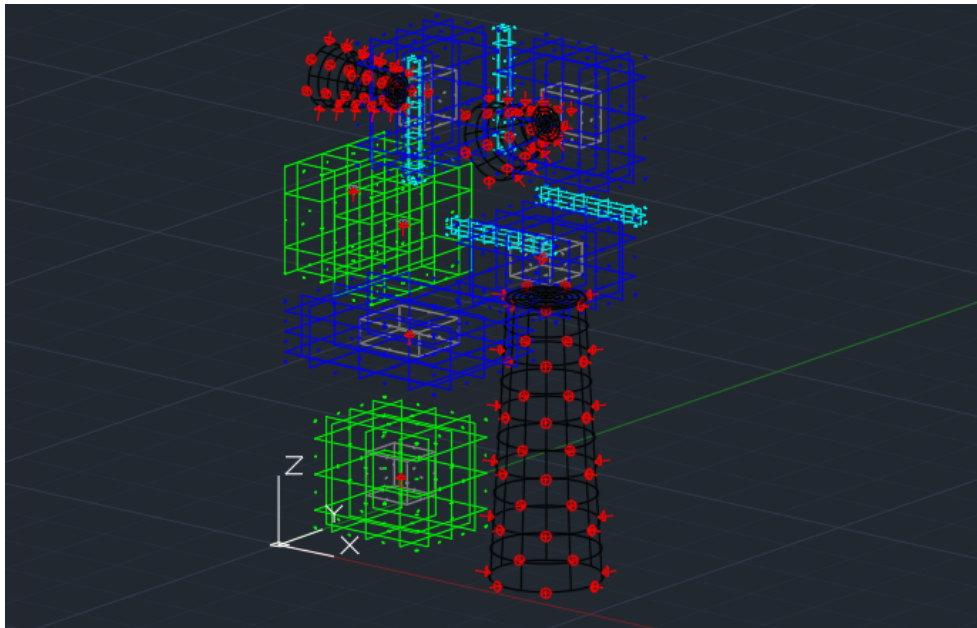


Figure 4.5: Mission 1 heat loads.

Orbit

The orbit chosen for Mission 1 is a sun-synchronous *LTAN* 10 : 30 *am*. The reason of this choice is the major availability of launch windows as piggy-back. An orbit representation is shown in Figure 4.6, while the other orbital data are reported in Table 4.7.

Orbital Parameter	Value
SSO <i>LTAN</i>	10 : 30 <i>am</i>
RAAN	106.982°
h	550 <i>km</i>
i	97.5088°
T0	01/08/2019 @10 : 00 : 00

Table 4.7: Mission 1 orbital data.

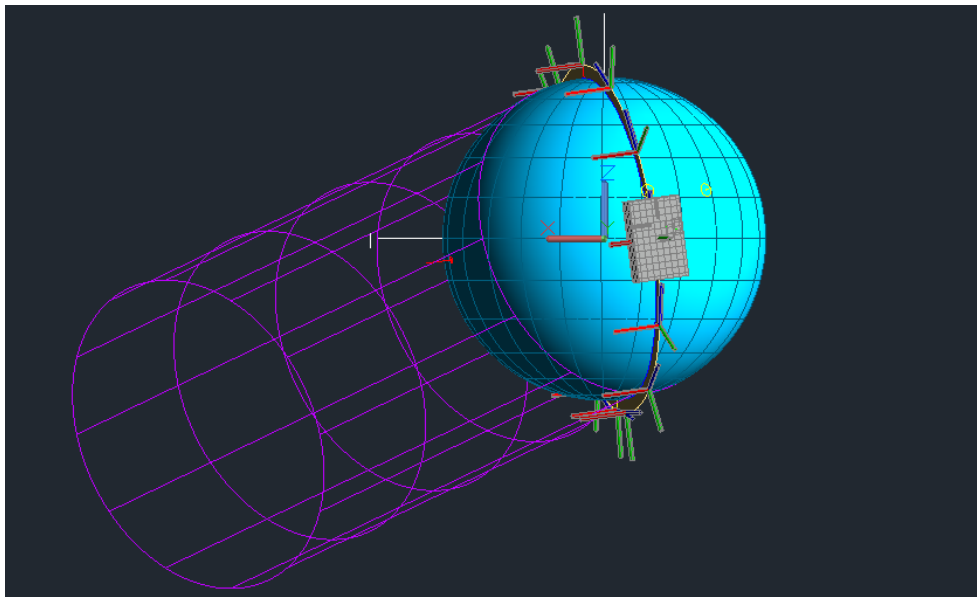


Figure 4.6: Mission 1 orbit.

Case Scenario

The case scenarios analysed for Mission 1 are three: the worst hot case, the worst cold case and a nominal scenario. The main characteristics for each scenario are listed in Table 4.8. The results and conclusion related to these analysis are discussed in Chapter 5.

Case	Orientation	Payload	Bus
Worst Hot Case	Sun Pointing: 6U/Y+	Off	On
Worst Cold Case	Nadir: 6U/Y- Velocity Vector: 2U/Z+	Off	Idle (3W)
Nominal Case	Nadir: 6U/Y- Velocity Vector: 2U/Z+	On	On

Table 4.8: Mission 1 case scenarios.

The Worst Hot Case is the sun-pointing scenario, in which the solar panel is perpendicularly directed to the Sun. In this situation the payload is off, while the bus is operative. Instead, the Worst Cold Case is the idle situation, so the spacecraft is nominal orientated but payload is off and bus is in Idle configuration so with reduced power. Finally there is the Nominal Case. In this scenario Mission 1 is operating so payload and bus are on, the orientation is, obviously, the nominal one.

4.2 Mission 2

Mission 2 is a project co-funded by ESA, in partnership with Italian company and four different payload providers, which encompasses the launch of two 6U CubeSats for Earth observation and validation of inter-satellite link technologies (GNSS reflectometry, multi-spectral observation, optical and RF ISL).

The purpose of the thermal analysis was to provide an effective representation of the thermal environment in order to support the feasibility of the project and the design of the TCS.

Using *Thermal Desktop* and the features described in the previous chapter the models of two spacecraft (defined as Mission 2.a and Mission 2.b) pictured in Figure 4.7 and Figure 4.8 have been built.

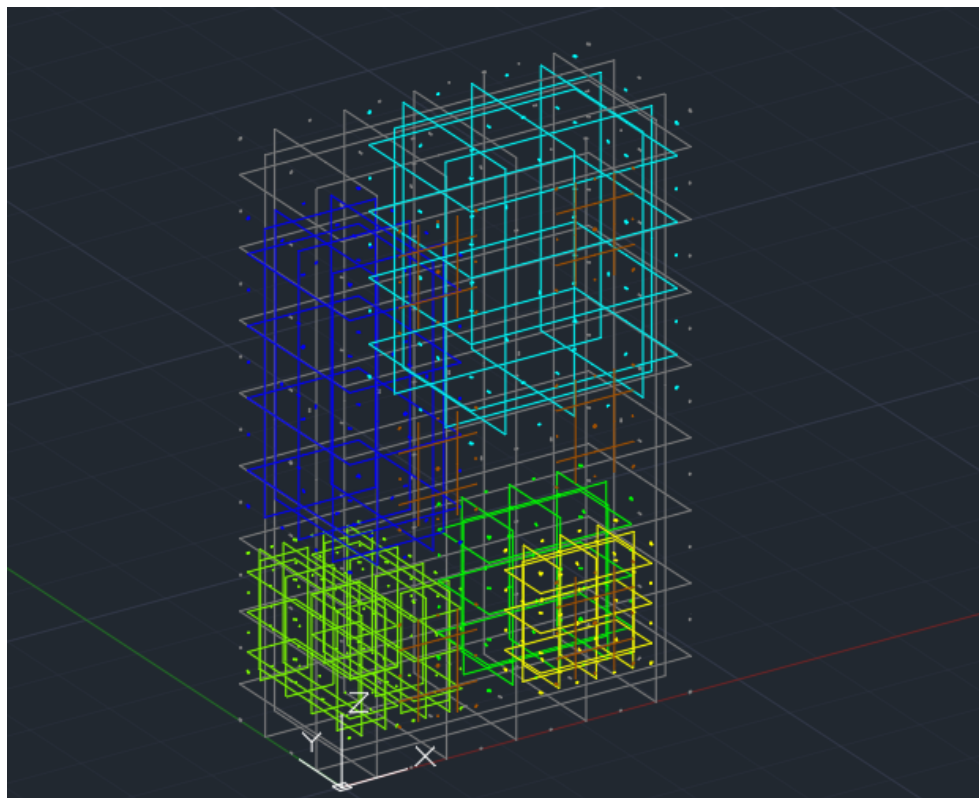


Figure 4.7: Mission 2.a overview.

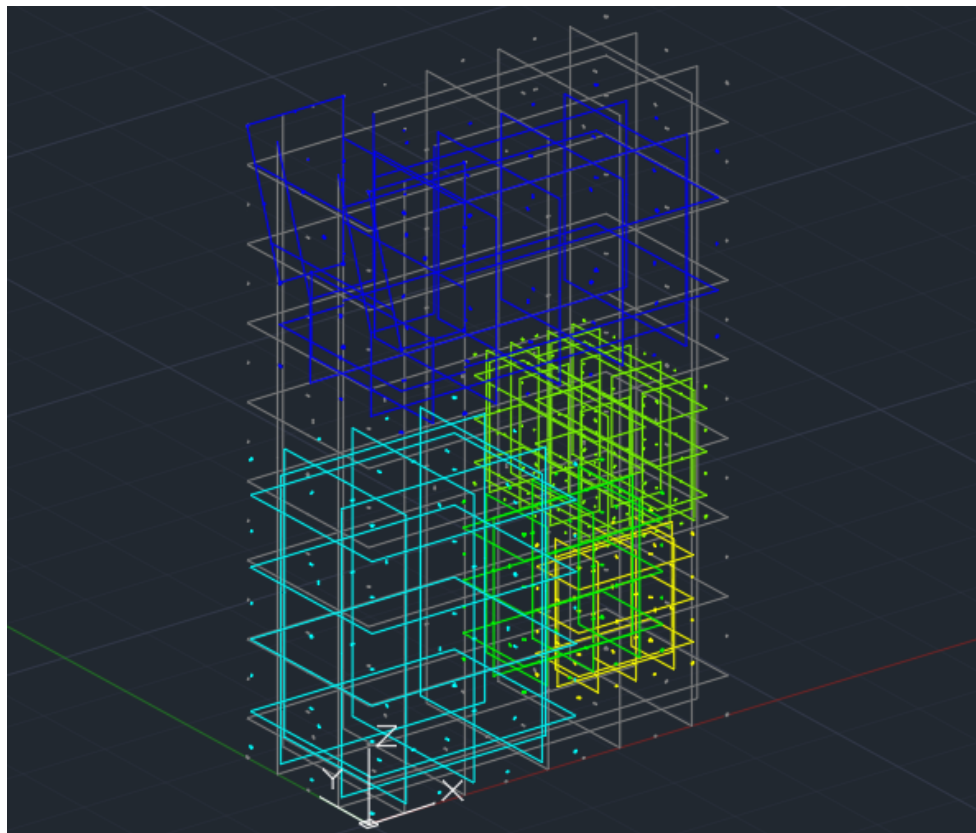


Figure 4.8: Mission 2.b overview.

Optical and Thermophysical Properties

The material's optical and thermophysical properties implemented in the model are summarized in Table 4.9 and Table 4.10[†].

Name	Conductivity $\left[\frac{W}{m \cdot K}\right]$	Density $\left[\frac{kg}{m^3}\right]$	Specific Heat $\left[\frac{J}{kg \cdot K}\right]$
Al7075	173	2810	960
FR4	0.23	1900	1200
Lithium Ion Cell	0.5	2140	870
Solar Cell	64	5323	322
Steel	55	7850	490
Copper	386	8940	390

Table 4.9: Mission 2 thermophysical properties.

[†]Values from *NASA Reference Publication 1121, April 1984* and *NASA/TM—2014-218195*.

Name	Solar Absorptivity	IR Emissivity
Al7075 Alodine	0.3	0.1
Al7075 Anodized	0.65	0.88
FR4	0.40	0.90
Black Painting	1	1
Solar Cell	0.90	0.80

Table 4.10: Mission 2 optical properties.

External Surfaces

The spacecraft's external surfaces are modelled with Finite Difference elements. The edge nodes are distributed on the surfaces and their number for the mesh has been chosen as a compromise between the analysis accuracy and execution time. A representation of the mesh is illustrated in Figure 4.9 and Figure 4.10, while in Table 4.11 and Table 4.12 are resumed the main characteristics of each surfaces for both CubeSats.

It is important to note that to distinguish the external face from the internal one there are two nodes in the same location but with different properties, while the coincident nodes belonging to two different surfaces have been merged to avoid errors during the analysis.

Face	Side	Material	Optical	Thickness [mm]	Mesh
3U/X+	Top/Out	Al7075	Alodine/Anodized	1.5	3x9
	Bottom/In	FR4	FR4	1.3	
3U/X-	Top/Out	Solar Cell	Solar Cell	0.5	3x9
	Bottom/In	FR4	FR4	2	
6U/Y+	Top/Out	Solar Cell	Solar Cell	0.5	6x9
	Separation	FR4	n.a.	2	
6U/Y-	Bottom/In	Al7075	Alodine	2.5	6x9
	Top/Out	FR4	FR4	5.5	
2U/Z+	Separation	Copper	n.a.	0.5	6x3
	Bottom/In	Al7075	Alodine	2.5	
2U/Z-	Top/Out	Al7075	Anodized	1	4x3
	Bottom/In	Al7075	Alodine	1	
2U/Z-	Top/Out	Al7075	Anodized	1	6x3
	Bottom/In	Al7075	Alodine	1	

Table 4.11: Mission 2.a external surfaces characteristics.

Face	Side	Material	Optical	Thickness [mm]	Mesh
3U/X+	Top/Out	Al7075	Alodine/Anodized	1.5	3x9
	Bottom/In	FR4	FR4	1.3	
3U/X-	Top/Out	Solar Cell	Solar Cell	0.5	3x9
	Bottom/In	FR4	FR4	2	
6U/Y+	Top/Out	Al7075	Alodine/Anodized	1.25	6x9
	Bottom/In	Al7075	Alodine	1.25	
6U/Y-	Top/Out	Solar Cell	Solar Cell	0.5	6x9
	Separation	FR4	n.a.	2	
	Bottom/In	Al7075	Alodine	2.5	
2U/Z+	Top/Out	Al7075	Anodized	1.25	4x3
	Bottom/In	Al7075	Alodine	1.25	
2U/Z-	Top/Out	Al7075	Anodized	1	6x3
	Bottom/In	Al7075	Alodine	1	

Table 4.12: Mission 2.b external surfaces characteristics.

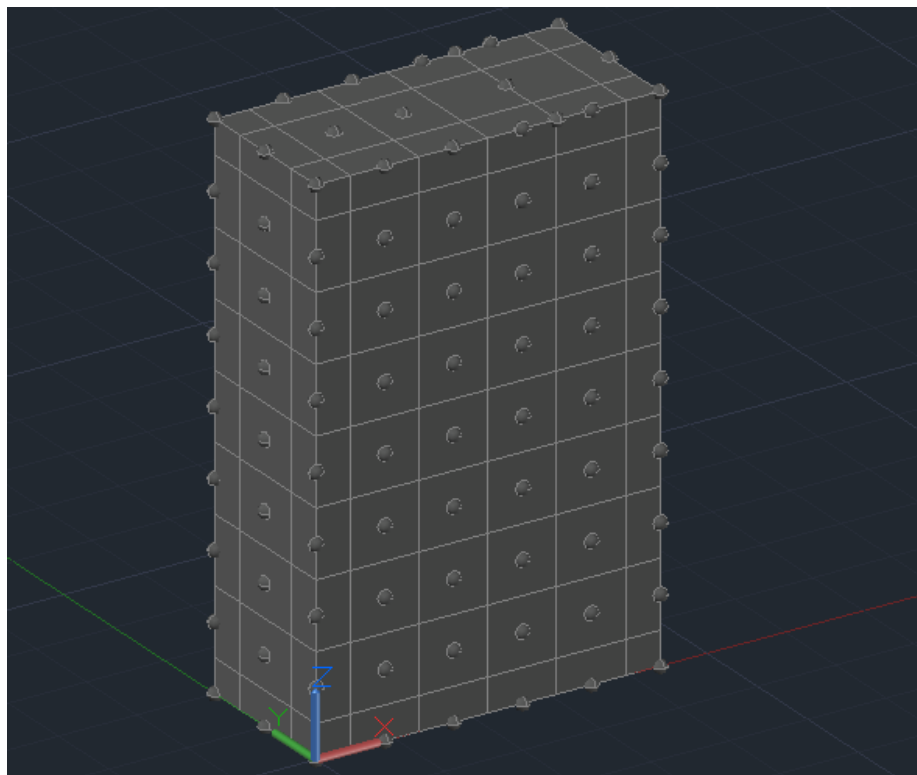


Figure 4.9: Mission 2.a external surfaces mesh.

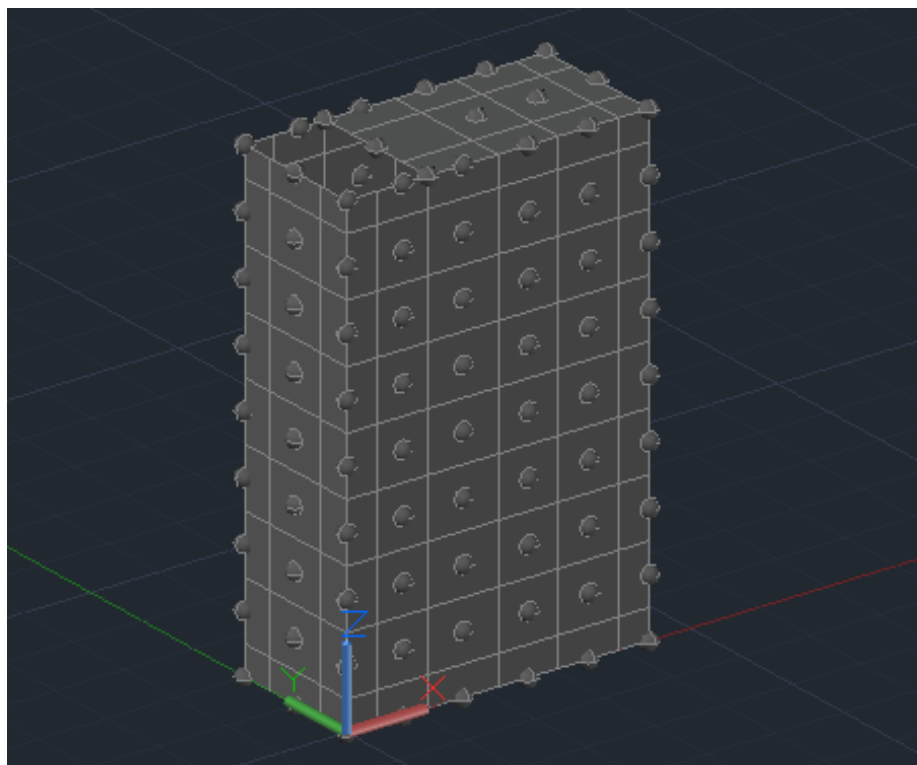


Figure 4.10: Mission 2.b external surfaces mesh.

For these missions several analysis have been executed to determine some aspects of the TCS. In particular the purpose is to better understand which superficial treatment is the most effective for the external 3U/X+ face of Mission 2.a, and the 3U/X+ and 6U/Y+ of Mission 2.b between alodine or anodizing.

Chromate conversion coating on an aluminium substrate is formerly known as Alodine, it is a type of conversion coating used to passivate the material. It is mainly utilized as a corrosion inhibitor, primer, decorative finish or to retain electrical conductivity. It is typically applied to everyday items such as hardware and tools, and can commonly be recognized by its distinctively iridescent, greenish-yellow color.

Anodizing instead, is an electrolytic passivation process used to increase the thickness of the natural oxide layer on the surface of metal parts. The process is called anodizing because the part to be treated forms the anode electrode of an electrolytic cell. Anodizing increases resistance to corrosion and wear, and provides better adhesion for paint primers and glues than bare metal does. Anodic films are also used to prevent galling of threaded components and to make dielectric films for electrolytic capacitors, but in particular they are most commonly applied to protect aluminium alloys.

The anodized aluminium layer is grown by passing a direct current through an electrolytic solution, with the aluminium object serving as the anode (the positive electrode). The current releases hydrogen at the cathode (the negative electrode) and oxygen at the surface of the aluminium anode, creating a build-up of aluminium oxide.

Payload and Bus Components

The components modelled inside the two spacecraft, shown in Figure 4.11 and Figure 4.12, are the following for both the missions:

- Two payload components;
- Two batteries;
- Two bus components.

As for Mission 1, these components have been modelled as aluminium boxes with a black body inside (the red boxes pictured in figures), where the heat loads are applied on, while the batteries have been modelled as FD solids.

In Table 4.13 and Table 4.14 are reported some of the main characteristics of the different components.

Component	Mesh	Material	Optical
Payload Component 1.a	4x3x5	Al7075	Alodine
Payload Component 2.a	4x3x5	Al7075	Alodine
Payload Component 2.a Antenna	4x4x4	Al7075	Alodine
Battery 1.a and 2.a	3x5x4	Lithium Ion Cell	Alodine
Bus Component 1.a	4x2x4	Al7075	Alodine
Bus Component 2.a	4x2x4	Al7075	Alodine
Black Body	1x1x1	FR4	Black Painting

Table 4.13: Mission 2.a payload and bus components characteristics.

Component	Mesh	Material	Optical
Payload Component 1.b	4x3x5	Al7075	Alodine
Payload Component 2.b	6x3x3	Al7075	Alodine
Battery 1.b and 2.b	3x5x4	Lithium Ion Cell	Alodine
Bus Component 1.b	4x2x4	Al7075	Alodine
Bus Component 2.b	4x2x4	Al7075	Alodine
Black Body	1x1x1	FR4	Black Painting

Table 4.14: Mission 2.b payload and bus components characteristics.

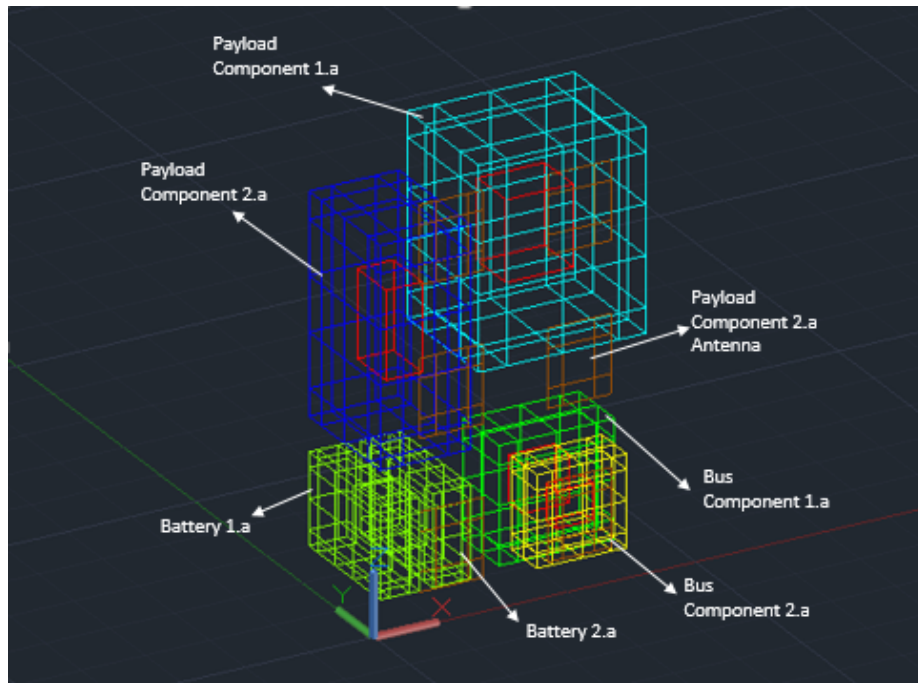


Figure 4.11: Mission 2.a payload and bus component.

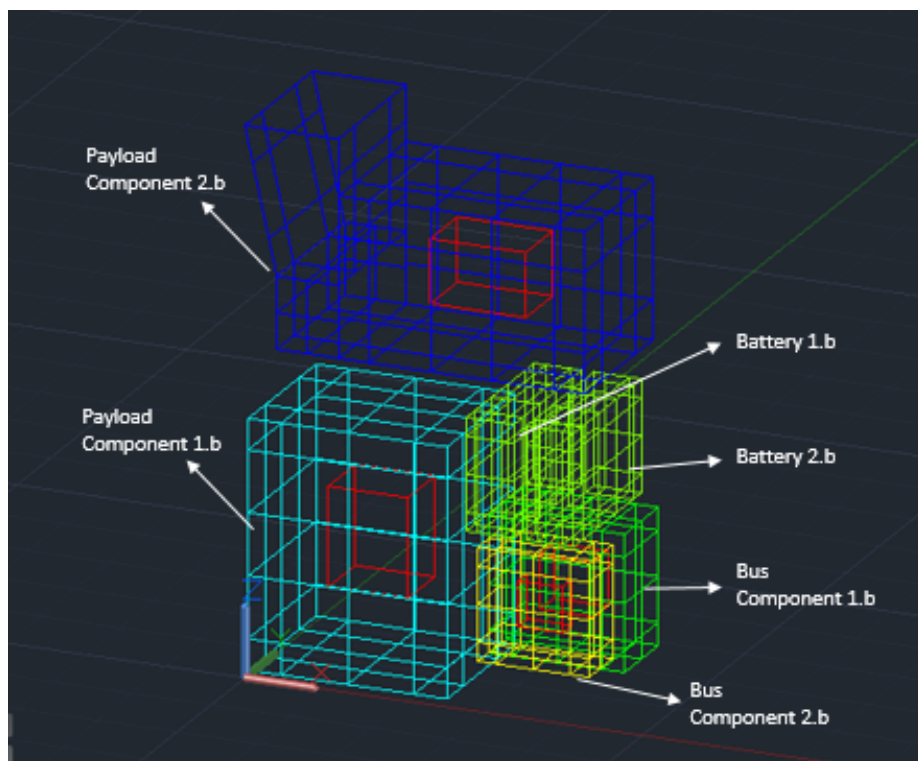


Figure 4.12: Mission 2.b payload and bus component.

Conductors

Unlike the previous mission, to connect the internal components to the external surfaces and to model the conductive paths at the interfaces it has been used the *Node-to-Node Contact* function, simulating the screw connections.

In Figure 4.13 is shown a conductors representation (red links in figure), while in Table 4.15 and Table 4.16 the input parameters used for the conductance calculation at the interfaces have been reported. Knowing steel thermophysical properties, the conductance coefficients are obtained inserting only the interface ratio *Area/Length*.

Interface	Area/Length [mm]
Battery – 6U/Y-	8
Battery – 6U/Y+	8
Bus Comp. 1.a - Bus Comp. 2.a	6
Bus Comp. 1.a – 6U/Y+	7
Payload Comp. 1.a – 6U/Y-	7
Payload Comp. 1.a – 6U/Y+	7
Payload Comp. 2.a – 6U/Y-	3
Payload Comp. 2.a – 6U/Y+	3

Table 4.15: Mission 2.a conductors parameters.

Interface	Area/Length [W/k]
Battery – 6U/Y-	8
Battery – 6U/Y+	11
Bus Comp. 1.b - Bus Comp. 2.b	6
Bus Comp. 1.b – 6U/Y+	7
Payload Comp. 1.b – 6U/Y-	5
Payload Comp. 1.b – 6U/Y+	7
Payload Comp. 2.b – 6U/Y-	5
Payload Comp. 2.b – 6U/Y+	7

Table 4.16: Mission 2.b conductors parameters.

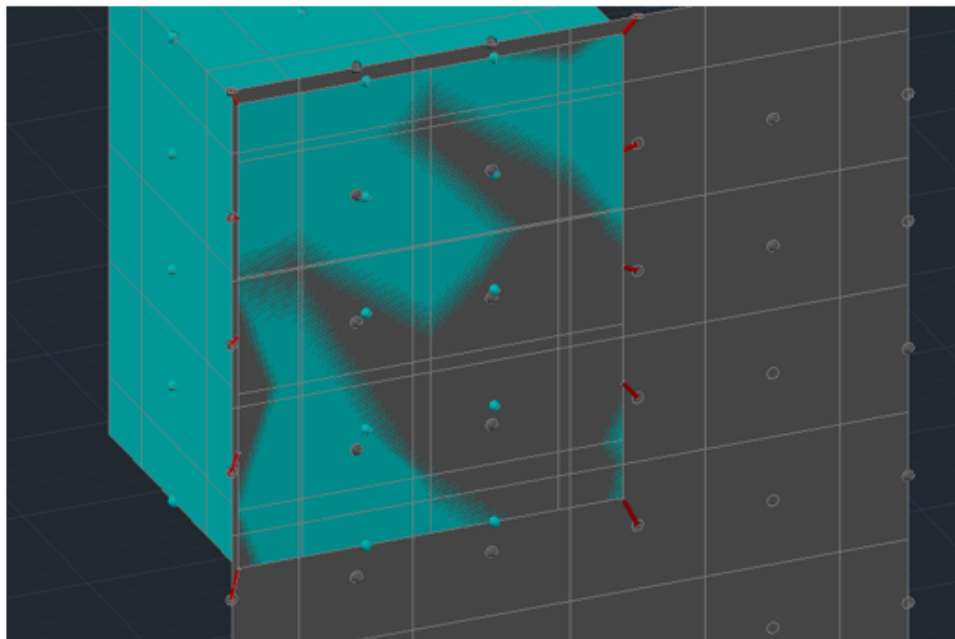


Figure 4.13: Mission 2 conductors.

Heat Loads

The heat loads, as previously for Mission 1, have been applied on the black body inside every component. These are solid heat loads, since they are applied to FD solids. Moreover, there are also surface heat load applied to the baffle of Payload Component 2.b, and heaters to the batteries, which are temperature dependent so they switch on only if $T < 5^\circ\text{C}$. The payloads heat loads for these mission are time dependent so they switch on only in a defined time per orbit. The heat loads included in the models, illustrated in Figure 4.14 and Figure 4.15, and their time dependency are reported in Table 4.17.

Heat Load	Power [W]	Time On
Payload Component 1.a	10	900 sec per orbit
Payload Component 2.a	12.5	955 sec per orbit
Payload Component 1.b	10	900 sec per orbit
Payload Component 2.b	8	240 sec per orbit
Payload Component 2.b Baffle	1	240 sec per orbit
Batteries	0.5	Temperature dependent
Bus Component 1.a and 1.b	3	Always On
Bus Component 2.a and 2.b	1	Always On

Table 4.17: Mission 2 heat loads.

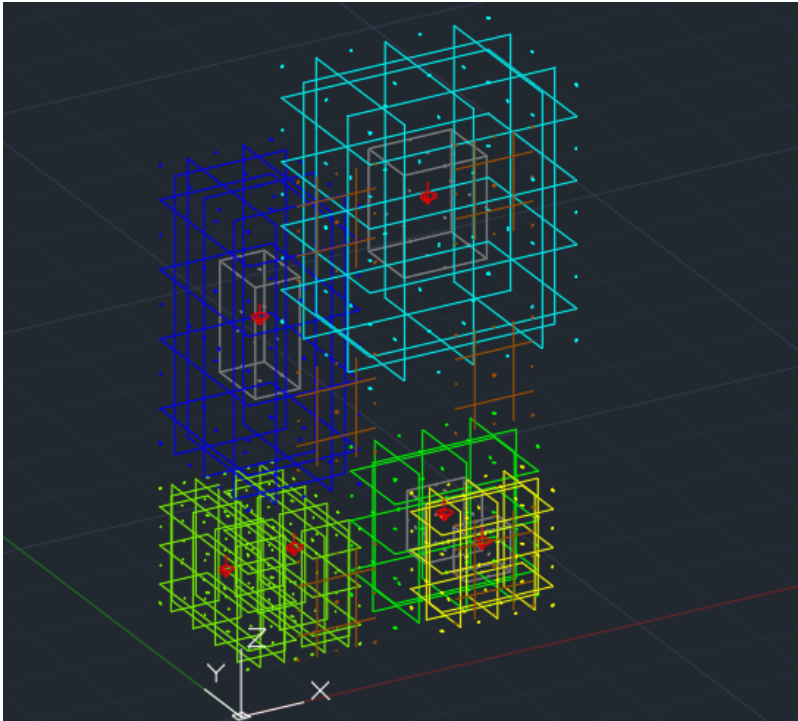


Figure 4.14: Mission 2.a heat loads.

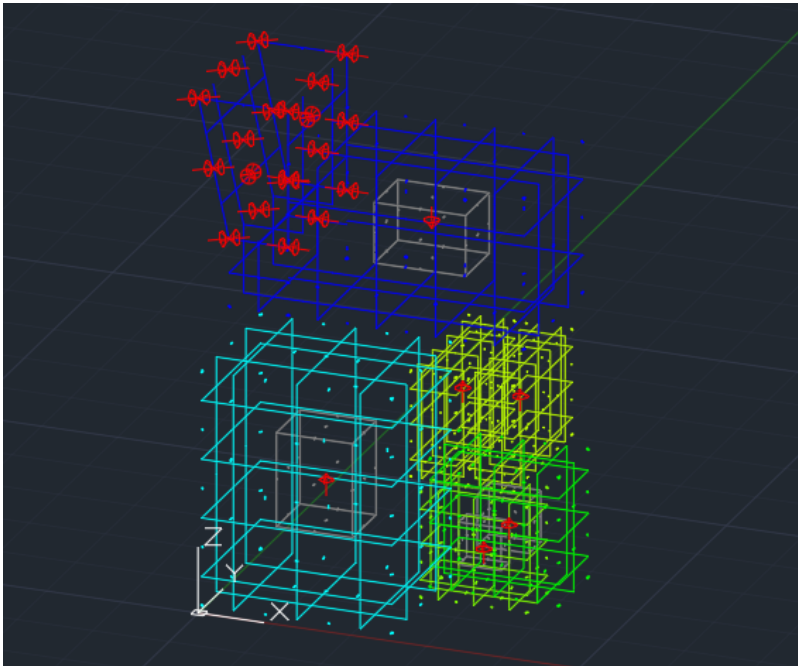


Figure 4.15: Mission 2.b heat loads.

Orbit

The orbit chosen for Mission 2, as for Mission 1, is a sun-synchronous $LTAN = 10 : 30 \text{ am}$. The reason of this choice is the major availability of launch windows as piggy-back. An orbit representation is shown in Figure 4.16, while the other orbital data are reported in Table 4.18.

Orbital Parameter	Value
SSO LTAN	10 : 30 <i>am</i>
RAAN	106.982°
h	550 <i>km</i>
i	97.5088°
T0	01/08/2019 @10 : 00 : 00

Table 4.18: Mission 2 orbital data.

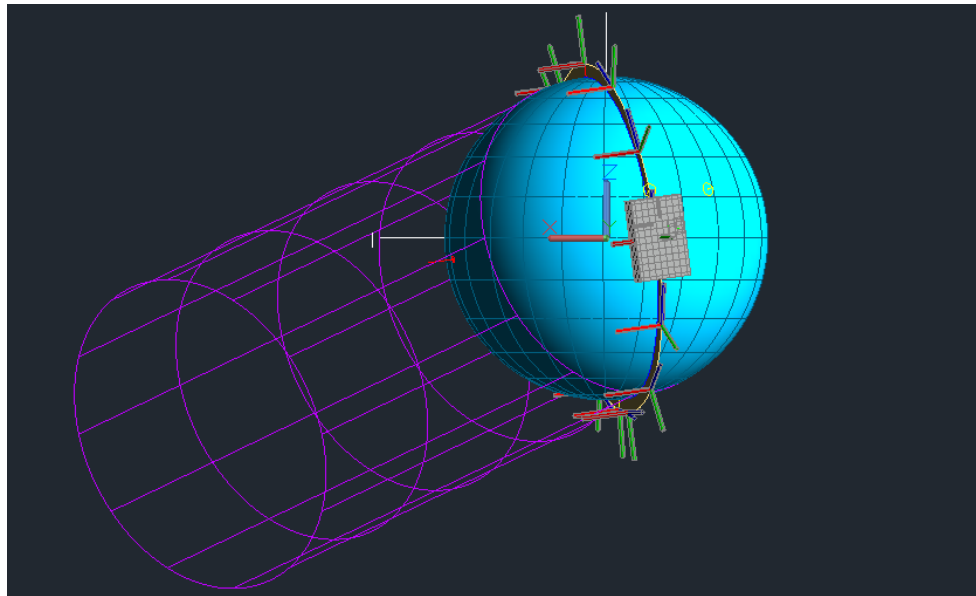


Figure 4.16: Mission 2 orbit.

Case Scenario

The case scenarios analysed for Mission 2 are four (two for each CubeSat): the worst hot cases and the worst cold cases. The main characteristics for each scenario are listed in Table 4.19.

The results and conclusion related to these analysis, included the choice between alodine and anodized, are discussed in Chapter 5.

Case	Orientation	Payload	Bus
Mission 2.a Worst Hot Case	Sun Pointing: 6U/Y+	Off	On
Mission 2.a Worst Cold Case	Nadir: 6U/Y- Velocity Vector: 2U/Z+	Off	On
Mission 2.b Worst Hot Case	Sun Pointing: 6U/Y-	Off	On
Mission 2.b Worst Cold Case	Nadir: 6U/Y+ Velocity Vector: 2U/Z-	Off	On

Table 4.19: Mission 2 case scenarios.

The Worst Hot Case is the sun-pointing scenario, in which the solar panel is perpendicularly directed to the Sun. In this situation the payload is off, while the bus is operative. Instead, the Worst Cold Case is the idle situation, so the spacecraft is nominal orientated but payload is off and bus is in Idle configuration so with reduced power.

Chapter 5

Results

Here are resumed the complete results of the analyses executed for Mission 1 and Mission 2 for the different case scenarios discussed previously.

5.1 Mission 1

5.1.1 Worst Hot Case

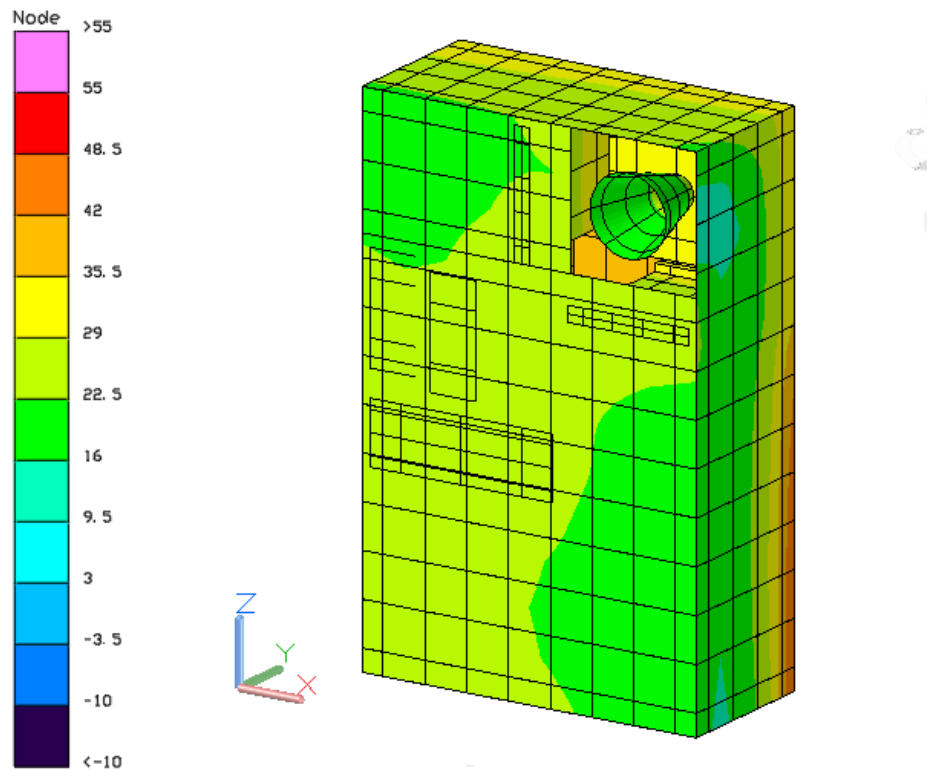


Figure 5.1: Mission 1 Worst Hot Case color post-processing.

6U/Y+

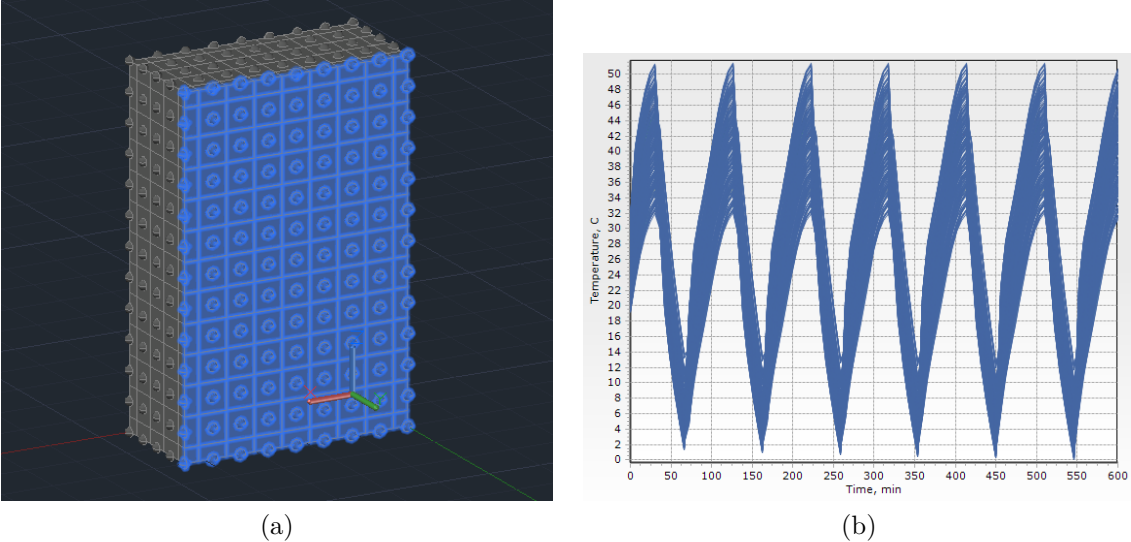


Figure 5.2: Mission 1 6U/Y+ Worst Hot Case x-y plotting.

6U/Y-

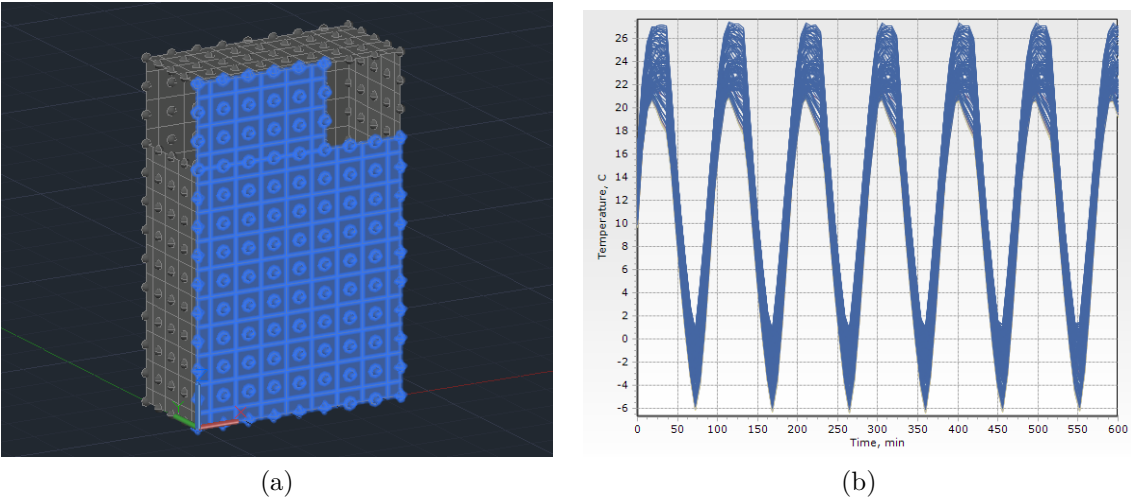
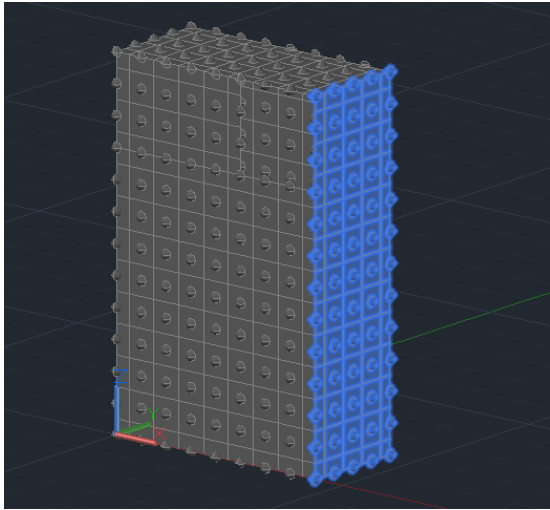
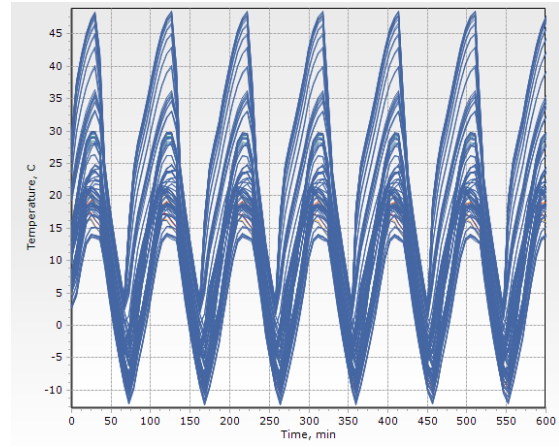


Figure 5.3: Mission 1 6U/Y- Worst Hot Case x-y plotting.

3U/X+



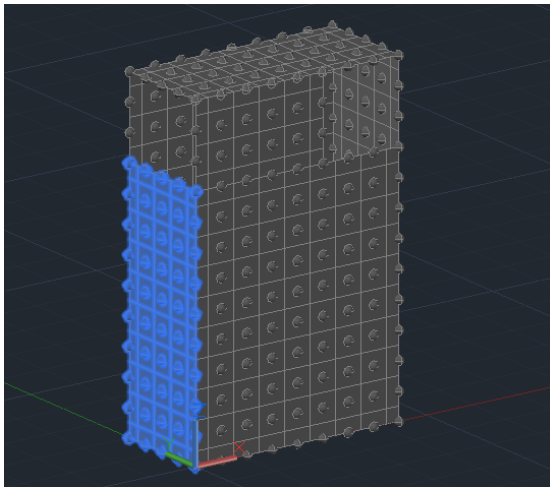
(a)



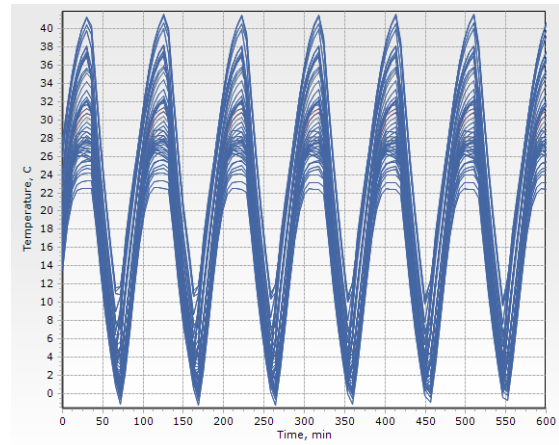
(b)

Figure 5.4: Mission 1 3U/X+ Worst Hot Case x-y plotting.

3U/X-



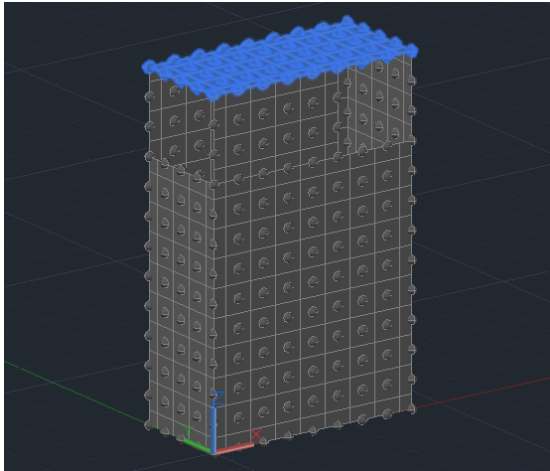
(a)



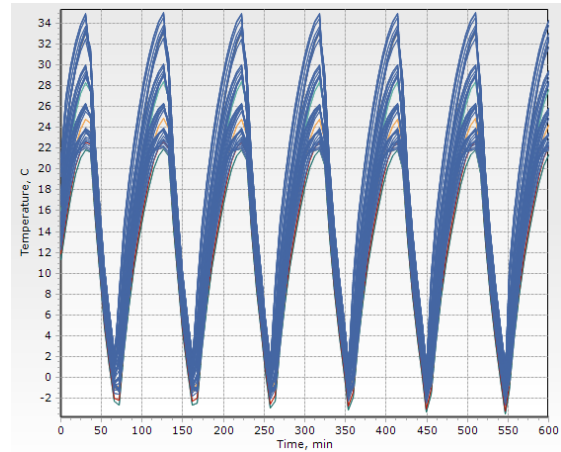
(b)

Figure 5.5: Mission 1 3U/X- Worst Hot Case x-y plotting.

2U/Z+



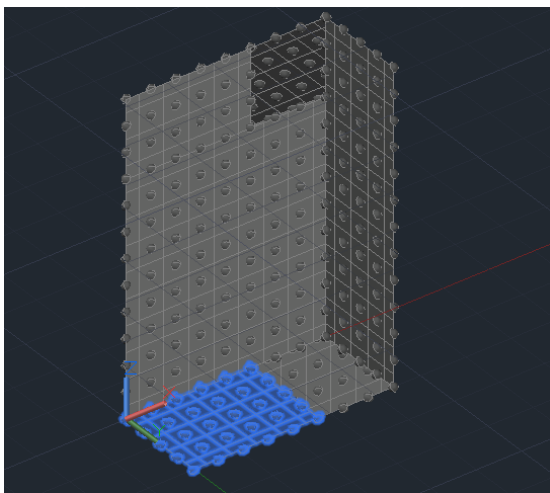
(a)



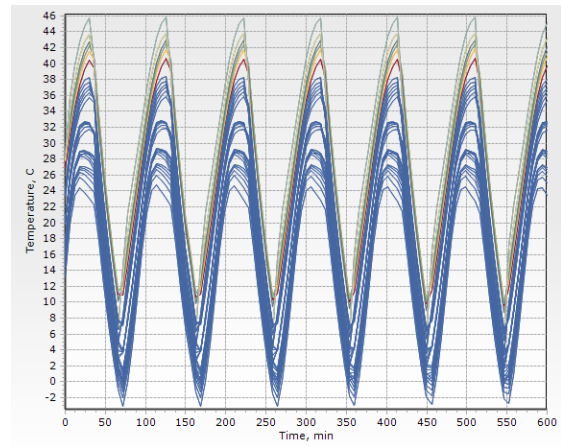
(b)

Figure 5.6: Mission 1 2U/Z+ Worst Hot Case x-y plotting.

2U/Z-



(a)



(b)

Figure 5.7: Mission 1 2U/Z- Worst Hot Case x-y plotting.

Camera 1

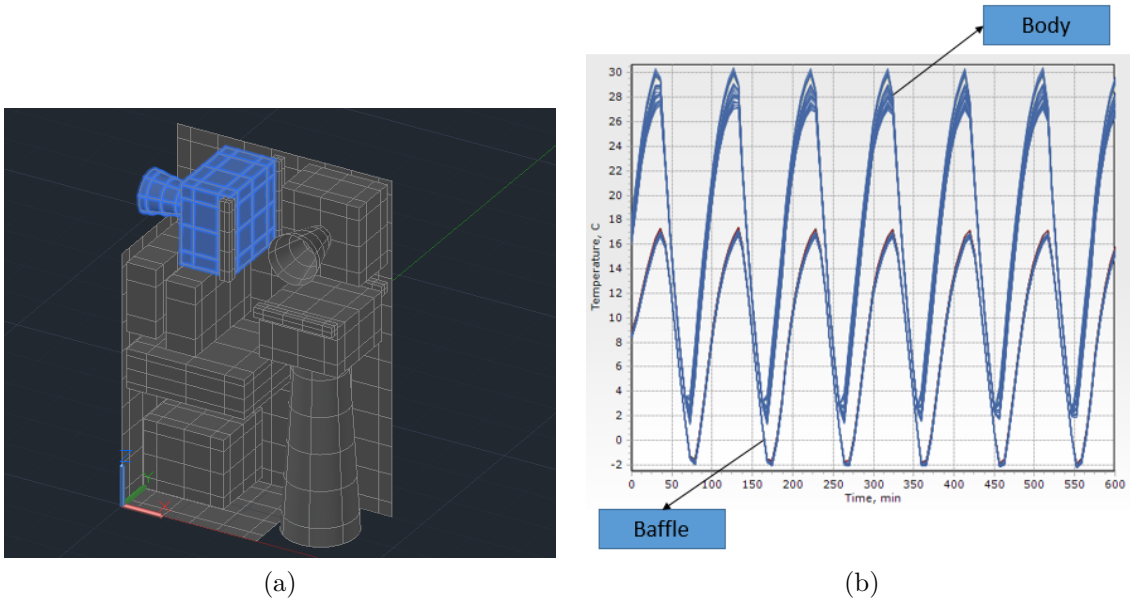


Figure 5.8: Mission 1 Camera 1 Worst Hot Case x-y plotting.

Camera 2

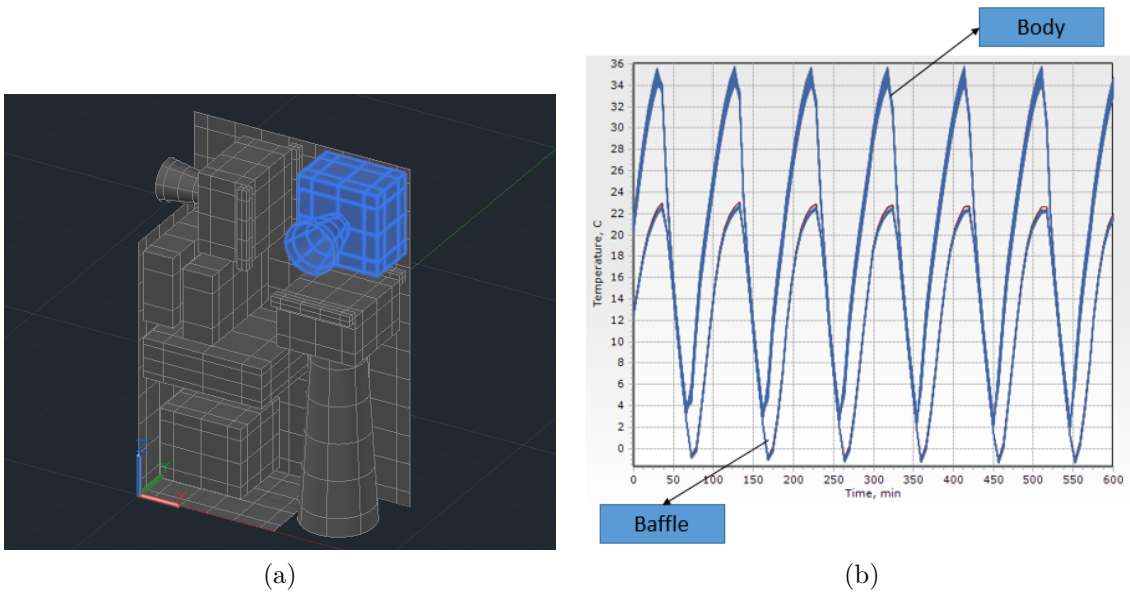


Figure 5.9: Mission 1 Camera 2 Worst Hot Case x-y plotting.

Camera 3

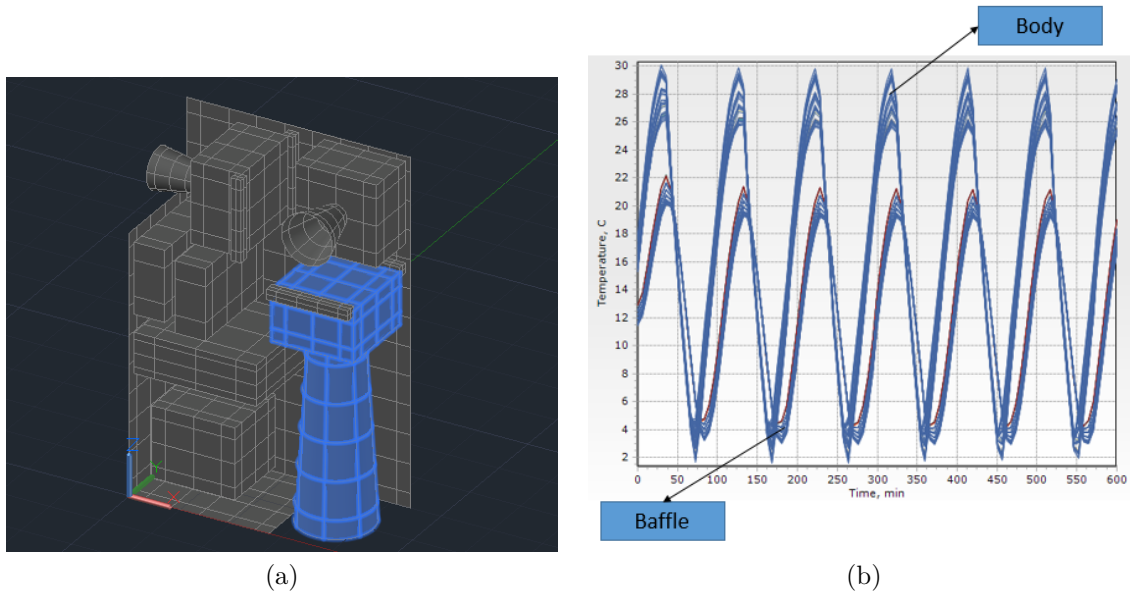


Figure 5.10: Mission 1 Camera 3 Worst Hot Case x-y plotting.

Brackets

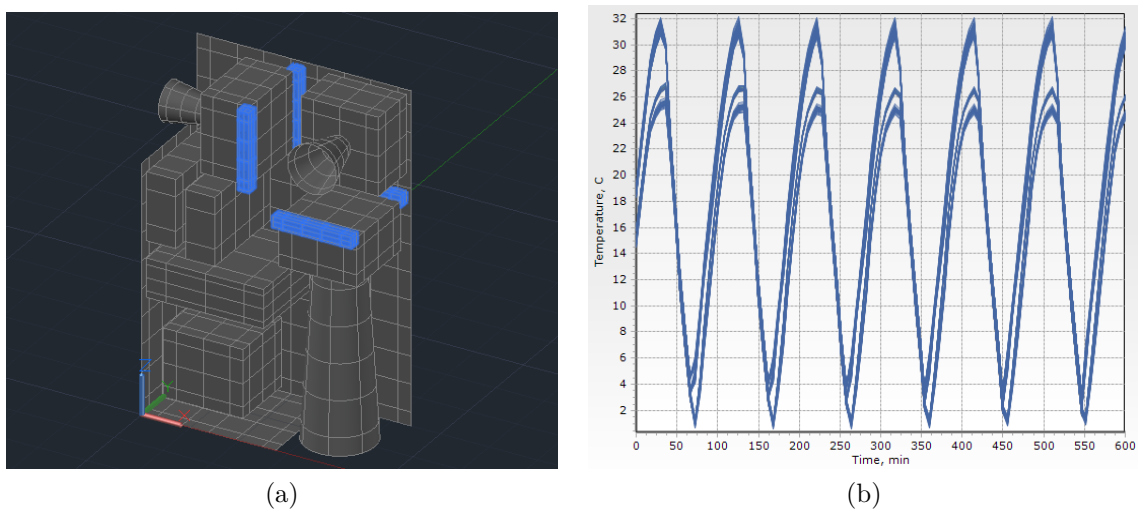
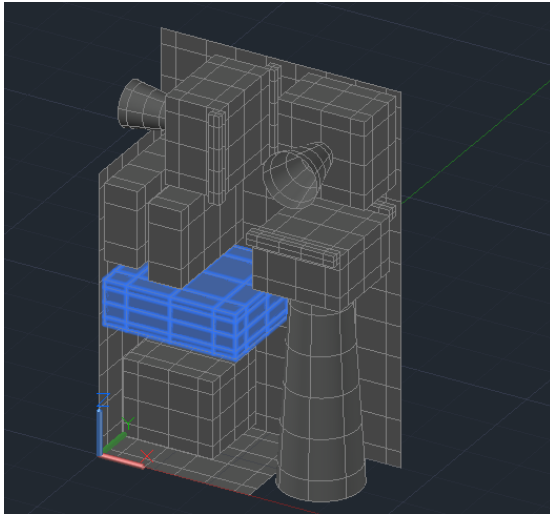
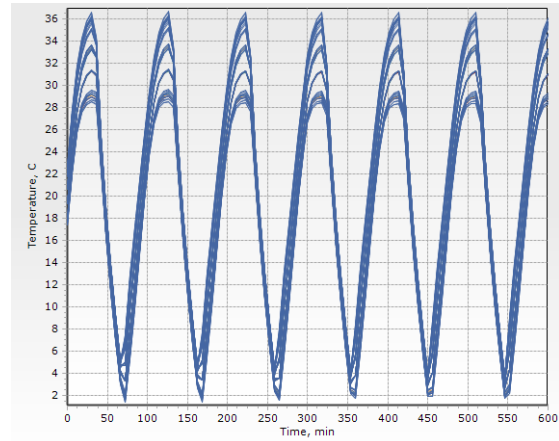


Figure 5.11: Mission 1 brackets Worst Hot Case x-y plotting.

Payload Component



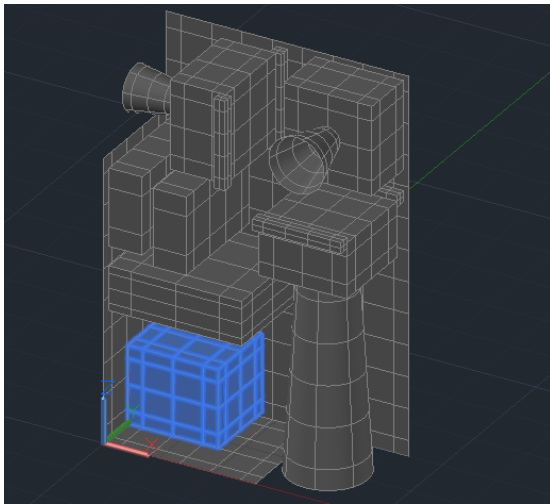
(a)



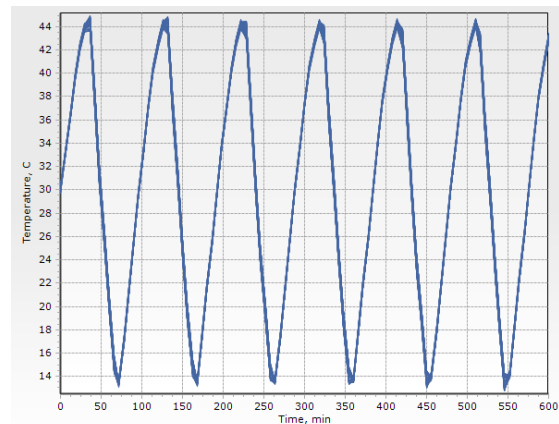
(b)

Figure 5.12: Mission 1 Payload Component Worst Hot Case x-y plotting.

Bus Component



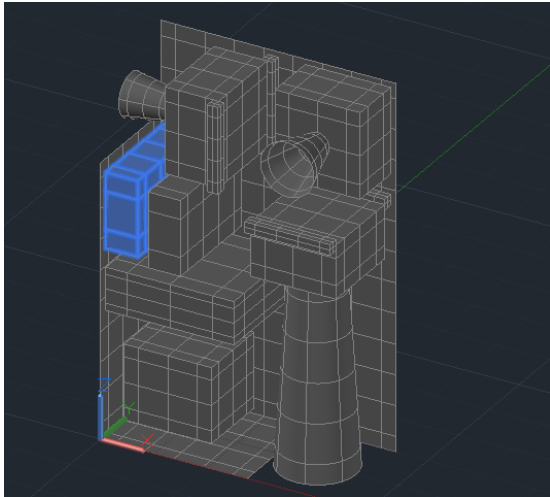
(a)



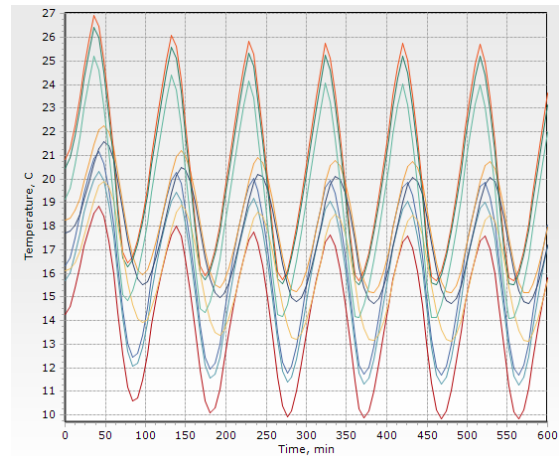
(b)

Figure 5.13: Mission 1 Bus Component Worst Hot Case x-y plotting.

Battery 1



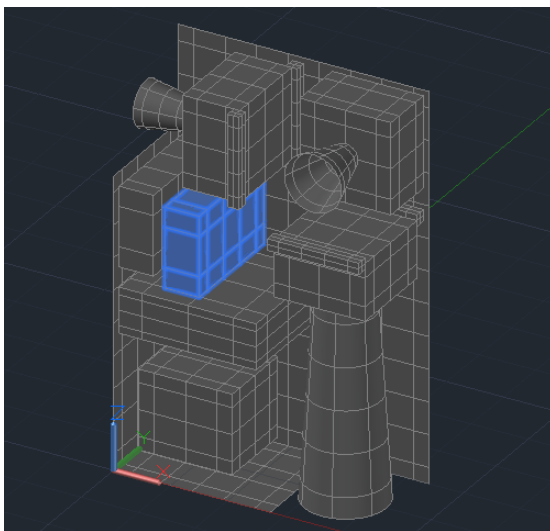
(a)



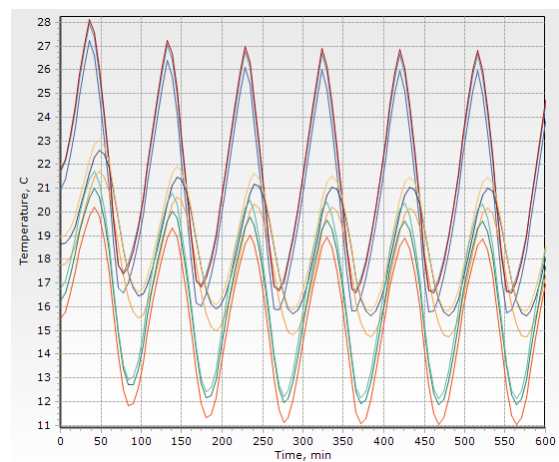
(b)

Figure 5.14: Mission 1 battery 1 Worst Hot Case x-y plotting.

Battery 2



(a)



(b)

Figure 5.15: Mission 1 battery 2 Worst Hot Case x-y plotting.

5.1.2 Worst Cold Case

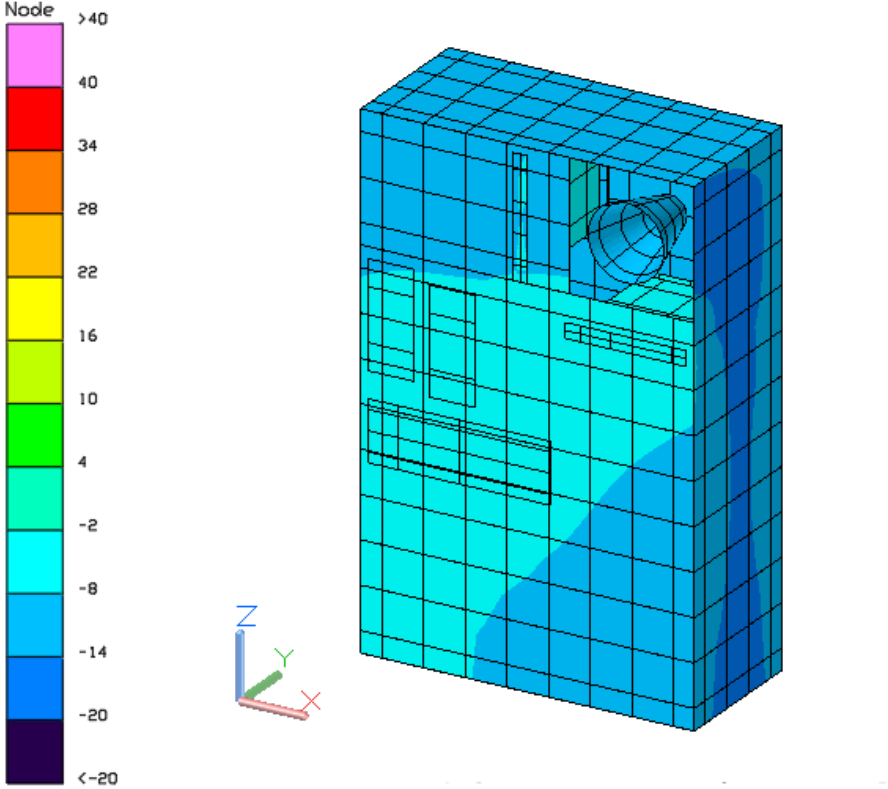
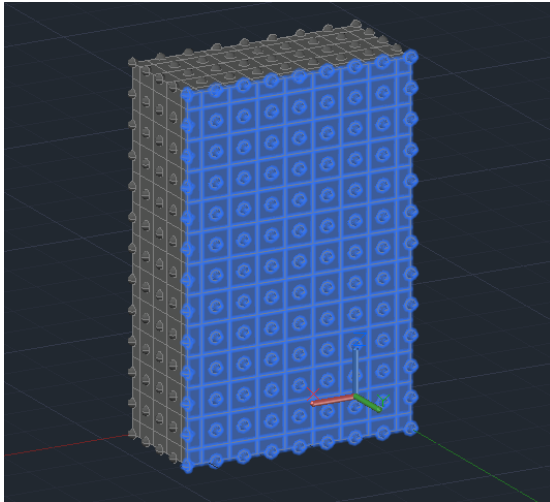
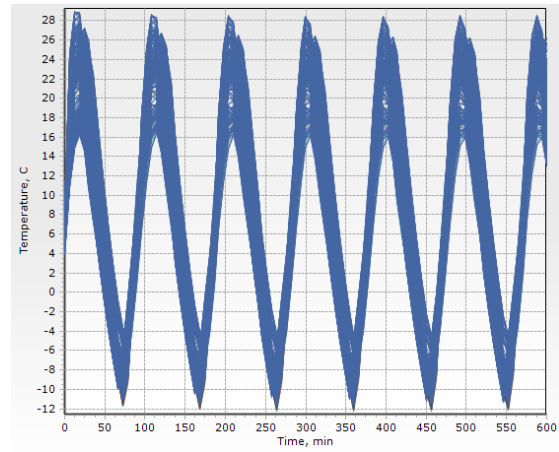


Figure 5.16: Mission 1 Worst Cold Case color post-processing.

6U/Y+



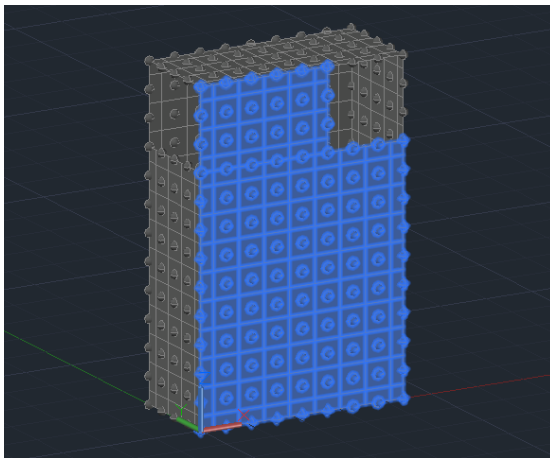
(a)



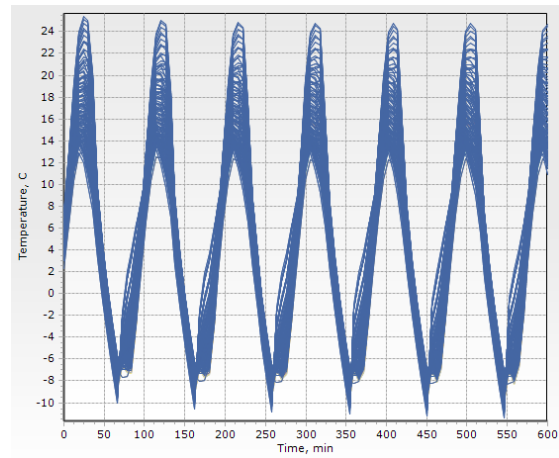
(b)

Figure 5.17: Mission 1 6U/Y+ Worst Cold Case x-y plotting.

6U/Y-



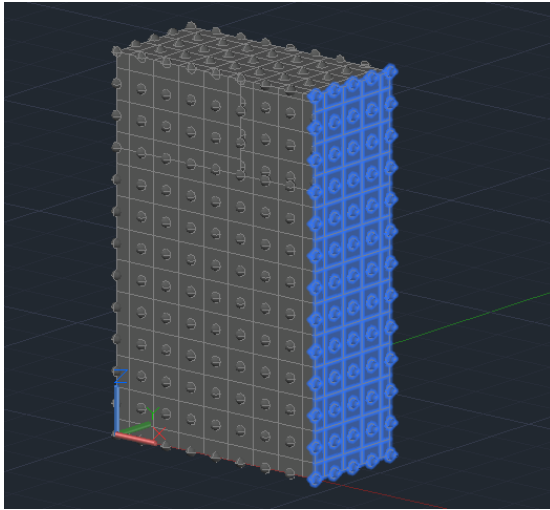
(a)



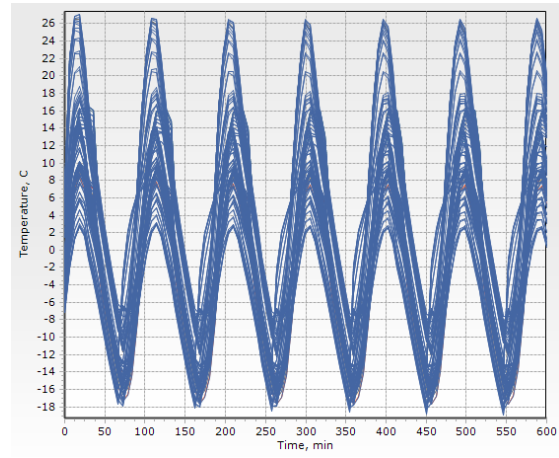
(b)

Figure 5.18: Mission 1 6U/Y- Worst Cold Case x-y plotting.

3U/X+



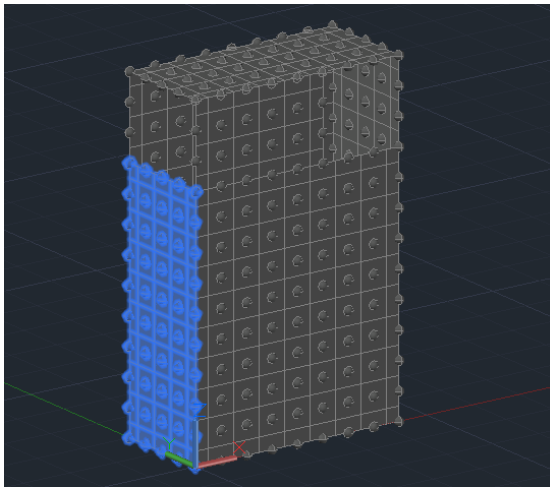
(a)



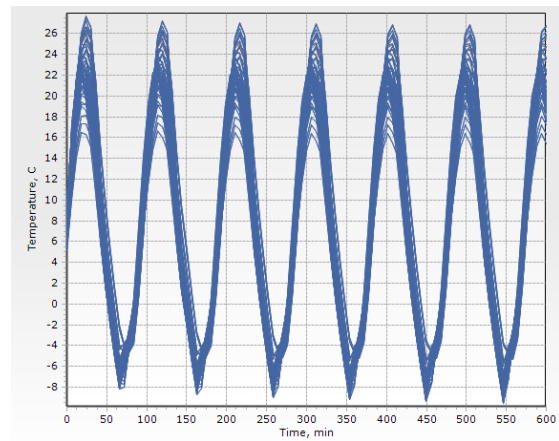
(b)

Figure 5.19: Mission 1 3U/X+ Worst Cold Case x-y plotting.

3U/X-



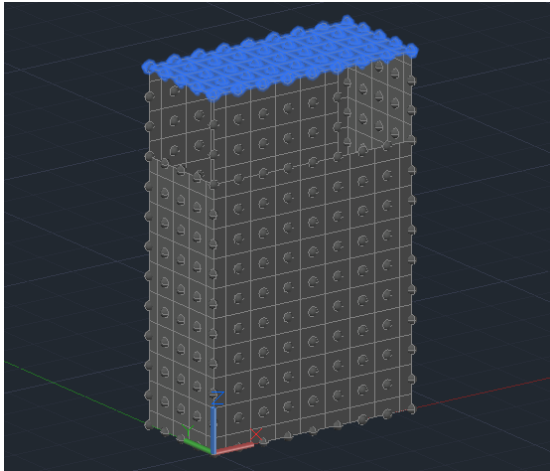
(a)



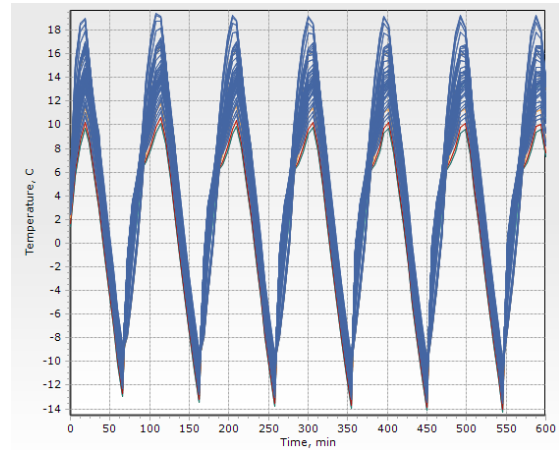
(b)

Figure 5.20: Mission 1 3U/X- Worst Cold Case x-y plotting.

2U/Z+



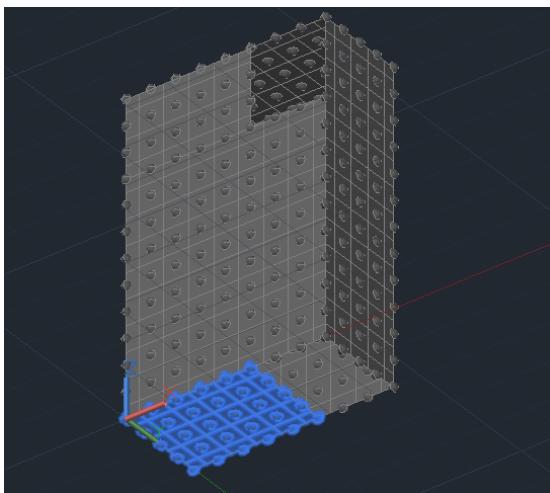
(a)



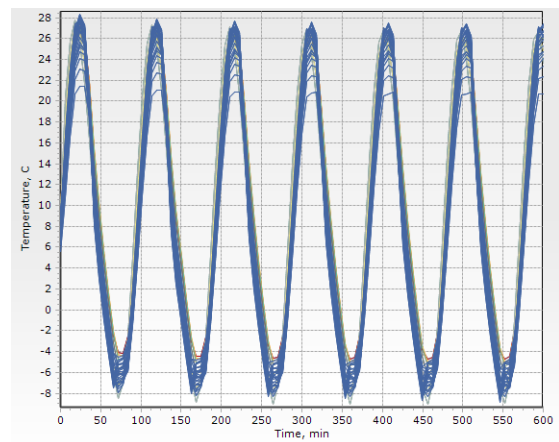
(b)

Figure 5.21: Mission 1 2U/Z+ Worst Cold Case x-y plotting.

2U/Z-



(a)



(b)

Figure 5.22: Mission 1 2U/Z- Worst Cold Case x-y plotting.

Camera 1

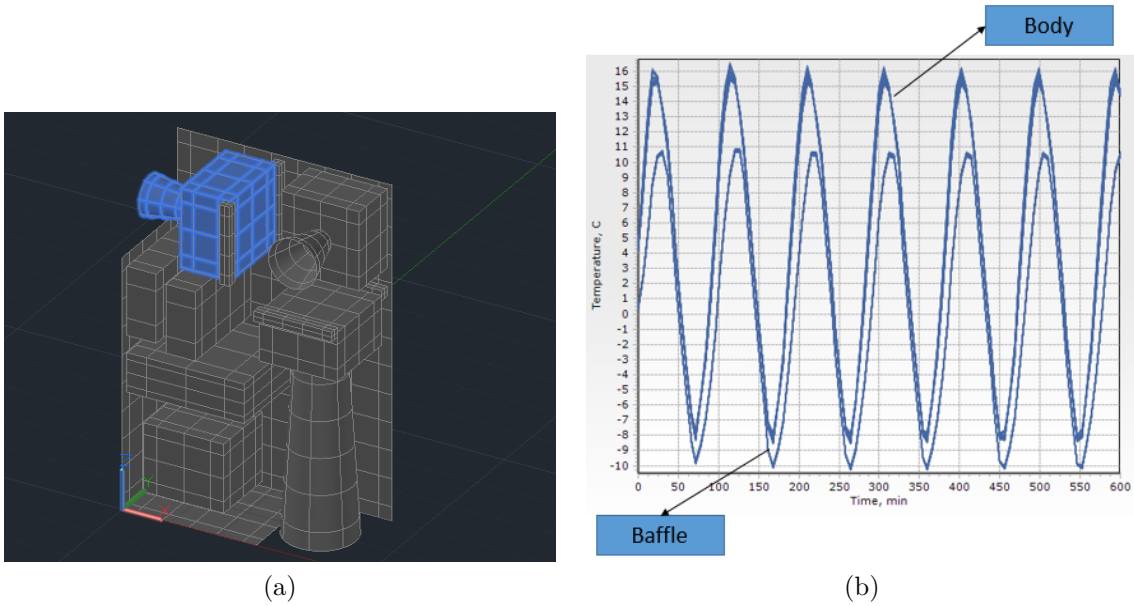


Figure 5.23: Mission 1 Camera 1 Worst Cold Case x-y plotting.

Camera 2

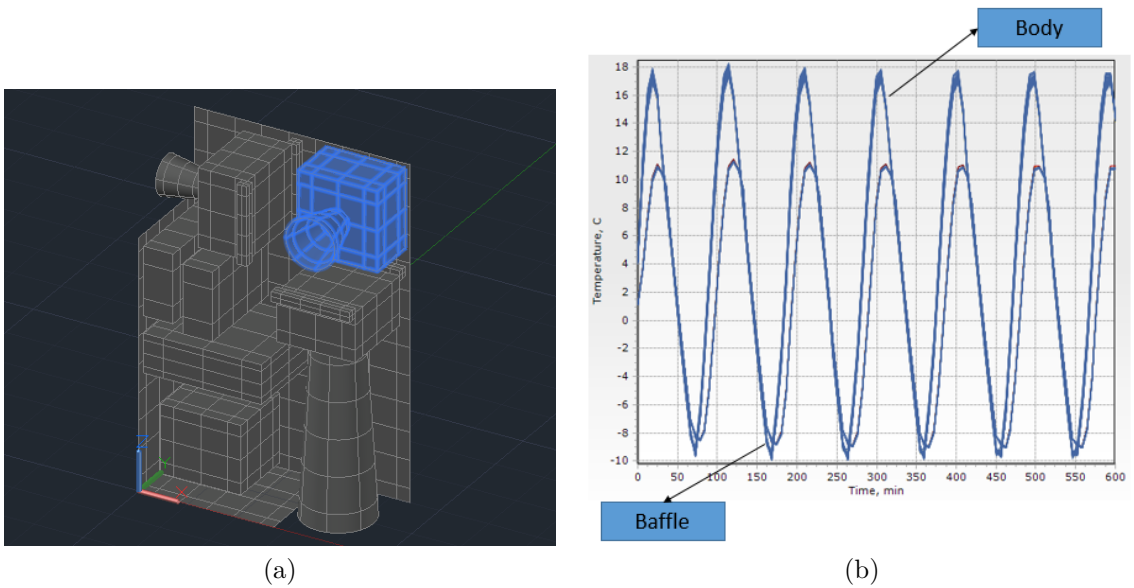


Figure 5.24: Mission 1 Camera 2 Worst Cold Case x-y plotting.

Camera 3

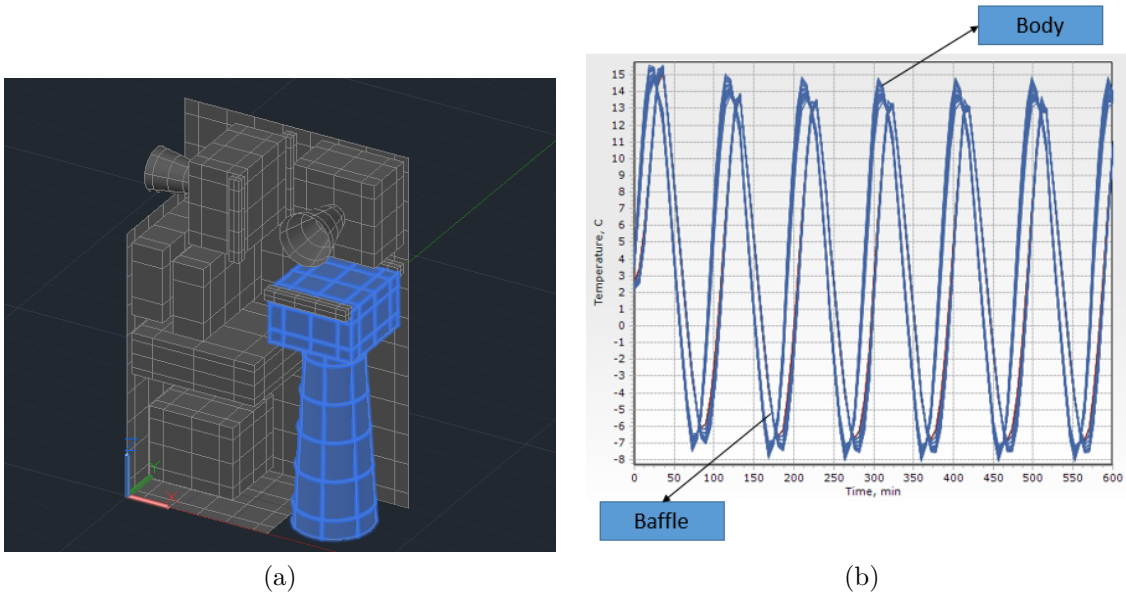


Figure 5.25: Mission 1 Camera 3 Worst Cold Case x-y plotting.

Brackets

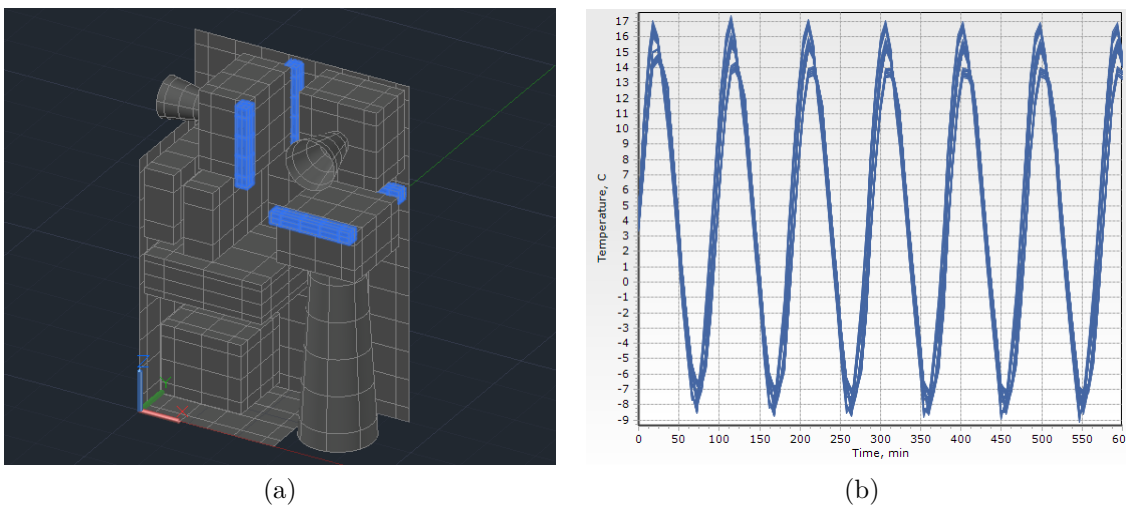
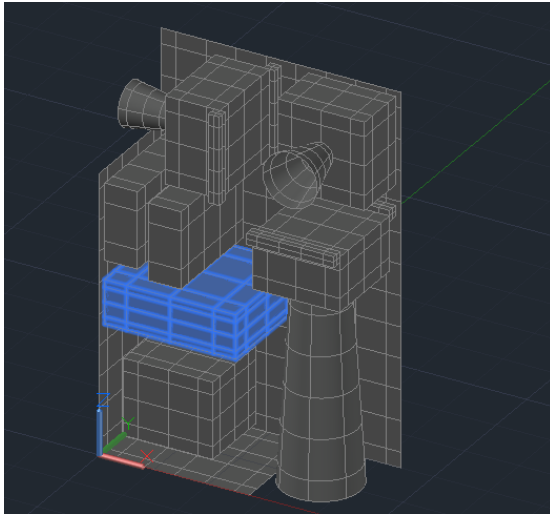
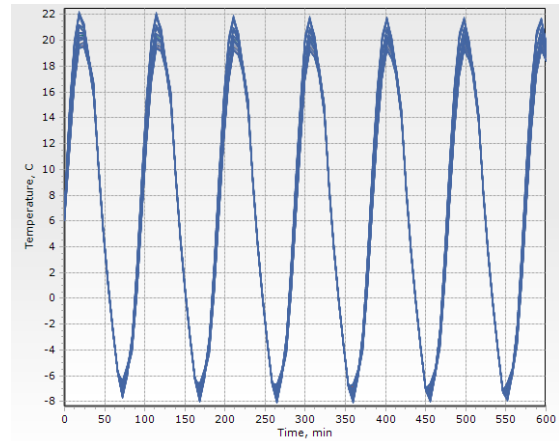


Figure 5.26: Mission 1 brackets Worst Cold Case x-y plotting.

Payload Component



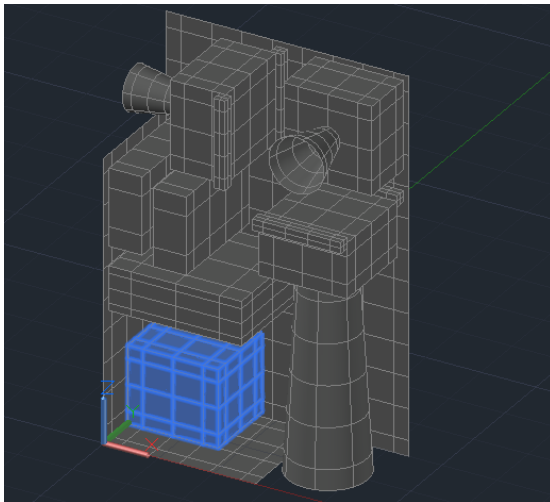
(a)



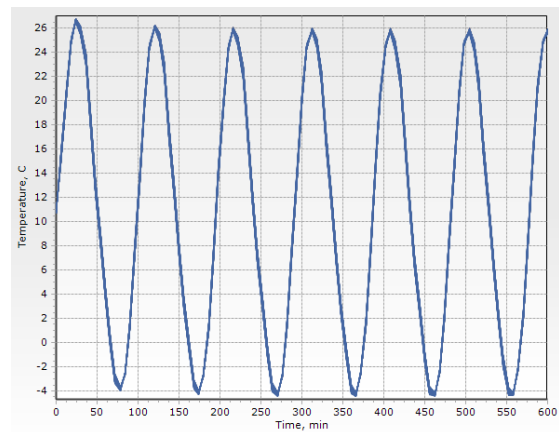
(b)

Figure 5.27: Mission 1 Payload Component Worst Cold Case x-y plotting.

Bus Component



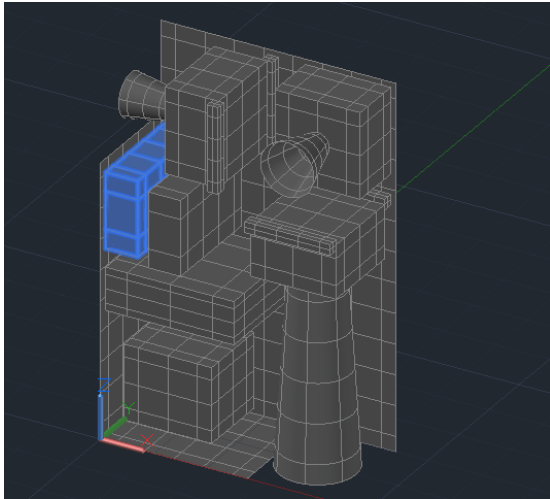
(a)



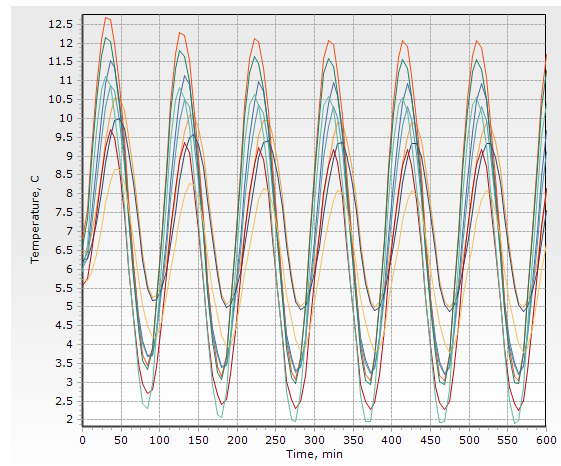
(b)

Figure 5.28: Mission 1 Bus Component Worst Cold Case x-y plotting.

Battery 1



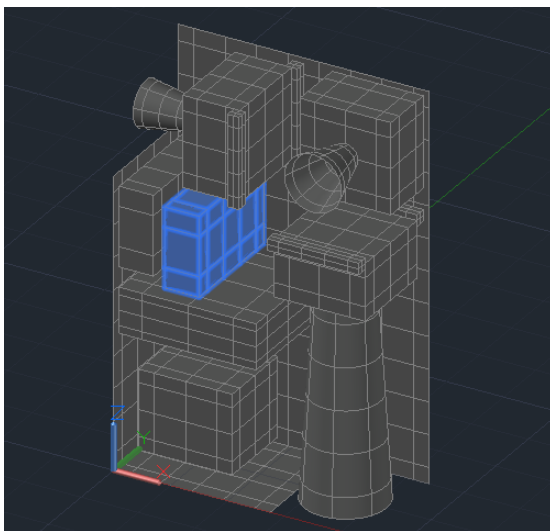
(a)



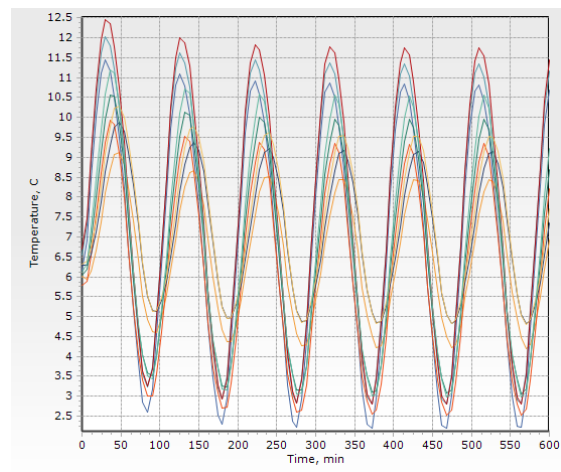
(b)

Figure 5.29: Mission 1 battery 1 Worst Cold Case x-y plotting.

Battery 2



(a)



(b)

Figure 5.30: Mission 1 battery 2 Worst Cold Case x-y plotting.

5.1.3 Nominal Case

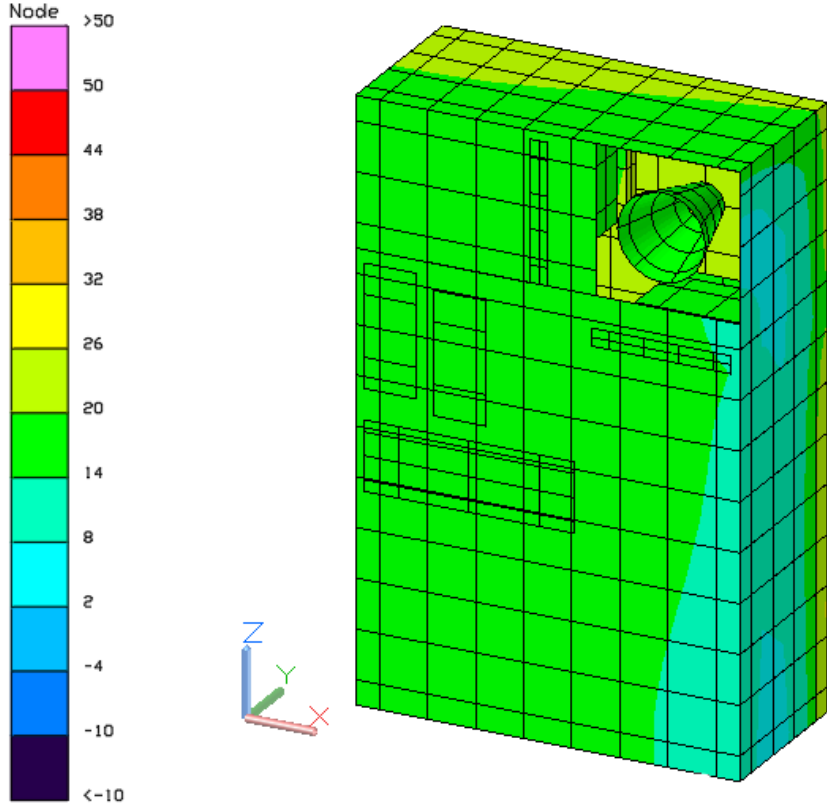
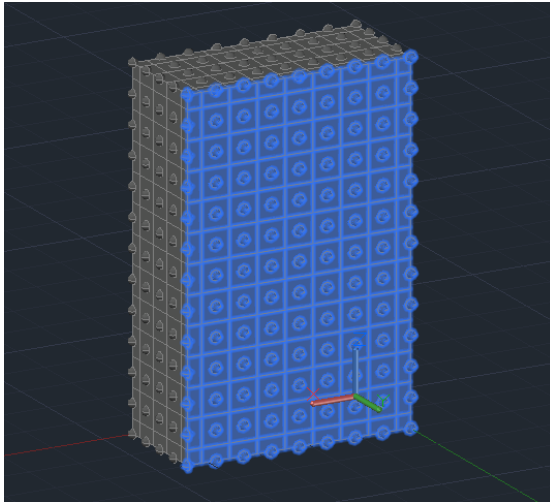
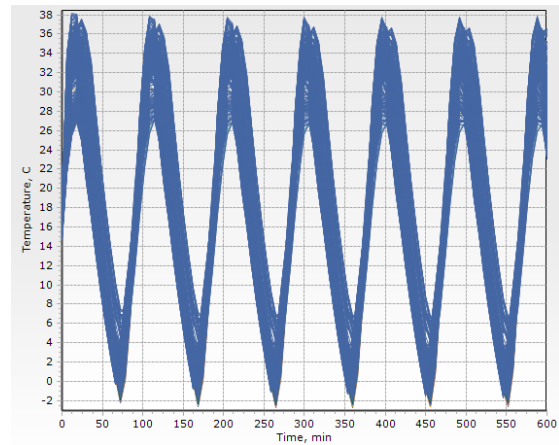


Figure 5.31: Mission 1 Nominal Case color post-processing.

6U/Y+



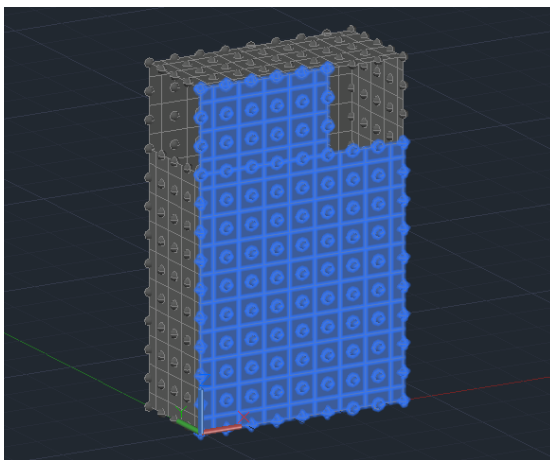
(a)



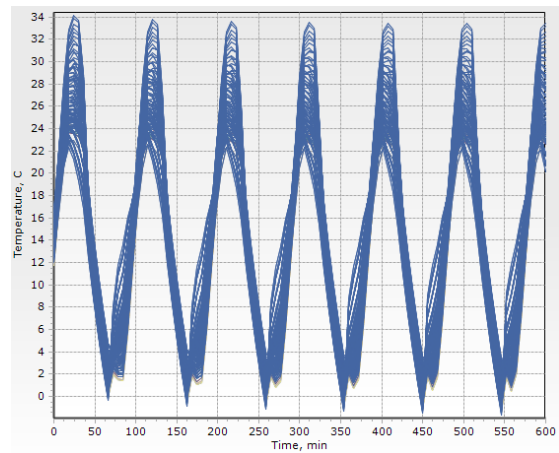
(b)

Figure 5.32: Mission 1 6U/Y+ Nominal Case x-y plotting.

6U/Y-



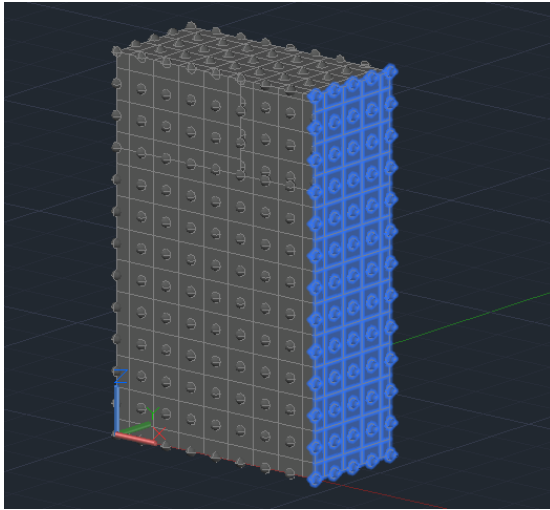
(a)



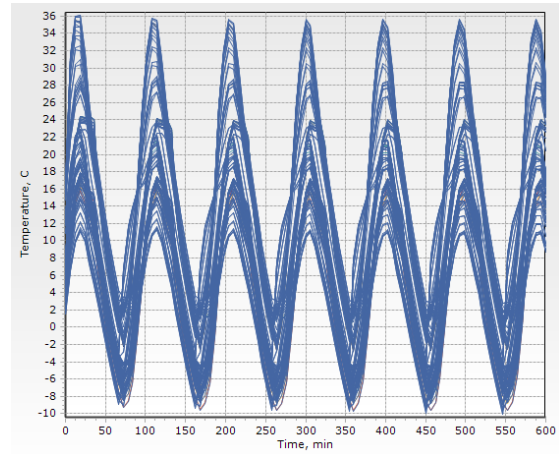
(b)

Figure 5.33: Mission 1 6U/Y- Nominal Case x-y plotting.

3U/X+



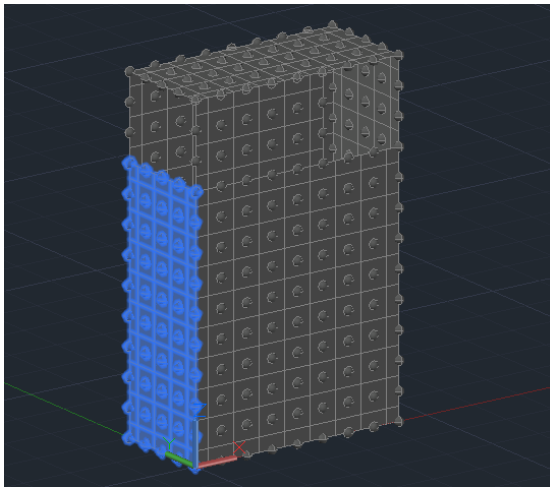
(a)



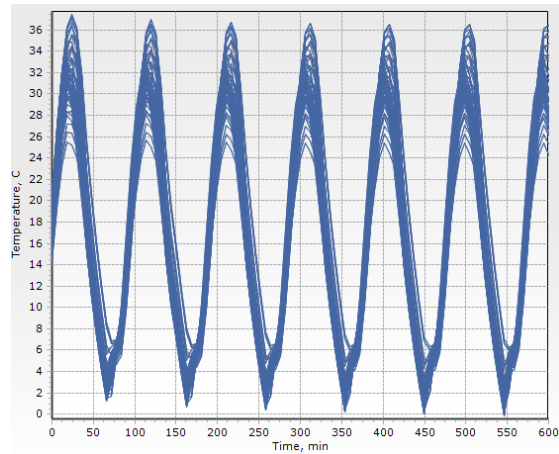
(b)

Figure 5.34: Mission 1 3U/X+ Nominal Case x-y plotting.

3U/X-



(a)



(b)

Figure 5.35: Mission 1 3U/X- Nominal Case x-y plotting.

2U/Z+

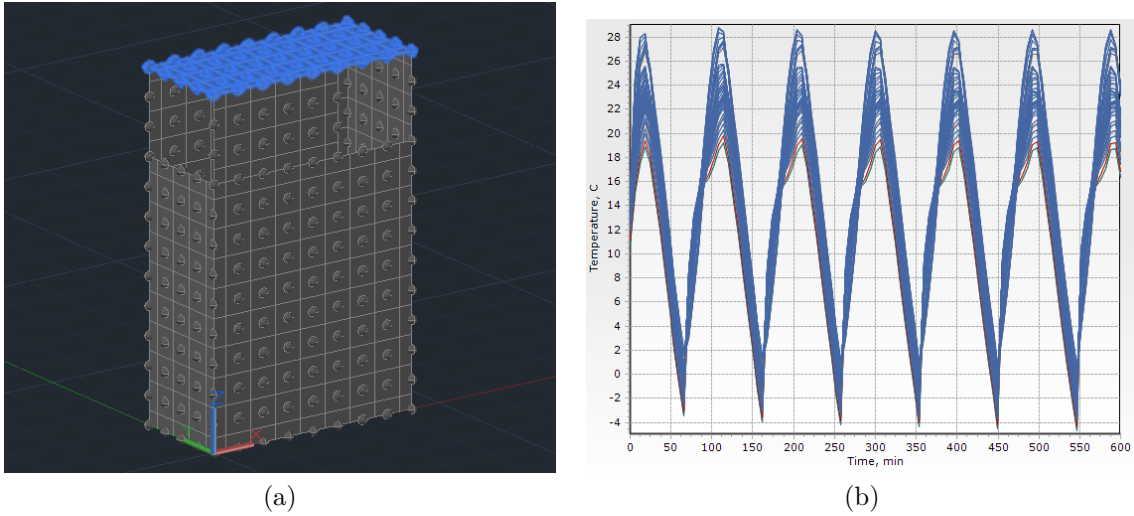


Figure 5.36: Mission 1 2U/Z+ Nominal Case x-y plotting.

2U/Z-

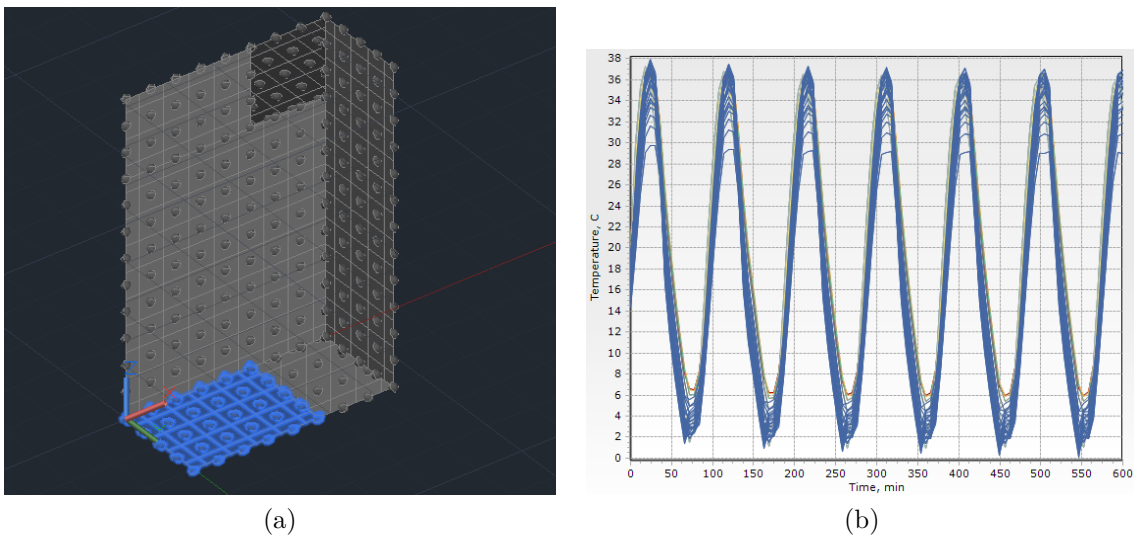


Figure 5.37: Mission 1 2U/Z- Nominal Case x-y plotting.

Camera 1

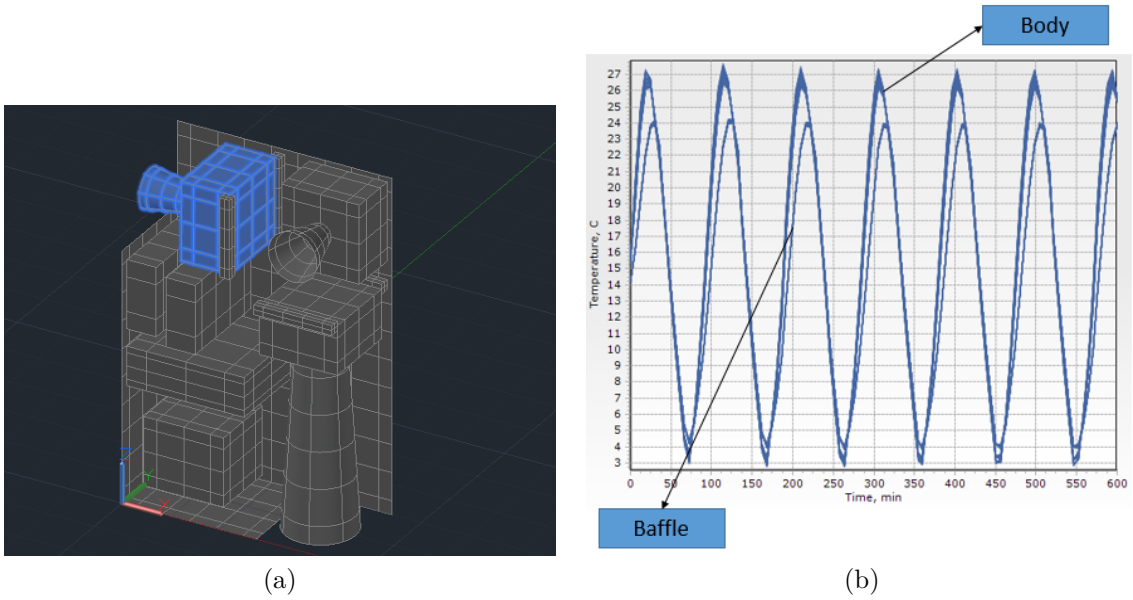


Figure 5.38: Mission 1 Camera 1 Nominal Case x-y plotting.

Camera 2

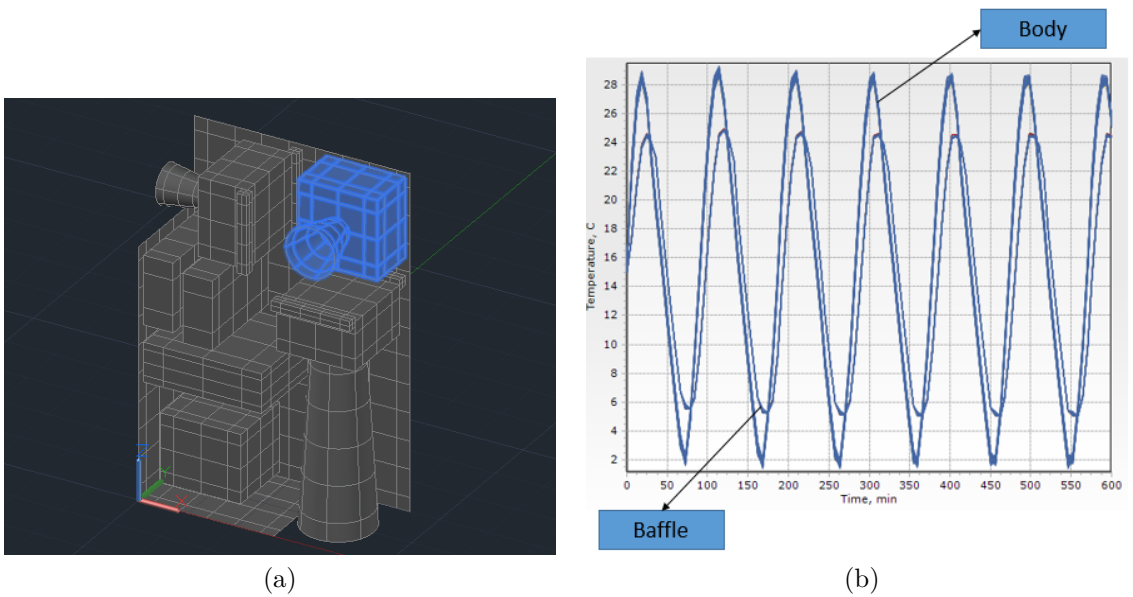


Figure 5.39: Mission 1 Camera 2 Nominal Case x-y plotting.

Camera 3

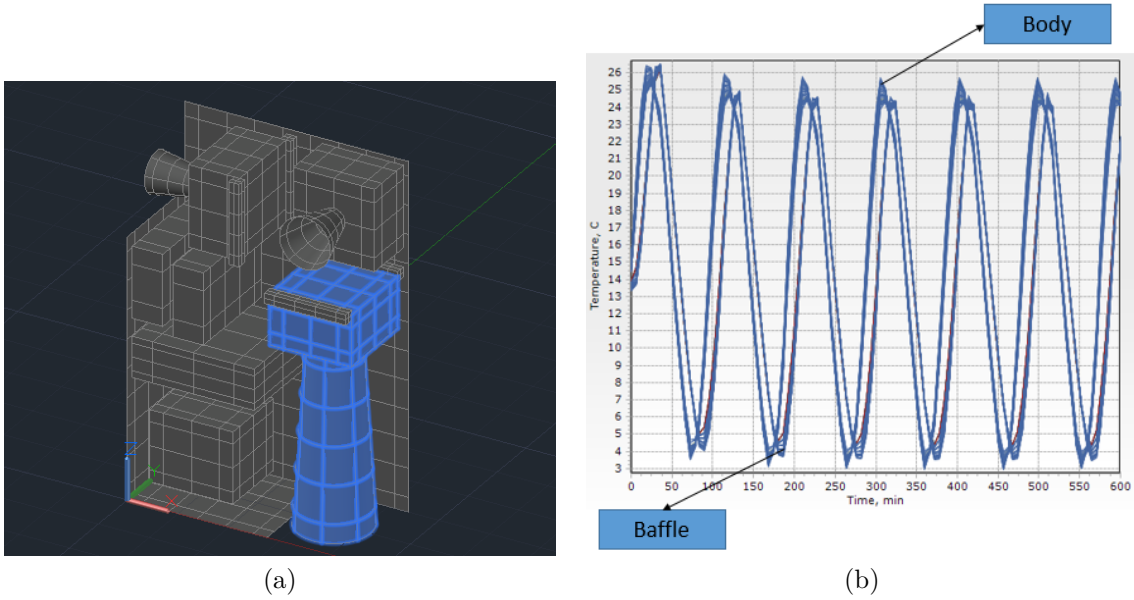


Figure 5.40: Mission 1 Camera 3 Nominal Case x-y plotting.

Brackets

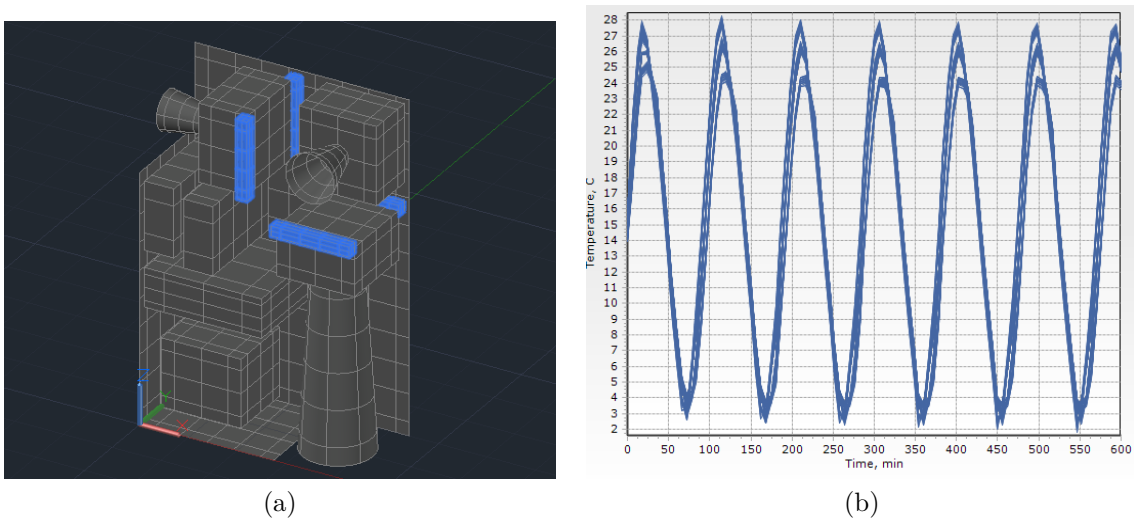
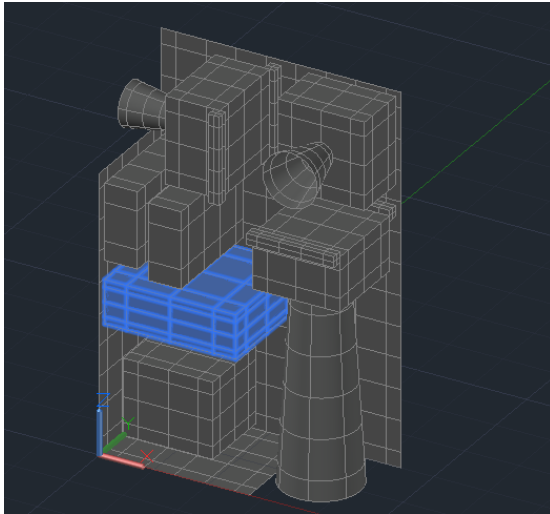
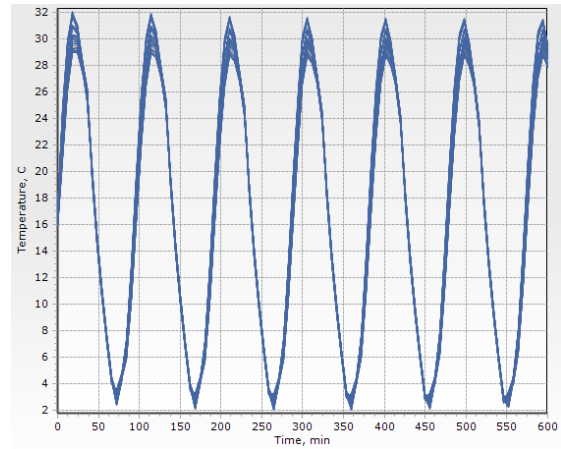


Figure 5.41: Mission 1 brackets Nominal Case x-y plotting.

Payload Component



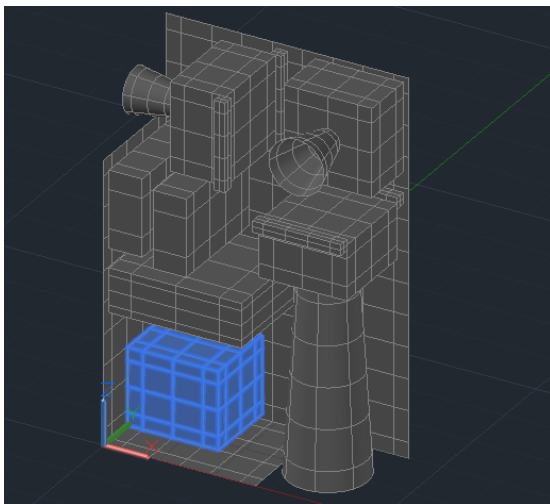
(a)



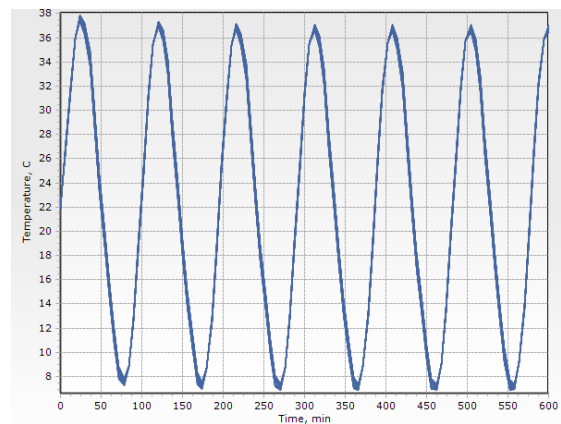
(b)

Figure 5.42: Mission 1 Payload Component Nominal Case x-y plotting.

Bus Component



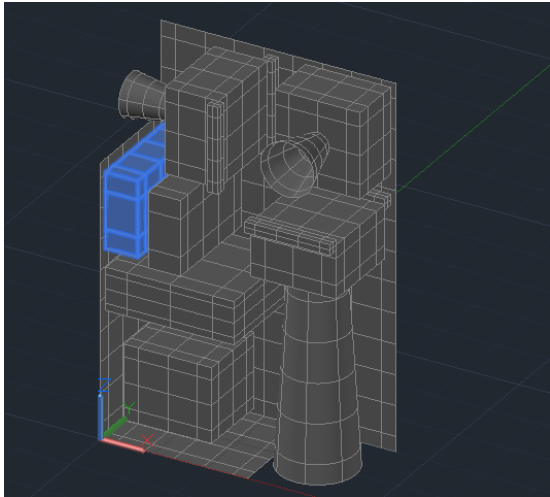
(a)



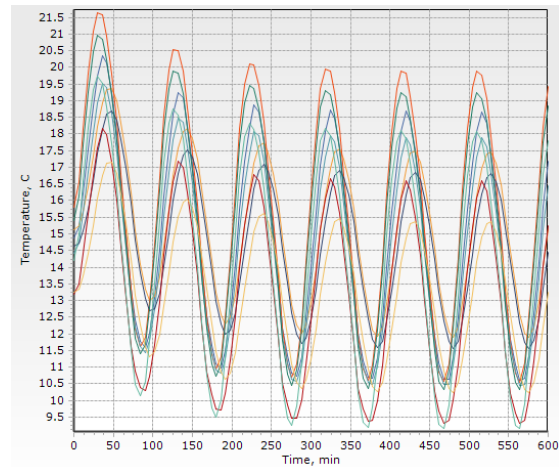
(b)

Figure 5.43: Mission 1 Bus Component Nominal Case x-y plotting.

Battery 1



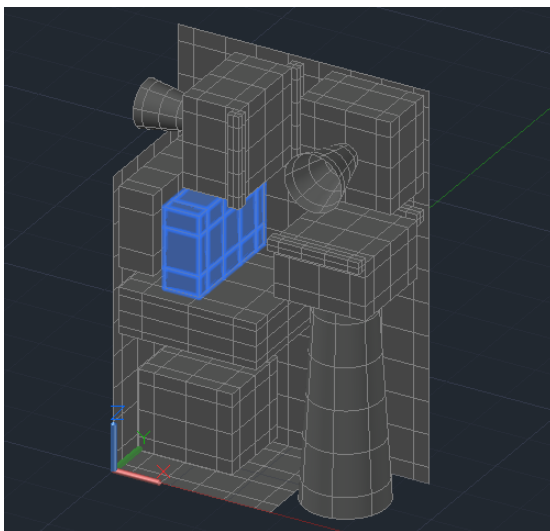
(a)



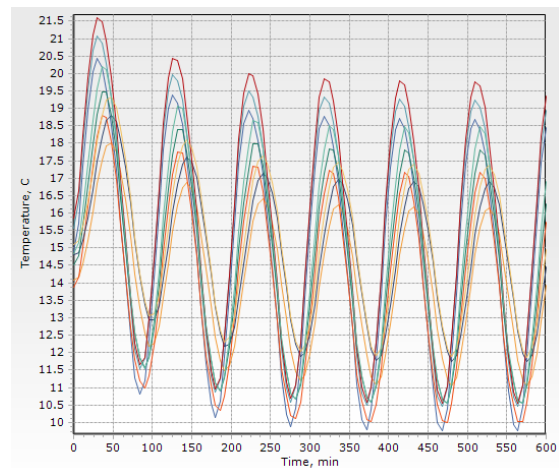
(b)

Figure 5.44: Mission 1 battery 1 Nominal Case x-y plotting.

Battery 2



(a)



(b)

Figure 5.45: Mission 1 battery 2 Nominal Case x-y plotting.

5.2 Mission 2

Unlike the previous Mission 1 in which the TCS was completely defined, for this thermal analysis it was requested to evaluate which superficial treatment was the most effective for different external surfaces of Mission 2.a and Mission 2.b.

Hence in this section, it is firstly reported the valuation between alodine and anodizing, then the results collected for the chosen alternative.

Finally it is discussed an additional case study, requested by the payload developer, in which the insertion of an extra PCB (printed circuit board), external to the payload, it is considered.

5.2.1 Alodine/Anodizing Valuation

The surfaces taken into consideration for the different superficial treatments are:

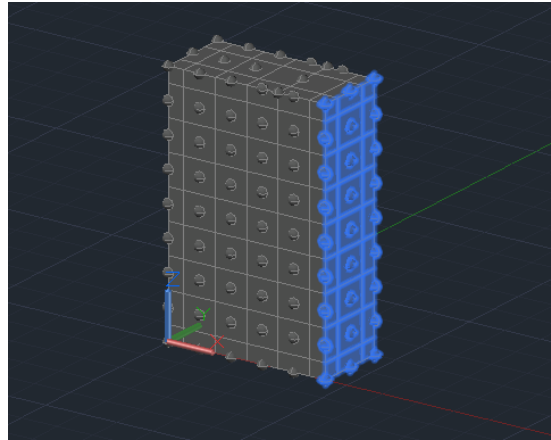
- Face 3U/X+ for Mission 2.a;
- Face 3U/X+ for Mission 2.b;
- Face 6U/Y+ for Mission 2.b.

Starting from Mission 2.a, it is possible to notice that with the 3U/X+ face anodized, the spacecraft reaches lower temperatures than with the alodine face, as shown in Figure 5.46. For this reason it has been preferred the solution with the face 3U alodine for Mission 2.a and Mission 2.b too.

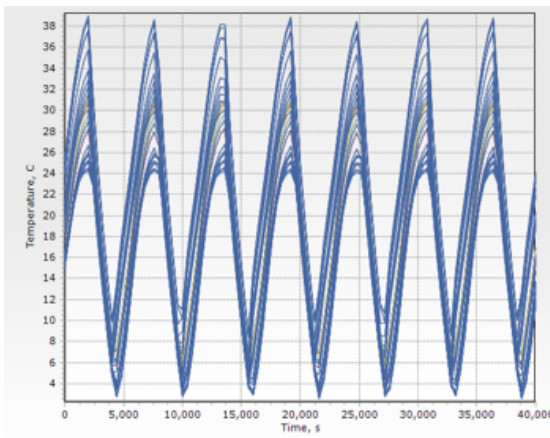
However, for Mission 2.b 6U/Y+ face it has been observed that the best solution is with the face anodised. In this way the spacecraft reaches lower temperatures then with alodine, as illustrated in Figure 5.47, but the internal components temperatures are still in the operational ranges. On the contrary with the 6U alodine the operational ranges are not ensured because the spacecraft reaches temperatures too high. As example in Figure 5.48 it has been reported the results for Mission 2.b Battery 1, where it easily to verify how in the worst hot case, the battery module temperature, with the face 6U alodine, exceeds the allowed limits.

So resuming, in the following sections have been collected the Mission 2.a and Mission 2.b results for the study case 3U/X+ alodine and 6U/Y+ anodised.

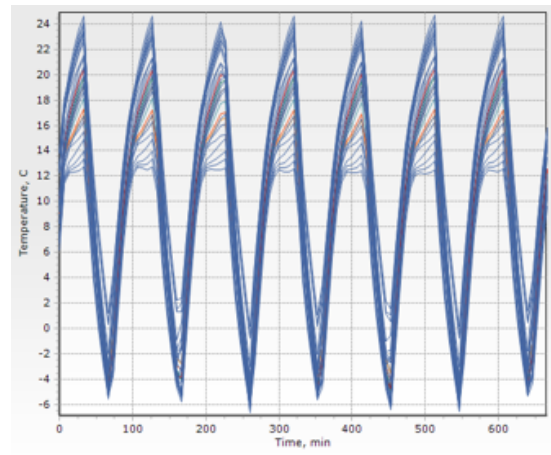
Mission 2.a 3U/X+



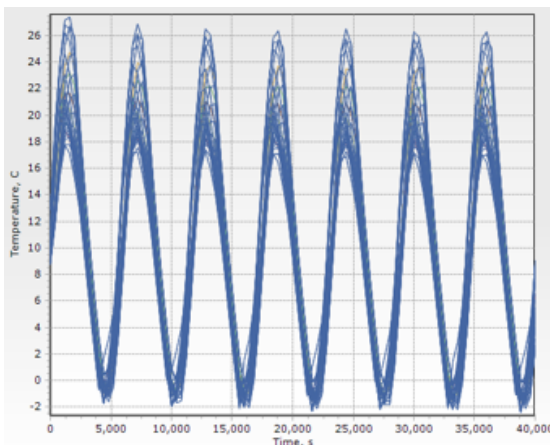
(a)



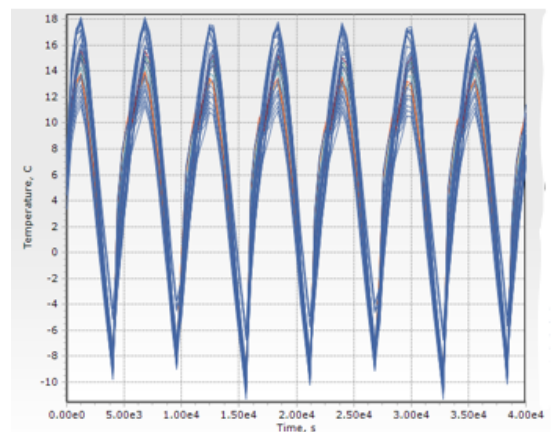
(b) Alodine Worst Hot Case



(c) Anodized Worst Hot Case



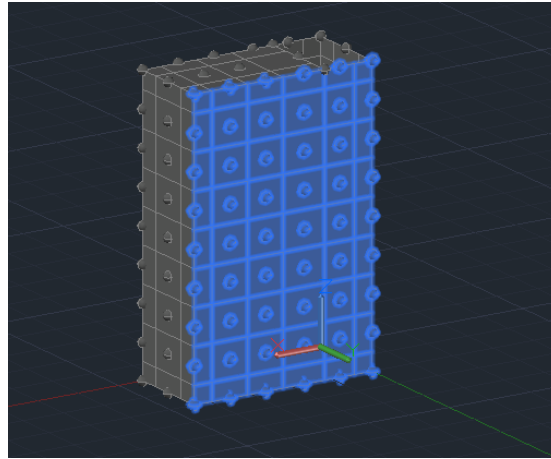
(d) Alodine Worst Cold Case



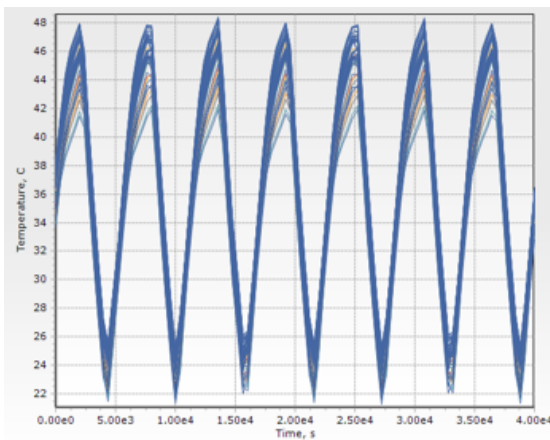
(e) Anodized Worst Cold Case

Figure 5.46: Mission 2.a 3U/X+ alodine/anodizing x-y plotting.

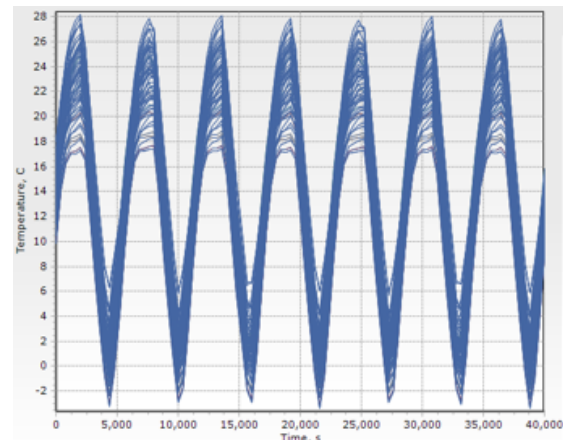
Mission 2.b 6U/Y+



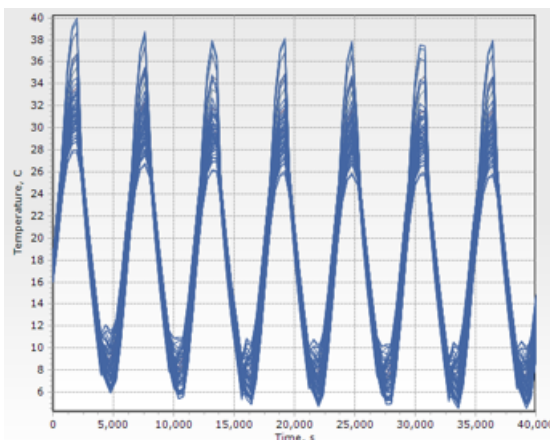
(a)



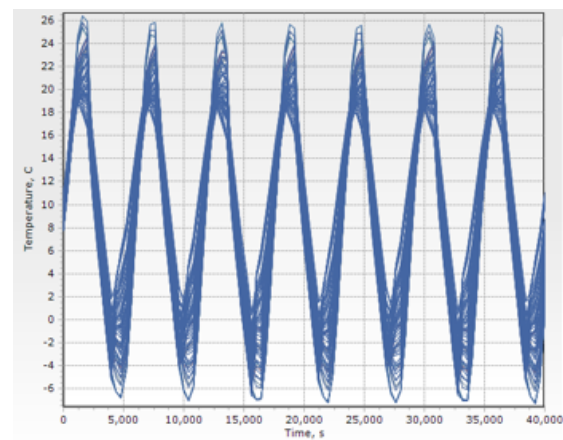
(b) Alodine Worst Hot Case



(c) Anodized Worst Hot Case



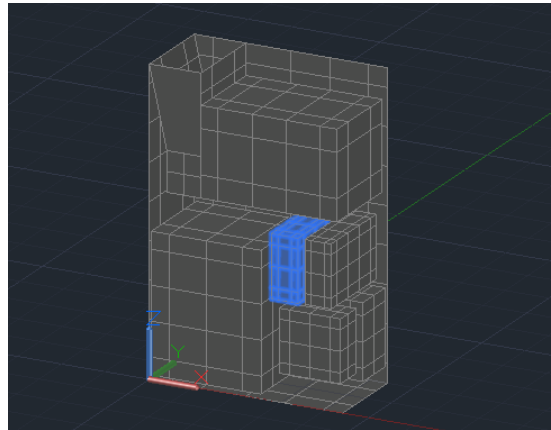
(d) Alodine Worst Cold Case



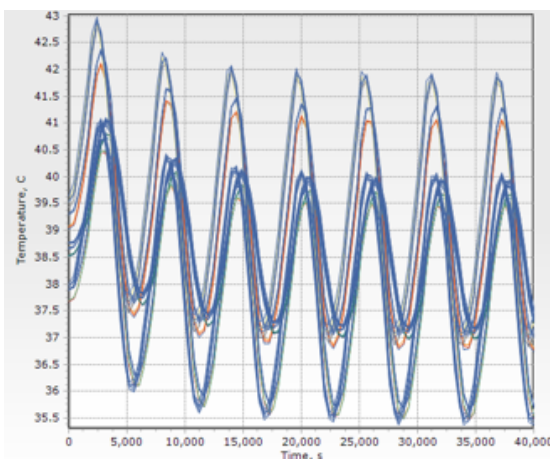
(e) Anodized Worst Cold Case

Figure 5.47: Mission 2.b 6U/Y+ alodine/anodizing x-y plotting.

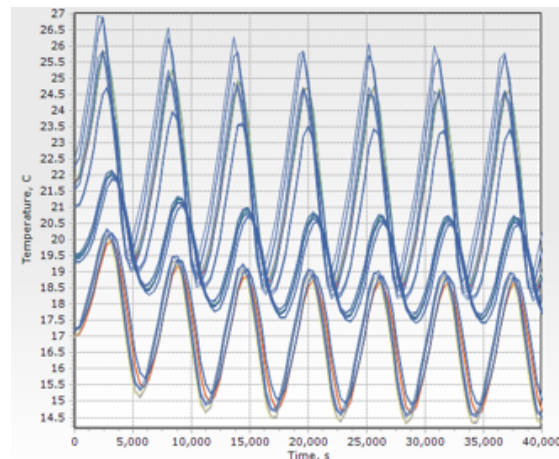
Mission 2.b Battery 1



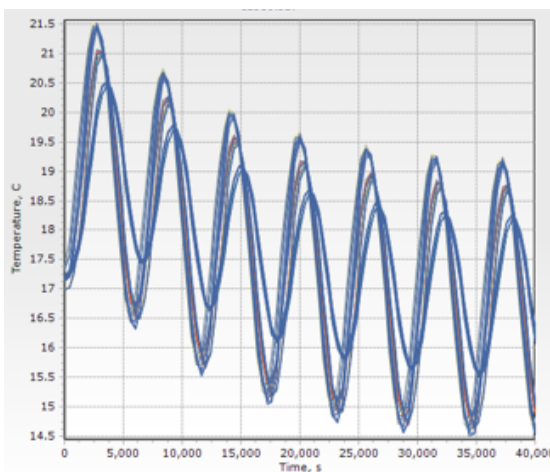
(a)



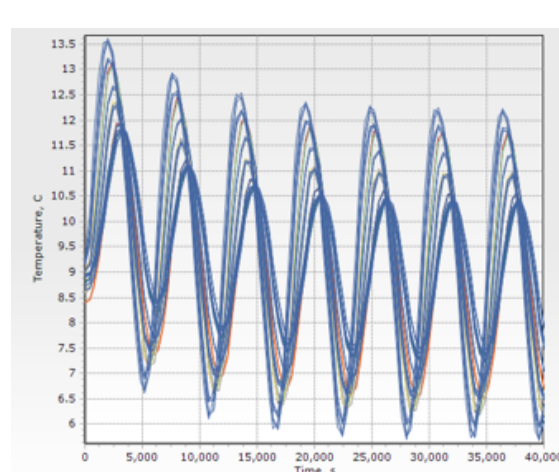
(b) With Face 6U Alodine Worst Hot Case



(c) With Face 6U Anodized Worst Hot Case



(d) With Face 6U Alodine Worst Cold Case



(e) With Face 6U Anodized Worst Cold Case

Figure 5.48: Mission 2.b Battery 1 alodine/anodizing x-y plotting.

5.2.2 Mission 2.a Worst Hot Case

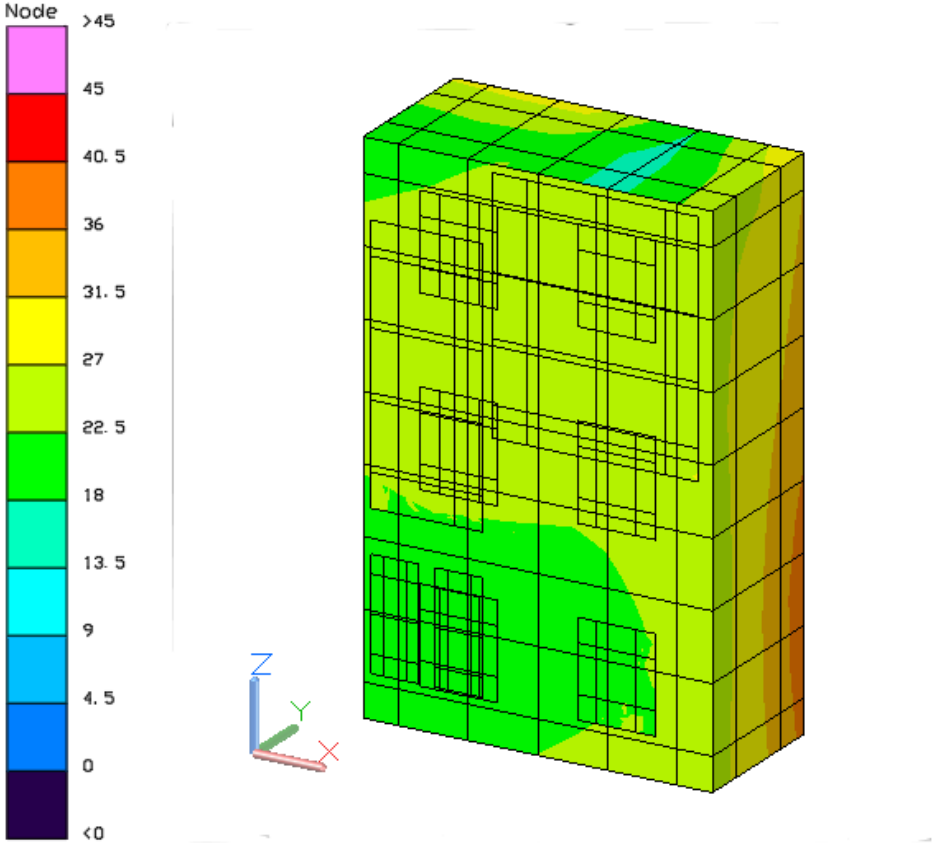
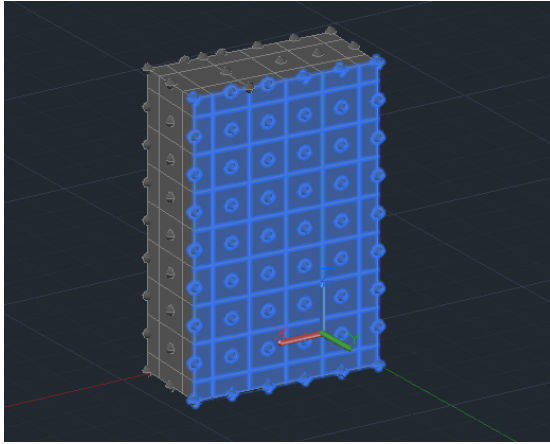
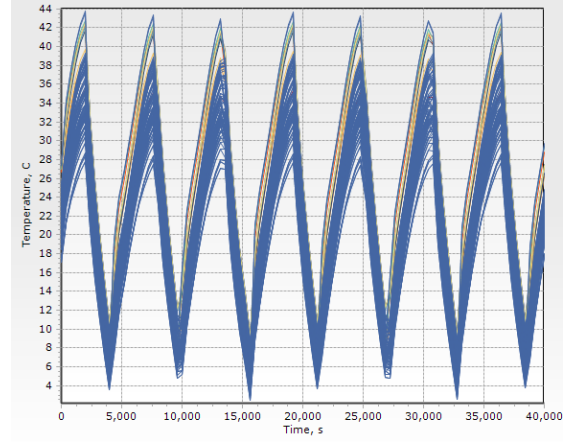


Figure 5.49: Mission 2.a Worst Hot Case color post-processing.

6U/Y+



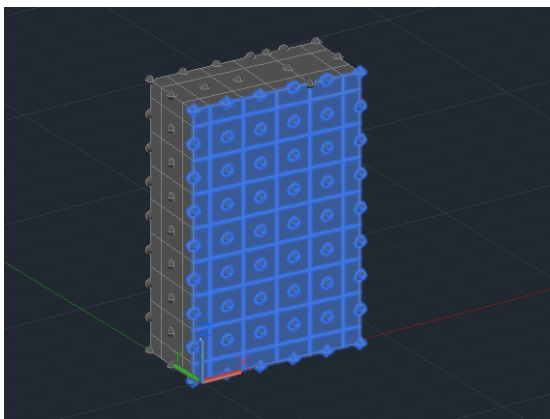
(a)



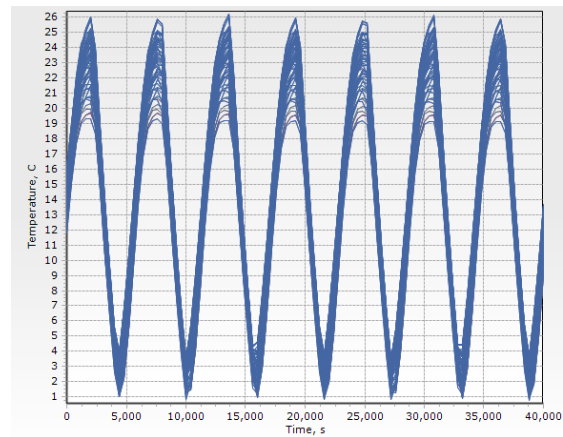
(b)

Figure 5.50: Mission 2.a 6U/Y+ Worst Hot Case x-y plotting.

6U/Y-



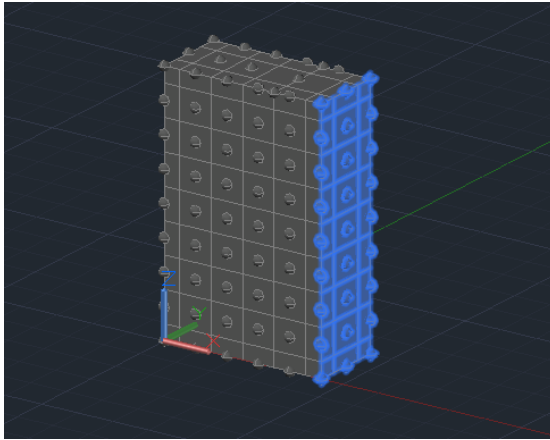
(a)



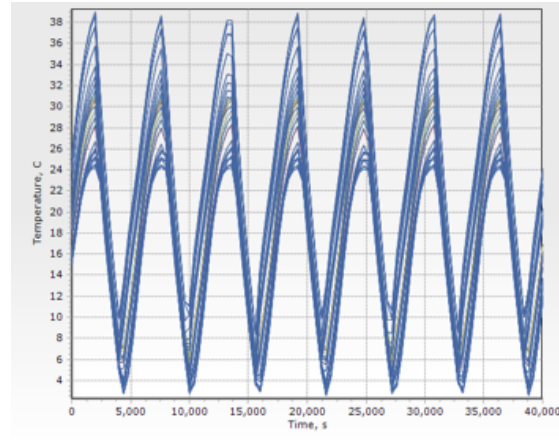
(b)

Figure 5.51: Mission 2.a 6U/Y- Worst Hot Case x-y plotting.

3U/X+



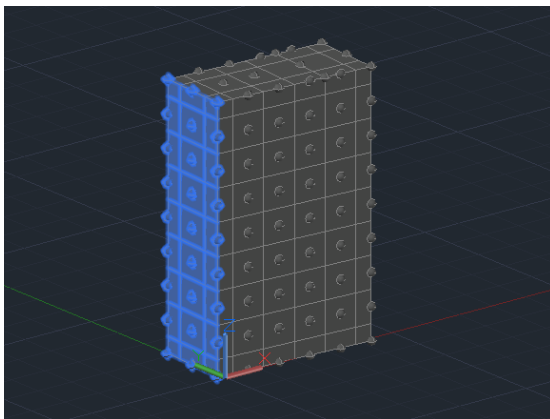
(a)



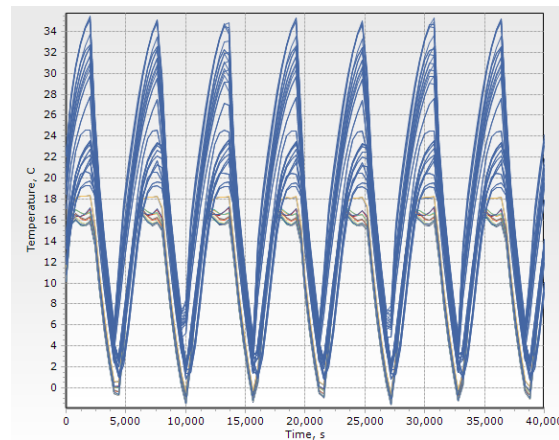
(b)

Figure 5.52: Mission 2.a 3U/X+ Worst Hot Case x-y plotting.

3U/X-



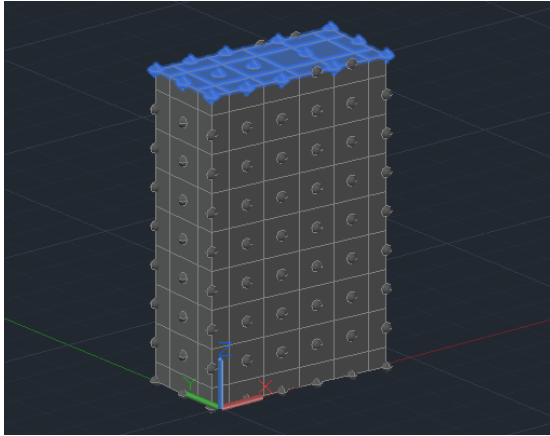
(a)



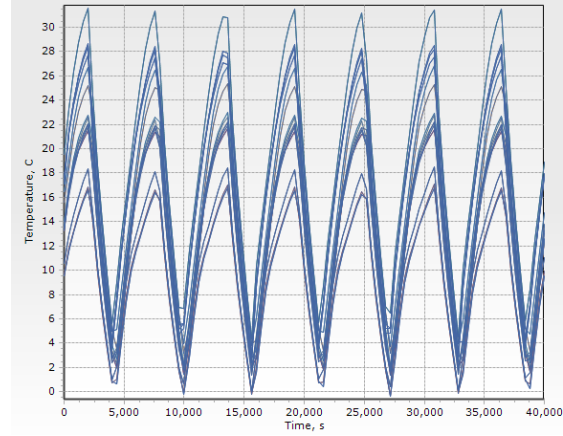
(b)

Figure 5.53: Mission 2.a 3U/X- Worst Hot Case x-y plotting.

2U/Z+



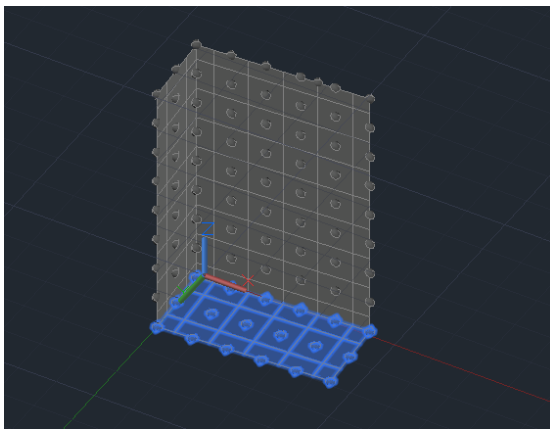
(a)



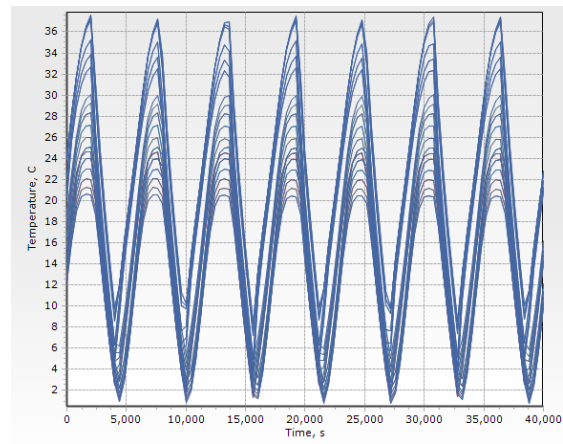
(b)

Figure 5.54: Mission 2.a 2U/Z+ Worst Hot Case x-y plotting.

2U/Z-



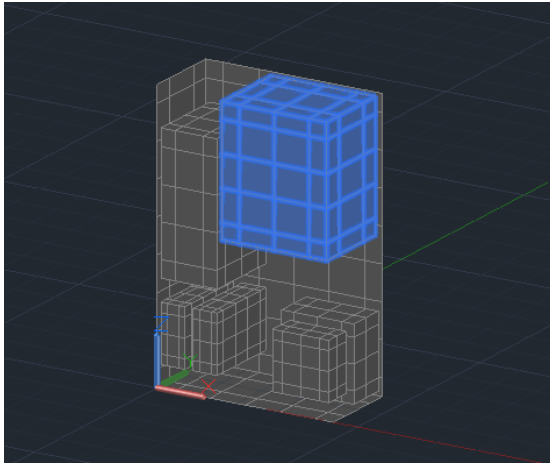
(a)



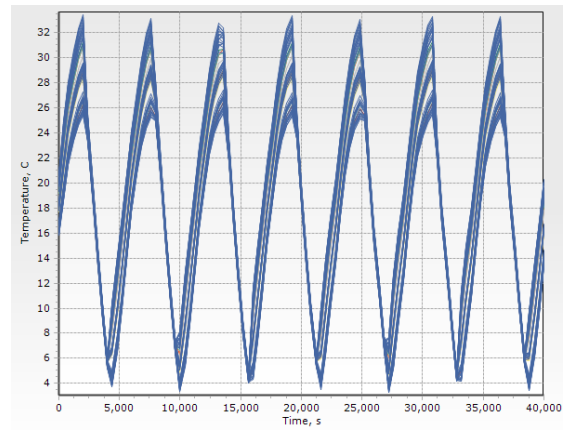
(b)

Figure 5.55: Mission 2.a 2U/Z- Worst Hot Case x-y plotting.

Payload Component 1.a



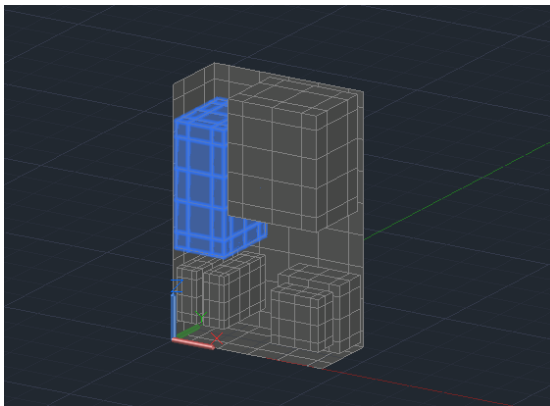
(a)



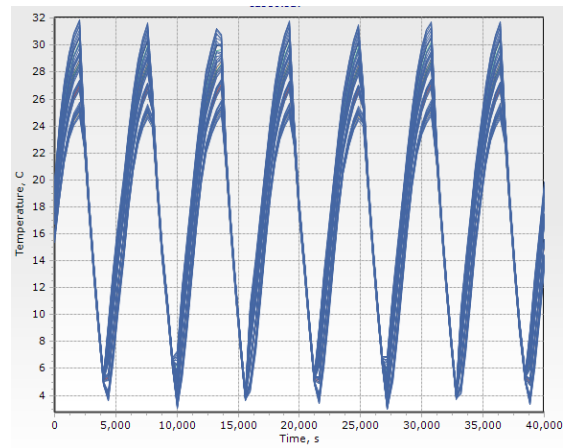
(b)

Figure 5.56: Mission 2.a Payload Component 1.a Worst Hot Case x-y plotting.

Payload Component 2.a



(a)



(b)

Figure 5.57: Mission 2.a Payload Component 2.a Worst Hot Case x-y plotting.

Payload Component 2.a Antenna

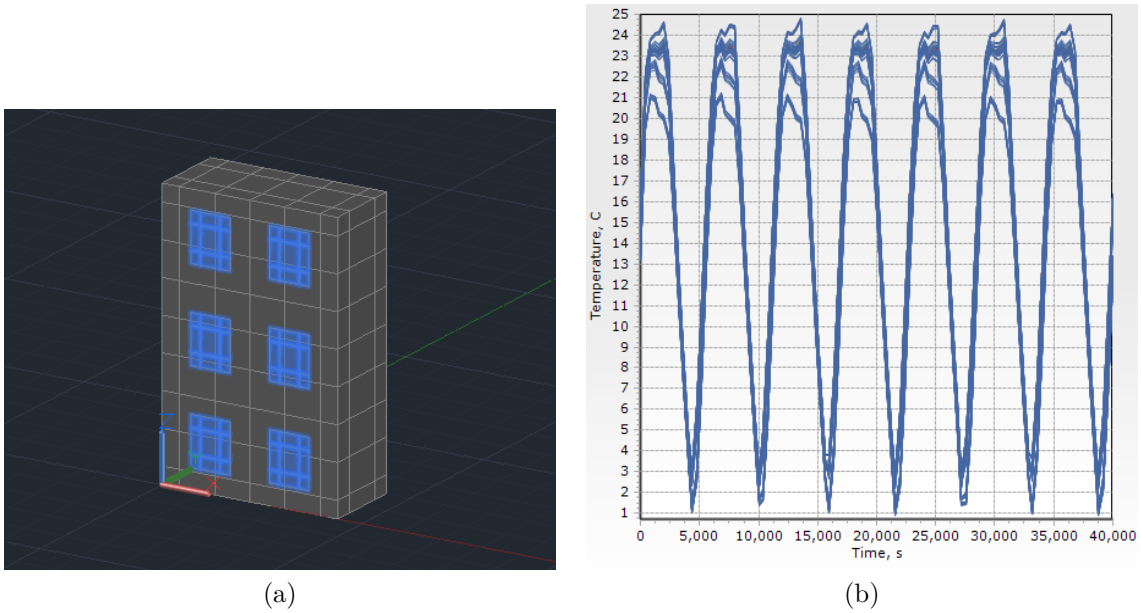


Figure 5.58: Mission 2.a Payload Component 2.a Antenna Worst Hot Case x-y plotting.

Bus Component 1.a

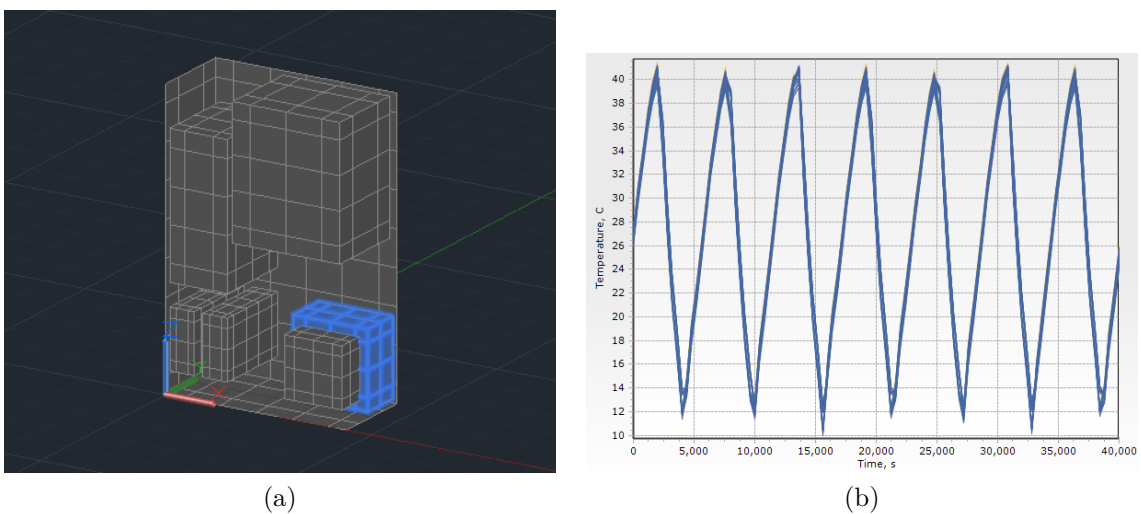
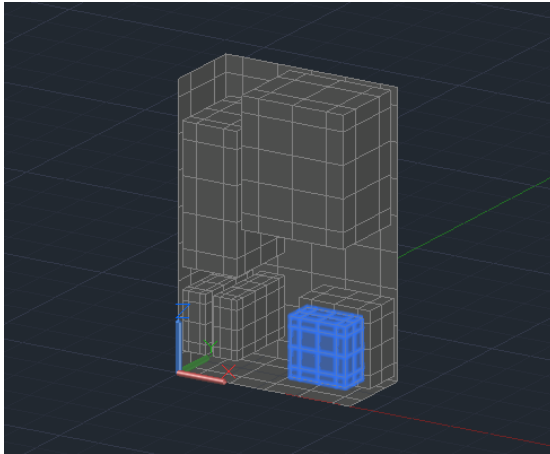
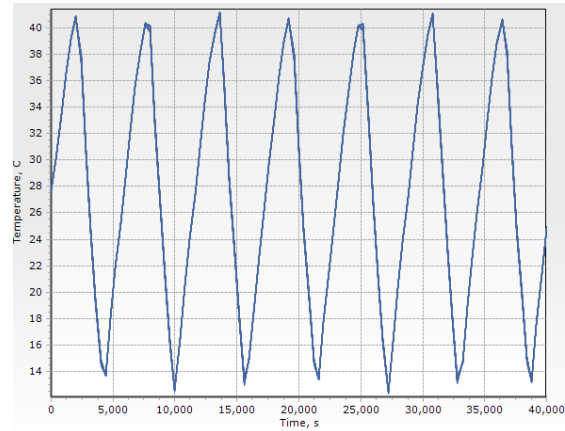


Figure 5.59: Mission 2.a Bus Component 1.a Worst Hot Case x-y plotting.

Bus Component 2.a



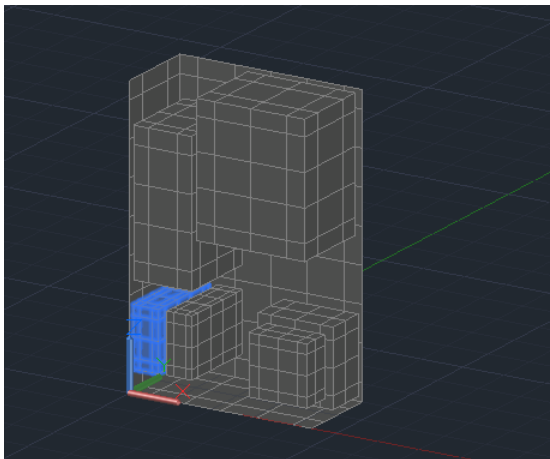
(a)



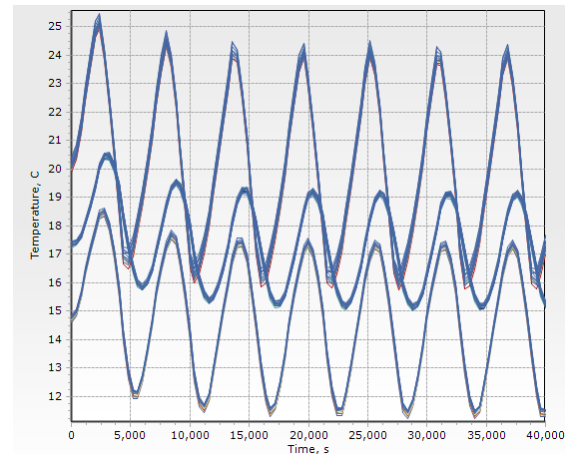
(b)

Figure 5.60: Mission 2.a Bus Component 2.a Worst Hot Case x-y plotting.

Battery 1.a



(a)



(b)

Figure 5.61: Mission 2.a Battery 1.a Worst Hot Case x-y plotting.

Battery 2.a

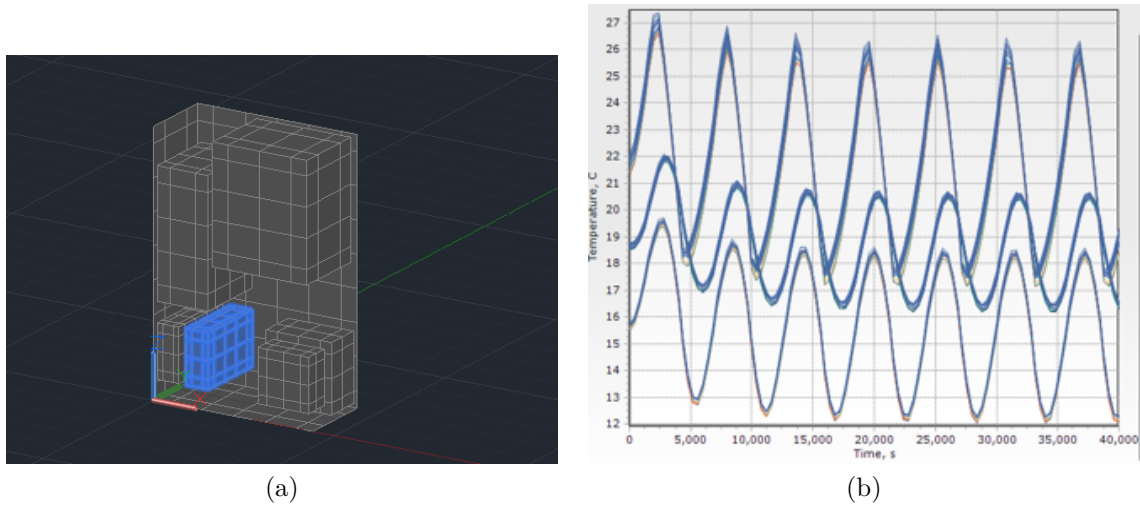


Figure 5.62: Mission 2.a Battery 2.a Worst Hot Case x-y plotting.

5.2.3 Mission 2.a Worst Cold Case

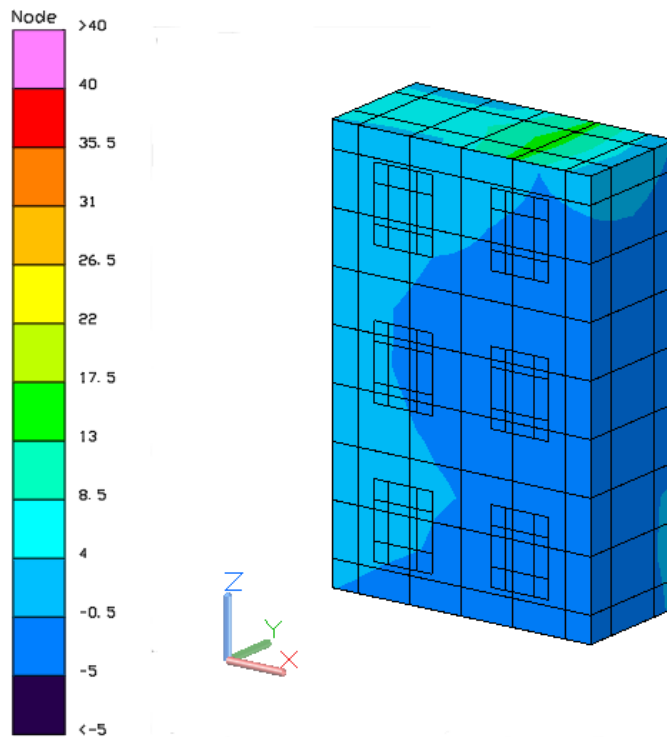
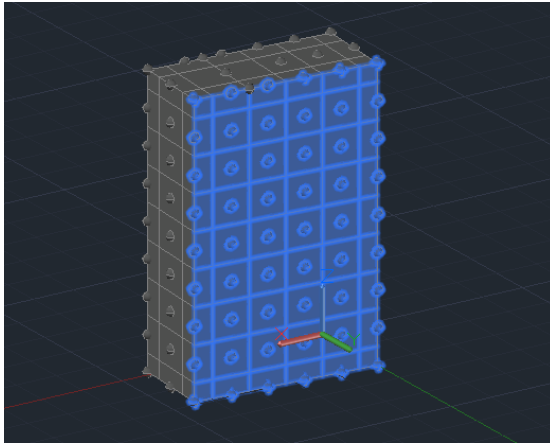
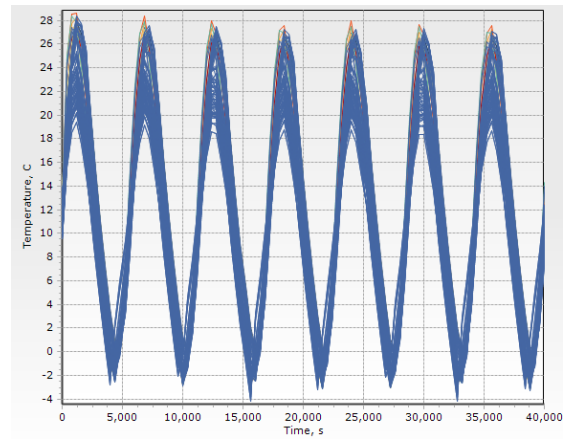


Figure 5.63: Mission 2.a Worst Cold Case color post-processing.

6U/Y+



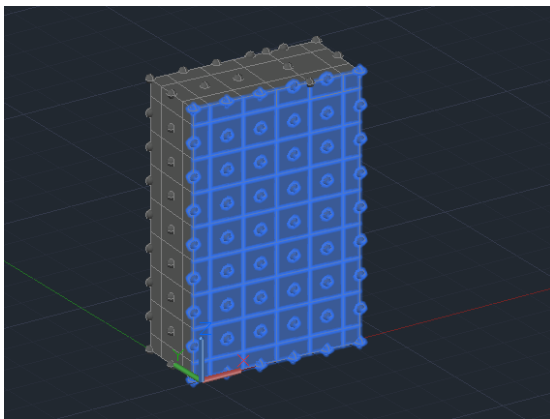
(a)



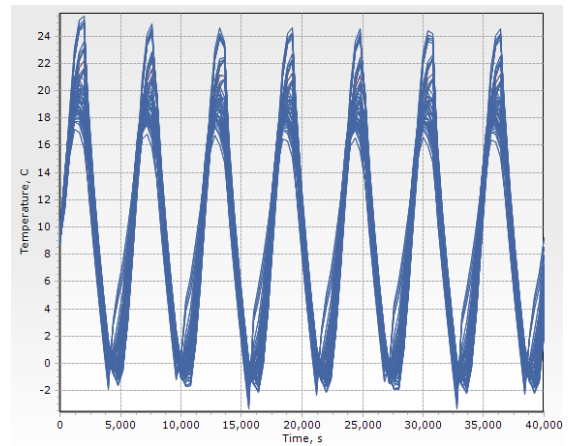
(b)

Figure 5.64: Mission 2.a 6U/Y+ Worst Cold Case x-y plotting.

6U/Y-



(a)



(b)

Figure 5.65: Mission 2.a 6U/Y- Worst Cold Case x-y plotting.

3U/X+

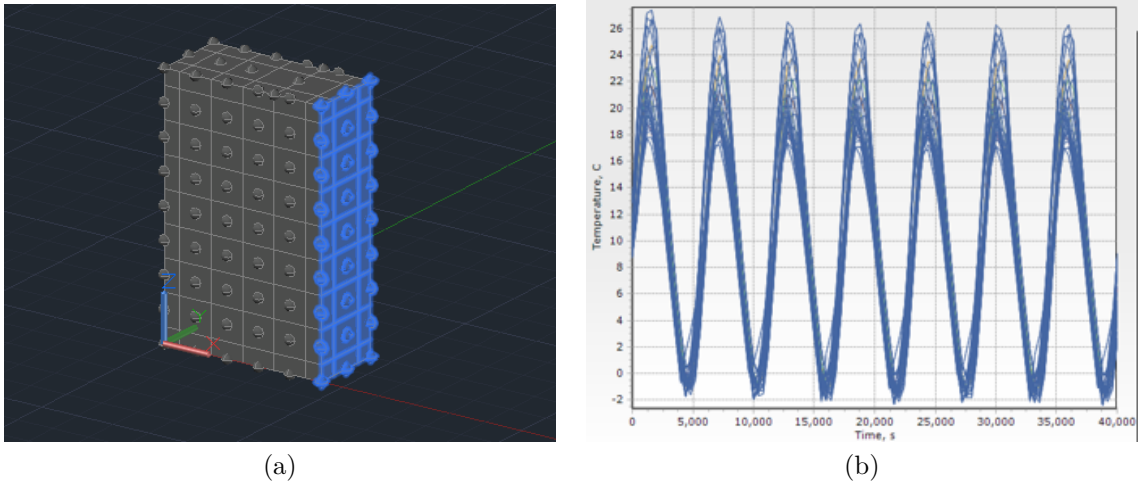


Figure 5.66: Mission 2.a 3U/X+ Worst Cold Case x-y plotting.

3U/X-

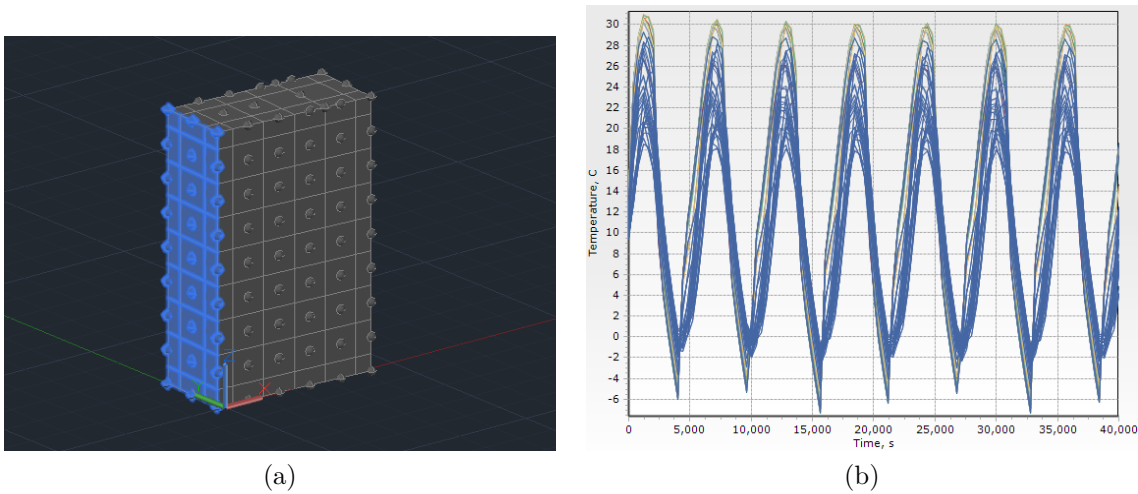
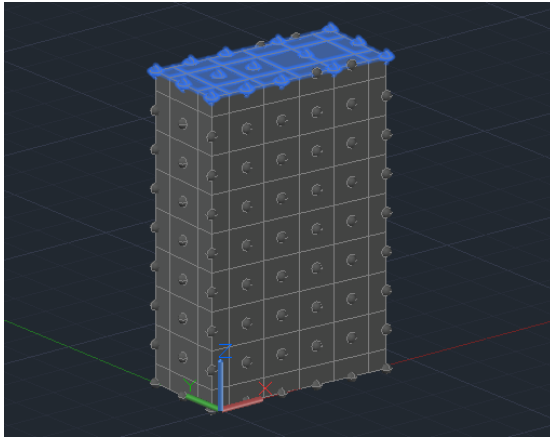
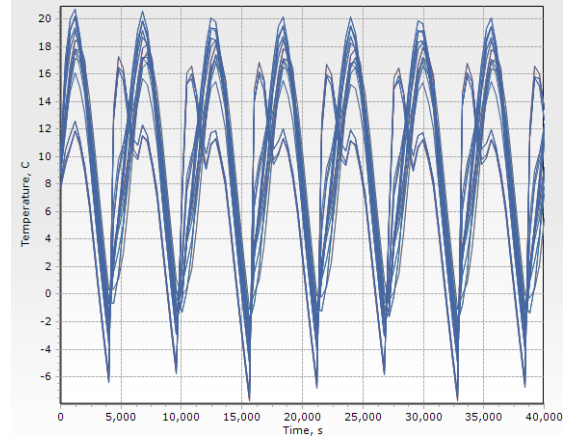


Figure 5.67: Mission 2.a 3U/X- Worst Cold Case x-y plotting.

2U/Z+



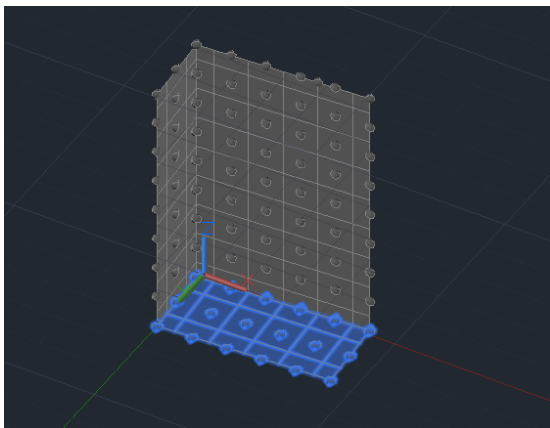
(a)



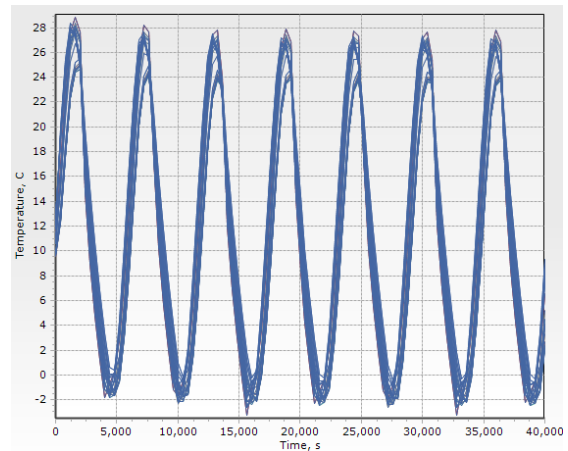
(b)

Figure 5.68: Mission 2.a 2U/Z+ Worst Cold Case x-y plotting.

2U/Z-



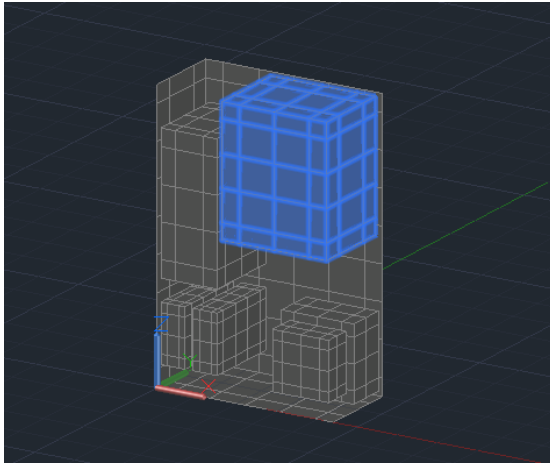
(a)



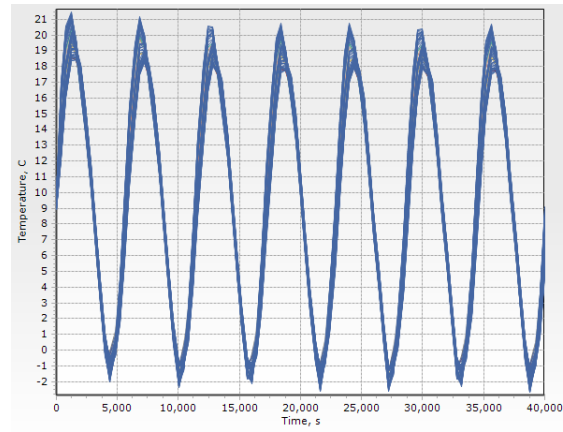
(b)

Figure 5.69: Mission 2.a 2U/Z- Worst Cold Case x-y plotting.

Payload Component 1.a



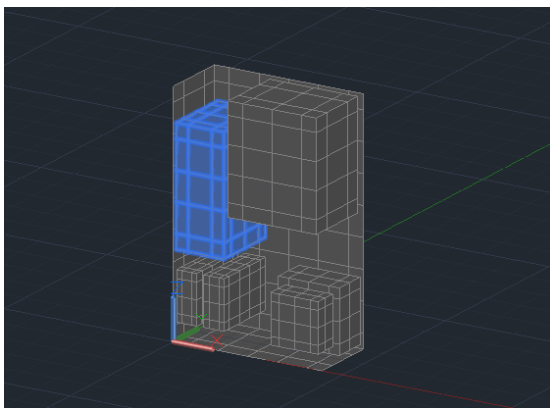
(a)



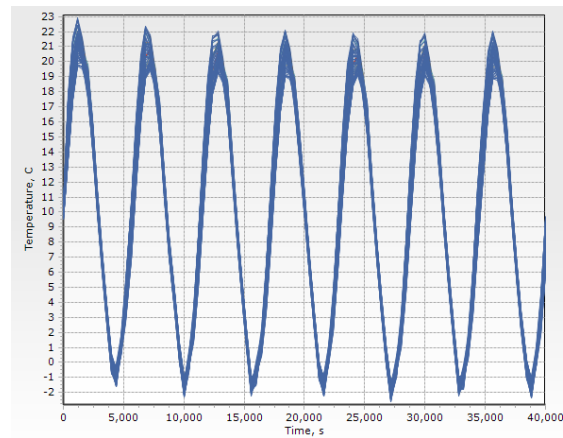
(b)

Figure 5.70: Mission 2.a Payload Component 1.a Worst Cold Case x-y plotting.

Payload Component 2.a



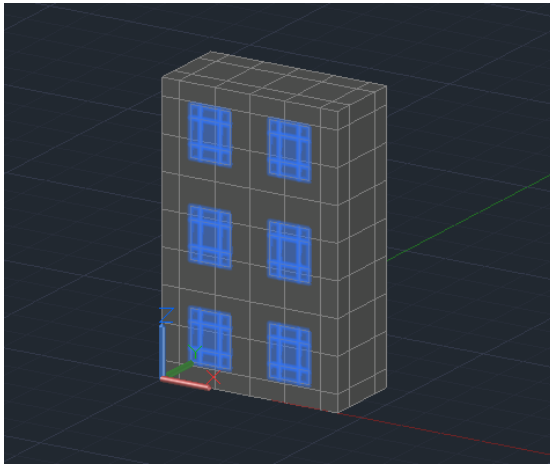
(a)



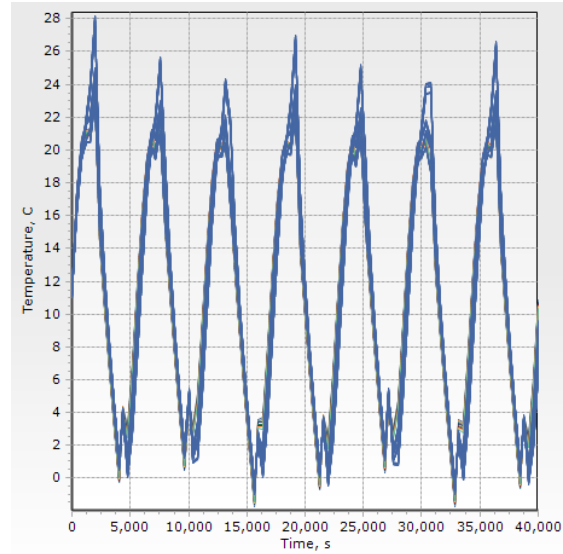
(b)

Figure 5.71: Mission 2.a Payload Component 2.a Worst Cold Case x-y plotting.

Payload Component 2.a Antenna



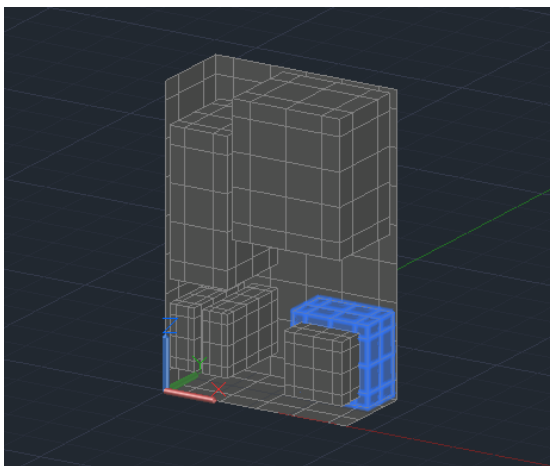
(a)



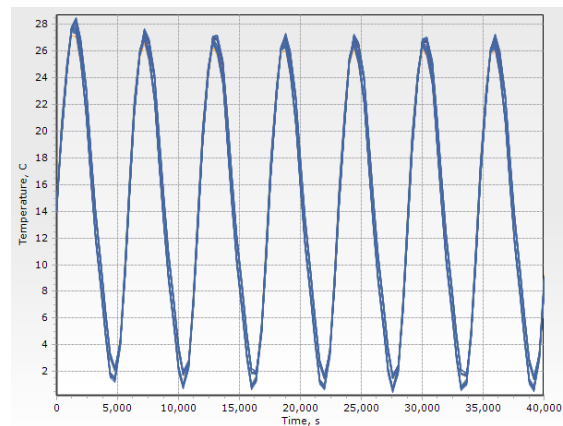
(b)

Figure 5.72: Mission 2.a Payload Component 2.a Antenna Worst Cold Case x-y plotting.

Bus Component 1.a



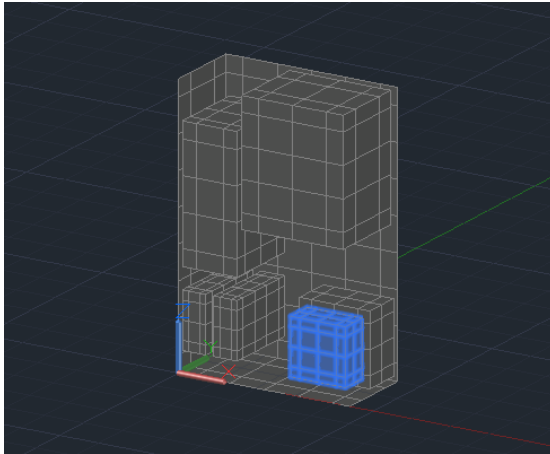
(a)



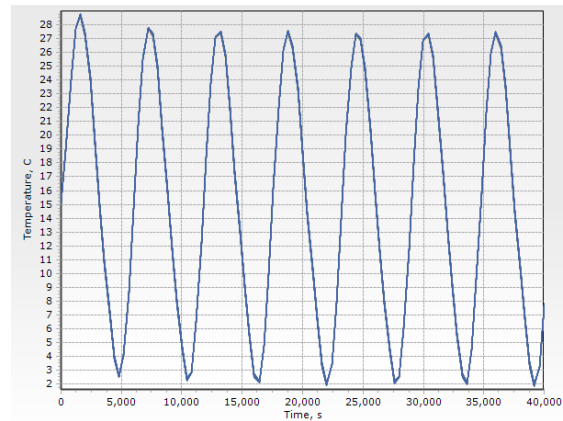
(b)

Figure 5.73: Mission 2.a Bus Component 1.a Worst Cold Case x-y plotting.

Bus Component 2.a



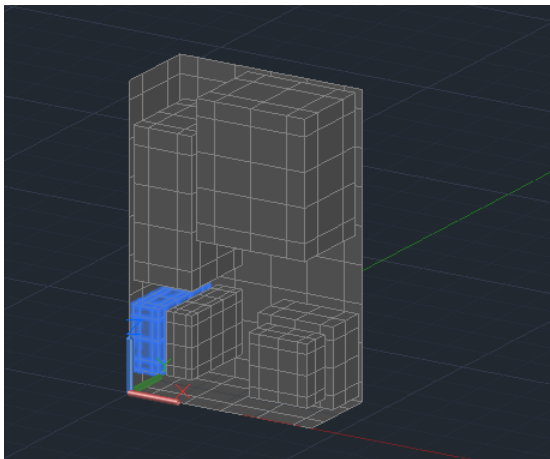
(a)



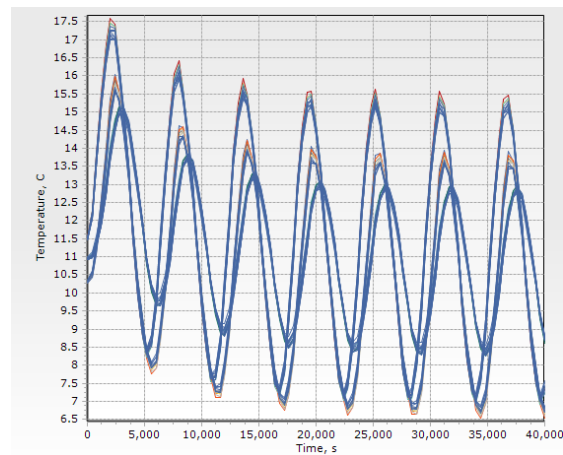
(b)

Figure 5.74: Mission 2.a Bus Component 2.a Worst Cold Case x-y plotting.

Battery 1.a



(a)



(b)

Figure 5.75: Mission 2.a Battery 1.a Worst Cold Case x-y plotting.

Battery 2.a

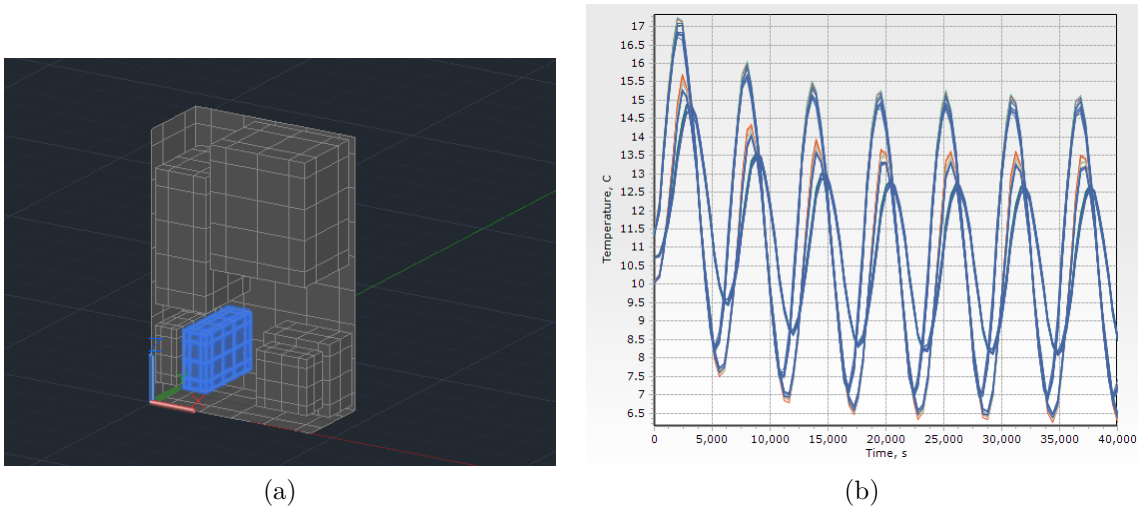


Figure 5.76: Mission 2.a Battery 2.a Worst Cold Case x-y plotting.

5.2.4 Mission 2.b Worst Hot Case

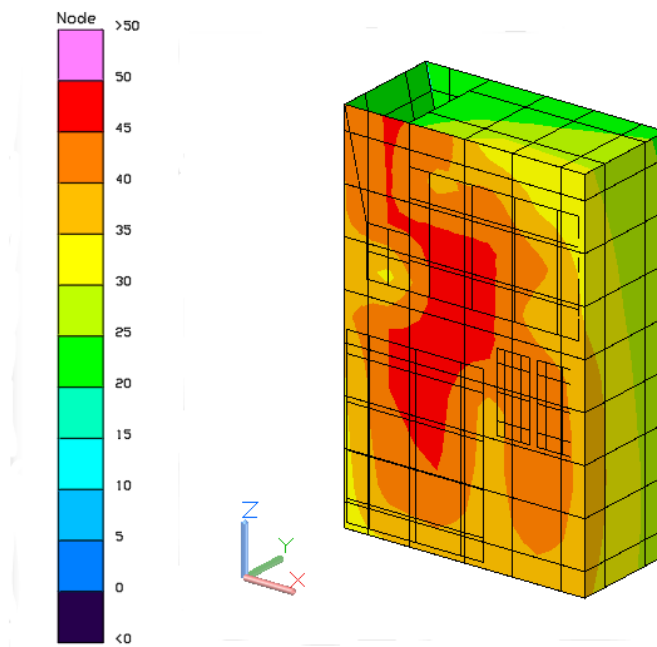
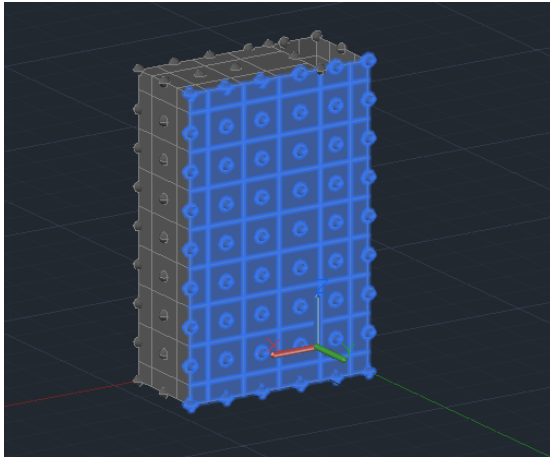
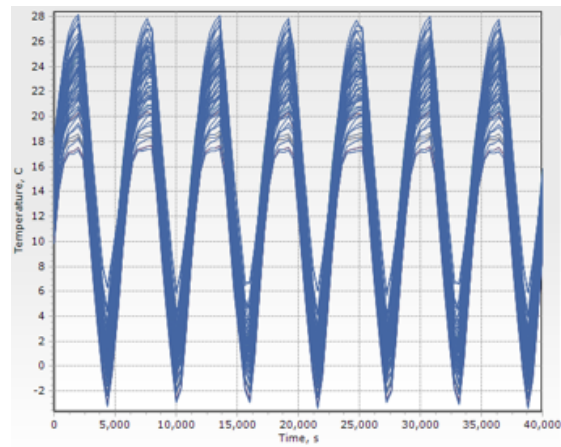


Figure 5.77: Mission 2.b Worst Hot Case color post-processing.

6U/Y+



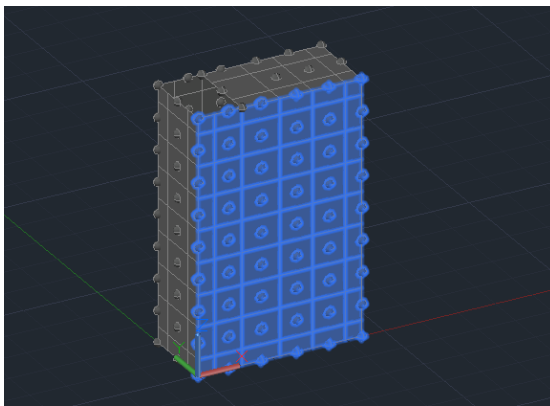
(a)



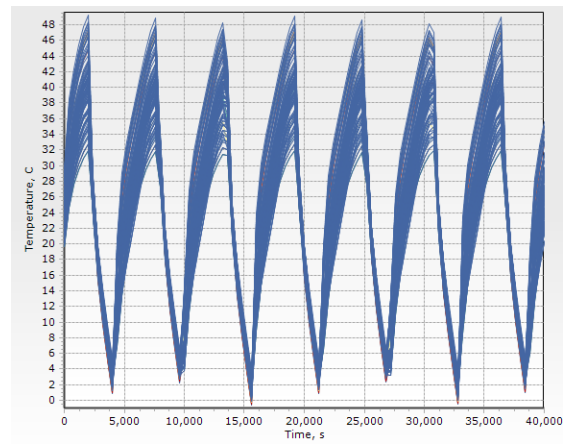
(b)

Figure 5.78: Mission 2.b 6U/Y+ Worst Hot Case x-y plotting.

6U/Y-



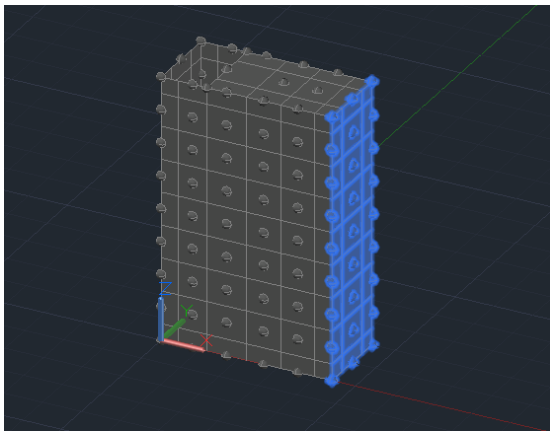
(a)



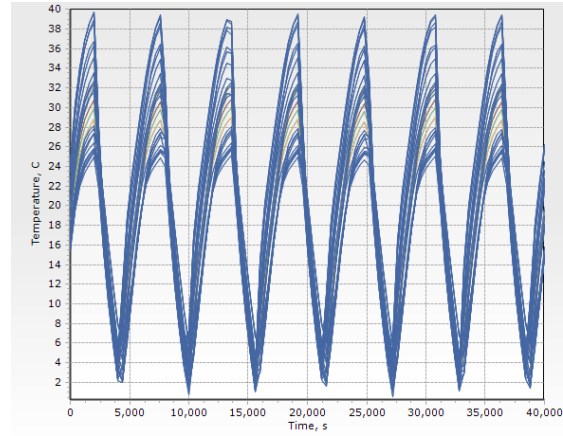
(b)

Figure 5.79: Mission 2.b 6U/Y- Worst Hot Case x-y plotting.

3U/X+



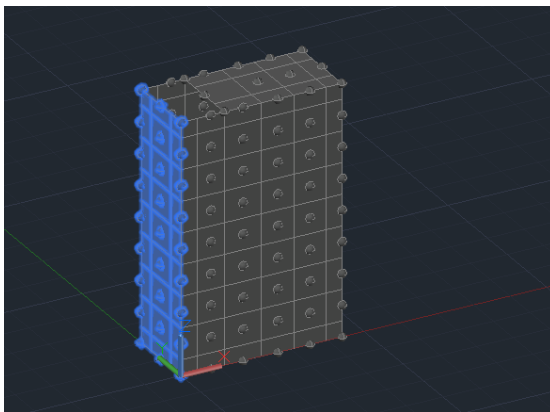
(a)



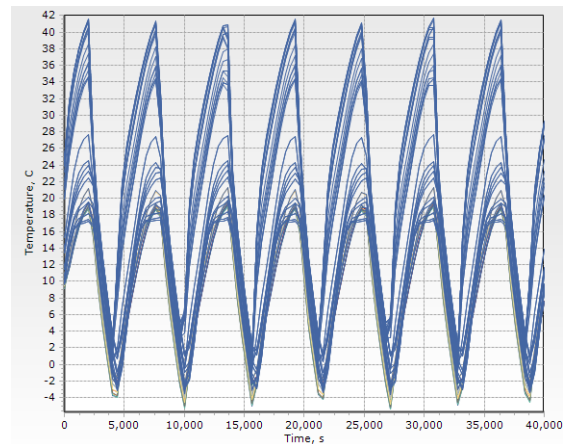
(b)

Figure 5.80: Mission 2.b 3U/X+ Worst Hot Case x-y plotting.

3U/X-



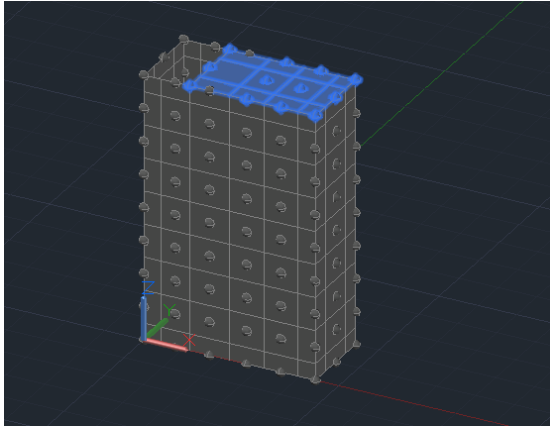
(a)



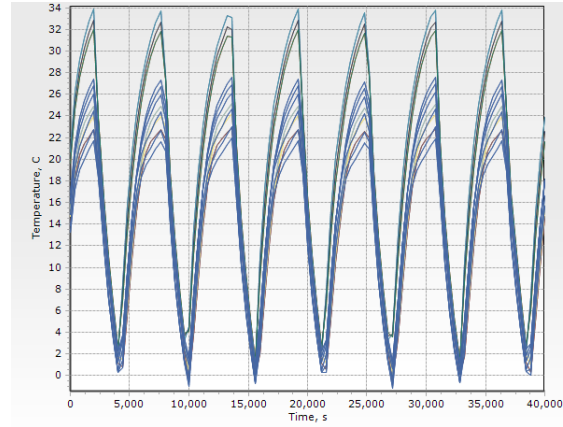
(b)

Figure 5.81: Mission 2.b 3U/X- Worst Hot Case x-y plotting.

2U/Z+



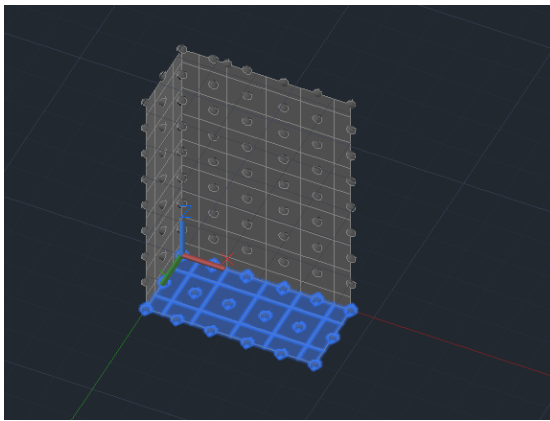
(a)



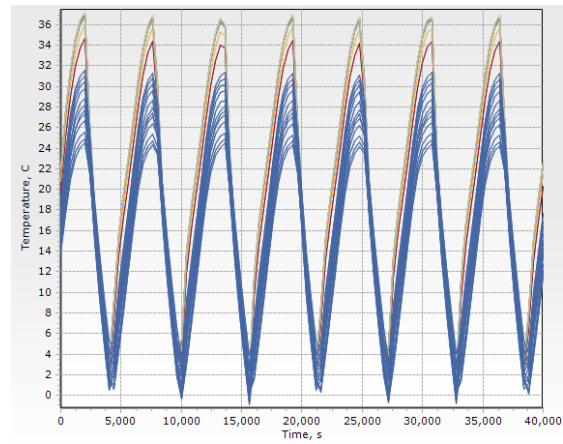
(b)

Figure 5.82: Mission 2.b 2U/Z+ Worst Hot Case x-y plotting.

2U/Z-



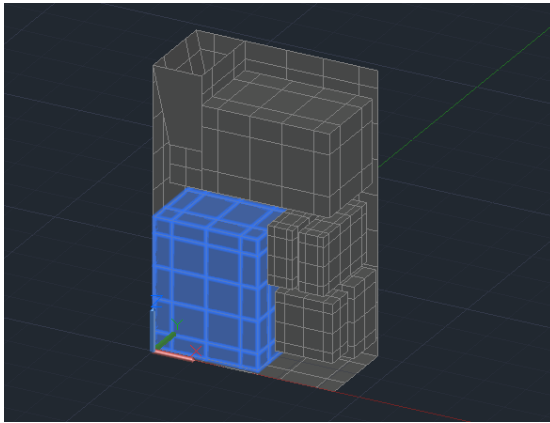
(a)



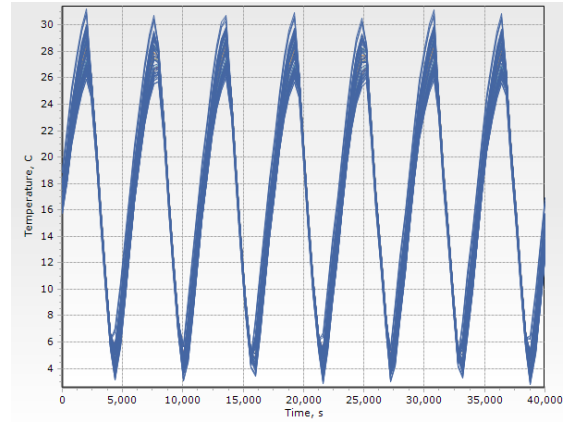
(b)

Figure 5.83: Mission 2.b 2U/Z- Worst Hot Case x-y plotting.

Payload Component 1.b



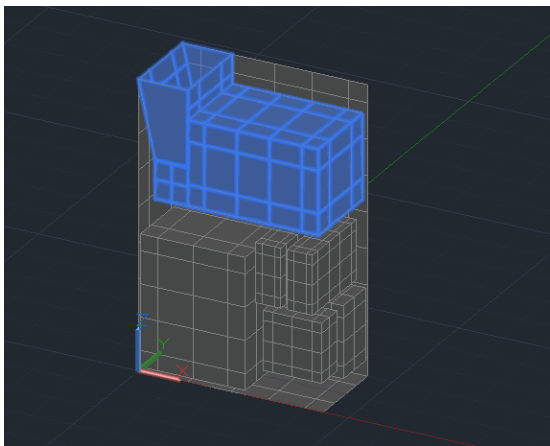
(a)



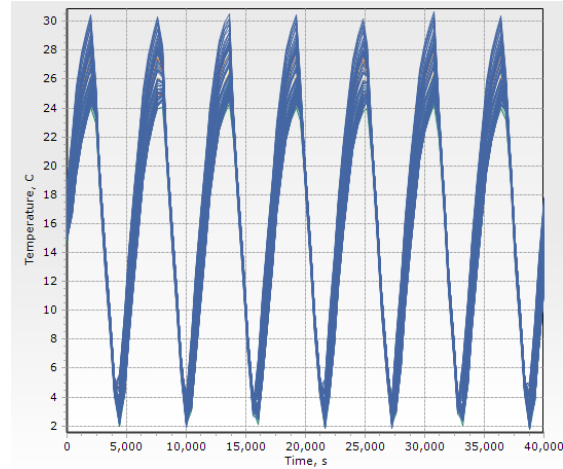
(b)

Figure 5.84: Mission 2.b Payload Component 1.b Worst Hot Case x-y plotting.

Payload Component 2.b



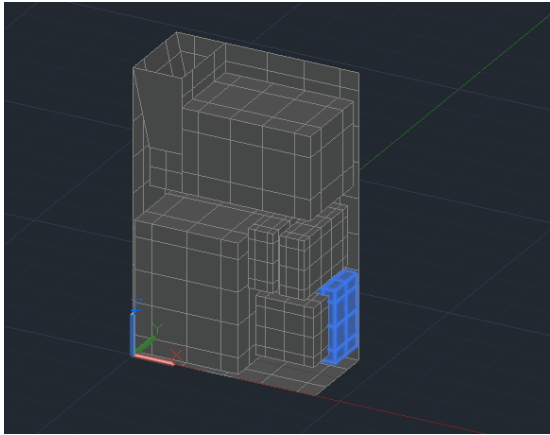
(a)



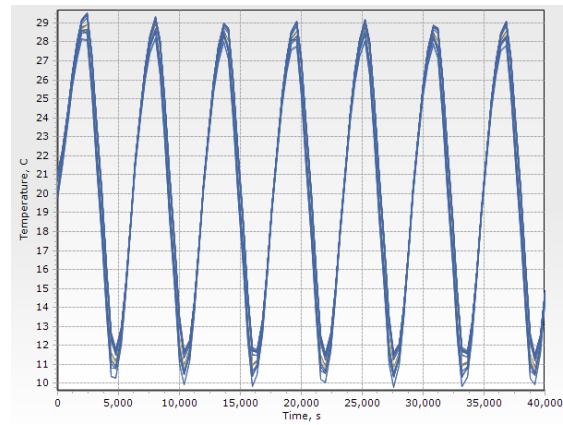
(b)

Figure 5.85: Mission 2.b Payload Component 2.b Worst Hot Case x-y plotting.

Bus Component 1.b



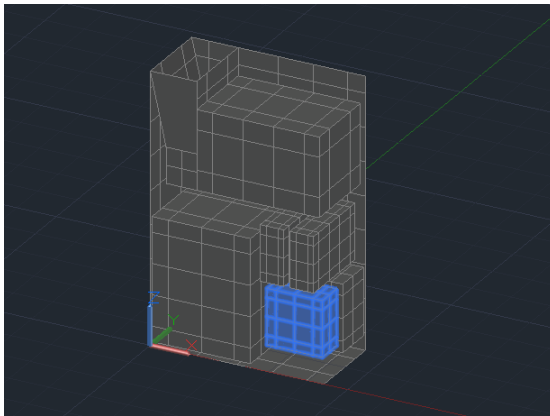
(a)



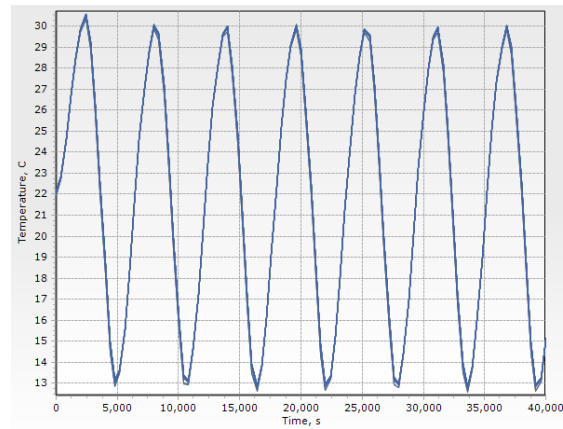
(b)

Figure 5.86: Mission 2.b Bus Component 1.b Worst Hot Case x-y plotting.

Bus Component 2.b



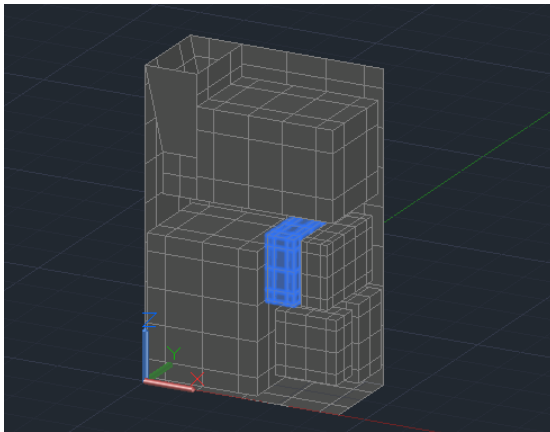
(a)



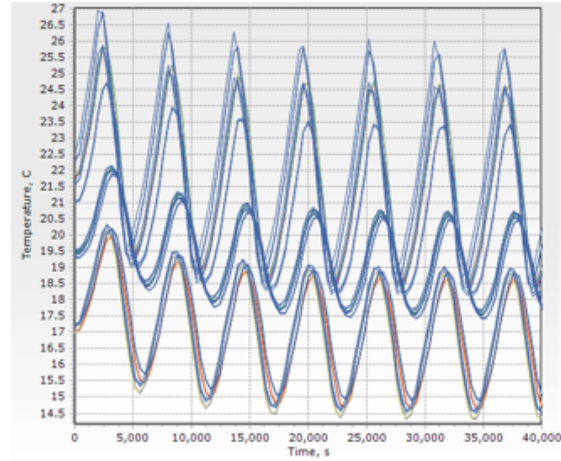
(b)

Figure 5.87: Mission 2.b Bus Component 2.b Worst Hot Case x-y plotting.

Battery 1.b



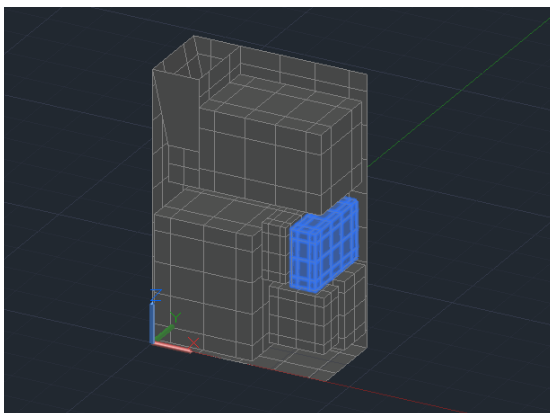
(a)



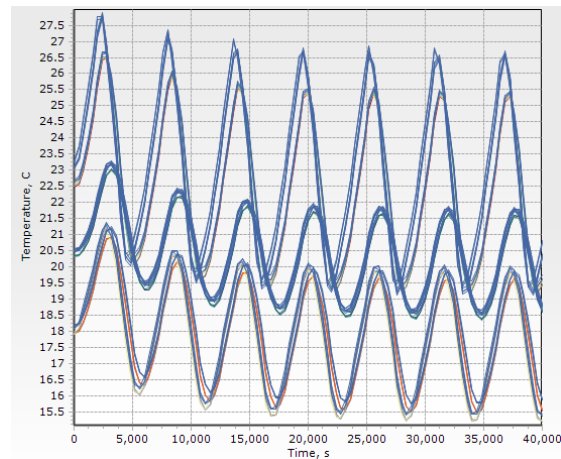
(b)

Figure 5.88: Mission 2.b Battery 1.b Worst Hot Case x-y plotting.

Battery 2.b



(a)



(b)

Figure 5.89: Mission 2.b Battery 2.b Worst Hot Case x-y plotting.

5.2.5 Mission 2.b Worst Cold Case

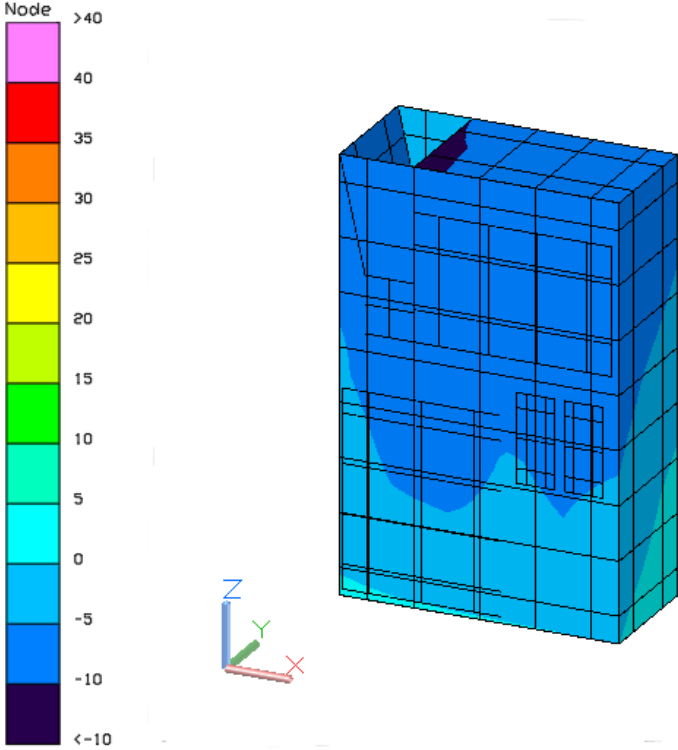


Figure 5.90: Mission 2.b Worst Cold Case color post-processing.

6U/Y+

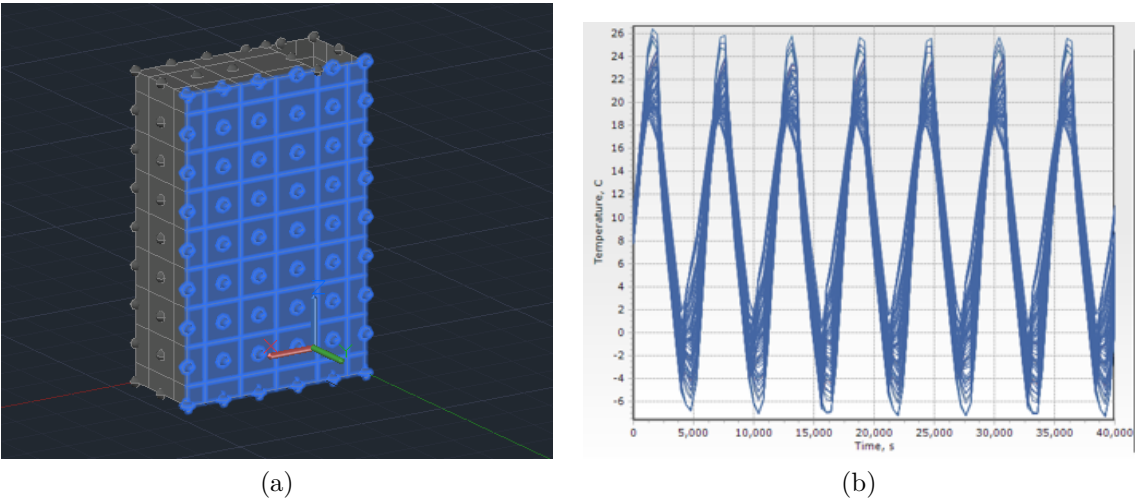


Figure 5.91: Mission 2.b 6U/Y+ Worst Cold Case x-y plotting.

6U/Y-

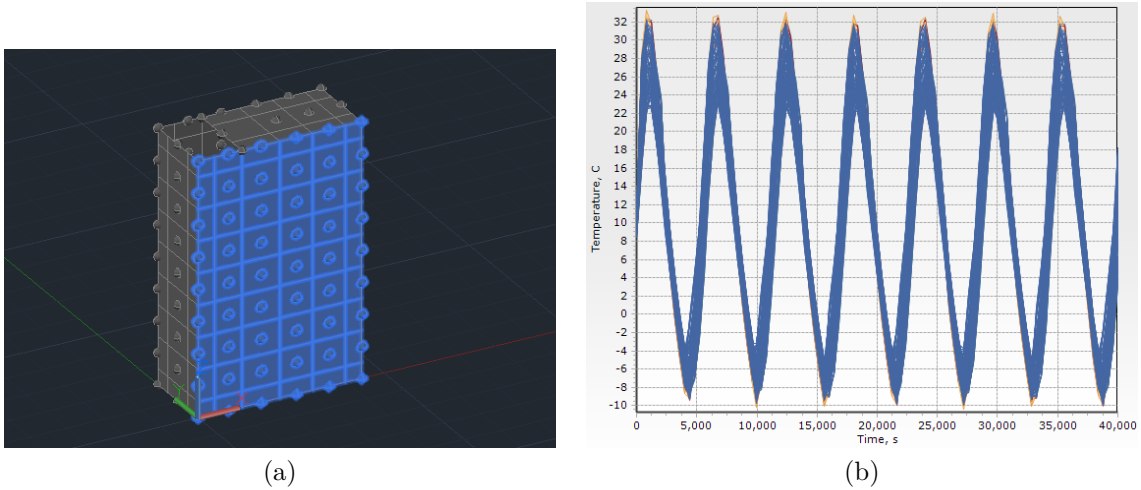


Figure 5.92: Mission 2.b 6U/Y- Worst Cold Case x-y plotting.

3U/X+

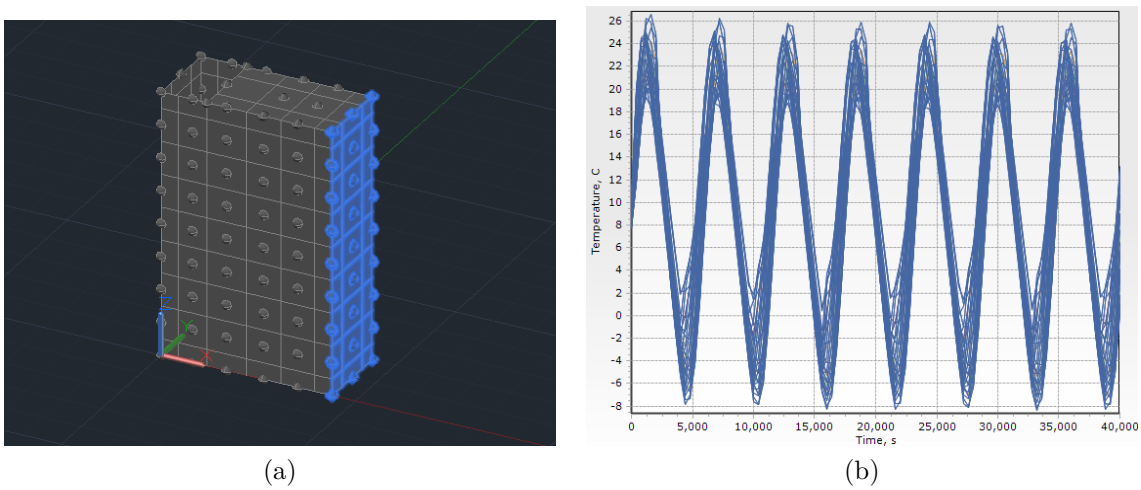


Figure 5.93: Mission 2.b 3U/X+ Worst Hot Case x-y plotting.

3U/X-

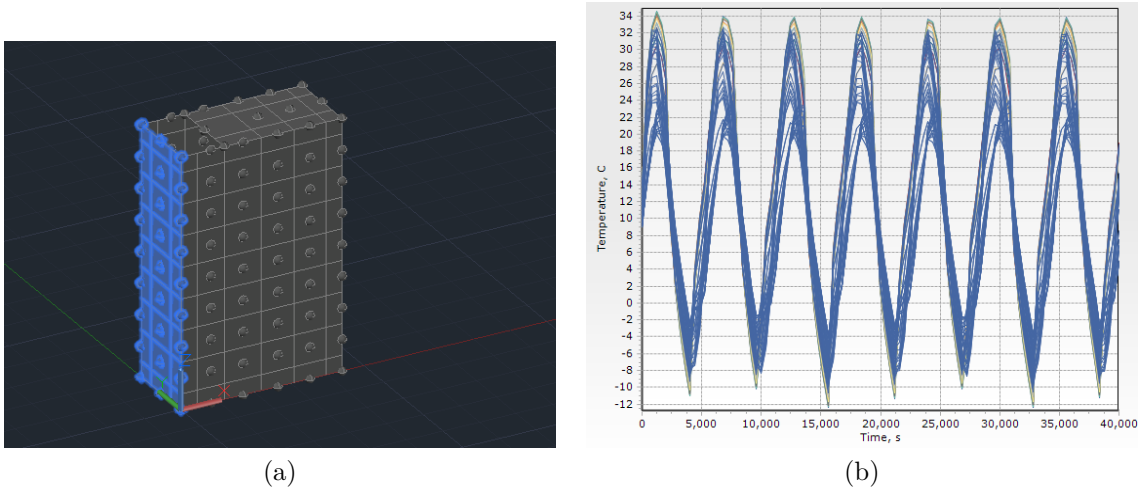


Figure 5.94: Mission 2.b 3U/X- Worst Cold Case x-y plotting.

2U/Z+

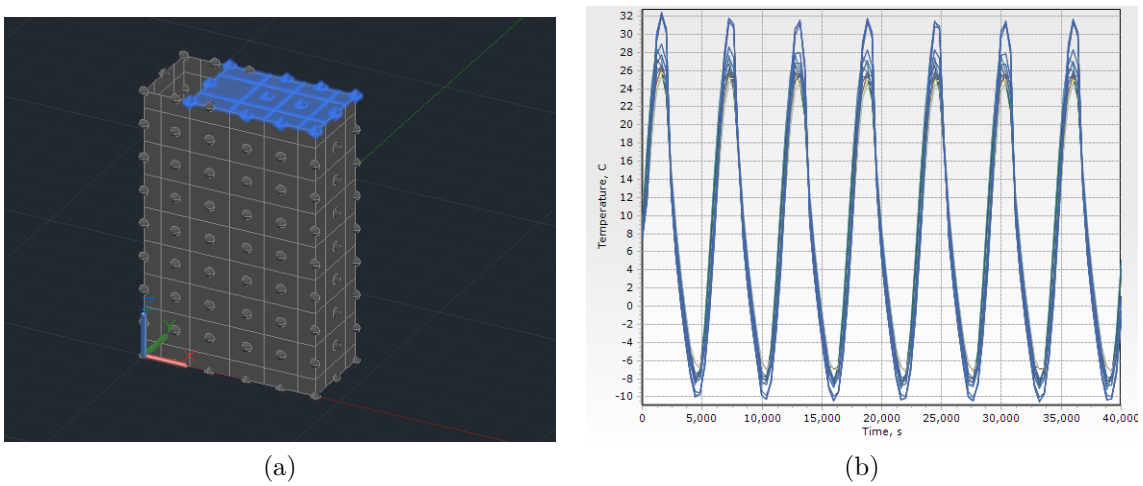


Figure 5.95: Mission 2.b 2U/Z+ Worst Cold Case x-y plotting.

2U/Z-

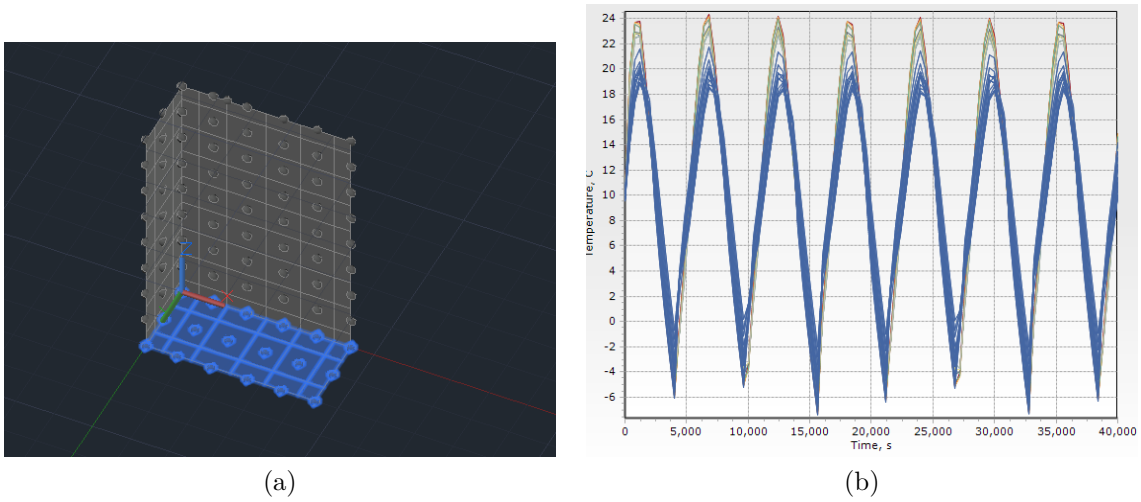


Figure 5.96: Mission 2.b 2U/Z- Worst Cold Case x-y plotting.

Payload Component 1.b

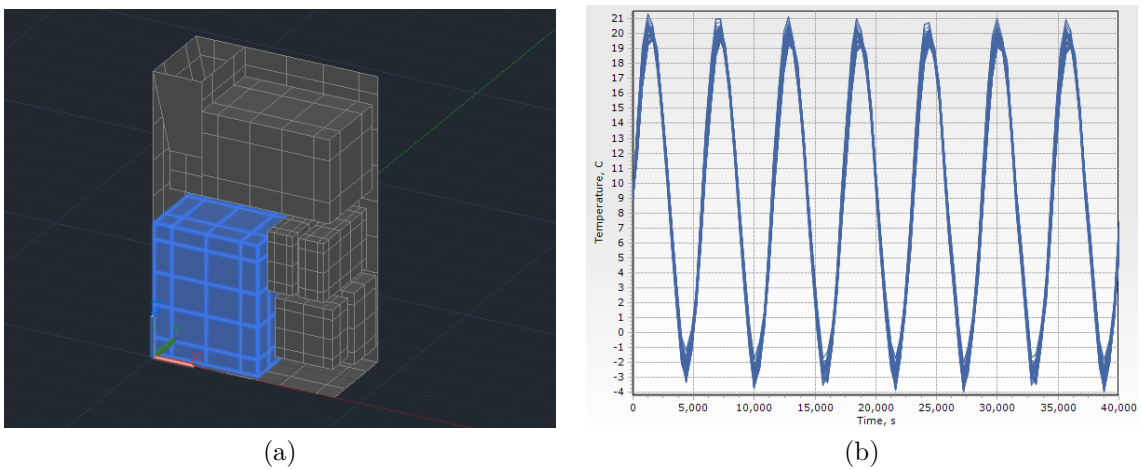


Figure 5.97: Mission 2.b Payload Component 1.b Worst Cold Case x-y plotting.

Payload Component 2.b

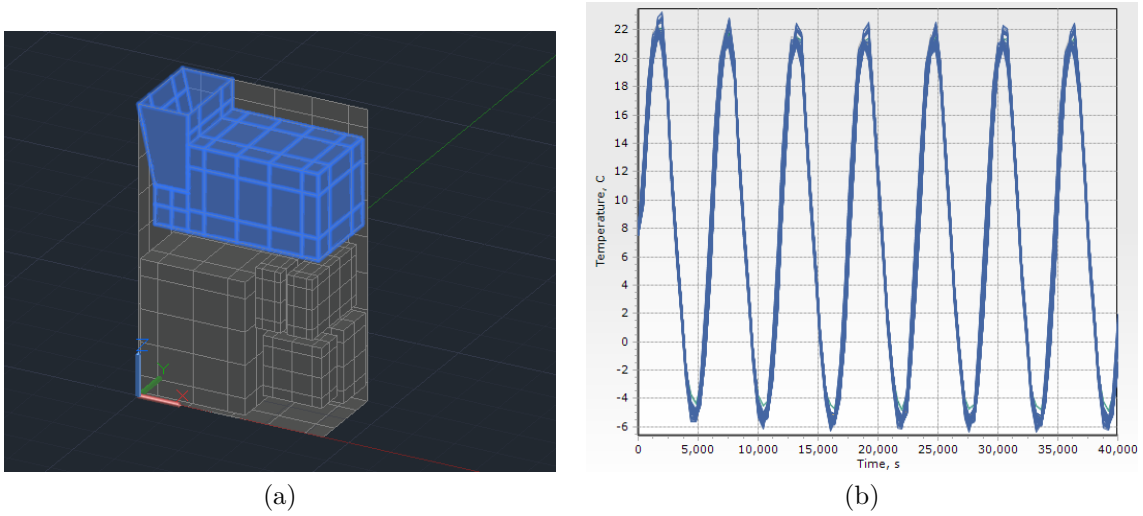


Figure 5.98: Mission 2.b Payload Component 2.b Worst Cold Case x-y plotting.

Bus Component 1.b

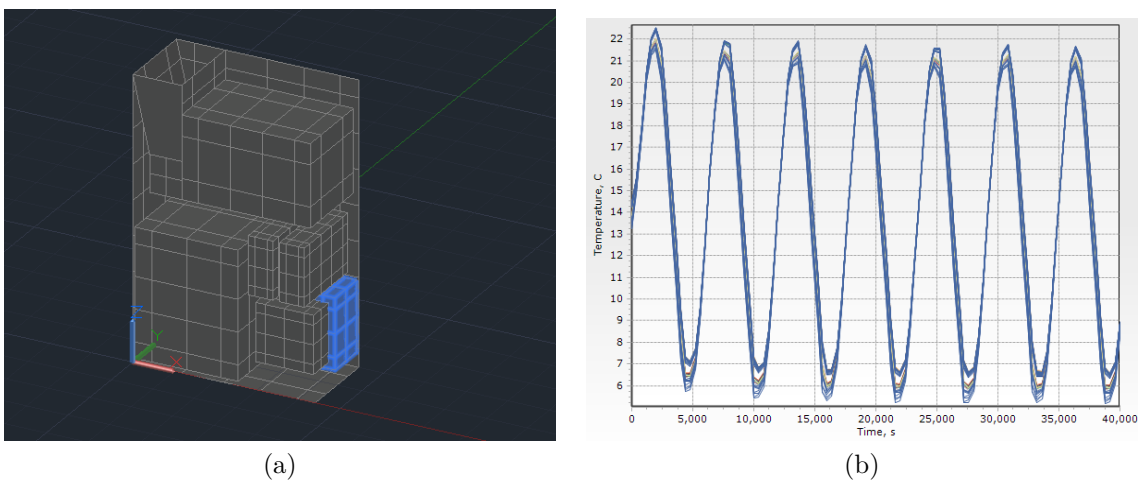


Figure 5.99: Mission 2.b Bus Component 1.b Worst Cold Case x-y plotting.

Bus Component 2.b

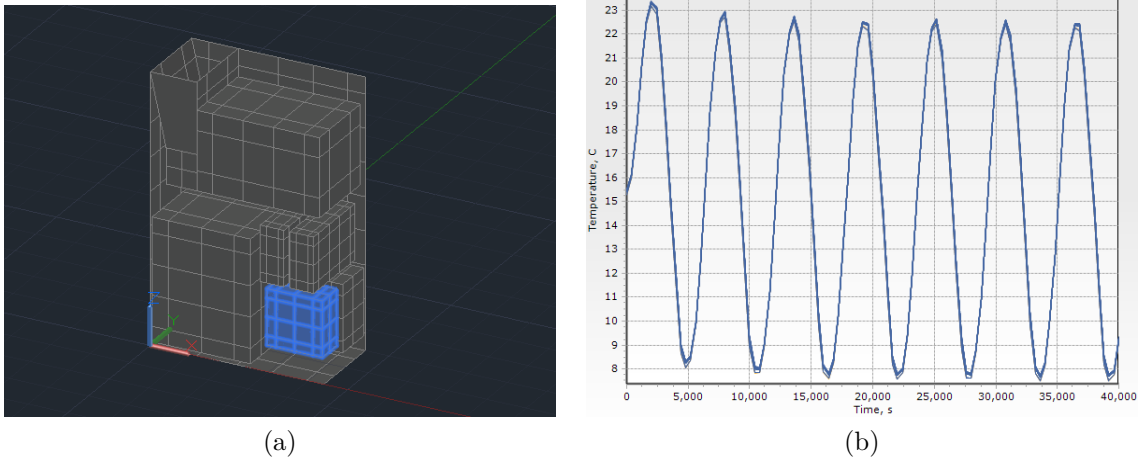


Figure 5.100: Mission 2.b Bus Component 2.b Worst Cold Case x-y plotting.

Battery 1.b

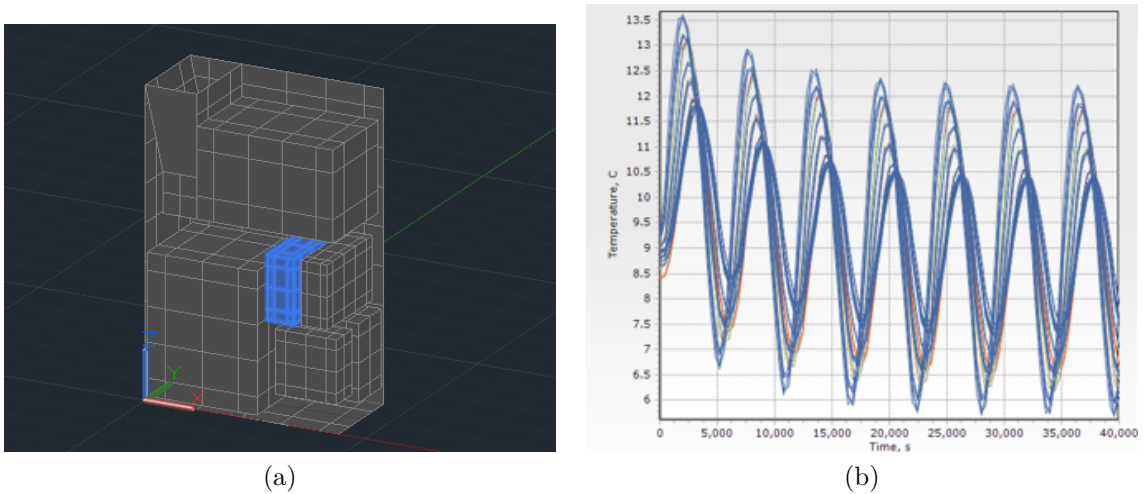


Figure 5.101: Mission 2.b Battery 1.b Worst Cold Case x-y plotting.

Battery 2.b

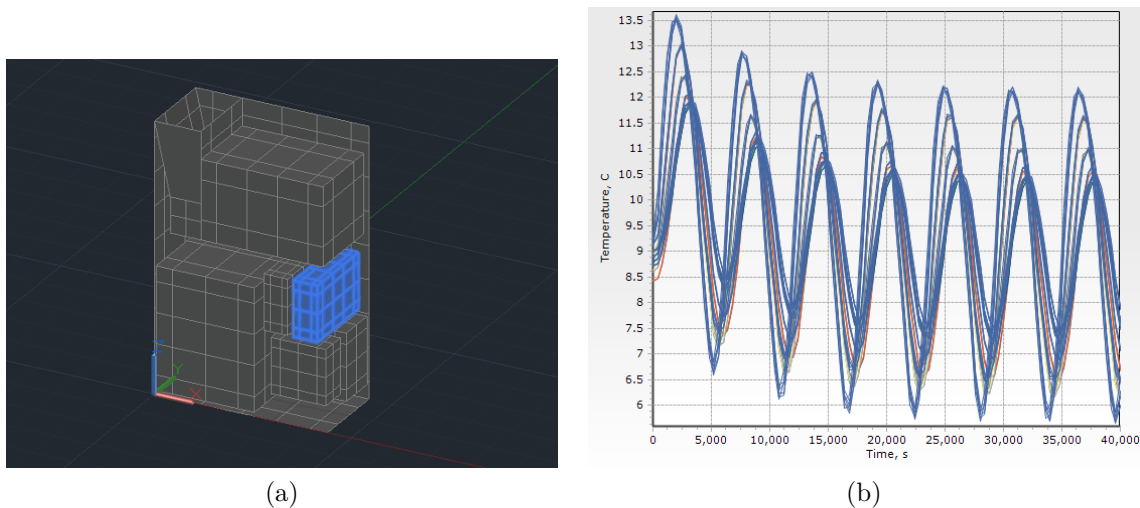


Figure 5.102: Mission 2.b Battery 2.b Worst Cold Case x-y plotting.

5.2.6 Payload PCB Addition

As previously discussed, at the end of the precedent analyses, it has been executed a further analysis adding two PCB, one in front of the other, at a distance of $2mm$, as it is shown in Figure 5.103.

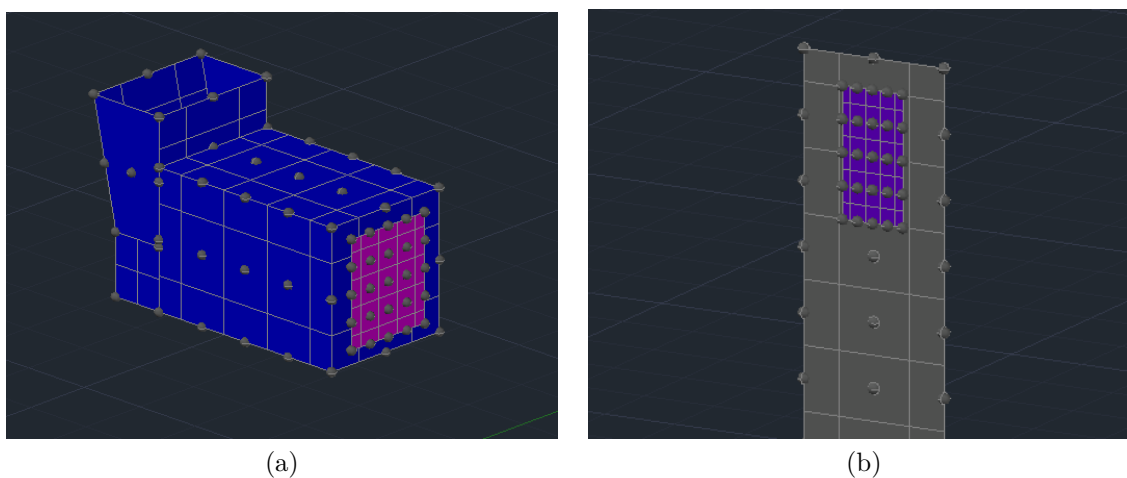
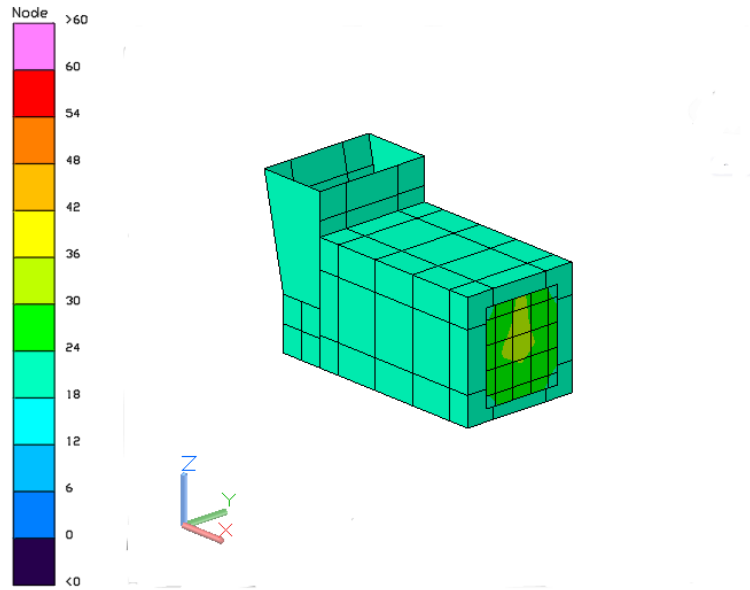


Figure 5.103: Mission 2.b Payload Component 2.b PCB (a) and 3U face PCB (b).

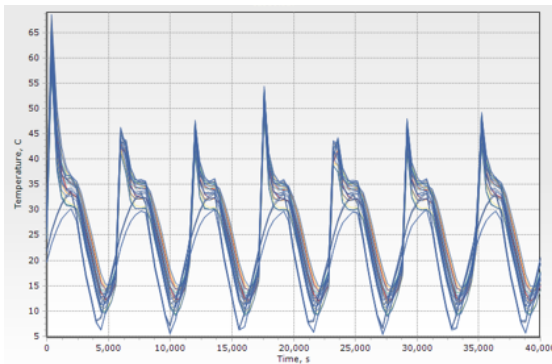
This new thermal analysis has been requested by the payload developer, and its purpose was to study the feasibility of adding an external PCB to the Payload Component 2.b and its interaction during the operation with the Bus PCB located on the 3U electronic board.

On the 3U face PCB is applied a constant heat load of $0.1W$, while on the Payload Component 2.b PCB the heat load is $3W$ but time dependent. It is active 350 sec per orbit.

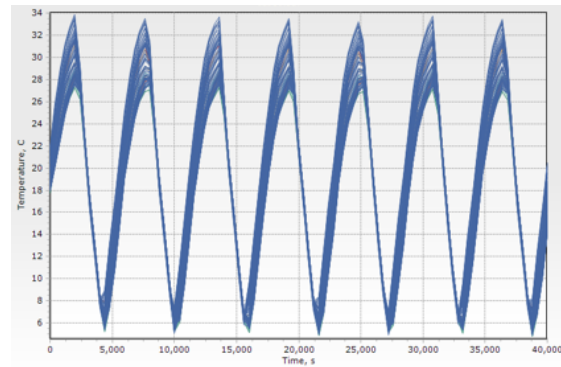
The analysis has been executed for the Worst Hot Case, so with the 6U/Y+ face in sun-pointing, and with the Payload Component 2.b and bus system operative. The final results are presented in Figure 5.104 and Figure 5.105.



(a)

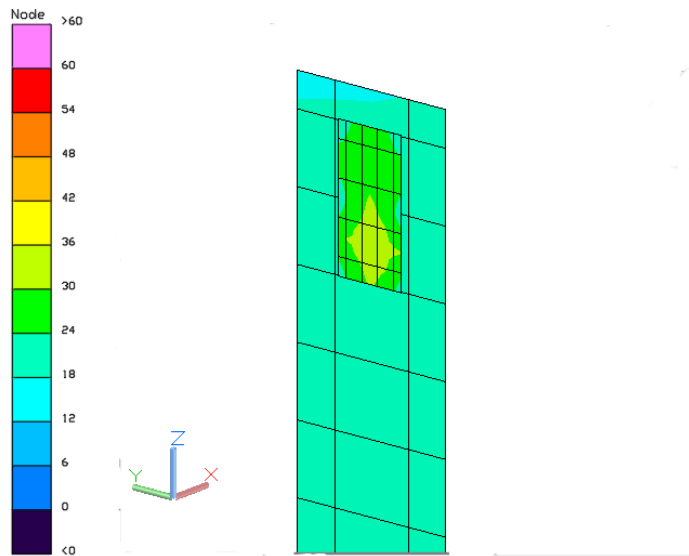


(b)

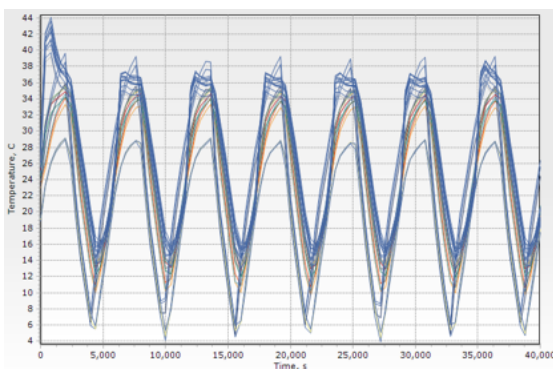


(c)

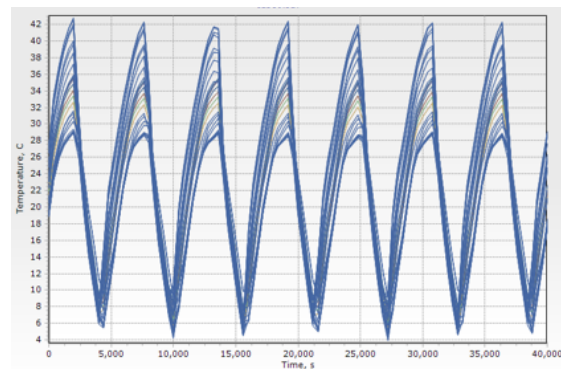
Figure 5.104: Mission 2.b Payload Component 2.b PCB color post-processing (a) and x-y plotting (b-c).



(a)



(b)



(c)

Figure 5.105: Mission 2.b 3U Face PCB color post-processing (a) and x-y plotting (b-c).

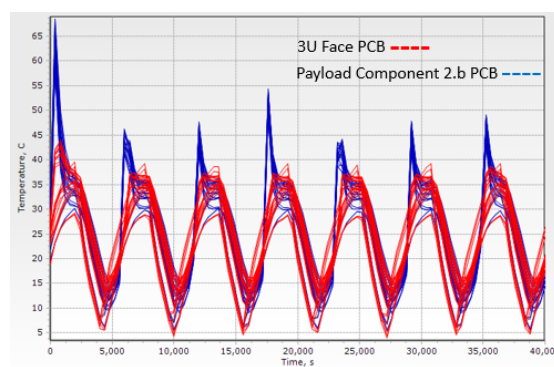


Figure 5.106: Mission 2.b Payload Component 2.b PCB vs. 3U Face PCB x-y plotting.

Chapter 6

Conclusions

Once all the results, from the previous analyses, have been collected, they can be discussed and some important observations can be done.

The principal purpose of Mission 1 and Mission 2 thermal analysis was to develop an as far as simple model which performs a quite effective representation of real spacecraft for the different case scenarios, in order to support the TCS design (see section 5.2.1) and give useful information about the mission feasibility and important input for the testing phase. The results, obtained from these analyses, have been discussed with *Tyvak International* systems and mechanical engineers, and shared with the partners companies involved into the project, including the *ESA*.

Regarding Mission 1, the degree of model accuracy reached has been judged positively for what requested in a first step of spacecraft design, so the collected results have ascertained the mission feasibility, since all the components are in their operative range, and they have been sent to the factories interested into the payload testing which was the most crucial for the project.

The only perplexity brought to light by these models regarded the batteries. In fact, as it can be noted in Figure 5.29b and Figure 5.30b, the battery module in the Worst Cold Case (section 5.1.2) reaches temperature too low to ensure the right battery charging. However in this design phase has to be considered a margin of few degrees which permits to the battery module temperature to be still considered into the operative range.

By the way thanks to this first thermal analysis could be taken precautions in the next design phases and the battery behaviour would be monitored with particular attention.

Instead talking about Mission 2, the analysis executed was more interesting, since it gave many important information.

As for Mission 1, it has been achieved a satisfying model accuracy for what requested at this phase of the project. In particular, all the components are in their operative range, so the mission feasibility has been ascertained and the testing phase has been started by the factories concerned with payload development.

Moreover, the results of Mission 2 thermal analysis have been really important for the TCS design, since thanks to this analysis it has been possible to to better understand which superficial treatment is the most effective for the external 3U/X+ face of Mission 2.a,

and the 3U/X+ and 6U/Y+ of Mission 2.b between alodine or anodizing. The analysis confirmed that the best solution for the study case was having the 3U/X+ alodine and 6U/Y+ anodised, as reported in section 5.2.1.

Regarding the last part of analysis instead, the PCB addition, *Tyvak International* and the payload developer considered themselves quite satisfied, since the results obtained corresponded to those hoped for. Moreover the model accuracy has been confirmed by the payload developers, whose thermal analysis gave the same results.

At this point the thermal analysis could be considered concluded and the mission project can proceed to the next steps of design and testing. For future phases of the project could be interesting to execute further thermal analyses to refine the model in order to obtain even more accurate results. Especially, for example, the battery module, which has been modelled in a particular simple way, or the contactors between crucial components, can be studied more deeply in order to represent their temperature trend in a more precise way.

Acronyms

ANSYS ANalysis SYstem

C&DH Command and Data Handling

CAD Computer Aided Design

CPL Capillary Pumped Loop

CPU Central Processing Unit

CSR Compressed Solution Results

DOF Degree Of Freedom

ESA European Space Agency

FDM Finite-Difference Method

FEM Finite-Element Method

FEMAP Finite Element Modeling And Postprocessing

FORTTRAN FORmula TRANslator

IMU Inertial Measurement Unit

GMM Geometric Mathematical Modeling

GNSS Global Navigation Satellite System

IR Infra Red radiation

ISL Inter-Satellite Links

JSC Johnson Space Center

LHP Loop Heat Pipe

MLI Multi Layer Insulation

MWR Method of Weighted Residuals
NASA National Aeronautics and Space Administration
NASTRAN NAsa STRuctural ANalysis
OSR Optical Solar Reflector
PCB Printed Circuit Board
PCM Phase Change Material
RF Radio Frequency
SHP Sorption Heat Pipe
SINDA Systems Improved Numerical Differencing Analyzer
SSM Second Surface Mirror
TCS Thermal Control System
TD Thermal Desktop
TMM Thermal Mathematical Modeling
TSS Thermal Synthesizer System
UV Ultra Violet radiation
VDA Vapour Deposition Aluminium

Bibliography

- [1] Wayne A. Shiroma, Larry K. Martin, Justin M. Akagi, Jason T. Akagi, Byron L. Wolfe, Bryan A. Fewell, Aaron T. Ohta, *CubeSats: A Bright Future for Nanosatellites*, Central European Journal of Engineering, 2010
- [2] Larson W. J., Wertz J. R., *Space Mission Analysis and Design*, Space Technology Library, 1991
- [3] David G. Gilmore, *Spacecraft Thermal Control Handbook*, D. G. Gilmore Editor, 2002
- [4] J. Meseguer, I. Pérez-Grande, A. Sanz-Andrés, *Spacecraft Thermal Control*, Woodhead Publishing in Mechanical Engineering, 2012
- [5] Chakravarti V. Madhusadana, *Thermal Contact Conductance*, Springer, 2014
- [6] J. R. Howell, R. Siegel, M. Pinar Mengüç, *Thermal Radiation Heat Transfer*, CRC Press, Taylor and Francis Group, 2010
- [7] R. R. McMurchy, R. G. Payne, R. L. Dotts, *Thermal Network Modeling Handbook*, TRW Systems under NASA contract 9-10435, 1972
- [8] T. D. Panczak, S. G. Ring, M. J. Welch, D. Johnson, B. A. Cullimore, D. P. Bell, *Thermal Desktop User's Manual*, C&R Technologies, Inc., 2017
- [9] S. G. Ring, D. Johnson, B. A. Cullimore, *SINDA/FLUINT User's Manual*, C&R Technologies, Inc., 2015

Acknowledgements

Una volta giunti alla fine di un lungo viaggio, come lo è stato arrivare alla fine di questo mio percorso universitario, spesso ci si guarda indietro e si riflette sulle difficoltà superate e su quanto si è cambiati lungo il tragitto, ma soprattutto ci si rende conto delle persone che sono state fondamentali al raggiungimento di un così importante traguardo. E' quindi proprio per questo motivo che mi sento in dovere di ringraziare tutti coloro i quali sono stati al mio fianco durante questo periodo, ed in un modo o nell'altro hanno contribuito al superamento di diversi ostacoli.

Per primi vorrei ringraziare la prof. Sabrina Corpino, per avermi dato la possibilità di realizzare questa tesi ed avermi insegnato tanto, oltre che appassionato, in tutti i suoi corsi; il prof. Fabrizio Stesina e Daniele Calvi, per essere sempre stati disponibili a sciogliere tutti i miei dubbi e ad aiutarmi nei momenti di bisogno.

Ringrazio anche moltissimo Fabio Nichele e con lui tutti i ragazzi di *Tyvak*, per avermi dato fiducia e l'opportunità di contribuire ad un vero progetto spaziale, imparando molto dal punto di vista professionale e umano, essendo sempre stati a disposizione ogni volta avessi necessità e non facendomi mai sentire un estraneo.

Un grazie va anche alla mia numerosa famiglia, ai miei genitori, a mia sorella, ai miei nonni, agli zii, i cugini, a loro che mi sono stati sempre vicino nonostante i 1000 km di distanza, che mi hanno supportato economicamente e soprattutto emotivamente, anche se li telefono meno di quanto dovrei. Che non hanno mai smesso di credere in me, anche magari quando io non ci credevo particolarmente.

Grazie ai miei compagni ingegneri di corso, con i quali ho condiviso ansie, gioie, difficoltà e distazioni ma soprattutto pranzi e cruciverba, e senza i quali molto probabilmente non sarei riuscito a superare tutti gli esami in tempo.

Grazie anche ai cosiddetti "amici di giù", quelli che non sento mai e che vedo ancora meno, quelli che nonostante tutto sono rimasti comunque al mio fianco, quelli che bastava un messaggio o una chiamata a qualsiasi ora per sapere che ci sei, quelli che ogni volta che siamo insieme è come se non ci fossimo mai separati.

Infine un grazie alla persona che conosco da meno tempo tra quelle citate, alla persona che mi ha conosciuto esattamente un mese prima di iniziare questo percorso di tesi, che mi ha visto spesso distratto, triste, disperato quando le analisi non davano i risultati sperati, che mi è stata più vicina di tutti in questi mesi, che mi ha aiutato a tirarmi su quando ne avevo bisogno, che non ha mai smesso di vedere il meglio di me e di ricordarmelo, che è riuscita e riesce ogni giorno a rendermi migliore di quello che sono. Grazie a tutti.